The Effect of Volatiles (H_2O, Cl and CO_2) on the Solubility and Partitioning of Platinum and Iridium in Fluid-Melt Systems

by

Fredrick Allan Blaine

A thesis
presented to the University of Waterloo
in fulfillment of the
thesis requirement for the degree of
Doctor of Philosophy
in
Earth Sciences

Waterloo, Ontario, Canada, 2010

© Fredrick Allan Blaine 2010

I hereby declare that I am the sole author of this thesis. This is a true copy of the thesis, including any required final revisions, accepted by my examiners.

I understand that my thesis may be made electronically available to the public

Abstract

Volatiles are a fundamental component of the Magmatic-Hydrothermal model of platinum group element (PGE) ore deposition for PGE deposits in layered mafic intrusions such as Bushveld and Stillwater. Volatiles have the potential to complex with PGEs in silicate melts and hydrothermal fluids, increasing PGE solubility; in order to assess the models of PGE ore deposition reliable estimates on the solubilities in the various magmatic phases must be known. However, experimental studies on the solubility and partitioning behaviour of PGEs in mafic magmatic-hydrothermal systems under relevant conditions are sparse, and the data that do exist produce conflicting results and new or adapted experimental methods must be applied to investigate these systems. Experimental results are presented here, investigating the effect of volatiles (i.e. H_2O, Cl and CO_2) on Pt and Ir solubility in a haplobasaltic melt and fluid-melt partitioning of Pt between an aqueous fluid and a haplobasaltic melt under magmatic conditions using a sealed-capsule technique. Also included are the details of the development of a novel experimental technique to observe fluid-melt partitioning in mafic systems and application of the method to the fluid-melt partition of Pt.

Solubility experiments were conducted to assess the effect of volatiles on Pt and Ir solubility in a haplobasaltic melt of dry diopside-anorthite eutectic composition at 1523K and 0.2GPa. Synthetic glass powder of an anhydrous, 1-atm eutectic, diopside-anorthite ($An_{42}Di_{58}$) haplobasalt composition was sealed in a platinum or platinum-iridium alloy capsule and was allowed to equilibrate with the noble metal capsule and a source of volatiles (i.e. H_2O, H_2O-Cl or H_2O-CO_2) at experimental conditions. All experiments were run in an internally-heated pressure vessel equipped with a rapid quench device, with oxygen fugacity controlled by the water activity and intrinsic hydrogen fugacity of the autoclave (MnO-Mn_3O_4). The resultant crystal- and bubble-free run product glasses were analyzed using a combination of laser ablation ICP-MS and bulk solution isotope-dilution ICP-MS to determine equilibrium solubilities of Pt and Ir and investigate the formation and contribution of micronuggets to overall bulk determined concentrations.

In water-bearing experiments, it was determined that water content did not have an intrinsic effect on Pt or Ir solubility for water contents between 0.9 wt. % and 4.4 wt. % (saturation). Water content controlled the oxygen fugacity of the experiment and the resulting variations in oxygen fugacity, and the corresponding solubilities of Pt and Ir, indicate that over geologically relevant conditions both Pt and Ir are dissolved primarily in the 2+ valence state. Pt data suggest minor influence of Pt^{4+} at higher oxygen fugacities; however, there is no evidence of higher valence states

for Ir. The ability of the sealed capsule technique to produce micronugget-free run product glasses in water-only experiments, allowed the solubility of Pt to be determined in hydrous haplobasalt at lower oxygen fugacities (and concentrations) then was previously observed. Pt and Ir solubility can be represented as a function of oxygen fugacity (bars) by the following equations:

$$[\boldsymbol{Pt}](\boldsymbol{ppb}) = \mathbf{1389}(\boldsymbol{fO_2}) + \mathbf{7531}(\boldsymbol{fO_2})^{\mathbf{1/2}}$$

$$[\boldsymbol{Ir}](\boldsymbol{ppb}) = \mathbf{17140}(\boldsymbol{fO_2})^{\mathbf{1/2}}$$

In Cl-bearing experiments, experimental products from short run duration (<96hrs) experiments contained numerous micronuggets, preventing accurate determination of platinum and iridium solubility. Longer run duration experiments showed decreasing amounts of micronuggets, allowing accurate determination of solubility; results indicate that under the conditions studied chlorine has no discernable effect on Pt solubility in the silicate melt from 0.6 to 2.75 wt. % Cl (saturation). Over the same conditions, a systematic increase in Ir solubility is found with increasing Cl content; however, the observed increase is within the analytical variation/error and is therefore not conclusive. If there is an effect of Cl on PGE solubility the effect is minor resulting in increased Ir solubilities of 60% at chlorine saturation.

However, the abundance of micronuggets in short run duration experiments, which decreases in abundance with time and increases with Cl-content, offers compelling evidence that Cl-bearing fluids have the capacity to transport significant amounts of Pt and Ir under magmatic conditions. It is suggested that platinum and iridium dissolved within the Cl-bearing fluid are left behind as the fluid dissolves into the melt during the heating stages of the experiment, leaving small amounts of Pt and Ir along the former particle boundaries. With increasing run duration, the metal migrates back to the capsule walls decreasing the amount of micronuggets contained within the glass. Estimates based on this model, using mass-balance calculations on the excess amount of Pt and Ir in the run product glasses (i.e. above equilibrium solubility) in short duration experiments, indicate *estimated* Pt and Ir concentrations in the Cl-bearing fluid ranging from tens to a few hundred ppm, versus ppb levels in the melt. Respective *apparent* (equilibrium has not been established) partition coefficients ($D^{i}_{fluid-melt}$) of $1x10^3$ to $4x10^3$ and 300-1100 were determined for Pt and Ir in Cl-bearing fluids; suggesting that Cl-bearing fluids can be highly efficient at enriching and transporting PGE in mafic magmatic-hydrothermal ore-forming systems.

Platinum solubility was also determined as a function of CO_2 content in a hydrous haplobasalt at controlled oxygen fugacity. Using the same sealed capsule techniques and melt composition as for

H_2O and Cl, a hydrous haplobasaltic melt was allowed to equilibrate with the platinum capsule and a CO_2-source ($CaCO_3$ or silver oxalate) at 1523 K and 0.2 GPa. Experiments were conducted with a water content of approximately 1 wt. %, fixing the log oxygen fugacity (bars) between -5.3 and -6.1 (log NNO = -6.95 @ 1573 K and 0.2 GPa). Carbon dioxide contents in the run product glasses ranged from 800-2500 ppm; and over these conditions, CO_2 was found to have a negligible effect on Pt solubility in the silicate melt. Analogous to the Cl-bearing experiments, bulk concentrations of Pt in CO_2-bearing experiments increased with increasing CO_2 content due to micronugget formation. Apparent Pt concentrations in the H_2O-CO_2 fluid phase, prior to fluid dissolution, were calculated to be 1.6 to 42 ppm, resulting in *apparent* partition coefficients ($D^{i}_{fluid-melt}$) of 1.5 x 10^2 to 4.2 x 10^3, increasing with increasing mol CO_2:H_2O up to approximately 0.15, after which increasing CO_2 content does not further increase partitioning.

As well, a novel technique was developed and applied to assess the partitioning of Pt between an aqueous fluid and a hydrous diopside-anorthite melt under magmatic conditions. Building upon the sealed-capsule technique utilized for solubility studies, a method was developed by adding a seed crystal to the capsule along with a silicate melt and fluid. By generating conditions favourable to crystal growth, and growing the crystal from the fluid, it is possible to entrap fluid inclusions in the growing crystal, allowing direct sampling of the fluid phase at the conditions of the experiment. Using a diopside seed crystal with the diopside-anorthite eutectic melt, it was possible to control diopside crystallization by controlling the temperature, thus allowing control of the crystallization and fluid inclusion entrapment conditions. Subsequent laser ablation ICP-MS analysis of the fluid inclusions allowed fluid–melt partition coefficients of Pt to be determined.

Synthetic glass powder of an anhydrous, 1-atm eutectic, diopside-anorthite ($An_{42}Di_{58}$) haplobasalt composition (with ppm levels of Ba, Cs, Sr and Rb added as internal standards), water and a diopside seed crystal were sealed in a platinum capsule and were allowed to equilibrate at experimental conditions. Water was added in amounts to maintain a free fluid phase throughout the experiment, and the diopside crystal was separated from the melt. All experiments were run in an internally heated pressure vessel equipped with a rapid-quench device, with oxygen fugacity controlled by the water activity and intrinsic hydrogen fugacity of the autoclave (MnO-Mn_3O_4). Experiments were allowed to equilibrate (6-48 hrs) at experimental conditions (i.e. 1498K, 0.2 GPa, fluid+melt+diopside stable) before temperature was dropped (i.e. to 1483K) to induce crystallization. Crystals were allowed to grow for a period of 18-61 hours, prior to rapid isobaric quenching to 293K at the conclusion of the experiment. Experimental run products were a crystal- and bubble-free glass and the diopside seed crystal with a fluid-inclusion-bearing overgrowth. Analysis of fluid inclusions

provides initial solubility estimates of Pt in a H_2O fluid phase at 1488 K and 0.2 GPa at or near ppm levels and fluid melt partition coefficients ranging from 2 – 48. This indicates substantial metal enrichment in the fluid phase in the absence of major ligands such as carbonate or chlorine.

The results of this study indicate that the volatiles studied (i.e. H_2O, CO_2, and Cl) do not have a significant effect on Pt and Ir solubility in a haplobasaltic melt at magmatic conditions. These results suggest that complexing of Pt and Ir by OH, Cl, and carbonate species in a haplobasaltic melt is insignificant and the presence of these volatiles will not result in significantly increased PGE contents over their dry counterparts, as has been suggested. Preliminary evidence of minor Cl-complexing of Ir is presented; however, resulting in only a slight increase (<100%) in Ir solubility at Cl-saturation. Significant partitioning of Pt and Ir into a fluid phase at magmatic conditions has been demonstrated; with estimates of fluid-haplobasaltic melt partition coefficients increasing from $1x10^1$ for pure water to up to an apparent $4x10^3$ with the addition of Cl or CO_2 to the system. This result indicates complexing of Pt and Ir with $OH < H_xCO_y \leq Cl$. Using these estimates, Cl- or CO_2-bearing magmatic fluids can be highly efficient at enriching and transporting platinum group elements (PGEs) in mafic magmatic-hydrothermal ore-forming systems.

Acknowledgements

I would like to thank my advisors Bob Linnen and Francois Holtz for their direction, help and support along the way as well as their friendship.

I would also like to thank Gerhard Brügmann, Joel Gagnon and Bryan Fryer for their help with analysis and interpretation and their expertise in working with some very difficult analyses.

There are many who have helped me along the way at Hannover and thanks go out to Harald, Antje, Marcus F., Melanie, Susi, Marcus N., Jasper, Dieter, Otto, Willie, Bettina and everybody else that made things a little easier at Hannover.

Thanks to all my friends who have helped me along the way and made my times both at Hannover and Waterloo unforgettable. To Piero, Kevin, Dominik, Roman, Francesco, Ronnie and Matthi, thank you for making Hannover feel like home and a place I will always miss. Thank you to Sean, Jen and Jesse who were my complaint-/vent-/support-circle throughout my graduate work.

A special thanks to my family for their love and support. I could not have done this without my parents who were always there when I needed advice and support, and always supported my decisions.

Finally, to Diane and Zinnia, who have been there for me through the hardest parts of this journey and are the reason its completion was possible, all my love and thanks.

This project was supported by the Hochschulvergabe Projekt N° 75 of the BGR (German Geological Survey), by the DFG (German Science Foundation, project Ho 1337/9) and by the Natural Science and Engineering Research Council of Canada.

Dedication

To my family

Table of Contents

List of Figures

List of Tables

Author's Note

The thesis presented here is written as a collection of individual first author papers, included as chapters 2-6, and an introductory and summary chapter. Each paper was written as a standalone paper and this requires that some information is repeated within other papers within this collection. This is especially true under the experimental and analytical methods sections of the individual papers. Where applicable and possible some liberty has been taken on the papers that have not been submitted to reference areas of the thesis where certain aspects of the research were covered in more detail in order to minimize this repetition.

The introductory chapter was written to provide the reader the necessary background to the problems addressed in this manuscript and underlines the necessity for the study presented within. As well, it ties together the individual chapters to the main theme of this manuscript which is to investigate the potential influences that volatile constituents can have on the formation of Platinum Group Element (PGE) ore deposits throughout the ore producing magma's evolution up to and including volatile saturation. This is accomplished through solubility studies designed to assess the role of H_2O, CO_2 and Cl on Pt and Ir solubility and partitioning studies to assess the potential of aqueous fluids to concentrate and transport PGEs which are addressed in Chapters 2 through 6.

Chapter 2 is entitled: "Platinum Solubility in a haplobasaltic melt at 1250°C and 0.2 GPa: The effect of water content and oxygen fugacity", published, Blaine et al. (2005). This paper addresses the influence water, the most abundant and arguably the most important volatile in magmatic systems, on Pt solubility in a basaltic melt analog. This study was conducted as a precursor to the fluid-melt partitioning study presented in Chapter 6, as water has the potential to affect Pt solubility in a silicate melt and prior to this study, consistent and interpretable, experimental data did not exist. As well as determining the effect of water on Pt solubility in a mafic melt, this study also provided valuable insight into the potential shortcomings of previous experimental techniques.

Chapter 3 is entitled: "The effect of Cl on Pt solubility in haplobasaltic melt: Implications for micronugget formation and evidence for fluid transport of PGEs", submitted. This paper addresses the effect of Cl, an extremely important volatile to metal enrichment and transport in ore forming systems, on Pt solubility in a basaltic melt. This is the first experimental paper to address this topic and provides important experimental data necessary for determining the role of Cl in PGE ore-forming systems. As well as determining the effect of Cl on Pt solubility in a mafic silicate melt, insight was also gained and data provided addressing the role of hydrothermal Cl-bearing fluids in the

concentration and transportation of Pt, a highly debated subject in PGE ore deposit research. Also presented in this chapter are new theories on the formation of micronuggets in experimental systems.

Chapter 4 uses the techniques developed in chapters 2 and 3 and applies them to another PGE of interest, iridium. This chapter is entitled "The effect of oxygen fugacity and Cl content on Ir solubility in a haplobasaltic melt: Evidence of Cl complexing in basaltic melts and aqueous brines"

Chapter 5 addresses the influence of carbon dioxide on Pt solubility, and is entitled "The effect of CO_2 on the solubility of Pt in a haplobasaltic melt at 1523K and 0.2 GPa and evidence for Pt-carbonyl complexing in magmatic fluids". Carbon dioxide is second only to water in abundance and is perhaps the most important volatile in mafic magmatic systems, from which reef-hosted PGE occurrences form. This paper addresses the effect of CO_2 on Pt solubility in a mafic silicate melt and gives insight into the potential for concentration and transport of PGEs in mixed H_2O-CO_2 fluids.

Chapter 6, reports the results of a technique development study to create a method for observing and quantifying fluid-melt partitioning of PGEs. The method developed has been utilized to give a first approximation of the fluid-melt partitioning of Pt, at P-T-X conditions approaching that of PGE ore-forming systems, necessary to assess the validity of the Magmatic- Hydrothermal model of PGE deposit formation. As well, the method sets the stage for future fluid-melt partitioning studies in basaltic systems for both the PGEs and other elements under controlled pressure, temperature and oxygen fugacity conditions for which there has not been a suitable method up to this point.

The final chapter provides a summary of the individual investigations under the blanket theme of this thesis and an overview of the potential influences of volatiles in PGE ore-forming magmatic systems. Suggestions for future research are also included in this section.

Though the papers are multi-author papers, experimental design and implementation, sample preparation, analyses, data collection and interpretation and writing were the responsibility of the first author, Fred Blaine. Robert Linnen and Francois Holtz were thesis advisors and had a role in the development and direction of the project and discussion throughout the PhD project. Gerhard Bruegmann and Joel Gagnon aided in instruction and development of analytical techniques as well as processing of analytical data, and were included as authors to recognize this contribution.

It is my hope that the reader will come away from reading this manuscript with an appreciation of the complexities of melt-volatile interactions in magmatic systems and also insight into the means by which to study these interactions experimentally. Although admittedly not the "Rosetta Stone" for the solution of the complex behaviors of PGEs, much progress has been made in

the understanding of the experimental difficulties and in the prevention of these difficulties. New experimental techniques have been developed and current techniques have been adapted for application to the study of PGE in basaltic systems while eliminating or at least minimizing potential problems associated with prior techniques. Application of the results of these studies and application of the developed techniques in increasingly complex experimental system will allow us to get one step closer to modeling PGE behavior in more and more complex natural systems.

Chapter 1: Introduction

1.1 Chemistry of the Platinum Group Elements (PGE)

Platinum group elements (PGE) consist of six elements: platinum (Pt), palladium (Pd), rhodium (Rh), iridium (Ir), ruthenium (Ru) and osmium (Os). This group of elements is in group VIII and group VIIIa of the transition elements in the periodic table. Further designation of these elements can be based on behavior, subdividing the PGEs into the iridium group PGEs (IPGE) which consists of Ir, Os, and Ru and the palladium group PGEs (PPGE) which consists of Pt, Pd and Rh (Barnes et al., 1985). Subdivision can also be based on the atomic weight, dividing the PGEs into light (Pd, Rh, Ru) and heavy (Pt, Ir, Os) groupings.

The PGEs are classed as highly siderophile elements (HSE) and along with Re and Au complete this geochemical grouping. Siderophile elements (iron-loving) have a strong affinity for forming metallic bonds and will readily form metallic bonds with other metals in a metallic phase over ionic bonds. As well as being siderophile the PGEs along with Au, Cu and Ag, are moderate to highly chalcophile (sulfur loving) and will form covalent bonds with sulfur over forming ionic bonds with oxygen. These two characteristics of the PGE exert the dominant control on their behavior in magmatic systems. If either a metallic phase or a sulfide phase coexists with a silicate phase, the PGEs will partition strongly out of the silicate phase, where the PGE are interpreted to exist covalently bonded to oxygen (Farges et al., 1999), and into the metallic or sulfide phase.

The solubility of the PGEs is highly dependent on the oxidation potential of the system. PGEs when present as a metal or alloy are in the zero-valent state and dissolve into an aqueous fluid or melt phase through an oxidation reaction (Equation 1.1). As a result, a dominant controlling factor for PGE solubility is oxygen fugacity in both aqueous and melts systems. The magnitude of the influence is dependent on the oxidation sate of the dissolved species as can be seen from Equations 1.1 through 1.3, and provides a means to determine the oxidation state of the PGE species by investigating the influence of changing oxygen fugacity on solubility. This is exemplified and covered in detail in Chapters 2 and 4 where the oxidation states of Pt and Ir are determined for silicate melts by conducting a series of experiments at varying oxygen fugacities. In Equation 1 the valence state is equal to 4x where x is equal to the stoichiometric amount of O_2 involved in the reaction.

$$Pt^{0}{}_{(s)} + xO_2 \Leftrightarrow PtO_{2x}$$ **Equation 1.1**

$$K = \frac{a\,PtO_{2x}}{aPt_s \times fO_2^x}$$ **Equation 1.2**

$$\log[Pt] = x \log f_{O_2} + K'$$ **Equation 1.3**

A good example of the control oxygen fugacity has on PGE solubility in nature is during the crystallization of chromite from a PGE-bearing melt. When chromite crystallizes there is a boundary layer effect which reduces the oxygen fugacity in the melt immediately surrounding the crystallizing chromite grain. Due to this drop in oxygen fugacity the PGE solubility decreases and can cause the formation/exsolution of a PGE alloy phase within this layer and as the chromite grows, the alloy phase is encompassed by the chromite and is trapped as an inclusion (Finnigan et al., 2008).

The aqueous geochemistry of platinum and palladium is relatively well constrained at low to moderate temperatures (up to 573K) although some variance is reported between various studies. There is a scarcity of experimental data for the remaining PGEs (Ir, Os, Ru, Rh) and few studies have looked at the aqueous geochemistry of any of the PGEs at increased, near magmatic, temperatures and there is a need for data in these areas (Wood, 2002), especially to determine the role of deuteric fluids in the genesis of PGE ore deposits. In historical studies it has been shown that PGEs can be transported as volatiles at magmatic temperatures (Fleet et al, 1993; 1995) and in sulphur-dominated vapour (Peregoedova et al. 2006); however transport by aqueous fluids at magmatic conditions is poorly understood. Over geologically relevant conditions in aqueous solutions the dominant oxidation state of all of the PGEs is 2+ (Hanley, 2005), at very oxidized conditions Pt(IV) could become dominant though likely not important in hydrothermal fluids. Various oxidation states of Os are also possible including Os(III), Os(VI) and Os(VIII) although little experimental work has been performed looking at osmium speciation in aqueous fluids.

At low to moderate temperatures Pt and Pd act as soft to moderate Lewis acids and preferentially form complexes with soft bases/ligands such as bisulphide, although complexation with intermediate ligands such as Cl is also possible (Wood, 2002; Hanley, 2005). At increased temperatures (above 573K) it is postulated that bonding with the PGEs will become increasing more "hard" causing complexation with Cl to become increasingly favored in hydrothermal fluids giving high T, Cl-bearing fluids a great potential for transporting the PGEs (Wood, 2002; Hanley, 2005). When PGEs dissolve from a metal or alloy where they are in the zero-valence state, the reaction is an oxidation reaction such as is shown in Equation 1.4 for Pt. It can be seen in Equation 1.4 through 1.6 that PGE solubility will be dependent on both the availability of oxygen (redox conditions) and on the

pH of the solution. From this it can be seen that the solubility of the PGEs will be highest in low pH fluids at oxidizing conditions.

$$Pt^{0}_{(s)} + \frac{1}{2}O_2 + 2H^{+} \Leftrightarrow Pt^{2+}_{(aq)} + H_2O \qquad \textbf{Equation 1.4}$$

$$\boldsymbol{K = \frac{aPt^{2+}}{(aH^{+})^{2} \times fO_2^{1/2}}} \qquad \textbf{Equation 1.5}$$

$$\boldsymbol{\sum Pt_{(aq)} = K \times (aH^{+})^{2} \times fO_2^{1/2}} \qquad \textbf{Equation 1.6}$$

1.2 Importance of PGE research

1.2.1 Core/Mantle segregation

The highly siderophile nature of the PGEs makes them very well suited to studying processes involved with core/mantle interaction and segregation. During the evolution of the Earth, when the metallic core separated from the silicate portion, which now forms the mantle and crust (bulk silicate Earth, BSE); the PGEs were partitioned strongly into the metallic core. This separation left a PGE-depleted BSE compared to the estimated bulk earth C1-chondritic values. Using estimates of PGE partitioning values these processes can be looked at in depth, and models of Earth's evolution can be developed. Using the current knowledge of partitioning of PGEs, there appears to be elevated PGEs remaining in the BSE which range from 1-7 ppb. This has led to the hypotheses that the PGEs and other siderophile elements were added to the BSE as a late-stage "veneer" that was added to the BSE after initial core-mantle separation (Chou, 1978; Righter, 2003). This model has been the focus of much research in recent years trying to constrain the values for PGE partitioning at mantle pressures by studies such as Righter (2003), Cottrell and Walker (2006), Ertel et al. (2006) and Righter et al. (2007). Enhanced solubility of the PGEs in a silicate melt at increased pressure (summarized in Lorand et al. 2008) has caused some researchers to question the necessity of the late veneer model, implying that higher PGE concentrations could be maintained in the BSE without the need of a late veneer.

1.2.2 PGE ore deposits

1.2.2.1 Role of volatiles in the genesis of PGE deposits

1.2.2.1.1 Non-conventional

It is well known that there are occurrences of PGEs at near economic levels in a variety of ore deposits that are known to be of a hydrothermal nature. Although usually not economic on their own and not ubiquitous to all deposits, PGEs can contribute greatly to the viability of these deposits. As well, the enrichment of the PGEs at these deposits that are of a definite hydrothermal nature provides evidence that aqueous fluids can transport and enrich PGEs.

Anomalous PGE occurrences in hydrothermal ore deposits have been found in Porphyry Cu deposits with preference to those formed in island-arc settings or alkaline rocks, unconformity U-Au deposits, sediment-hosted stratiform Cu deposits (Kupferschiefer) and Jacutinga-type ironstone deposits (Wood, 2002). There are also hydrothermal platinum deposits, namely the New Rambler (USA), Waterberg Deposit (S. Africa) and the Copper Hill Deposit (Australia). Marathon and Lac des Isles are also proposed to have been formed through hydrothermal processes. In the aforementioned deposit types it is postulated that PGE-chlorine complexing dominates in the fluid responsible for the concentration and transport of the PGEs at low to moderate temperatures and at relatively oxidizing and acidic conditions, which is determined by associated mineralogy (Wood, 2002). In deposits such as these, an increase in fluid pH, decrease in redox potential and/or a decrease in temperature could cause the deposition of PGEs.

As well as the PGE-bearing deposits that are associated with Cl-bearing fluids, there are also a number of deposits that are of hydrothermal origin and are interpreted to have resulted from bisulphide complexation. These deposits have formed at more reducing conditions and higher pH than the previously mentioned deposits and include, volcanogenic massive sulphide, Ni-Mo-PGE-Au deposits in black shales, Salton Sea, Ophiolites and footwall hosted ores of the Sudbury Igneous Complex (Wood, 2002).

1.2.2.1.2 PGE occurrences in association with layered mafic intrusions

There has been substantial research into PGE deposits over the last 30+ years without consensus on the processes involved in the formation of reef-hosted platinum group element deposits. The role of volatiles in the genesis of PGE deposits in layered intrusions is one of the most poorly understood aspects and many ideas have been put forth. A strong correlation between PGE contents

and chlorine concentrations have been observed in a number of PGE deposits, including three of the world's largest PGE deposits Bushveld (S. Africa), Stillwater (U.S.A) and the Great Dyke Deposit (Zimbabwe) (Boudreau and Meurer, 1999). Although this correlation is prevalent and would seem to hint at a coincidental process resulting in the observed behavior, it has been largely ignored, especially in papers that support the magmatic R-factor model of PGE enrichment. This correlation has been used to argue for the validity of the magmatic-hydrothermal model of PGE enrichment using the elevated Cl concentrations to indicate the presence of late stage Cl-bearing hydrothermal fluids which acted as a transport and concentrating medium for the PGEs.

1.2.2.2 R-Factor Model

Proponents of the R-factor model, dubbed "downers" because PGE enrichment is thought to involve downwards migration of sulphide (Mungall and Naldrett, 2008), hold that PGE enrichment is due predominantly to partitioning of the PGEs between a silicate melt and an exsolved sulphide phase. In this model a mafic to ultramafic melt reaches saturation in a sulphide melt through magma mixing; assimilation of, or interaction with, a crustal component (i.e. sulphur-bearing sediment); and/or decreasing temperature. When the silicate melt reaches saturation in a sulphide melt, the exsolved sulphide will strip the chalcophile elements including the PGEs from the silicate melt due to the very high sulphide/silicate melt partition coefficients resulting in a sulphide phase enriched in PGEs and a highly depleted silicate melt. The relation between the concentrations in the coexisting silicate and sulphide phases can be modeled using the R-factor equation (Equation 1.7; Campbell and Naldrett, 1979)

$$\boldsymbol{C_{sul} = D_i^{sul/sil} \times C_o \times \frac{(R+1)}{R+D_i^{sul/sil}}} \qquad \textbf{Equation 1.7}$$

Where:

C_{sul} is the final concentration of element "i" in the sulphide melt, R (hence R-factor) is the mass ratio of silicate to sulphide melt, C_o is the initial concentration of element "i" in the bulk original silicate+sulphide melt and $D_i^{sul/sil}$ is the sulphide-silicate melt partition coefficient for element i.

Due to the high density of the sulphide in relation to the silicate melt, upon exsolution and coalescence the sulphide will descend through the magma chamber and into the quasi-crystalline mush at the bottom of the magma chamber (Mungall and Naldrett, 2008). Repeated injections of fresh undepleted magma through this sulphide will further enrich the sulphide in chalcophile elements including the PGE. Enrichment can continue in this manner until the sulphide reaches equilibrium

with the undepleted silicate melt. The repeated injection of fresh magma is a key assumption of this model because in order for the sulphide to become sufficiently enriched in the PGEs, the sulphides must interact and scavenge chalcophile elements from a very large volume of silicate melt.

The R-factor model has abundant support due to its succinct explanation of the majority of Ni-rich, PGE-poor deposits. Two such deposits, Voisey's Bay and Norilsk-Talnakyth nickel deposits, show very compelling evidence that they formed due to a process such as the R-factor model. At these deposits the host gneisses were sulphur bearing and evidence in the form of reaction haloes indicated that there was substantial interaction between the host rock and the silicate melt which would provide the necessary sulphur for saturation of a sulphide phase (Naldrett, 1999). Internal geochemical evidence also supports the R-factor model at these deposits as there is evidence that the magmas entering the chamber underwent significant depletion in the chalcophile elements followed by intruding magmas that were successively less depleted (Brügmann et al. 1993; Naldrett, 1999). This is evident in the rocks immediately overlying the PGE enrichment which are highly depleted and which become less depleted going up the stratigraphic column.

Although the R-factor adequately describes the formation of the majority of nickel-rich, PGE-poor deposits and has been proposed for many Ni deposits, it has not been able to explain all the features of PGE-rich nickel deposits hosting reef-type PGE deposits. However, dynamic models such as that of Kerr and Leitch (2005) can explain some of the features of high-grade, low-sulphide deposits. Due to the fundamental nature of the R-factor equation and of highly chalcophile element behaviour, small to moderate R-factors will provide the largest amount of highly chalcophile element enrichment, owing to the fact that the initial sulphide melt exsolved will contain very high concentrations of PGE and deplete the melt strongly in these elements. Increasing the R-factor serves to dilute the sulphide melt in the highly chalcophile elements preventing the preservation of economic levels of PGE, however high R-factors can allow significant enrichments and large tonnages for the higher abundance, moderately-chalcophile elements such as Ni and Cu. The low R-factors required for the PGEs are the primary shortcoming of the R-factor model for PGE-rich deposits as it requires that a small amount of sulphide melt is able to interact, equilibrate and scavenge PGEs from a very large amount of silicate melt, >100's of km^3, in the case of a PGE-rich deposit such as Bushveld.

1.2.2.3 Magmatic-Hydrothermal Model

There has been a significant amount of work initially proposed by Ballhaus and Stumpfl (1986) and subsequently spearheaded by other researchers (Boudreau and Meurer, 1999; Meurer et al., 1999; Willmore et al. 2000; Boudreau, 2008) looking at the possibility and evidence for

magmatic-hydrothermal redistribution and concentration of PGEs in reef-hosted deposits. The resultant models are dubbed "uppers" because the source of the PGEs is below the deposit and transported upwards in an exsolved aqueous fluid. Historically there has been a lot of resistance to this model due to lack of experimental evidence and the wide acceptance of the R-Factor model. The magmatic-hydrothermal model still holds support in its explanation of geochemical and structural features within the two largest PGE-bearing layered intrusions; Stillwater and Bushveld. In this model, the magma becomes fluid saturated and a chlorine-bearing aqueous fluid exsolves from the melt due to decreasing temperature, and crystallization within magma. If there is a significantly high fluid/melt partition coefficient for the PGEs, the aqueous fluid will scavenge the PGEs leaving a depleted magma. The fluid can then travel upward in the deposit, where it can reach a fluid-undersaturated magma and dissolve into that magma, with the PGEs dissolving into that magma if the magma is not saturated in PGEs, or into a sulphide phase. This process can continue with multiple saturation events, continuously moving upwards enriching the overlying magma in PGEs, until eventual deposition of the PGEs. However the experimental results of this study indicate that other factors and mechanisms may come into play which can enhance the effectiveness of this model and are discussed in detail in Chapters 2 and 4.

The support for this model comes in the geochemical, petrological and structural features of the reef hosted PGE occurrences. This includes elevated Cl, and incompatible elements associated with the PGE enrichment in the Bushveld and Stillwater deposits (Boudreau and Meurer, 1999), and the pegmatitic nature of the Merensky Reef, Bushveld (Ballhaus and Stumpfl, 1986) both indicating the presence of fluids. As well, in the Merensky Reef there is a general association and occurrence of the PGE-bearing phases at the intercumulus silicate-sulphide interface indicating late-stage formation of the PGE-bearing phases which is counterintuitive to the early PGE-rich sulphides that would be formed using the R-factor model (Ballhaus and Stumpfl, 1986)

1.3 History of experimental work on PGE solubility in silicate melts and fluids

Due to the growing economic importance of the PGEs in the early 1990s as well as their use in the determination of processes involved in early Earth formation there was an increase in experimental studies on PGE behaviour throughout this period. The advancements in experimental design and the development of new analytical techniques have allowed for significant progress in the study of PGE behaviour and have opened the door for new studies on more advanced systems. Although historically there have been a number of partitioning studies for the PGE looking at

distribution coefficients for sulphide melt-silicate melt (Ballhaus and Ulmer, 1995; Bezmen et al., 1994; Fleet et al.,1999; Makovicky and Karup-Moller, 2000; Peach et al., 1994 Van Orman et al., 2006), mineral-silicate melt (Brenan et al., 2003; 2005; Righter et al., 2004) and metal-silicate melt (Cottrell and Walker, 2006; Righter, 2003; Righter et al. 1997; 2007). These studies have resulted in a good understanding of the solubility of PGEs in metal and sulphide phases over recent years, especially after the recognition of PGE micronuggets in the sulphide, metal and silicate phases and subsequent analyses by microanalytical techniques such as laser-ablation ICP-MS. However there is still some debate on the origin of micronuggets (discussed later) and the true solubilities of PGE in the silicate melt phase (Cottrell and Walker, 2006, Ertel et al. 2008) requiring new or adapted techniques to observe PGE solubility in the silicate phase at P-T-X conditions relevant to nature. Only recently have studies expanded to study PGE solubility outside of dry, volatile-free systems and as a result there are still relatively few partitioning studies looking at fluid-melt partitioning of the PGEs and more data are required, requiring new or adapted experimental techniques to observe increasing complex systems.

1.3.1 Solubility Experiments

1.3.1.1 Stirred Crucible Method (Mechanically Assisted Equilibration)

In early studies on metal solubility, a method was utilized using a crucible composed of metal, to contain the melt of interest, and as the source of metal for saturation of the melt. Due to the relatively large volume of these crucibles and the length of time needed to reach equilibrium relying solely on convection, a modification of the method was implemented using a metal rod of the same metal as the crucible to stir the melt throughout the duration of the experiment. The stirred crucible method was predominantly developed and used in the PGE solubility studies of Ertel (Ertel et. al. 1999; summarized in Ertel et al., 2008). For these studies a crucible composed of either pure PGE metal or a PGE alloy was used for the source of the desired PGE for melt saturation. A glass powder of the composition of the desired melt was added to the crucible and the assemblage was heated in a gas-mixing furnace to the temperature of interest at fO_2-controlled conditions using different gas mixtures added to the furnace. At various time points during the duration of the experiment a alumina rod could be dipped into the melt and then removed along with a small sample of melt; the sample could then be quenched and analyzed for PGE content. After sampling, the experiment could be continued either at the same fO_2 or the fO_2 could then be varied to observe solubility at another oxygen fugacity.

This method is very good except for a few limiting factors. On the positive side, temperature is easy to control and oxygen fugacity can be controlled very precisely which, as discussed before, is extremely important to the study of PGE solubility. It is also possible to observe PGE solubility at a number of different fO_2's in a single experiment by varying the fO_2 between sampling episodes. Another benefit to this method is the large sample size which allows for multiple sample extractions and analyses.

The restrictions of this experimental technique are that all experiments are conducted at 1 atm pressure, and at this pressure all experiments are dry, volatile-free. A second drawback is the presence of ubiquitous PGE micronuggets at lower oxygen fugacities and extremely long equilibration times (>600 days, Ertel et al., 1999). The micronugget problem will be addressed in detail in a separate section as it is a natural as well as an experimental phenomenon, somewhat unique to the PGEs, and requires careful consideration. Because in initial studies bulk solution analyses were used, the presence of micronuggets masked any true solubility trends and this method was only applicable over a certain oxygen fugacity range and was not able to measure solubilities at low fO_2. Later studies used laser ablation ICP-MS to analyze for PGEs and were able to determine micronugget-free solubilities at lower oxygen fugacities extending the range of oxygen fugacities that are possible to study.

It has been suggested that the presence of micronuggets is caused by physical agitation of the stirring rod knocking off small particles of the rod which were then were entrained within the melt (Ertel et al. 1999). Further evidence that this was not the case and that micronugget formation was due to other experimental aspects was obtained over the duration of the current study and is discussed throughout this document as it applies to individual sections.

1.3.1.2 Wire-loop Method

The wire-loop method was used primarily in PGE-solubility studies conducted by Borisov (Borisov and Palme, 1997; Borisov and Palme, 2000; summarized in Borisov, 2001). This method used a wire loop made of either the PGE of interest or a PGE alloy as the source for the metal of interest. A glass powder is secured in the metal loop with an organic glue mixture which volatilizes upon heating of the sample leaving only the melt droplet, held within the metal loop by the surface tension of the melt, once the experiment has reached temperature. Experiments are run in gas-mixing furnaces which provide the same temperature control and oxygen fugacity control as those used for the stirred crucible method, and as well the drawbacks of only being able to study 1 atm, dry volatile-free systems. At the conclusion of the experiment the wire loop is removed from the furnace and

quenched, the wire loop removed and the resultant glass analyzed. Multiple extractions of melt are not possible using this method but with their small sample size it is possible to conduct multiple experiments at the same time. The absence of mechanical mixing causes increased equilibrium time versus the stirred crucible method but the small sample size and therefore small transport length for the PGEs counteracts this, keeping run times within reason. Micronuggets are a problem using this method at low oxygen fugacities, again masking solubility trends at low PGE solubilities if bulk analytical techniques are used. Again laser ablation analysis is utilized with this method to alleviate the micronugget problem.

1.3.2 Micronuggets

Micronuggets are submicron-scale PGE-rich inhomogeneities. Micronuggets can be found in the melt, mineral, and perhaps even in fluid phases, as high concentration anomalies in both experimental and natural systems. It is the author's opinion that micronuggets, when formed from oversaturation conditions in a silicate melt, are somewhat analogous to colloids in that they remain suspended, with a nearly homogeneous distribution and do not coalesce (although over great lengths of time coalescence may be possible). More details of micronugget formation in experiments and nature will be presented throughout this thesis as they are a somewhat unique phenomenon to PGEs and are integral to the experimental and analytical design and interpretation of any experimental results and their application to nature.

The nature of micronuggets in experimental melts is not fully understood and there is some contention as to how they form in experimental systems. The most widely accepted hypothesis is that the micronuggets are a "contaminant" and are not representative of a phase that was dissolved in the melt (Ertel et al., 1999, 2001, 2006, 2008; Fortenfant et al., 2003; Blaine et al. 2004, Brenan et al., 2005; Chapters 3-5 of this manuscript; among others). In this case, the melt can be analyzed by microanalytical techniques and the effect of micronuggets can be removed, as discussed below. Other researchers believe that these PGE nuggets are the result of quenching. These researchers believe the PGEs contained within the micronuggets were originally dissolved in the melt (Cottrell and Walker, 2006) and form on quenching of the experiment shown by textural observation of micronuggets in quenched glasses; in this case bulk-analytical techniques can/should be utilized to determine solubilities. These two conflicting techniques and interpretations provide very different estimates on PGE solubility with inclusion of the micronuggets adding significantly to the estimates on solubility. However, some distinction must be made between the two experimental techniques utilized; in the studies documented in Ertel et al. (2008), as well as Borisov and Palme (1994) using the stirred-crucible and wire-loop methods, respectively, very rapid quench is possible; in the studies

of Cottrell and Walker a piston cylinder apparatus is utilized which will have slower quench rates (> 1 min to cool to room temperature, Manning and Boettcher (1994)). Although the observed behaviours are the same (formation of micronuggets) the slight differences in technique may result in different mechanisms. Current experimental data cannot disprove or discount the formation of micronuggets on quench in the experiments of Cottrell and Walker (2006) and further studies are required, for all experimental techniques. For these reasons new techniques were utilized for the studies presented in this thesis and are discussed in their relevant chapters.

It is the author's belief that the micronuggets present in the experimental melts were not dissolved in the melt prior to quench (at least using wire-loop and stirred-crucible methods), are problematic in experimental systems, and wherever possible, care must be taken in the experimental design to minimize micronugget contamination. The presence of micronuggets precludes any bulk solution analytical methods, where the entire sample is dissolved and analyzed. When analyzed with bulk solution methods the presence of micronuggets results in an overestimation in solubility. Newer microanalytical techniques such as ion microprobe and laser ablation inductively coupled plasma have been used with success to determine inherent solubilities in analytical products by subtracting the influence of micronuggets which occur as high intensity, transient peaks in the signal (Chapters 3-5; Fortenfant et al., 2003; Blaine et al., 2004; Brenan et al., 2005). In most cases the micronugget signals using these methods are easy to observe as they are many times above background in signal intensity and can be removed from the integrated regions of the spectra.

Although inherent solubilities can be determined by microanalytical techniques it is best to eliminate the micronugget problem if possible and because of the presence of micronuggets in nature it would be very beneficial to understand their formation. It is the author's opinion that early studies had some problems which made micronugget formation unavoidable. The primary reason was in the design of the experiments which, generally began at oxidizing conditions (or with glasses synthesized at oxidizing conditions) which allowed large quantities (100's of ppm) of Pt and other PGEs to be dissolved in the melt. When experiments were then conducted at more reducing conditions, where solubilities were lower, equilibrium was always approached from oversaturation. Due to oversaturation the PGEs could not reside in the melt and could form small alloy- or pure-metal nuggets within the melt and due to their small size (and perhaps like charge) these nuggets could be remain suspended and not coalesce into large nuggets or be transferred to the crucible or wire-loop. This problem was the same for the stirred-crucible and the wire-loop methods as well as partitioning studies. It was also the nature of the studies (especially the stirred-crucible method) to begin at high oxygen fugacities (high PGE solubility) and systematically decrease oxygen fugacity (lower PGE

solubility). It is the author's opinion that at a certain point the PGEs would simply exsolve forming the micronuggets, and the bulk concentration in the melt would no longer vary with oxygen fugacity. This was the exact behavior observed (Borisov and Palme, 1997; Ertel et al., 1999) showing a flattening out of PGE solubility with fO_2 (with considerable scatter) and caused some researchers (Amosse et al., 1990) to suggest zero-valent solution of some PGEs, though with introduction of LA-ICPMS this idea was subsequently dismissed as it was clear that micronuggets contributed significantly to the apparent solubilities. The problem of determining PGE solubility for oversaturated conditions is addressed and summarized in Blaine et al. (2004) (Chapter 2) where similar problems were encountered and subsequently resolved.

Another problem suggested by Borisov and Palme (1997) is complexation of the PGEs with carbon species or formation of PGE-carbon species/colloids within the melt due to the presence of CO_2/CO mixtures used in the gas-mixing furnaces. This observation is qualitative and it may have been purely coincidental that the oxygen fugacities, below which there were micronugget problems, coincided with the switch to CO_2/CO gas mixtures. In the current study, experiments were designed to determine the effect of CO_2 on Pt solubility in a haplobasaltic melt (Chapter 4). The results and implications are discussed within Chapter 4. A second problem associated with the wire-loop method is the use of organic glue, which could also contribute to the micronugget problem which is also addressed in Chapter 4.

In the experiments of this study, micronuggets were prevalent in a number of experiments, especially those where Cl and CO_2 were components, which provide important insights into the nature of micronuggets and the systems in which they form. In these cases, the presence of micronuggets was beneficial and provided much information. The occurrence of micronuggets in these experiments is summarily explained in the discussion of each of the individual studies (Chapters 2-4). The implications to natural systems are also presented in these chapters.

1.3.3 Experimental studies on the solubility of PGEs in a volatile phase

Fluid-melt partitioning experiments in general are inherently quite difficult, require elaborate experimental set-ups in order to achieve reliable results and many of the current experimental techniques are problematic in key areas. Mafic systems are especially problematic where the low viscosity of the melt precludes the direct trapping of inclusions in a quenched glass which is a method available for use in felsic systems. It is also not possible to perform experiments in these systems, where the capsule is simply quenched and the free fluid removed because of the formation of quench products due to the reduced solubility of components within the fluid phase at room temperature.

Due to the use of platinum or noble metal capsules to contain the experiment, leaching of the capsule to dissolve quench products would also result in leaching of the capsule material giving non-representative results.

One method suitable for use in mafic systems is to determine partitioning calculated from the amount of an element lost from a melt to a known amount of fluid. However, the most suitable capsule material for these experiments is generally a PGE or PGE alloy due to their high melting temperature and workability. Determination of a PGE's solubility using these materials would be overly complicated by potential contamination from the capsule and alloy formation which would reduce the activity of the PGEs in the system. Another possibility would be Re but is too brittle for practical use. This mass-loss method, although unsuitable for PGEs, was used as part of this study to determine partitioning of other elements and is discussed further later in this paper.

The absolute best way to observe an element's solubility in a fluid at magmatic conditions is either to sample the fluid at T and P or to measure the solubility in situ at the magmatic T and P using advanced spectroscopic techniques. In situ measurement is only now becoming possible using diamond anvil cells and x-ray spectroscopy using synchrotron radiation, but in reality is still very limited and requires a very complex experimental set-up with only moderate controls on oxygen fugacity. Because direct sampling at magmatic temperatures and pressures is not possible, the second best means of observing the composition of magmatic fluids is to trap the fluid at the temperature and pressure of interest in a trapping medium.

The diamond-trap method (Kessel et al., 2004) allows sampling of fluid and quench products but is only a viable method under restricted temperature and oxygen fugacities within the stability field of diamonds. This technique is not viable at the high temperature, and moderately oxidizing conditions used for the study of PGE solubility in basaltic magmas.

Another trapping technique is the fractured-quartz method. In the fractured-quartz method, pre-fractured quartz crystals are used in the experiment and healing of the fractures during the experiment traps fluid inclusions which are analyzed at the conclusion of the experiment using a microanalytical technique such as laser ablation ICP-MS (e.g., Hanley et al. 2005, Hanley and Heinrich 2007; Pettke et al. 2002, Simon and Pettke 2009). Any constituents which were dissolved at experimental conditions and precipitated during quench are also contained within the inclusion and analyzed when the inclusion is ablated; therefore the analysis is representative of the fluid that was trapped. However, the major limitation of this method is there is no control on the time at which the fractures heal and trap inclusions allowing inclusions to be trapped at any time during the experiment,

even during the initial heating stages, thus fluids that are not in equilibrium are potentially trapped. Trapping of non-equilibrium fluids over arrange of conditions results in spurious data non-representative of the fluids at the conditions of interest (Hanley et al. 2005, Hanley and Heinrich, 2007; Pettke et al. 2002; Simon and Pettke, 2008). Secondly, this method is only possible using quartz-rich melt compositions and cannot be used to examine mafic systems where PGE occurrences are found.

A final method in use to determine the solubility of metals at high temperature is to extrapolate low-temperature thermodynamic data. This method was used extensively in the 1990s by authors such as Gammons and Bloom (1993), Gammons et al. (1992), Sassani and Shock (1990, 1998), Wood et al. (1994) and Gammons (1995, 1996) among others. Most of the data was determined from experiments that were performed at temperatures of less than 573K and were then extrapolated to magmatic temperatures. These extrapolations were very useful in demonstrating that, even at moderate hydrothermal temperatures, fluids have the potential to dissolve large amounts (ppm levels) of PGEs. These models indicate that significant Pt solubilities can occur in the presence of complexing ligands such as HS and Cl. In the case of Cl it was found that significant solubilities only occur at low pH and highly oxidizing conditions at low to moderate temperatures. It was suggested in these studies and by other researchers (Wood, 2002; Hanley, 2005) that Pt becomes a "harder" Lewis acid with increasing temperature and that Cl could become a major complexing agent at magmatic temperatures. The major shortcoming of these experiments was the inability to provide direct experimental evidence of PGE solubility at the temperatures of mafic magma and extrapolation to these temperatures can introduce large amounts of uncertainty. Xiong and Wood (2000) also show that there are significant problems with PGE-solubility data extrapolated to high temperature.

1.4 The role of volatiles in evolving magmatic systems

Volatiles are a very important component of all magmatic systems and control many of the properties of these systems. A few of the properties that the presence of volatiles can influence are the melting and crystallization temperatures, density, viscosity, phase relations, diffusivity, fragility and crystal habit (cf. Volatiles In Magma, Reviews in Mineralogy Vol. 30, MSA , 1994). Volatiles are present to some extent in all magmatic systems and through ascent (depressurization) and/or crystallization nearly all magmas reach volatile saturation at some point in their history, although it should be noted though that some volatile solubilities (i.e. Cl in some cases and S) can increase with decreasing pressure (Carroll and Webster, 1994; Mavrogenes and O'Neill, 1999). The nature of the exsolved volatile phase(s) is dependent on the composition of the dissolved volatiles and magma, but

is generally either an aqueous or carbon dioxide-rich volatile as the dominant phase (+\- other phases), a hydrosaline melt/brine or a sulphide melt. These exsolved volatile phases can be very important to ore deposit formation and modeling as they can provide a mechanism for enrichment and transport of metals.

Three volatiles were studied in this thesis; H_2O, Cl and CO_2. Methods were developed for each of the volatiles to determine the effects of each of the individual volatiles on PGE solubility. These are important volatiles to understanding PGE behavior and the following section will provide a brief summary about what is known about the behavior of each volatile and their effect on magmatic systems. Although the review below is somewhat outside of the scope of this thesis, understanding the effects of volatiles on melt properties and their incorporation into a silicate melt is necessary to fully understand the potential effects that volatiles can have on PGE behavior.

1.4.1 Water

Water is the most abundant volatile in magmatic systems and has the greatest influence on melt properties. Even at very low concentrations i.e., a few hundred ppm, water can have dramatic effects on the physiochemical aspects of a magma. Water can change the melting temperature, density, viscosity and its presence can affect the entire magmatic cycle (Lange, 1994). Water is important during the melting of source rock (i.e. water is a flux), the assimilation of country rock, and the rise of the magma to its eventual emplacement and/or extrusion. Water increases element diffusivity in a magma, causing increased crystal size and can also change the phase relations of a system, causing dramatic changes in the phases of a crystallizing or melting system. An important factor in water's dramatic effects is the low molecular weight of water resulting in a large mole fraction of water at even low water contents.

1.4.1.1 Solubility and speciation

The solubility of water is strongly dependant on the composition of the silicate melt (Holtz et al., 1992; 2000; Behrens et al., 2001; Behrens and Jantos, 2001; Benne and Behrens, 2003), however, when melt composition is expressed on an 8-oxygen basis, some broad similarities exist and water solubilities (on a mol/mol basis) are similar between different compositions (Burnham et al., 1994). The solution mechanism for water involves the incorporation of water into the silicate structure through the breaking of bridging oxygen (BO) bonds. As a result, there is an increased solubility of water in silicic magmas where there is a larger number of BO, as compared to mafic magmas which have a lower abundance of BO. Water solubility has a strong relation to the NBO/T (Non-bridging oxygen per tetrahedral unit) value of magma and generally increases with silica content although

there are other compositional factors that can affect water solubility among magmas with similar NBO/T values.

Water dissolves into magma in two forms, either as a charged OH-species or as molecular water (McMillan and Carroll, 1994). The amount of each can be observed using IR and NMR spectroscopy and it has been determined that the amounts of each are dependent on a number of factors. In early studies, the speciation of water was determined for melts using spectroscopy on quench glasses and only with the advent of diamond-anvil cells have in-situ, at-temperature spectroscopic measurements been made on melts (Shen and Keppler, 1995). These measurements are necessary due to the dependence of speciation on quench rate resulting in glasses that were not necessarily representative of the melt.

The assimilation of water into magmas will be explained in more detail in the following sections as the speciation and incorporation of water into magma has a dramatic effect on the viscosity of melts and is a direct result of the incorporation of water into the silicate structure.

1.4.1.2 Physical effects

1.4.1.2.1 Melting temperature

The addition of even small amounts (<1 wt. %) of water will decrease the melting temperature of a silicate minerals and this effect is observed to be the most dramatic in the most silica-rich (polymerized) systems. For example the anhydrous melting temperature of pure dry quartz is lowered by 500 K when a 0.5 GPa P_{H2O} is present (Mysen and Richet, 2005). In more depolymerized melts the effect is less profound although it is still significant as in the diopside-anorthite system where the anhydrous eutectic temperature is decreased by 64 K when 1 GPa P_{H2O} is present (Yoder, 1965). In a crystallizing system, the presence of water lowers the solidus temperatures and will result in lower crystallization temperatures.

1.4.1.2.2 Density

The density of magma can be estimated from the molar volume ($\overline{V}$) contributions of each component of the magma and their molar masses. Water has a light molar mass and has a large molar volume as compared to the major components of a silicate melt, ie. SiO_2, Al_2O_3, etc., and its presence will therefore decrease the density of the melt. Although it is possible to analyze a quenched silicate glass and determine some properties of the melt (e.g. solubility, speciation, etc.), a direct comparison between silicate glass and melt density is not possible. Glasses containing significant water require that the glasses are quenched from a melt at high pressures, which results in a compaction of the glass

and in different density values for glasses synthesized at different pressures. In order to compare these different glasses it is necessary to "relax" the glasses by heating them to under the glass transition temperature at atmospheric pressure. After this relaxation it is possible to analyze the glasses and calculate the density.

There has been some debate over the true molar volume values of H_2O in silicate glasses and melts. Ochs and Lange (1999) have determined that the molar volume in silicate glasses is constant and is independent of composition. This has been demonstrated in rhyolitic, andesitic and basaltic compositions. The calculated molar volume is found to be the same as the densest polymorph of ice (Ice VII) which has a value of 12.0 ± 0.5 cm^3/mol, translating to a density of 1.5g/cm^3. This value is also found to be independent of the speciation of water dissolved in the glass (OH^- or molecular H_2O) showing the volume change of reaction between these species to be zero in silicate glasses. Considering the relatively high density of this polymorph the change in density of a silicate glass with addition of water is less then would be initially predicted.

It has also been speculated that the molar volume of water in silicate melts is independent of composition (Ochs and Lange, 1999) who determined a molar volume of 22.9 ± 0.6 cm^3/mol with a partial molar thermal expansivity ($\overline{\alpha}$) of 9.5 ± 0.8 cm^3/mol per Kelvin and a molar thermal compressibility ($\overline{\beta}$) of -3.2 ± 0.6 x 10^{-4} cm^3/mol per bar for compositions ranging from NBO/T of 0 (rhyolite and albite) and an intermediate melt with an NBO/T of 1.9. Recently it has been speculated by other researchers (Mysen and Richet, 2005) that this is only valid in a narrow range of pressures and compositions. Isothermal compressibility (β) and the coefficient of thermal expansion (α) are important factors for the calculation of the density of a melt at high pressures and temperatures. These two factors are dependent on composition and therefore the model of Ochs and Lange (1999), must be used with some caution at high temperatures and pressures and with silicate compositions that are significantly different from those of the experiments.

1.4.1.2.3 Viscosity

The addition of water to a silicate melt dramatically lowers the viscosity of the melt and this effect is most profound for highly polymerized melts and low water contents (summarized in Chabiron et al., 2004). At low water contents, there is a very large effect with the addition of water and this effect decreases with increasing water content. In less polymerized melts the addition of water still decreases viscosity but the effects are less profound.

How water affects viscosity and the nature of the decreasing effect with increasing water content is still under debate. The decrease in viscosity is due to the incorporation of water into the silicate structure and there are various solution mechanisms that could result in this effect. At low water contents, water is dissolved primarily as OH^- groups with decreasing amounts of OH^- and increasing amounts of molecular H_2O at higher water contents (Chabiron et al. 2004). Degrees of polymerization for a silicate tetrahedron can be notated using Q^n notation where 'n' is equal to the number of bridging (Si-O-Si) bond in the tetrahedron and varies from zero (fully depolymerized) to four (fully polymerized). Zotov and Keppler (1998) demonstrated that the abundance of Q^4 species decreases with increasing water content and the abundance of Q^3 and Q^2 species increases through equations 1.8 through 1.10 which both cause depolymerization of the melt.

$$\mathbf{2Q^4 + H_2O \leftrightarrow Q^3(OH) + Q^3(H)} \qquad \textbf{Equation 1.8}$$

$$\mathbf{3Q^4 + 2H_2O \leftrightarrow Q^2(OH,H)_2 + 2Q^3(H,OH)} \qquad \textbf{Equation 1.9}$$

$$\mathbf{2Q^4 + 2H_2O \leftrightarrow 2Q^2(OH,H)_2} \qquad \textbf{Equation 1.10}$$

In the first reaction a bond between two Q^4 groups (Si and a bridging O) is broken and a water molecule gives up a hydrogen atom to balance the O and the remaining OH-group balances the Si resulting in two Q^3 groups with one NBO each. In the second reaction a Q^2 group forms in a similar way except that two bridging O bonds are broken in a single Q^4 group resulting in a Q^2 group with two NBOs. As well in this reaction two Q^3 groups can be formed (Equation 1.9) with water balancing the Si and O from the other two Q^4 groups as in the first reaction or a second Q^2 group can be formed (Equation 1.10). These reactions differ from those given in Mysen and Richet (2005) because the equations here are shown balanced. As well, Q^2 can form from reaction of water with Q^3 groups through Equation 1.11, and also causes depolymerization of the melt.

$$\mathbf{2Q^3 + H_2O \leftrightarrow Q^2(OH) + Q^2(H)} \qquad \textbf{Equation 1.11}$$

It has been observed that at low water contents the abundance of Q^3 groups increases with increasing water content but levels off at higher water contents (Zotov and Keppler, 1998). The abundance of Q^2 groups increases steadily with increasing water content although their abundance is much less than that of the Q^3 groups, so the Q^2 species do not affect viscosity as much as the Q^3. This decrease in formation of Q^3 groups may be attributed to Equation 1.12, where there is competition

between H- and the M- (network modifying cations, e.g. Na, K) ions at high water contents (Mysen and Richet, 2005).

$$M_2O + H_2O \leftrightarrow 2M(OH) \qquad \textbf{Equation 1.12}$$

This reaction would result in polymerization of the melt through formation of Q^4 groups and result in increased viscosity. This may be the cause of the lessening of the effect of water on viscosity at higher water contents and not the dissolution of OH groups changing to molecular water at higher water contents. This topic is still under debate as there is support for both sides and further spectroscopic studies will hopefully clarify this problem.

1.4.1.2.4 Diffusivity

The addition of water to a melt increases diffusivity in that melt. This is due to the relation between diffusivity and viscosity. According to the Eyring equation (Chakraborty, 1995; Mungall, 2002), an increase in the viscosity of a melt will decrease the diffusivity of a given species in the melt. This is important in silica-rich, highly polymerized systems with high water contents and results in increased crystal growth rates and fewer, larger crystals. The effect of volatiles on diffusivity will be limited to their effects on viscosity for the purposes of this chapter and the remainder of the thesis and will not deal with individual species. Therefore it is sufficient to say for the remainder of the chapter if a volatile increases viscosity it will decrease diffusivity and vice versa.

1.4.2 Carbon dioxide

Carbon dioxide is the second most abundant volatile in magmatic systems after water and also plays a major role in magmatic processes. The effects of carbon dioxide are generally less profound than water but it can still have a large effect on density, viscosity, phase relations and melting/crystallization temperatures. In many respects CO_2 influences melt properties in a manner quite different from that of water.

1.4.2.1 Solubility and speciation

Carbon dioxide solubility and speciation are interesting topics and have been the focus of several studies. Carbon dioxide dissolves into melts in two forms; as molecular CO_2 and as CO_3^{2-}. Many factors influence the solubility and speciation of CO_2 in a melt, but in general CO_2 solubility increases with increasing pressure and decreases with increasing temperature.

In mafic magmas, such as basalt (including mafic alkaline melts; basanite, leucitites and nephelinites) where the melt is highly depolymerized, CO_2 dissolves solely as the CO_3^{2-} species

(Lowenstern, 2000) and can reach solubilities of a few weight percent. In polymerized silicic magmas such as rhyolite, CO_2 dissolves solely as molecular CO_2 and has much lower solubilities typically less than 1 wt. % except at pressures greater than 3GPa. In intermediate compositions both molecular CO_2 and CO_3^{2-} species are found (King and Holloway, 2002). As well, the equilibrium reaction between molecular CO_2 and carbonate (Equation 1.13) shifts towards molecular CO_2 at higher temperatures indicating that molecular CO_2 contents can also become significant at higher temperatures in mafic, depolymerized melts (Nowak et al, 2004). The reason molecular CO_2 is not recognized to be substantial in mafic glasses is due to the low abundance at temperatures near the glass transition temperature. The solubility of CO_2 and the ratio of molecular CO_2 to CO_3^{2-} are strongly dependant on a number of factors, and this makes modeling of CO_2 dissolution difficult.

$$\mathbf{CO_{2(melt)} + O^{2-}_{(melt)} \leftrightarrow CO_3^{2-}_{(melt)}} \qquad \textbf{Equation 1.13}$$

The solubility/abundance of molecular CO_2 appears to be correlated with the ionic porosity of the magma, or in other words the amount of "open" space within the silicate melt structure (King and Holloway, 2002). This is understandable as CO_2 is a neutral molecule within the melt, is not incorporated into the melt and fills in the structural voids. Factors that increase the ionic porosity in the melt will increase the amount/solubility of molecular CO_2 (King and Holloway, 2002). Molecular CO_2 is unlikely to be found in melts with <~48% ionic porosity (King and Holloway, 2002). Aside from effects on ionic porosity there are only very weak associations of molecular CO_2 solubility and composition, i.e. $X_{(Si+Al)}$, X_{Ca} etc, with increasing solubility with an increase in Si+Al and decreasing solubility with increasing Ca (King and Holloway, 2002). Molecular CO_2 solubility is a near-linear function of the mole fraction of CO_2 in the fluid and therefore can be described as following Henrian behaviour, this remains true at low pressures but there is some deviation at higher pressures in rhyolites (Tamic et al. 2001) and possibly in intermediate compositions as well, as is suggested by King and Holloway (2002).

By contrast, CO_3^{2-} in the melt does not follow Henrian behaviour and its solubility is not a direct function of the mole fraction of CO_2, except at low pressures where Henrian behaviour was found in basalts (Dixon and Stolper, 1995).

1.4.2.2 Physical effects

The solution reaction of CO_2 in silicate melts through the formation of CO_3^{2-} complexes should cause polymerization of the melt, which should cause the opposite physical effects as water; i.e. increased melting temperature and increased viscosity. In reality though, much of the effects of

CO_2 on physical melt properties is analogous to that of water and is attributed to unidentified factors other than melt polymerization (Mysen and Richet, 2005).

1.4.2.2.1 Melting temperature

The effect of CO_2 on melting temperature of silicates minerals is dependent on the speciation of CO_2 in the melt. In melts where the dominant species is molecular CO_2 there is only a slight decrease in melting temperature with the addition of CO_2. An example of this is in the melting of albite; melting temperature (~1573K) is lowered by less than ten degrees with the addition of CO_2 at 2 GPa (Mysen and Richet, 2005). In case where the dominant species is carbonate there is a larger effect as in the case of the melting of diopside which shows a decrease in melting temperature of approximately 75 degrees at 2 GPa from ~1923K to 1848K (Mysen and Richet, 2005). The melting point depression in the presence of CO_2 is also positively correlated with pressure.

1.4.2.2.2 Density

Only one study examines the effect of CO_2 on melt density and that is by Bourgue and Richet (2001). In this study they determined the effect of CO_2 on a potassium-silicate melt ($KS_{1.3}$) and found that there was a linear decrease in melt density with increasing CO_2 content, with a constant molecular volume of CO_2 in the melt of 25.6 ± 0.8 cc/mol. It was also found that CO_2 does not affect the coefficient of thermal expansion (α) for this melt and that in the glass CO_2 was dissolved solely as carbonate, which was attributed to the formation of carbonate complexes with free potassium.

The effect of CO_2 on density should be dependent on the speciation of CO_2 in the melt. In the above mentioned case and in other melts where CO_2 is dissolved in the melt as carbonate which is incorporated into the melt structure, the effect should be a decrease in density with increasing CO_2 content due to the low mass and high molecular volume. In the case where CO_2 is dissolved into a melt as molecular CO_2 which occupies open space within the melt it would be logical that an increase in CO_2 content would cause an increase in density as long as the structure of the melt was not modified significantly by the CO_2 molecules. In silicic magmas, where molecular CO_2 is dominant, the solubility is very low and any change in density is likely to be insignificant.

1.4.2.2.3 Viscosity

The study by Bourgue and Richet (2001) also is the only study that studied the effect of CO_2 on melt viscosity. They observed that CO_2 affects viscosity in a manner similar to water and decreases viscosity substantially at low CO_2 concentrations and the effect decreases with increasing CO_2. It was also found that at higher temperatures there is a lessening of the effect of CO_2 on viscosity. Again it should be noted that in this case the CO_2 was dissolved as carbonate and this effect

would not be expected or may not have as dramatic of an effect in systems where molecular CO_2 is dominant.

1.4.3 Chlorine

The halogens, consisting of F, Cl, Br and I, form a minor but important group of volatiles. The most abundant volatiles in this group are F and Cl. Chlorine and fluorine behave very differently in magmas and their importance is different in different areas. Fluorine is an important volatile in the formation of pegmatites whereas Cl plays an important role in ore-forming systems (e.g. porphyry systems) where an exsolved aqueous phase with chlorine provides a very efficient way of concentrating and transporting metals.

1.4.3.1 Solubility and speciation

Chlorine dissolves into a silicate melt by associating with the network modifying M-cations in the melt (i.e. Na, K, Ca, etc.), and there is little to no Si-Cl or Al-Cl association (Sandland et al., 2004). The solubility of Cl is strongly dependant on pressure, temperature and composition of the silicate melt. Although many gasses/volatiles show a negative molar volume change upon dissolution, Cl shows a positive change and results in an increase in Cl solubility with decreasing pressure when the melt is saturated in a Cl-bearing vapour (Signorelli and Carroll, 2000) for compositions in the range of rhyolite to phonolite. However, Cl shows a more typical behaviour showing increased solubility with increased pressure when the melt is saturated in a brine (Webster, 2004; Aiuppa et al., 2009). Very limited data indicates that Cl shows a negative temperature correlation with increasing temperature resulting in a decrease in Cl solubility, for example there is a decrease from .05 – 0.04wt.% solubility with a temperature increase from 1473-1563K in a rhyolitic (liparite) system (Carroll and Webster, 1994).

Chlorine does not form bonds with Al and it follows that an increase in alumina content will decrease the Cl solubility in a silicate melt. This was demonstrated in phonolitic and rhyolitic systems. Signorelli and Carroll (2000) studied two phonolites; a peralkaline phonolite and a peraluminous phonolite and demonstrated that the solubility of Cl was significantly higher in the peralkaline compared to the peraluminous phonolite. In rhyolitic systems, Cl solubility increases from a metaluminous rhyolite to peralkaline rhyolites (Metric and Rutherford, 1992). It was also found that the Cl solubility in phonolites is roughly twice that as in rhyolites under similar conditions (Signorelli and Carroll, 2000). Chlorine has been found to preferentially associate with cations with higher ionization potentials and will associate with Ca over Na over K (Mysen and Richet, 2005).

A further complication of Cl solubility and speciation is its behaviour in silicate melt-H_2O-XCl systems (where X = mol fraction Cl). In these systems, an immiscible brine and aqueous fluid coexist at high Cl contents and low pressures. In supercritical systems where there is only one fluid the Cl content in the melt increases with increasing Cl content in the fluid. In subcritical systems with both a saline brine and an aqueous fluid present there is a maximum Cl content in the melt and the Cl content does not increase above this point with increasing Cl content. At high pressures (200 and 250 MPa) under supercritical, one fluid conditions, there is a smooth increase in Cl content in the melt. At lower subcritical pressures there is a definite maximum Cl content in the melt at which the brine and fluid become immiscible leading to invariant Cl concentrations in the melt (Signorelli and Carroll, 2000; Webster et al., 2002).

In silicate melt-H_2O-XCl systems there is also an interaction between Cl and H_2O at high Cl and/or H_2O contents. It has been found (Webster et al. 1999, Stelling et al., 2008) that at high water contents an increase in water content will decrease the solubility of Cl in a silicate melt and at high Cl contents an increase in Cl content decreases H_2O solubility.

1.4.3.2 Physical effects

Compared to water and carbon dioxide, the incorporation of Cl has a small effect on the physical properties of silicate melts although its effects are not trivial. Because Cl forms bonds solely with the M-cations in a melt it removes these cations from their network-modifying positions and results in polymerization of the silicate melt. This polymerization results in an increase in viscosity (decrease in diffusivity) with increasing Cl content. This polymerizing effect also has the effect of increasing the liquidus and solidus temperatures of complex silicate melts but in simple silicate melts such as albite it can decrease solidus temperatures by up to 200K at pressures of several hundred MPa (Wyllie and Tuttle, 1964).

1.5 The potential role of volatiles in magmatic PGE ore-forming systems and the necessity for investigation

In a recent paper, Naldrett et al. (2009), it was implicitly stated that in order for the proposed model for the formation of the Merensky Reef of the Bushveld complex to be valid, the solubilities of the PGE in the silicate phase must be orders of magnitude higher than experimentally determined solubilities for dry diopside-anorthite systems. This statement emphasizes the need for more relevant experimental data for the assessment of models of PGE deposit formation; as mentioned above, by far

the bulk of PGE-bearing experimental studies have investigated dry, diopside-anorthite systems or more felsic fluid-melt systems; these studies are not directly applicable to natural ore-forming systems in reef hosted PGE deposits. The sparseness of data for hydrous systems is due in part to the difficulty in the experiments themselves and also to the need to use simplified systems to aid in interpretation.

The parental magmas of the PGE-bearing layered Stillwater and Bushveld complexes are believed to be relatively volatile rich and have contained approximately 1% water (Boudreau and McCallum 1992, Boudreau, 2008 ; Meurer et al., 1999), Cl (Willmore et al., 2000; Meurer et. al, 1999) and CO_2 (Mathez et al., 1988). Some potential effects of these volatiles are hypothesized in these studies, although the effects of these volatiles on PGE behaviour in both a magmatic-hydrothermal fluid and the silicate melt are poorly understood. These studies interpret that the primary effect of fluids is as a transport medium for the PGEs upon late-stage exsolution from the silicate melt. However, there are two main stages that volatiles could play a role in metal concentration and transport, during the initial volatile-bearing melt stage and at a later stage when the magma reaches volatile saturation. The purpose of this study is to assess the effect and potential role of volatiles throughout these two stages using a diopside-anorthite eutectic silicate melt analog.

Due to the effect of volatiles on the physiochemical parameters noted above it is foreseeable that volatiles could affect the solubility of metals such as the PGE in melts through affecting the physical properties of the melt or by complexing of the metal within the melt. All the volatiles investigated in this study and discussed above form charged species within the melt OH^-, CO_3^{2-} and Cl^- and have the potential to complex metals within a silicate melt. The complexing of metals by ligands within a silicate melt had not been demonstrated and was believed not to occur until recently where it was demonstrated by Farges et al. (200), where MoS_x complexes are present in a silicate melt. As well, Botcharnikov et al. (2010) determined that Au shows evidence of complexing with Cl and a S species in a silicate melt, causing increased Au solubility. These are the first documented cases of complexing by ligands in a silicate melt causing increased metal solubility. In this study the effect of H_2O and mixed H_2O-Cl and H_2O-CO_2 fluids on the solubility of Pt and Ir are determined to assess the potential for these volatiles to complex PGEs as well as determine the solubilities of these metals in volatile bearing silicate melts to further assess the ore deposit models. The details of these experiments and interpretations are found in Chapters 2 through 5 and are summarized in Chapter 7 of this document.

In order to assess the role of late-stage magmatic hydrothermal fluids in enriching and transporting the PGEs, a new experimental technique was developed and was applied to the diopside-anorthite-H_2O system. The details of the experimental design and results are presented in Chapter 6.

Chapter 2 - Platinum solubility in a haplobasaltic melt at 1250°C and 0.2 GPa: The effect of water content and oxygen fugacity (Blaine et al., 2005)

2.1 Introduction

The Platinum group elements (PGE), Pt, Rh, Pd, Ir, Os, Ru, along with Au and Re are classified as the highly siderophile elements. In the past few years there has been increased interest in the high temperature geochemistry and behaviour of PGEs due to their importance to ore deposits and the understanding of early Earth formation and core segregation.

The highly-siderophile nature of PGEs makes them ideal candidates for studying the segregation of the Earth's iron-rich core from the silica-rich mantle. In order to fully understand this process, the partitioning of PGE between metal and silicate phases must be determined. To date, two approaches have been used: 1) direct experimental determination of partition coefficients between coexisting iron-rich metal and silicate phases (e.g., Ballhaus et al., 1994; Ballhaus and Ulmer, 1995) and 2) determination of solubilities in the silicate phase and subsequent calculation of metal/silicate partition coefficients (e.g., Ertel et al. 1999). There are several problems with the first method. Very low PGE concentrations in the silicate phase makes analysis difficult and incomplete separation of the iron-rich metal and silicate portions can cause higher apparent solubilities in the analyzed silicate phase. The second method is simpler because the PGE concentrations in the silicate phase are a result of saturation of the melt with respect to the PGE of interest instead of a Fe-PGE alloy (Ertel et al. 1999).

Current estimates of PGE partitioning cannot explain the apparently elevated levels of PGEs in the mantle. Although the PGE abundances can be explained with the late veneer model (O'Neill et al., 1995) and using this model the abundances do not rely solely on PGE partitioning, there is still some controversy as to how metal-silicate partition coefficients depend on temperature, pressure, and sulfur and oxygen fugacity. However, there has been very little investigation into the effect of volatiles on PGE solubility at elevated pressures.

The economic interest in PGEs has increased over the past few years and hence research into the formation of PGE deposits has grown accordingly. In order to create a robust model to explain the formation of PGE deposits, reliable estimates of PGE solubilities in silicate melts must be available at conditions relevant to the formation of the deposit. PGE behaviour in basaltic magmas has been examined from two perspectives, from direct observation of natural systems and using an experimental approach. There is an extensive body of literature on PGE ore deposits but there have been few experimental studies and PGE behaviour is not well constrained at low oxygen fugacities (Borisov and Palme, 1997; Ertel et al., 1998, 1999; Fleet et al., 1999a,b; Amosse et al., 2000; Fortenfant et al., 2002). Most natural basaltic systems have oxygen fugacities lower than those represented by previous studies, and more data is required at the oxygen fugacities representative of natural systems. Also, the majority of the previous experimental studies have investigated PGE behaviour at 101 kPa and in dry systems. Natural systems contain volatiles and the incorporation of volatiles, such as water, in silicate melts is strongly dependent on pressure; therefore experiments at atmospheric pressure are insufficient to understand PGE solubilities in natural melts.

Water is the most important volatile in magmatic systems, is present to some extent in all natural silicate melts and can have various effects on melt properties. Boudreau et al., (1988) and Boudreau (2002) concluded that the parental basaltic magmas associated with large PGE deposits, such as the Bushveld and Stillwater, had significant water contents (up to 1 wt. %). It has also been proposed that water was present during core formation and that the Earth accreted wet (Righter and Drake, 1997, 1999). Modeling of these systems relies on estimates of PGE solubility. Considering that water has the potential to change Pt solubility and therefore change partitioning behaviour, it is necessary to determine the effect of water, if any, on PGE behaviour in silicate melts.

In this study we performed experiments at elevated pressure to clarify the role of water on Pt solubility in a haplobasaltic melt, which can be considered as a simple analog to natural basaltic systems.

2.2 Experimental methods

Our experiments were conducted through hydration of a synthetic silicate glass at high pressure and temperature and equilibrating the resulting hydrous melt with the platinum capsule holding the experimental charge. This technique allows saturation of the silicate melt in platinum at the conditions of interest (P, T and water activity (a_{H_2O})).

It is a common practice to synthesize starting glasses from oxides and carbonates in platinum crucibles at 101 kPa. Due to the high oxygen fugacities present in normal furnaces, large amounts of platinum can be dissolved into such starting glasses (Borisov and Palme, 1997; Ertel et al., 1999). For example, Farges et al. (1999) found that up to 200 ppm platinum can be dissolved in calcium aluminosilicate glasses prepared using platinum crucibles at atmospheric pressure and oxygen fugacity (f_{O_2}). It is very difficult in studies of PGE solubility to reach equilibrium from high degrees of oversaturation, i.e., utilizing a starting glass with Pt concentrations orders of magnitude greater than the solubility at the experimental conditions. In the initial experiments of this study it was found that anomalously high platinum contents were present in end-product glasses after normal experimental durations when using starting glasses synthesized in platinum crucibles. Ertel et al. (1999) also observed non equilibrium conditions i.e., decreases in Pt concentrations with time, using the stirred crucible technique after >800 hours of run duration using glasses with higher starting Pt concentrations. In order to minimize the run times needed to reach equilibrium at low Pt solubilities (low oxygen fugacities) it was necessary to synthesize a relatively platinum-free starting glass. The procedure for glass synthesis in this study differs from standard methods of synthesizing glasses in the use of alumina instead of platinum crucibles.

Starting glasses with a diopside-anorthite dry eutectic composition ($An_{42}Di_{58}$) were prepared from reagent grade component oxides and carbonates. Prior to use, the components were dried for a minimum of twelve hours to remove water; MgO and Al_2O_3 were dried at 1073K and $CaCO_3$ and SiO_2 were dried at 473K in 1 atm furnaces and were stored in a desiccator. The individual components were then weighed and sintered at 1273K overnight in a covered alumina crucible, to remove CO_2 from the carbonate components. This material was placed in a new alumina crucible, covered with an alumina plate, and placed in a preheated oven at 1473K. Temperature was then increased rapidly (600K/hour) to 1773K. This temperature regimen was used to prevent the formation of thermal cracks in the crucible. The melt was left for approximately twenty minutes at this temperature. The crucible was then quickly removed from the oven and placed in water resulting in rapid quenching of the glass. The glass was then removed from the crucible, ground to a fine powder in an agate mortar, re-melted using the same process and quenched again to increase homogeneity.

Glasses were analyzed for major element composition using a Cameca SX-100 electron microprobe, with a 15keV accelerating voltage, a 6 nA beam current and a 10 μm beam. Transects were performed to check for glass homogeneity. The average glass composition obtained, of seven experiments analyzed (H_2O-2 through H_2O-8), in weight percent normalized to 100% is:

50.39(0.37)% SiO_2, 15.98(.25)% Al_2O_3, 24.03(.38)% CaO and 9.56(.21)% MgO, 1σ standard deviations of all microprobe analyses are given in brackets. This composition is close to the diopside-anorthite dry eutectic composition used in previous studies (e.g. Borisov and Palme, 1997; Ertel et al., 1998, 1999). Starting glasses were also analyzed by ID-MC-ICPMS (explained in detail in Section 3.2) to determine platinum concentrations. The starting glass used in this study contained 50.3 ppb Pt. Although the glasses did not come in direct contact with Pt, the starting oxides and carbonates might have contained trace amounts of platinum. Platinum crucibles are also used regularly in the furnaces where the starting glass was synthesized and thus Pt-bearing aerosol particles may have caused the contamination. Only one sample of the starting glass was analyzed and therefore the starting Pt concentration may vary slightly between runs.

After synthesis starting glasses were ground in an agate mortar and pestle to a grain size of <200μm. Experimental charges consisting of ~300 mg of haplobasaltic glass and varying amounts of distilled water were loaded into platinum tubes (2.5cm L x 4mm o.d./3.6mm i.d.). After the sample was loaded into the capsule and weighed the open end of the capsule was crimped. The capsule was then dipped in liquid nitrogen to minimize loss of water and sealed by welding. It was then allowed to reach room temperature and reweighed to ensure that there was no loss of water during the welding. Water was added such that the resulting glasses and melts contain between 1 and ~ 5 wt. % (saturation; Berndt et. al, 2002). Two experiments (H_2O-7 and H_2O-10) had small amounts (< 0.5 wt. %) of excess water, otherwise the experiments were conducted at water undersaturated conditions.

The platinum capsules were composed of pure platinum and therefore any effect of alloys can be dismissed and the activity of platinum is assumed to have been unity, at the P-T-X conditions of the experiment. Experiments were conducted at 1523 K ± 10 K and 200 MPa + 0.4/ -0.02 MPa. Temperature was controlled using two S-type thermocouples and was monitored with the use of two additional S-type thermocouples. Run durations ranged from 21 to 68.8 hours. The oxygen fugacity of the experiments is imposed by the intrinsic hydrogen fugacity of the autoclave. The intrinsic f_{H_2} is well characterized through multiple experiments at different temperatures and the corresponding f_{O_2} falls on the MnO-Mn_3O_4 buffer curve at water-saturated conditions (Berndt et al., 2002). More details of this are outlined in Section 4. At the conditions of the experiment, 1523K, 200 MPa and water saturated conditions, f_{O_2} = $10^{-3.6}$ bar, calculated from O'Neill et al. (1993).

All experiments were conducted in vertically mounted internally heated pressure vessels (IHPVs) equipped with a rapid quench device. This method allows the melt to be quenched to a

crystal and bubble-free glass at a cooling rate of >200K/min (Berndt et al., 2002). After quenching, the samples were removed from the sample holder and weighed to ensure there had been no loss of water during the experiment.

The experimental glasses were removed from the capsule and broken into 3-4 large pieces for various analyses. No visible Pt contamination was noted on the exterior of the glass samples, but steps were taken (see below) to ensure there was no surface contamination. All end-product glasses were clear with no noticeable coloration or crystallization. Results for individual runs are summarized in Table 2.1.

Table 2.1 - Summary of run conditions and analysis of run product glasses

Sample Name	Length of Experiment (hours)	Water Content wt.% (Added)	Water Content wt. % (KFT)	Platinum Concentration (melt) (ppb) +/- 5% error	log $fO_{2(exp)}$
H_2O-1	66.5	1.92	1.87 +/- 0.02	36.0	-4.7
H_2O-2	48	1.94	1.86 +/- 0.03	34.0	-4.7
H_2O-3	21	1.94	1.85 +/- 0.03	51.5	-4.7
H_2O-4	48	0.95	0.86 +/- 0.04	17.3	-5.8
H_2O-5	48	2.88	[1]2.51 +/- 0.05	75.6	-4.3
H_2O-6	48	3.75	[1]3.40 +/- 0.04	94.0	-4.0
H_2O-7	48	4.71	[1]4.39 +/- 0.05	133	-3.7
H_2O-8	48	2.91	[1]2.71 +/- 0.05	82.9	-4.2
H_2O-10	68.8	4.77	[1]4.20 +/- 0.05	114	-3.8

[1] possible incomplete collection of water during KFT analysis

2.3 Analytical techniques

2.3.1 Analysis of Water Content

2.3.1.1 Fourier Transform Infrared Spectroscopy (FTIR)

Pieces of run-product glasses were prepared as 500µm thick doubly-polished sections for Fourier transform infrared spectroscopy (FTIR). Near-infrared spectra with a resolution of 4 cm^{-1} were collected using a BRUKER IFS 88 spectrometer with an IR-Scope II microscope, using a tungsten light source, a CaF_2 beam splitter, and an MCT narrow range detector. A slit aperture of ~150 µm x 150 µm was used and multiple measurements were made on the same polished section. The peak heights near 4500 cm^{-1} and 5200 cm^{-1} were compared to determine if the distribution of

water was homogeneous throughout the sample. From the time series experiments, used to determine minimum time for equilibrium (discussed in Section 4.1), two pieces of the run-product glass were analyzed (~2mm x 2mm), one from the top and one from the bottom of the capsule; for other experiments, one piece of glass was analyzed. In all experiments the water was distributed evenly, even after the shortest run duration. Peak heights of a given sample were identical within error of the measurement which is introduced by instabilities in the baseline, which varied by up to .003 absorbance units. This results in an estimated maximum variation in absolute water content of 0.2 wt. % for a given experiment. Absorption coefficients of glasses are strongly dependant on composition (e.g., Ohlhorst et al. 2001) and the lack of absorption coefficients for Di-An glasses precluded an exact calculation of water contents from FTIR spectra.

2.3.1.2 Karl Fischer Titration (KFT)

End product glasses were analyzed for total water content using Karl Fischer titration (KFT) (cf. Behrens et al., 1996 for details on the method). Glasses with greater than 3 wt. % water degassed violently, even with slow heating, which may have lead to in incomplete collection of the water and consequently underestimation of water content. However, the amount of underestimation is not likely to be large because the KFT measured water contents agreed well with those calculated from the amount of water added to the capsule. This also indicates that the capsules remained sealed throughout the experiment. The values for water content obtained by KFT were used for the redox calculations below. The error in analysis is given in Table 1 and was used for calculating corresponding errors in oxygen fugacity.

2.3.2 Pt Analysis

Platinum was analyzed in experimental glasses by isotope-dilution multi-collector inductively coupled mass spectroscopy (ID-MC-ICPMS). Contamination of the samples with capsule material was a large concern and care was taken to minimize this problem. Due to the small absolute amounts of platinum dissolved in the glasses any contamination by capsule material would be noticed immediately due to very high apparent concentrations. Glasses were removed from the capsule and thoroughly cleaned in multiple stages. A large piece(s) of the glass of approximately 100 mg was placed in a Teflon Savillex bomb. To clean the sample 1ml dilute (1:20) HF was added and the sample was placed in an ultrasonic bath for one minute. This was to loosen any platinum metal that may have been attached to the surface without leaching Pt from the sample. The samples and containers were then rinsed thoroughly with high purity water. Water was then added to the container and it was again placed in an ultrasonic bath for five minutes. The water was then discarded and the sample was allowed to dry overnight.

After cleaning, the samples were crushed to a fine powder using an agate mortar and pestle. The samples were then weighed placed in a clean Savillex bomb and spiked with a ^{198}Pt-enriched platinum solution. The samples and spike were then digested using 0.5 ml concentrated HF + 0.5 ml concentrated HCl + 0.5 ml concentrated HNO_3. All acids used were suitable for trace analysis; HCl and HNO_3 were distilled and HF was doubly distilled. The containers were sealed and placed on a hot plate at 393K for 24 hours. After one hour the samples were removed from the hotplate and placed in an ultrasonic bath for five minutes before being returned to the hotplate. After 24 hours of digestion the containers were uncovered, put back on the hot plate and the acids were allowed to evaporate. After the samples were thoroughly dried, 0.5ml of concentrated HNO_3 was added to the sample and allowed to evaporate on the hot plate. A further 0.2ml concentrated HNO_3 was added and again allowed to evaporate. The final stage of the digestion process was the addition of 2ml of 0.8N HNO_3 saturated with Br_2. The Savillex bombs were then sealed tightly and placed again on the hotplate overnight. This final step ensured that the platinum present was in the highest valence state which was required for subsequent column separation.

Bio-Rad AG 1X8 resin (200-400 mesh) was prepared the day before column separation by adding of 0.8N HNO_3 saturated with Br_2. Resin was added to the column and two 1ml aliquots of 0.8N HNO_3 saturated with Br_2 were added and allowed to pass through the column. The samples were then loaded onto the column and again two 1ml aliquots of 0.8N HNO_3 saturated with Br_2 were added. The resin was then cleaned by adding 5ml 10N HNO_3 to the column. After the resin was cleaned, 10ml of 14N HNO_3 was added to the column, eluting the Pt, and the solution was collected. Samples were evaporated and then stored until analysis.

Analysis was done using either the multicollector ICP-MS at the University of Muenster, a Micromass Isoprobe, or a NU Instruments MC-ICP-MS at the MPI for Geochemistry in Mainz. All wet chemistry was performed at the MPI in Mainz.

2.4 Results

2.4.1 Attainment of Equilibrium

Attainment of equilibrium was determined through time series experiments. The duration after which there was no subsequent change in concentration with time was considered to be the minimum time needed to reach equilibrium. Equilibrium of the systems was determined through leveling off of concentrations over time to a constant value (Figure 2.1).

The time series experiments contained 2 wt. % H_2O and equilibrium was approached from oversaturation. The majority of experiments (excluding one at 1 wt. % H_2O) were conducted with greater water contents and equilibrium was approached from undersaturation. Water decreases the viscosity of the melt and, as shown by the Eyring equation (Chakraborty, 1995), element diffusivity increases with decreasing viscosity. Therefore, it can be assumed that equilibration times are shorter for experiments with greater water contents. Equilibrium was reached between 24 and 48 hrs of run duration (Figure 2.1). Consequently, all subsequent experiments had run times of 48 hrs or longer. Concentrations from experiments with durations less than 48 hours were not used for calculations as they were not representative of equilibrium condidtions.

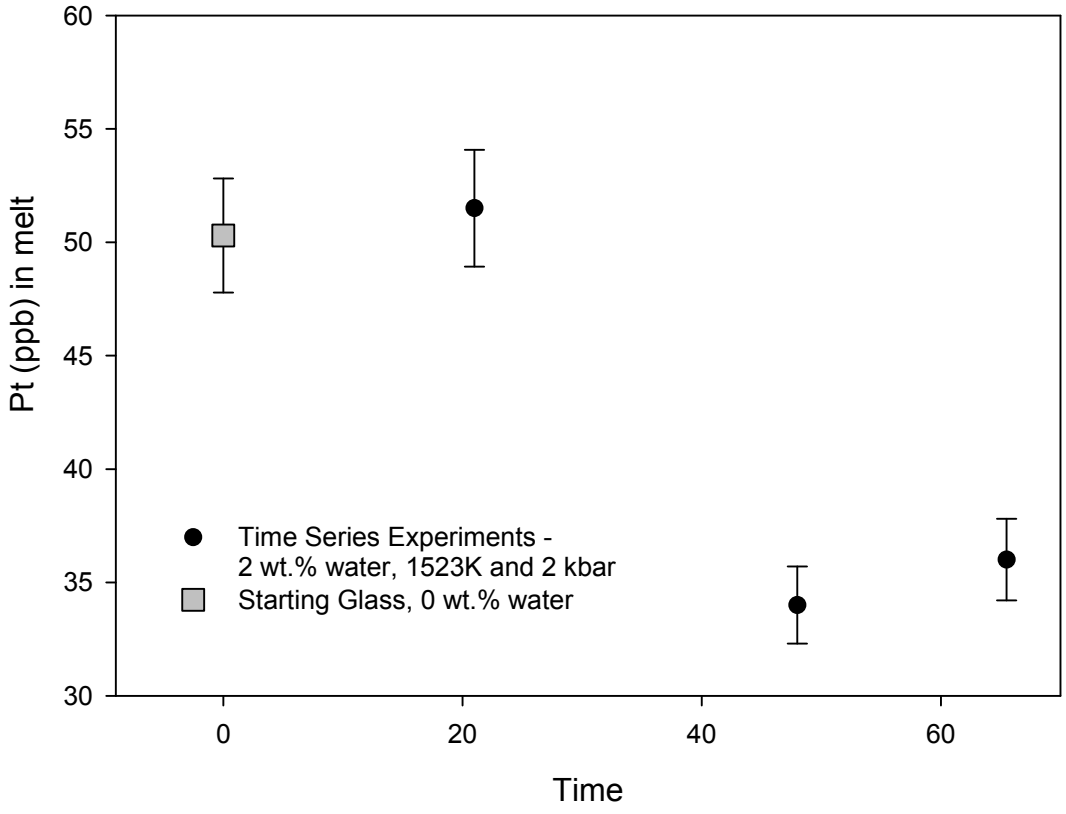

Figure 2.1 - Platinum concentration versus time in time series experiments. Leveling off of concentrations to a constant value (within error) after 48 hours indicates equilibrium was reached between 24 and 48 hours run duration. Error bars represent an estimated 5% analytical error in Pt analysis.

2.4.2 Effect of Water

It is clear that platinum solubility increases with increasing water content of the melt (Figure 2.2). However, water content was not the only variable since the water activity influences the prevailing f_{O_2}, which is controlled by the dissociation reaction of water:

$$H_2O \Leftrightarrow H_2 + \frac{1}{2}O_2 \qquad \textbf{Equation 2.1}$$

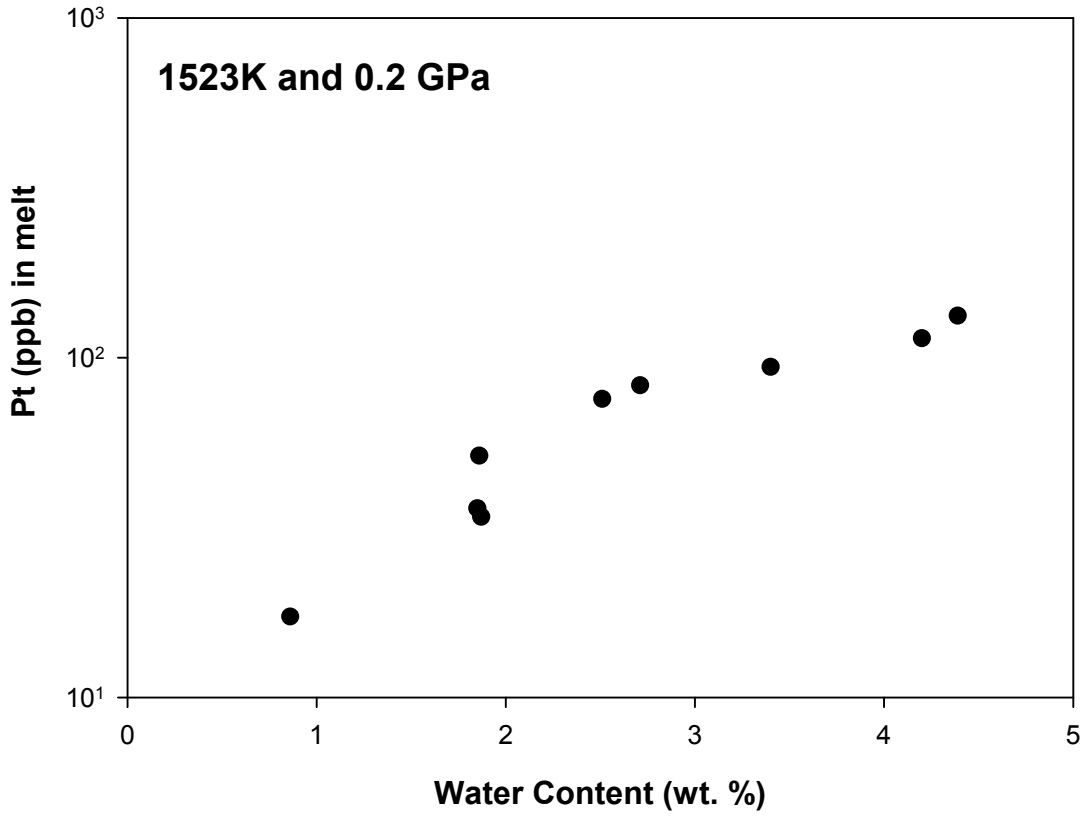

Figure 2.2 - Platinum concentrations versus water contents in the melt showing an increase in platinum solubility with an increase in water content from 1 wt. % to saturation. Error bars, representing an estimated 5% analytical error in Pt content and error in water content given in Table 1, are smaller than the symbol size.

The platinum capsule is permeable to hydrogen and therefore the hydrogen fugacity in the experimental charge is controlled by the intrinsic f_{H_2} of the autoclave. This f_{H_2} is well characterized and was identical in all experiments, as discussed in Section 2.2. Increasing the water content in the melt increases the activity of water in the melt and therefore increases the oxygen fugacity of the experiment. Water activities in the experimental charges were calculated from the water content of the melt using Equation 2.2 from Burnham (1994):

$$\alpha H_2O = k\left(\mathrm{X}_{H_2O(melt)}\right)^2 \text{ at } \mathrm{X}_{H_2O(melt)} < 0.5 \qquad \textbf{Equation 2.2}$$

From the water activities, the oxygen fugacity of the experiments can be calculated using Equation 2.3 (modified from Whitney, 1972):

$$f_{O_2(\exp)} = f_{O_2(water-saturated)} + 2a_{H_2O(\exp)} \qquad \textbf{Equation 2.3}$$

Figure 3 shows that there is a linear dependence between log platinum solubility and log f_{O_2}. Since there is a linear trend between platinum solubility and oxygen fugacity it suggests that the solubility mechanism for Pt is an oxidation reaction such as that given in Equation 2.4.

$$Pt^0{}_{(s)} + xO_2 \Leftrightarrow PtO_{2x} \qquad \textbf{Equation 2.4}$$

The dominant valence of platinum can also be estimated from the slope of the solubility versus oxygen fugacity trend from Equation 2.5, where b is a constant and the valence of Pt is equal to 4x:

$$\log[Pt] = x \log f_{O_2} + b \qquad \textbf{Equation 2.5}$$

The log Pt solubility vs. log oxygen fugacity trend follows closely to an ideal slope of ½ as shown on Figure 2.3. Therefore, over the conditions studied, platinum is dissolved in the melt primarily in the 2+ valence state. At the redox conditions of this study the predicted valency of platinum from dry studies (Borisov and Palme, 1997; Ertel et al., 1999; Fortenfant et al., 2002) is also 2+. Since there is no deviation in the slope of Pt solubility versus oxygen fugacity from ½, with varying water content, it can be concluded that water has no intrinsic effect on Pt solubility. This conclusion is further supported through comparison to dry systems, discussed below.

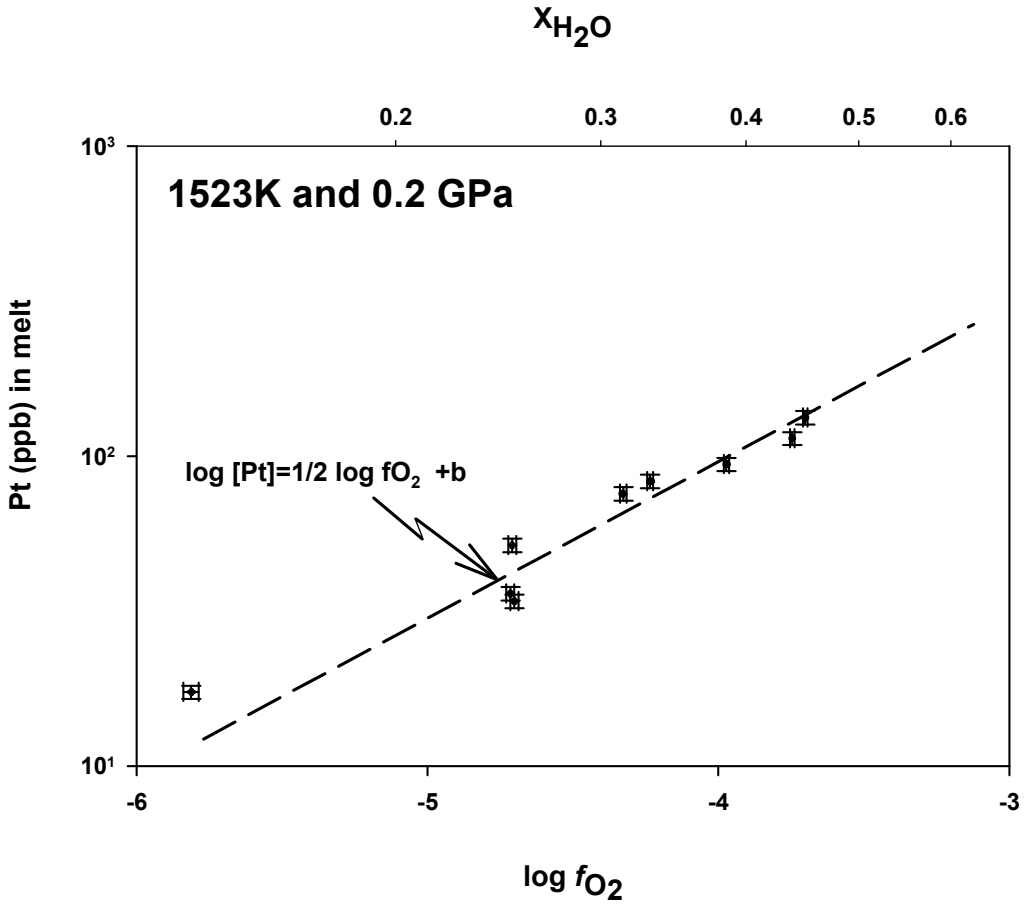

Figure 2.3 - Platinum concentration in a haplobasaltic melt versus calculated f_{O_2} and corresponding $X_{H_2O(melt)}$ calculated from Burnham, 1994. The trend is linear and has a slope near to 1/2 indicating platinum is dissolved in the melt primarily in the 2+ valence state. Error bars correspond to an estimated 5% error in Pt, errors in f_{O_2} are calculated from the errors in water content given in Table 1.

2.5 Discussion

2.5.1 The effect of water

We are aware of only two studies that have examined the effect of water on platinum solubility, namely Bezmen et al. (1998), and Ertel et al. (1998). The study of Ertel et al. (1998) is the only one to report a systematic data set allowing estimation of the effect of water on platinum solubility. Bezmen et al. (1998) reported only "spasmodic increases" in platinum solubility with increasing water contents and predicted increasing platinum solubility with decreasing oxygen fugacity.

Ertel et al. (1998) studied the effect of water and f_{O_2} on platinum solubility in a Di-An eutectic melt at 1573K and 200 MPa using a sealed capsule technique in an IHPV nearly identical to that used in this study. The main difference between the study of Ertel et al. (1998) and the present study is in the method of starting glass preparation, discussed below. Ertel et al. (1998) observed a small influence of f_{O_2}, and a negative influence of water content, on platinum solubility. By contrast we have shown that f_{O_2} is the controlling factor on platinum solubility and that the only role of water is to change f_{O_2}. It should also be noted that the observed platinum concentrations of Ertel et al. (1998) were at ppm levels, whereas those of this study are at ppb levels.

Ertel et al. (1998) used run durations of 12h, which were demonstrated in our study to be insufficient to ensure equilibrium even from low starting Pt concentrations. Moreover without the use of alumina crucibles for glass preparation the initial Pt concentrations were likely at the ppm-level.

We believe that Ertel et al. (1998) observed a kinetic effect resulting from the addition of varying amounts of water. Increasing the water content will decrease the viscosity of the melt, and will therefore decrease the amount of time needed for the system to reach equilibrium. If experimental charges did not reach equilibrium and all experiments had the same run durations, those experiments with greater water contents would be closer to equilibrium. If the starting glasses used were oversaturated with respect to platinum, as was the case in preliminary experiments of this study, the experiments with higher water contents would have had lower platinum concentrations due solely to being closer to equilibrium. This could produce the interpreted trend of decreasing Pt "solubility" with increasing water content observed by Ertel et al. (1998) but the Pt concentrations would not be representative of equilibrium conditions.

It was found in anhydrous studies using the stirred crucible (Ertel et al., 1999) and wire-loop techniques (Borisov and Palme, 1997) that micronugget formation, explained in detail below, was a problem at low oxygen fugacities and that platinum solubilities could not be determined at oxygen fugacities less than $f_{O_2} = 10^{-3.5}$ bar, Figure 2.4. The oxygen fugacities of this study cover a range of oxygen fugacities down to a f_{O_2} value of $10^{-5.8}$ bar, which is much lower than was possible for Pt solubility studies in dry systems. The data of this study thus cannot be compared directly to those of the dry studies. However, the solubility trend observed in this study, extrapolated to higher oxygen fugacities, overlaps that of the dry studies (Figure2. 4). The anhydrous melt compositions of this and the previous studies are nearly identical and the effects of slightly different temperatures among the

studies (most of the data within 50 K) will be small compared to the effects of oxygen fugacity. Therefore, the overlap of anhydrous and hydrous data sets further indicates that water has no intrinsic control on platinum solubility in a haplobasaltic melt and that the observed trends are due solely to varying oxygen fugacities. This conclusion is in agreement with Righter et al. (1999), who found that water had no effect on metal-silicate melt partitioning for the less siderophile elements Ni, Co, Mo and W for water contents of up to 4 wt. %.

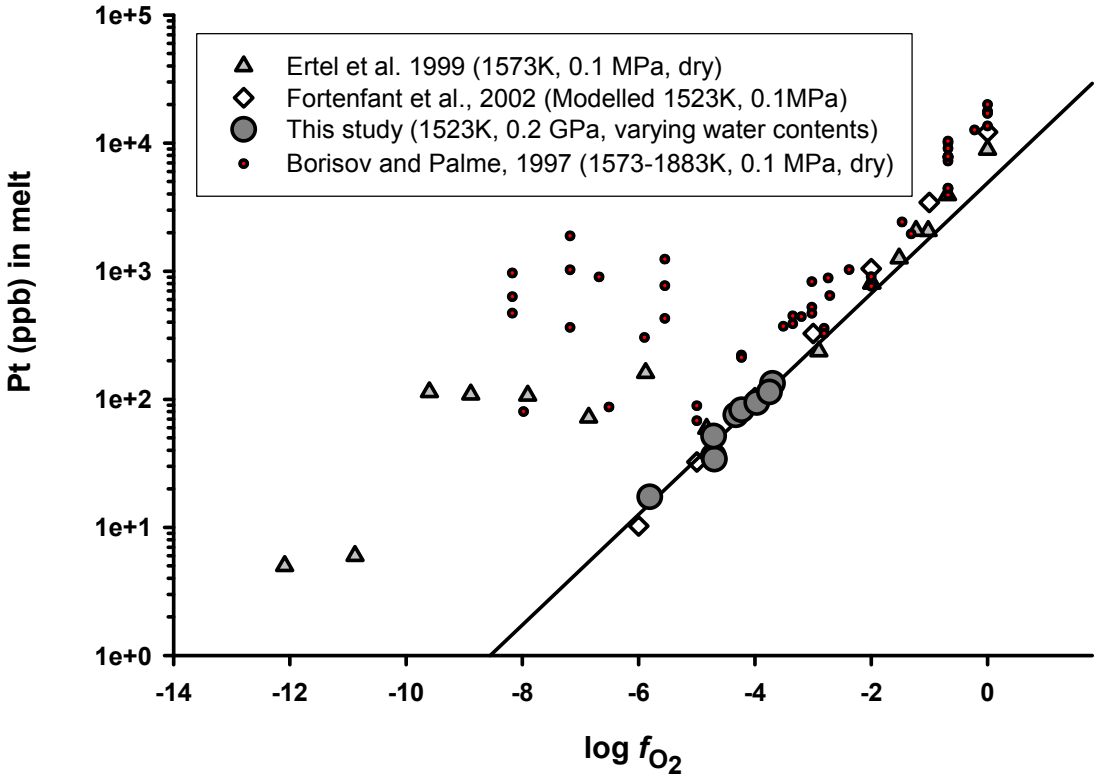

Figure 2.4 - Combined data of this study (hydrous) and previous studies (anhydrous). The linear trend is calculated from the data of this study and when extrapolated fits well with those of the dry studies. This indicates water content has no intrinsic effect on platinum solubility. Deviation from the linear trend at low oxygen fugacity in anhydrous studies is due to micronugget contamination, which was not evident in this study. Error bars are smaller than the symbol size for this study and are not given for the previous studies.

2.5.2 Eliminating the Micronugget Effect: An Extension of Previous Studies

A problem with many experiments on PGE behaviour is the formation of "micronuggets" which are sub-microscopic, high concentration inhomogeneities in glasses. The exact nature of the micronuggets is unknown and is not clear how they form. Ertel et al. (1999, 2001) and Borisov and

Palme (2000) observed that micronuggets form at low oxygen fugacities, in experiments at conditions of low PGE solubility. The presence of micronuggets results in an overestimation of Pt solubility.

Many experiments on PGE solubility begin at a high oxygen fugacity (high concentration) and the oxygen fugacity is progressively lowered e.g., the stirred crucible technique explained and used in Ertel et al. (1999). In experiments such as these, there is a minimum oxygen fugacity and in turn, a minimum concentration at which the solubilities of certain PGEs (e.g. Pt, Ir) appear to level out, when PGEs are analyzed by bulk methods. Any further reduction in oxygen fugacity results in PGE concentrations that produce a level, although scattered trend with no discernable trend of solubility versus oxygen fugacity. Prior to the discovery of the micronugget effect, it was proposed that at these oxygen fugacities it was possible to have PGEs dissolved in a zero valence state (Borisov and Palme, 1997; Ertel et al., 1999). Some researchers also proposed an increase in solubility with decreasing oxygen fugacity, which would suggest a negative valence state for platinum at low f_{O_2} conditions (Amosse et al., 2000).

A solution to the micronugget problem was to introduce microanalytical techniques such as LA-ICPMS to analyze the glasses for PGEs (e.g. Ertel et al., 1999; 2001). Using these techniques it was possible in some instances to essentially subtract the influence of micronuggets to obtain the "background" concentrations in the glasses. Although in these cases it was still not possible to measure platinum solubility without micronuggets at low oxygen fugacities (less than $f_{O_2} = 10^{-3.0}$ bar).

In this study, the final Pt concentrations in the glasses were all reached from a low starting Pt concentration in the glass, allowing the determination of Pt solubilities down to more reduced conditions ($f_{O_2} = 10^{-5.8}$ bar) without evidence of micronugget formation. This suggests that the formation of micronuggets is not dependant on oxygen fugacity, but rather is a limitation of the experimental method.

2.6 The effect of oxygen fugacity on Pt solubility

The results of this study indicate that, within error, Pt is dissolved solely in the 2+ valence state under the f_{O_2} conditions of this study. Furthermore, there is no evidence of a change of valence of platinum to a 0-valence state or a solubility minimum for platinum as suggested by previous studies (Borisov and Palme, 1997; Ertel et al., 1999; Amosse et al, 2000). A linear fit of the data combined from this and previous studies produces a slope of .48 (Equation 2.6) and has an R- squared

value = .992, giving an effective valence of Pt of 1.92 indicating that throughout the entire f_{O_2} range studied, platinum is, within error, entirely in the 2+ valence state.

$$\log[Pt] = m \times \log f_{O_2} + b \qquad \textbf{Equation 2.6}$$

In order to evaluate the possibility of a minor amount of Pt in the 4+ valence state at high f_{O_2}, as suggested by Ertel et al. (1999), the influence of platinum in both the 2+ and 4+ valence states was determined by using a non-linear regression of the solubility data with f_{O_2} (Equation 2.7), summarized in Figure 2.5. The equation form is taken from Ertel et al. (1999) and is a common form used in platinum solubility studies. Determined equilibrium solubilities in this study were combined with those of the higher f_{O_2} data set of Ertel et al. (1999). This allowed regression over a larger range of f_{O_2}, from pure oxygen to 10^{-5} bar. The resulting fit is given below (Equation 2.7), with 1σ errors given in square brackets:

$$[Pt]_{total(ppb)} = 1389[377] \times f_{O_2} + 7531[326] \times f_{O_2}^{\frac{1}{2}} \qquad R^2 = .997 \qquad \textbf{Equation 2.7}$$

This is of the form:

$$[Pt]_{total} = [Pt^{4+}] + [Pt^{2+}] \qquad \textbf{Equation 2.8}$$

Using this equation at very oxidizing conditions (pure O_2), the amounts of Pt at saturation, in the 2+ and 4+ valence states, respectively is 7531 and 1389 ppb. This results in a ratio of 2+/4+ of 5.42. However at conditions relevant to PGE ore deposit formation, FMQ-2 (Ballhaus and Sylvester, 2000) (f_{O_2} = 10^{-10} bar @1573K, 200 MPa, calculated from Schwab and Kuenstner, 1982), the amounts in the 2+ and 4+ valencies are 0.12 ppb and 3.7×10^{-7} ppb, respectively, giving a 2+/4+ ratio of 3.3×10^{5}.

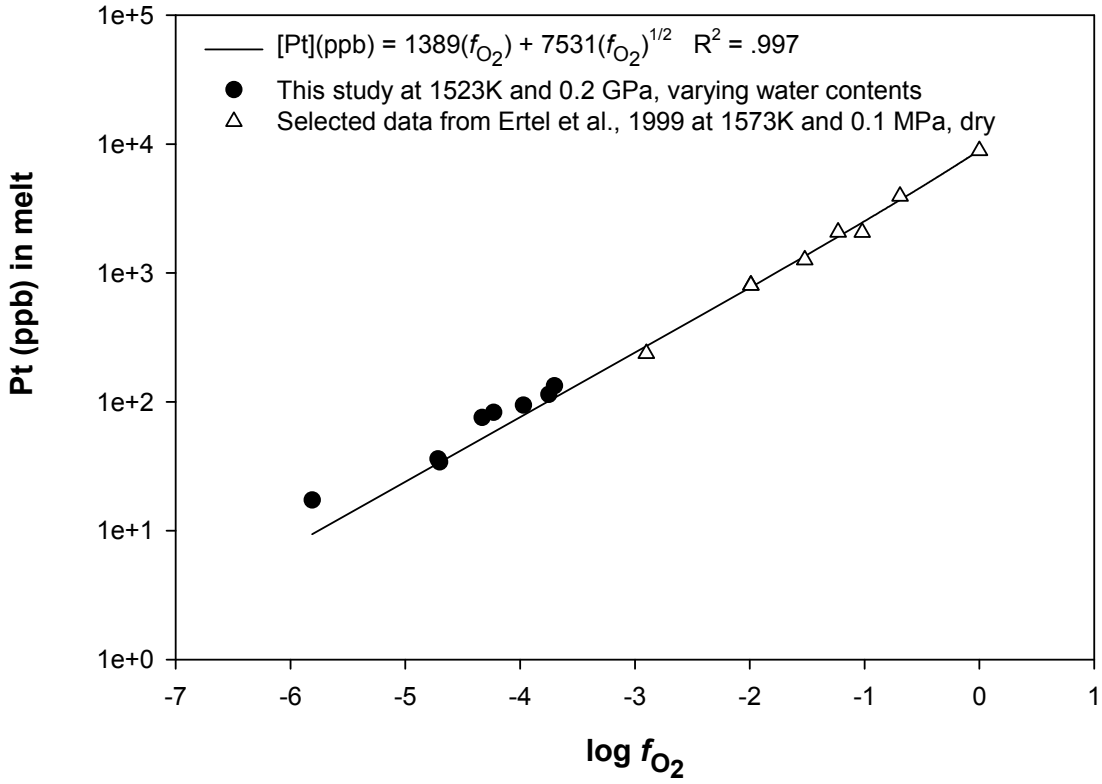

Figure 2.5 - Non-linear regression plot of the data of this study combined with selected data of Ertel et al. (1999). High f_{O_2} data that showed no influence of micronugget contamination was selected from Ertel et al. (1999) for the regression. Error bars are smaller than the symbol size and are not given for the previous studies.

It remains for interpretation whether the deviation from ideal slope of ½ is a result of the influence of Pt dissolved in the 4+ valence state or if it is just an experimental or analytical relic. However at geological conditions the proportion of Pt dissolved in the 4+ valence state will be negligible.

Previous studies into platinum solubility were conducted at 101 kPa. The experiments in this study were conducted at elevated pressure in order to dissolve substantial amounts of water into the melt and are therefore also more representative of natural systems. There is a slight possibility that any effect water has on platinum solubility is cancelled out by an equal and opposite effect of pressure, though this is highly unlikely. The effect of pressure on platinum solubility is assumed to be minimal at the 200 MPa pressures used in this study.

2.7 Conclusions

This study used a sealed capsule technique combined with rapid quench as an effective means for determining the effect of water on metal solubility in a silicate melt at high temperature, and at a pressure analogous to natural systems. There was no evidence of micronugget formation using this technique and platinum solubilities were determined at oxygen fugacities lower than previously possible.

The extrapolation of the platinum solubility versus oxygen fugacity trend obtained in this study overlaps with data obtained for anhydrous systems. This indicates that for the conditions studied the dominant control on platinum solubility is oxygen fugacity and its solubility is not directly affected by water content. Thus, platinum solubility is not affected by water with water contents up to saturation of a haplobasaltic silicate melt, if f_{O_2} is constant. Water content can affect oxygen fugacity by changing the water activity in a system. This change in oxygen fugacity in turn will change the solubility of platinum.

At lower oxygen fugacities platinum continues to be dissolved into a silicate melt predominantly in the 2+ valence state (at oxygen fugacities at least as low as 10^{-5} bar). There is no indication of a change in valence of platinum to zero-valency, dissolution of metallic platinum, at low oxygen fugacities.

2.8 Addendum – Bezmen et al. (2008): Conflicting results

After the publication of Blaine et al. (2005) a study was presented by Bezmen et al. (2008) that showed conflicting results to those presented here. Although they did not challenge the data of this study (discussed below), their interpretation conflicts with data that has been obtained in subsequent experiments in the overall study detailed in this thesis (i.e. Chapter 6). As it applies directly to the topic discussed in this chapter, discussion of these results will be included here.

Bezmen et al. (2008) studied Pt solubility in a hydrous $Di_{55}An_{35}Ab_{10}$ synthetic melt at 1473 K and 0.2 GPa in the presence of a free fluid (H_2O) phase, using an internally heated vertical gas pressure vessel without the ability for rapid quench. Similar to this study they used noble metal capsule for the source of PGE; however, they implemented a double capsule technique for control of oxygen fugacity. Over the oxygen fugacity range from Hematite-Magnetite through Wüstite-Iron the solubilities that they determined were orders of magnitude higher than that found in this study and studies of Borisov and Palme (1997), Ertel et al. (1999) and Fortenfant et al. (2003).

Comparing the data of Blaine et al. (2005) and Bezmen et al. (2008); Bezmen et al. (2008) states that the increase in Pt solubility is due to the presence of a free fluid-phase in the experiments of Bezmen et al. (2008). Bezmen et al. (2008), also states that at fluid undersaturated conditions (such as those in Blaine et al., 2005) the melt behaves as an anhydrous melt, thus explaining the lack of effect of H_2O on Pt solubility observed by Blaine et al. (2005). Some fundamental flaws are present in the study of Bezmen et al. 2008. The most evident flaw is that they use a bulk analytical technique (Neutron Activation analysis, NA) for the analysis of Pt and to this author's opinion they fail to demonstrate that micronuggets are not present and do not influence the concentrations measured. Bezman et al. 2008, utilized XPR (X-ray Para-magnetic Resonance) spectroscopy to conclude that there was no metallic Pt present in the glasses however did not take into account possible differences in XPR spectra for crystalline versus non-crystalline Pt metal, possible presence of colloidal Pt or other possible phases that could form Pt-micronuggets. There was no demonstration to this author's opinion that these glasses were micronugget-free (in the sense that micronuggets are high concentration anomalies that are not representative of Pt dissolved in the melt at experimental conditions and not the strict "metallic" Pt micronuggets of Bezmen et al. 2008) and that the Pt measured within the glasses was representative of true solubilities at experimental run conditions. Laser-ablation ICPMS of the experimental run products of Bezmen et al. (2008) would provide undisputable or at least widely accepted evidence that the observed concentrations represented solubilities under the experimental conditions; however, Bezmen et al. (2008) failed to do this. It has been demonstrated throughout this thesis study (in Chapters 3, 4, 5 and 6) that Pt (and Ir) solubility does not vary with the presence or absence of a free fluid phase (H_2O, Chapter 6; H_2O-Cl, Chapters 3 and 4; or H_2O-CO_2, Chapter 5) at constant oxygen fugacity, under equivalent conditions to Blaine et al. (2005). The results and interpretation of Bezmen et al. (2008) cannot therefore be accepted at face value without further consideration.

2.9 Addendum II – Ertel et al. (2006): Effect of pressure on Pt solubility

In the current study it was demonstrated that the Pt solubility data obtained for a hydrous diopside-anorthite melt observed at 0.2 GPa was consistent, within error and at the same oxygen fugacity, with the data of the same melt composition under anhydrous conditions and 1 atm (Borisov and Palme, 1995; Ertel et al. 1999, Fortenfant et al. 2003). Based on the data of Holzheid et al. (2000) it was assumed that pressure had negligible effect and the two data sets could be compared directly. The data of this study was therefore interpreted to indicate that H_2O had negligible effect on Pt solubility.

A subsequent study by Ertel et al. (2006) indicates that at increased pressure there is an effect of pressure on Pt solubility in an anhydrous diopside anorthite melt. Ertel et al. (2006) indicate increasing Pt solubility in the silicate melt with increasing pressure from 1 atm to 0.5 GPa to 14 GPa; showing an approximate 3 order of magnitude increase in Pt solubility in the silicate melt at 14 GPa versus 1 atm data. If a linear behaviour is adopted for the effect of pressure on Pt solubility, this may suggest that there should be a slight increase in Pt solubility at the experimental pressures used in this study. However, the data of this study does not indicate this at the low comparative pressure (0.2 GPA) of this study, barring the unlikely scenario that the presence of water decreases solubility by the same amount that pressure increases it, and furthermore this decrease shows no variation with water content. However, it is noted that although at the pressures of this study the effect of pressure appears negligible it is not implied that pressure does not have an effect at higher pressures, as investigated by Ertel et al. (2006). At the low relative pressures of this study, it is held that the interpretations of the data in this study are correct.

Chapter 3 - The effect of Cl on Pt solubility in haplobasaltic melt: Implications for micronugget formation and evidence for fluid transport of PGEs

3.1 Introduction

For a number of years a correlation between Cl and Pt has been noted in the world's largest platinum deposits, namely the Bushveld and Stillwater deposits of South Africa and Montana, as well as the Great Dyke in Zimbabwe. At these deposits, anomalously high Cl contents have been inferred from the presence of Cl-rich apatites (Boudreau and McCallum 1992, Willmore et al. 2000, 2002 and Mathez and Webster 2005) which suggests that a Cl-rich volatile phase was present during the crystallization of the intrusion. Brine fluid inclusions have also been observed at these deposits, e.g. Ballhaus and Stumpfl (1986), Hanley et al. (2008). At the Bushveld deposit the Cl contents in the apatites drop sharply above the Merensky Reef (the dominant PGE-rich horizon) and above this horizon the apatite compositions are increasingly more F-rich. The exact cause or implications of this correlation has remained enigmatic, although it has been suggested that it represents a late stage exsolution of a Cl-rich volatile phase which migrated upwards, transporting and/or remobilizing PGEs and depositing them at the ore horizons in these layered intrusions (Boudreau et al., 1986, 1999).

Chlorine isotope studies (Willmore et al., 2002) suggest that this Cl was introduced with the parental magmas at Bushveld and was not introduced during the later stages or from an outside source. In order to explain the role of Cl in the parental magmas and its close spatial association with PGE deposition and enrichment, the influence of Cl on the behavior of PGEs needs to be determined. It is generally recognized that under specific conditions, high temperature aqueous fluids have the capacity to transport PGEs (e.g. Wood, 1987; Mountain and Wood, 1988; Ballhaus et. al. 1994; Sassani and Shock, 1998; Gammons, 1995; 1996; Xiong and Wood, 2000; Hanley et al. 2005; Simon and Pettke, 2009), and Cl-bearing aqueous fluids have been proposed as potential enrichment and transport mechanism for PGE (Wood, 1987; Ballhaus and Stumpfl, 1986; Boudreau and Meurer 1999, Hanley et al., 2005). However, it is not certain whether the volume proportion of these fluids (aqueous fluid to melt ratio) is significant, i.e., that fluid transport is an important ore-forming

process. In order to assess whether the volume proportions are significant, reliable fluid-melt partitioning estimates are needed. To do this there are two areas that need to be addressed experimentally; assess the solubility of Pt in a Cl-bearing aqueous fluid at magmatic conditions and assess the effect of Cl on the solubility of Pt in the silicate melt, i.e., does Pt-Cl complexing occur in a silicate melt.

It has been recently shown that sulphur can complex metals in silicate melts, in the case of Mo complexes (Farges et al., 2006) and both sulphur and chlorine in the case of Au (Botcharnikov et al., 2010). Chlorine complexing in silicate melts could allow for increased Pt solubility in the silicate melt and influence validity of ore deposit models for the PGEs. Previously Blaine et al. (2005) demonstrated that water has no effect on Pt solubility at fixed f_{O_2}, thus there is no evidence to support complexing of Pt with water (or OH^-). In the current study the role of Cl on Pt solubility in hydrous synthetic basaltic melt is determined to establish whether or not Cl can increase a magmas capacity to carry Pt.

3.2 Experimental methods

Platinum solubility was determined in a Cl-bearing, hydrous, Fe-free basalt at high pressure and high temperature. Experiments were conducted in an internally-heated pressure vessel and the sample container (sealed noble metal capsule) was used as the source of the noble metal for the equilibration between Pt and melt. For the majority of the experiments the capsules used were pure platinum but a series of experiments were run using $Pt_{80}Ir_{20}$ alloy capsules. The use of a Pt-Ir alloy for the capsule material allows determination of the solubilities of both Pt and Ir during the same experiment, although only the results for Pt are addressed in this paper. Where Pt-Ir alloys were used an activity correction was applied to correct for the reduced activity of Pt in the experiment and is outlined below.

Experimental charges were prepared by sealing approximately 300mg of glass with a composition corresponding to that of the 1 atmosphere eutectic point of the dry diopside-anorthite system ($An_{42}Di_{58}$). The glass was powdered to a grain size of <200μm and varying amounts of distilled water (from approximately 3mg to 14mg, corresponding to 1 - 4.5 wt. % water) were added into Pt or Pt-Ir capsules (25mm length x 4mm outer diameter/3.6mm inner diameter), along with a source of chlorine. In most experiments chlorine was added as a solid $MgCl_2$ and $CaCl_2$ mixture with an Mg:Ca ratio equivalent to that of the starting glass. In early experiments chlorine was added as $MgCl_2$ and $CaCl_2$ in solution, but this resulted in inhomogeneous Cl distribution throughout the

capsule with a concentration gradient over the length of the capsule, likely due to low total volatile contents, and only the results for the experiment Cl-1 are included in this study. This inhomogeneity in Cl distribution was eliminated in experiments using solid salts. The salts were mixed with the haplobasaltic glasses prior to loading into the capsules in approximately 1 g batches to obtain Cl contents between 1 and ~3 wt. %, mixed thoroughly, and were stored in a drying oven at 373K prior to loading.

In experiments using capsules composed of pure platinum, the activity of platinum is assumed to have been unity at the P-T-X conditions of the experiments. For experiments using $Pt_{80}Ir_{20}$ alloy capsules, Pt activities were taken from Tripathi and Chandrasekharaiah (1983), where Pt activity in a $Pt_{80}Ir_{20}$ alloy at temperatures of 1383K, 1468K and 1573K is 0.80. To determine absolute solubilities (activity = 1), concentrations in the resultant experimental glasses was divided by the corresponding activities. The effect of pressure on metal activities was assumed to be negligible.

Experiments were conducted at 1523 K ± 10 K and 200 MPa + 0.4/ -0.02 MPa. Temperature was controlled using two S-type thermocouples and was monitored with the use of two additional S-type thermocouples. In a previous study on the investigation of the effect of water on Pt solubility in a synthetic basalt at the same P-T conditions, Blaine et al. (2005) performed time series experiments and demonstrated that equilibrium between the Pt capsule and melt is reached between 48 and 65.5 hours (same melt composition and amount of added glass as in this study). Following this earlier work experiments were initially run using similar durations. However, in the Cl-bearing experiments significant Pt heterogeneity was evident (in the form of micronuggets) which required longer run durations to dissipate. Details of this behaviour are outlined below.

All experiments were conducted at the Institut für Mineralogie at the Leibniz University of Hannover, Germany, in a vertically mounted, internally-heated pressure vessel equipped with a rapid quench device. This apparatus allows the melt to be quenched to a crystal- and bubble-free glass at a cooling rate of >200 K/min (Berndt et al., 2002). The oxygen fugacity of the experiments is imposed by the intrinsic hydrogen fugacity of the autoclave. The intrinsic f_{H_2} is well characterized through multiple experiments at different temperatures and the corresponding f_{O_2} falls on the $MnO\text{-}Mn_3O_4$ buffer curve at water-saturated conditions (Berndt et al., 2002). At the conditions of the experiments, 1523 K, 200 MPa and water-saturated conditions the f_{O_2} calculated from O'Neill and Pownceby (1993) is $10^{-3.6}$ bar.

After quenching, the samples were removed from the sample holder and weighed to ensure there had been no loss of water during the experiment. The experimental glasses were removed from

the capsule and broken into 3–4 large pieces for various analyses. No visible Pt contamination was noted on the exterior of the glass samples, but steps were taken (see below) to ensure there was no surface contamination when using bulk solution methods for Pt analysis. All end-product glasses were clear with no noticeable coloration or crystallization. Electron microprobe analysis (EMPA) of polished sections of the quenched products (glasses) showed homogeneous distribution of chlorine after 68 hours or more using solid Cl-salts as the source for Cl. Results for individual runs are summarized in Table 3.1.

3.3 Analytical techniques

3.3.1 Microprobe – Major elements and chlorine

The major element compositions of the glasses were determined using either a Cameca SX-100 electron microprobe at the University of Hannover or a Cameca SX-50 at the University of Toronto, with a 15 keV accelerating voltage, a 4-6 nA beam current, and a 10 μm defocused beam. Transects were performed to check for glass homogeneity and consisted of a minimum of ten analyses. In all glasses there was no indication of glass heterogeneity and composition varied only slightly between experiments due to the small differences in the amount of salt added. Average run product normalized to anhydrous, Cl-free glass compositions (in wt %) are CaO = 23.50 (0.38), MgO = 9.99 (0.28), Al_2O_3 = 16.75 (0.70), and SiO_2 = 49.75 (0.41), with 1σ standard deviations given in brackets. Results for individual runs are shown below in table 3.2, indicating only minor variation in Ca and Mg with increasing Cl content.

Table 3.1- Summary of experimental conditions and glass analysis

Sample Name	Capsule material	Experiment Duration (h)	$Cl_{(melt)}$ (Wt.%)$_c$	$H_2O_{(melt)}$ (Wt. %)$_{(f)}$	Log Oxygen Fugacity (bars)	$Pt_{(melt)}$ (LA) (ppb)$_{c,d}$ Activity corrected solubility	$Pt_{(melt)}$ (ID) (ppb) Activity corrected solubility
Short run duration experiments not used in interpretation as discussed in text							
Cl-1	Pt	65.5	0.56 (.03)	1.24(.12)$_{(a)}$	-5.33	22 (6)	22
PtIr-10*	$Pt_{80}Ir_{20}$	68	2.75 (.09)	2.03(.07)$_{(b)}$	-4.82	118 (14)	1612
PtIr-11	$Pt_{80}Ir_{20}$	68	2.25 (.06)	2.25(.06)$_{(b)}$	-4.65	19379 (2162)	7304
Cl-4	Pt	74	0.92 (.06)	1.54(.15)$_{(a)}$	-5.05	71 (30)	18419$_e$
Cl-5	Pt	74	2.00 (.06)	2.14(.21)$_{(a)}$	-4.70	976 (54)	1375
Cl-6	Pt	74	2.53 (.09)	1.01(.10)$_{(a)}$	-5.81	229 (47)	1543
PtIr-7	$Pt_{80}Ir_{20}$	92.8	2.12 (.07)	1.60(.05)$_{(b)}$	-5.10	294 (48)	310
PtIr-8	$Pt_{80}Ir_{20}$	92.8	1.79 (.05)	3.59(.08)$_{(b)}$	-4.04	3155 (430)	13422
PtIr-9	$Pt_{80}Ir_{20}$	92.8	1.85 (.06)	2.96(.09)$_{(b)}$	-4.27	8600 (2649)	7311
Longer run duration experiments used for interpretation as discussed in text							
PtIr-13	$Pt_{80}Ir_{20}$	96	0.89 (.02)	3.63(.10)$_{(b)}$	-3.97	80 (27)	332
PtIr-14	$Pt_{80}Ir_{20}$	96	0.69 (.05)	4.4(.10)$_{(b)}$	-3.75	134 (22)	322
PtIr-15	$Pt_{80}Ir_{20}$	96.1	0.68 (.06)	2.12(.09)$_{(b)}$	-4.60	45 (9)	298
PtIr-16	$Pt_{80}Ir_{20}$	96.1	2.52 (.08)	3.83(.08)$_{(b)}$	-4.02	171 (32)	39063$_e$
PtIr-17*	$Pt_{80}Ir_{20}$	96.1	1.90 (.07)	4.38(.08)$_{(b)}$	-3.83	122 (13)	45
Cl-9	Pt	122.8	0.17 (.03)	1.45(.14)$_{(a)}$	-5.07	13 (3)	na
Cl-11	Pt	130	0.84 (.06)	2.20(.22)$_{(a)}$	-4.56	18 (5)	na
Cl-12	Pt	130	1.51 (.03)	2.29(.23)$_{(a)}$	-4.58	40 (16)	157
Cl-13	Pt	130	2.04 (.05)	2.41(.24)$_{(a)}$	-4.54	18 (6)	54
Cl-7	Pt	144	0.80 (.04)	1.56(.16)$_{(a)}$	-5.02	17 (1)	135
Cl-8	Pt	144	1.49 (.02)	1.39(.14)$_{(a)}$	-5.25	21 (2)	401

Pt(LA) – Pt concentration as determined by laser-ablation ICP-MS
Pt(ID) – Pt concentration as determined by bulk solution isotope dilution ICP-MS
a – determined by mass difference (EMPA)
b – determined by KFT
c – 1 σ errors given in brackets
d – Calculated from 195-Pt signal
e – likely contamination of ID analysis
f – errors given in brackets
*** - Saturated in a volatile phase as evidenced by hissing on opening of capsule**
na – not analyzed

Table 3.2- Summary of microprobe analyses

Sample Name	CaO	MgO	SiO_2	Al_2O_3	Cl
PtIr-7	23.10(0.11)	10.15(0.11)	48.67(0.18)	15.97(0.18)	2.12(0.07)
PtIr-8	23.27(0.15)	10.05(0.16)	48.85(0.24)	16.03(0.20)	1.79(0.05)
PtIr-9	23.17(0.21)	9.99(0.43)	48.92(0.29)	16.06(0.18)	1.85(0.06)
PtIr-11	22.93(0.19)	10.17(0.17)	48.51(0.18)	16.14(0.11)	2.25(0.06)
PtIr-12	22.88(0.14)	10.05(0.12)	50.32(0.25)	16.73(0.19)	0.02(0.01)
PtIr-13	22.95(0.19)	9.99(0.17)	49.72(0.17)	16.45(0.16)	0.89(0.02)
PtIr-14	22.93(0.28)	10.11(0.18)	49.66(0.20)	16.61(0.33)	0.69(0.05)
PtIr-15	22.91(0.25)	10.15(0.14)	49.73(0.26)	16.54(0.14)	0.68(0.06)
PtIr-16	23.15(0.18)	10.02(0.17)	48.27(0.19)	16.04(0.13)	2.52(0.08)
PtIr-17	23.20(0.18)	10.00(0.11)	48.82(0.22)	16.07(0.11)	1.90(0.07)
Cl-1	23.46(0.27)	9.68(0.16)	50.04(0.25)	16.27(0.27)	0.56(0.03)
Cl-4	23.46(0.16)	9.63(0.13)	49.65(0.24)	16.33(0.19)	0.92(0.06)
Cl-5	23.45(0.20)	9.85(0.09)	48.79(0.20)	15.92(0.12)	2.00(0.06)
Cl-6	23.69(0.31)	9.83(0.16)	48.17(0.38)	15.78(0.12)	2.53(0.09)
Cl-7	23.54(0.19)	9.73(0.16)	49.59(0.21)	16.33(0.17)	0.80(0.04)
Cl-8	23.63(0.24)	9.62(0.18)	49.04(0.22)	16.22(0.16)	1.49(0.02)
Cl-9	23.21(0.22)	9.41(0.14)	50.30(0.19)	16.92(0.16)	0.17(0.03)
Cl-11	22.68(0.23)	9.66(0.19)	48.70(0.28)	18.12(0.16)	0.84(0.06)
Cl-12	22.68(0.27)	9.49(0.12)	48.29(0.29)	18.03(0.19)	1.51(0.03)
Cl-13	22.59(0.16)	9.54(0.17)	47.94(0.28)	17.89(0.17)	2.04(0.05)

3.3.2 Karl Fischer Titration (KFT)

Run-product glasses were analyzed for total water content using KFT (cf. Behrens et al., 1996 for details on the method). Glasses with more than 3 wt. % water degassed violently, even with slow heating. This degassing may have led to incomplete collection of the water and consequently underestimation of water content, however the underestimation is assumed to be slight. Water contents determined by KFT were higher than calculated from water added to the capsule (by 42% to 90% relative), due to the hydroscopic nature of the salts which took on significant water during capsule preparation despite efforts to minimize this effect. However, KFT measurements are representative of water contents in the melt at experimental conditions and were used to calculate the redox conditions of the experiments as outlined below. The water contents of the glasses are included in Table 3.1 along with associated errors.

3.3.3 Microprobe – Water contents

In instances where KFT values were not available due to lack of material, the water contents were determined using an EMPA mass difference (100%-yield) calculation as outlined in Morgan and

London (1996) and King et al. (2002). To achieve this, lower beam currents (4 nA at University of Toronto) were utilized. For water determination ten-point transects were performed and average mass differences obtained were used to calculate the water content. Where available, analyses by KFT were used to calculate a linear correction factor (showing good correlation with $R^2 = .902$) to calculate water contents from microprobe measurements. Water contents estimated from EMPA yields for glasses using a linear correlation were determined to be suitable for the purposes of this study (estimated +/- 10% relative) for samples where lack of material prevented KFT analyses.

3.3.4 Fourier Transform Infrared Spectroscopy (FTIR)

Selected pieces of run-product glasses were prepared as 500µm thick, doubly polished sections for FTIR analysis. Near-infrared spectra with a resolution of 4 cm^{-1} were collected using a Bruker IFS 88 spectrometer with an IR-Scope II microscope, a tungsten light source, a CaF_2 beam splitter, and a mercury cadmium telluride (MCT) narrow range detector. A slit aperture of 150 µm x 150 µm was used, and multiple measurements were made on the same polished section. The peak heights near 4500 cm^{-1} and 5200 cm^{-1} were compared and it was determined that the distribution of water was homogeneous throughout the sample. FTIR was used solely for the purpose of determining the distribution of water within the experimental glass as absorption coefficients for the glass composition used are not characterized.

In all experiments the water was distributed uniformly, even after the shortest run duration. Peak heights of a given sample were identical within error of the measurement. Measurement error is introduced by instabilities in the baseline, which varied by up to 0.003 absorbance units. This results in an estimated maximum variation in absolute water content of 0.2 wt. % for a given experiment.

3.3.5 Isotope Dilution ICP-MS

Platinum was analyzed in bulk experimental glasses by isotope dilution inductively coupled mass spectrometry (ID-ICP-MS), using either the Micromass Isoprobe multicollector ICPMS at the University of Muenster, or a NU Instruments multicollector ICPMS at the Max Planck Institute for Geochemistry in Mainz. All wet chemistry was also performed at the MPI in Mainz.

Contamination of the samples with Pt-bearing capsule material was a large concern using a bulk solution analytical method and care was taken to minimize this problem. Because of the small absolute amounts of platinum dissolved in the glasses, any contamination by capsule material would be readily apparent due to very high concentrations (apparent solubilities). Any analyses showing anomalously high Pt concentrations were treated as suspect and were discarded and reanalyzed using laser ablation ICP-MS as outlined below.

For analysis, glasses were removed from the capsule and thoroughly cleaned in multiple stages. A large piece(s) of the glass (~100 mg) was placed in a Teflon Savillex bomb. To clean the sample, 1 mL of dilute (1:20) HF was added and the sample was placed in an ultrasonic bath for 1 minute. This process served to loosen any platinum metal that may have been attached to the surface without leaching Pt from the sample. The samples and containers were then rinsed thoroughly with high-purity water. Water was then added to the container, and it was again placed in an ultrasonic bath for 5 minutes. The water was then discarded, and the sample was dried overnight. After the cleaning stages, the samples were crushed to a fine powder using an agate mortar and pestle, which was cleaned thoroughly between samples with distilled HNO_3. The samples were then weighed, placed in a clean Savillex bomb, and spiked with a ^{198}Pt-enriched platinum solution. The samples and spike were then digested using a solution of 0.5 mL concentrated HF, 0.5 mL concentrated HCl and 0.5 mL concentrated HNO_3. All acids used were suitable for trace analysis; HCl and HNO_3 were distilled, and HF was doubly distilled. The containers were sealed and placed on a hot plate at 393 K for 24 hours. After 1 hour, the samples were removed from the hotplate and placed in an ultrasonic bath for 5 minutes before being returned to the hotplate. After 24 hours of digestion the containers were uncovered, returned to the hot plate, and the acids were allowed to evaporate. After the samples were thoroughly dried, 0.5 mL of concentrated HNO_3 was added to the sample and was allowed to evaporate on the hot plate. A further 0.2 mL concentrated HNO_3 was added and the sample allowed to evaporate. The final stage of the digestion process was the addition of 2 mL of 0.8N HNO_3 saturated with Br_2. The Savillex bombs were then sealed tightly and placed on the hotplate overnight. This final step ensured that the platinum present was in the highest valence state which was required for subsequent column separation.

Bio-Rad AG 1X8 resin (200–400 mesh) was prepared the day before column separation by adding of 0.8N HNO_3 saturated with Br_2. Resin was added to the column and two 1-mL aliquots of 0.8N HNO_3 saturated with Br_2 were added and allowed to pass through the column. The samples were then loaded onto the column, and again two 1-mL aliquots of 0.8N HNO_3 saturated with Br_2 were added. The resin was then cleaned by adding 5 mL of10N HNO_3 to the column. After the resin was cleaned, 10 mL of 14N HNO_3 was added to the column, eluting the Pt and the solution was collected. Samples were evaporated and then stored until analysis by MC-ICP-MS.

3.3.6 Laser Ablation ICP-MS

The laser-ablation ICP-MS analytical facility at the Great Lakes Institute for Environmental Research, University of Windsor, Canada, was used to determine both the possible presence of micronuggets and Pt concentrations in glasses. Laser ablation analysis was performed on polished

chips of sample glass devoid of visible surface contamination using a 266nm Nd-YAG laser with 1.25 kiloampere power and a 20Hz repetition rate. Use of a 2 mm diameter pinhole and 10X-objective resulted in a laser spot size of 140 μm and samples were analyzed by boring into the sample at a rate determined by the laser. Samples were analyzed using a Thermo Electron X series II quadrupole ICP-MS using an argon carrier gas. Background acquisition was obtained for 60 seconds with the laser off, followed by sample acquisition for a maximum of 180 seconds. Data was collected for the following isotopes, ^{43}Ca and ^{25}Mg (high resolution, 20 ms dwell times) ^{191}Ir, ^{193}Ir, ^{195}Pt, ^{196}Pt (low resolution, 100 ms dwell times). Calcium was used as an internal standard using values obtained by electron microprobe analysis to correct for variances in ablation yield. Analyses were calibrated using two analyses of NIST 610 standard, run at the beginning and end of each acquisition set; if acquisition sets contained more than 20 analyses, a two more NIST 610 analyses were performed mid way through the acquisition set. Acquired LA data was reduced and interpreted using a combination of Thermo Electron's Plasmalab software and in-house developed tools based on Longerich et al. (1996).

A typical analysis with two micronuggets is shown in Figure 3.1, with the micronuggets appearing as the short duration high intensity peaks occurring at 85000 and 114000 milliseconds. Where these peaks occur they are excluded from the integrated regions in order to get a baseline concentration representing the concentration in the micronugget-free melt. The most appropriate isotope for Pt concentration calculations was ^{195}Pt, because this isotope has the highest abundance, the spectra have a low background and the most stable signal.

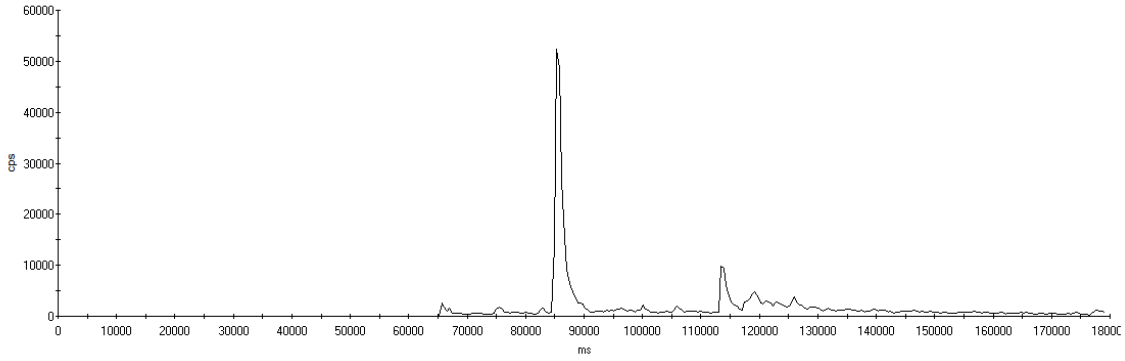

Figure 3.1 – Typical LA-ICPMS result for 195-Pt, showing two discreet "micronuggets" evident by the short duration high intensity peaks at 85000 and 114000 milliseconds (ms). The peaks are surrounded by regions of stable count rates which are used for the integration of the data to determine baseline "micronugget-free" solubilities. Laser switched on at 65000 ms

3.4 Attainment of equilibrium

Although equilibrium should be reached within 48-66 hours as demonstrated in Blaine et al. (2005), it is clear by comparing experiments of different run durations that concentrations and distribution of Pt within the experimental glasses vary with run duration. This is especially clear using the results from the bulk ICP-MS analyses (see "Pt (ID)" data in table 1) but is also evident from the laser ablation data. Comparing shorter run duration experiments with longer run duration experiments, when analyzed by bulk solution ICP-MS there is a clear indication that there are lower Pt contents (at comparable oxygen fugacities) with increasing run duration (for example, compare experiments Cl-5 and Cl-13 in table 1). Using laser ablation analyses it is clear that the increased concentrations in the short run duration experiments are due to an increased abundance of micronuggets in the glasses (Figure 3.2). In the shortest run duration experiments, Pt distribution in the glasses is very inhomogeneous and it is not possible to measure a clear micronugget-free baseline concentration. In longer run duration experiments the micronugget distribution is more regular, the amount of micronuggets decreases and reliable concentrations can be obtained using LA-ICPMS. Therefore to obtain reliable estimates of Pt solubility it is only possible to use the data obtained from longer run duration experiments where the distribution of micronuggets is such that one can get a clear resolution of micronugget-free baseline concentrations. This was found to occur after more than 93 hours. This behaviour is discussed in detail in the following sections.

PtIr-11 – 68 hours, 19379 ppb Pt (LA-ICPMS)

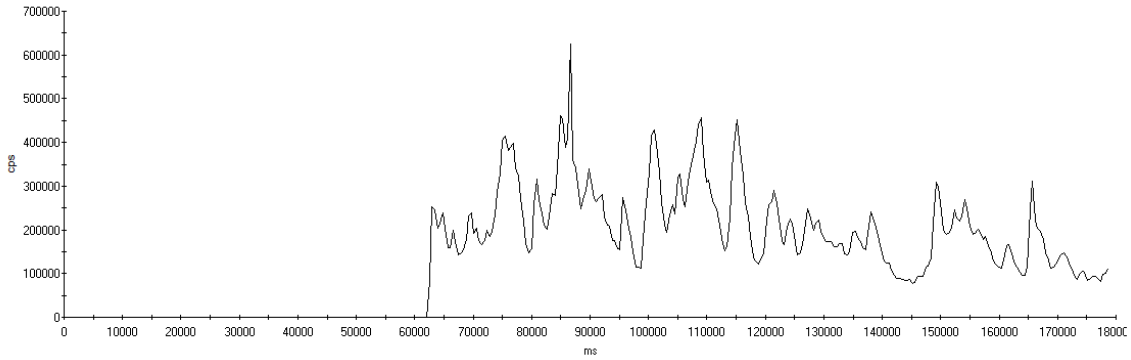

Cl-5 – 74 hours, 976 ppb Pt (LA-ICPMS)

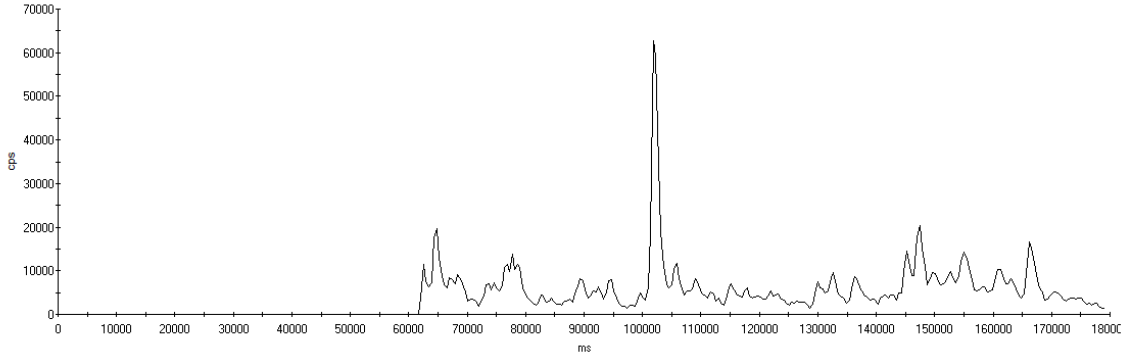

Cl-13 – 130 hours, 18 ppb Pt (LA-ICPMS)

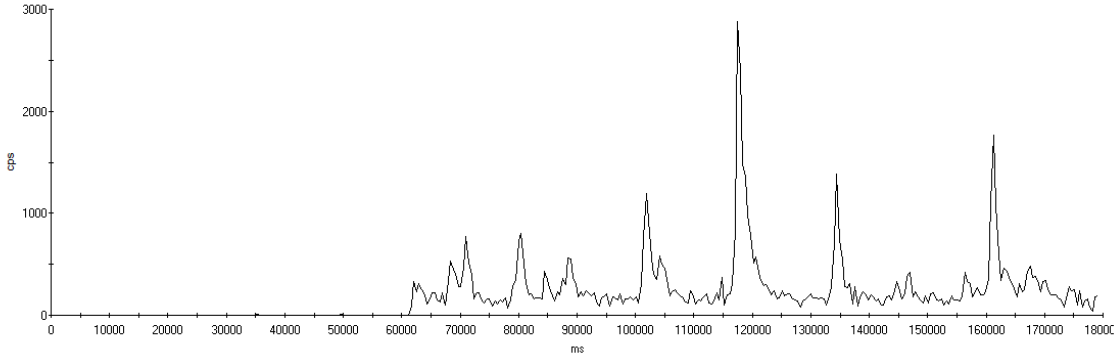

Figure 3.2 –LA ablation analyses of three individual samples with similar water and chlorine contents as a function of time (in milliseconds). The experimental duration for the synthesis of the three samples differs as indicated in the figure. For PtIr-11, variable though consistently high count-rates preclude baseline concentration calculations. Cl-5 shows a still variable spectrum, but with much lower count-rates with evidence of individual "micronuggets". Cl-13, the longest duration experiment, shows easily identifiable "micronuggets" and a lower and more stable baseline. Note the change of scale of the Y-axis for the analysis of Cl-13

3.5 Results and Discussion

The most direct evidence of Cl-complexing of platinum in the melt would be an increase in platinum solubility with increasing Cl content, where all other variables are constant. However, other factors must also be considered to interpret Pt solubility data. Platinum solubility is highly dependent on the prevailing oxygen fugacity of the experiments due to the oxidation reaction which forms charged Pt-species in the melt upon dissolution of the metallic zero-valent Pt from the capsule (Equation 3.1), where the valence of platinum is equal to 4 times the stoichiometric coefficient of O_2. In these experiments, oxygen fugacity is controlled by varying water contents through the dissolution reaction of water (Equation 3.2). Hydrogen fugacity is fixed and controlled by intrinsic hydrogen fugacity of the autoclave. The capsules are permeable to H_2 at experimental conditions but are not permeable to water. The intrinsic f_{H_2} is well characterized through multiple experiments at different temperatures and the corresponding f_{O_2} falls on the MnO-Mn_3O_4 buffer curve at water-saturated conditions (Berndt et al., 2002). At the conditions of the experiment, 1523K, 200 MPa and water saturated conditions, f_{O_2} = $10^{-3.6}$ bar, calculated from O'Neill et al. (1993). At water-undersaturated conditions, the water activity in the melt can be estimated from the water concentration in experimental glasses (for example using the model of Burnham, 1994), allowing further calculation of the prevailing oxygen fugacity in the capsule using Equation 3.3. Details of these calculations can be found in Blaine et al. (2005).

The majority of experiments were run at volatile undersaturated conditions without the presence of a free volatile phase. In these cases, for the purposes of this study, it is assumed that chlorine has a negligible effect on oxygen fugacity, i.e., that Cl did not change the activity of water in the system. It must be noted; however, that at high near-saturation Cl levels there is evidence that increased Cl content may result in an increase in water activity (Aranovich and Newton, 1996; Botcharnikov et al. 2004; Webster and Mandeville, 2007), however this effect cannot be quantified for these experiments. Increased water activity would result in an increase in oxygen fugacity and result in a possible underestimation of oxygen fugacity at high Cl contents.

Two experiments were conducted at volatile saturated conditions evidenced by pressurization of the capsule after the experiment and hissing upon opening. The saturation content of 2.75 wt. % Cl in the melt of experiment PtIr-10 corresponds well with Cl solubility estimates from Webster et al. (1999) and coexisted with Cl-rich brine. PtIr-17 was saturated in water with 4.38 wt. % water in the glass and is consistent with the saturation value of 4.25 wt. % water determined in Blaine et al. (2005) showing a slight increase in water solubility with the presence of Cl, although this value is lower than

that determined for a natural trachybasalt by Stelling et al. (2008). The oxygen fugacities for the two experiments at volatile saturated conditions were estimated solely from the water content of the glass because the fluid compositions are not known exactly. The difference in oxygen fugacity between Cl-bearing, fluid saturated experiments and a Cl-free water saturated experiment is assumed to be low. Sufficient data is not available to assess the potential change in oxygen fugacity with Cl saturation (as would be implied by Stelling et al, 2008) for PtIr-10, however it was excluded from calculations for reasons discussed below.

$$Pt^{0}_{(metal)} + xO_2 \Leftrightarrow PtO_{2x(melt)} \qquad \textbf{Equation 3.1}$$

$$H_2O_{(gas)} \Leftrightarrow H_{2(gas)} + \frac{1}{2}O_{2(gas)} \qquad \textbf{Equation 3.2}$$

$$\log f_{O_2(\exp eriment)} = \log f_{O_2(water-saturated)} + 2\log a_{H_2O(\exp eriment)} \qquad \textbf{Equation 3.3}$$

The Pt solubility data of this study are compared to the data obtained for a chlorine-free system in Figure 3 (data from Blaine et al., 2005). The Cl-free trend data is a regression of data obtained in both a hydrous, diopside-anorthite system (Blaine et al. 2005, where water was deemed not to have any effect on Pt solubility) and anhydrous data for the equivalent diopside anorthite system from Borisov and Palme, 1997 and Ertel et al., 1999. Considering the previous observation on the attainment of equilibrium data, data from short run duration experiments were removed and only experiments with run durations of 96 hours or more were used. Some experiments with shorter run durations exhibited fewer micronuggets and reliable LA analyses could be obtained, however to maintain consistency, only experiments longer than 96 hours (where all experiments were able to be analyzed reliably) were used for calculations.

Figure 3.3 shows that there is no discernable effect of Cl on Pt solubility over the entire range of Cl contents investigated in this study. All data plot predominantly along the Cl-free trend line determined for both hydrous (Blaine et al. 2005) and anhydrous diopside melts (Borisov and Palme 1997; Ertel et al. 1999) indicating that Cl has a negligible effect on the intrinsic solubility of Pt in a haplobasaltic melt.

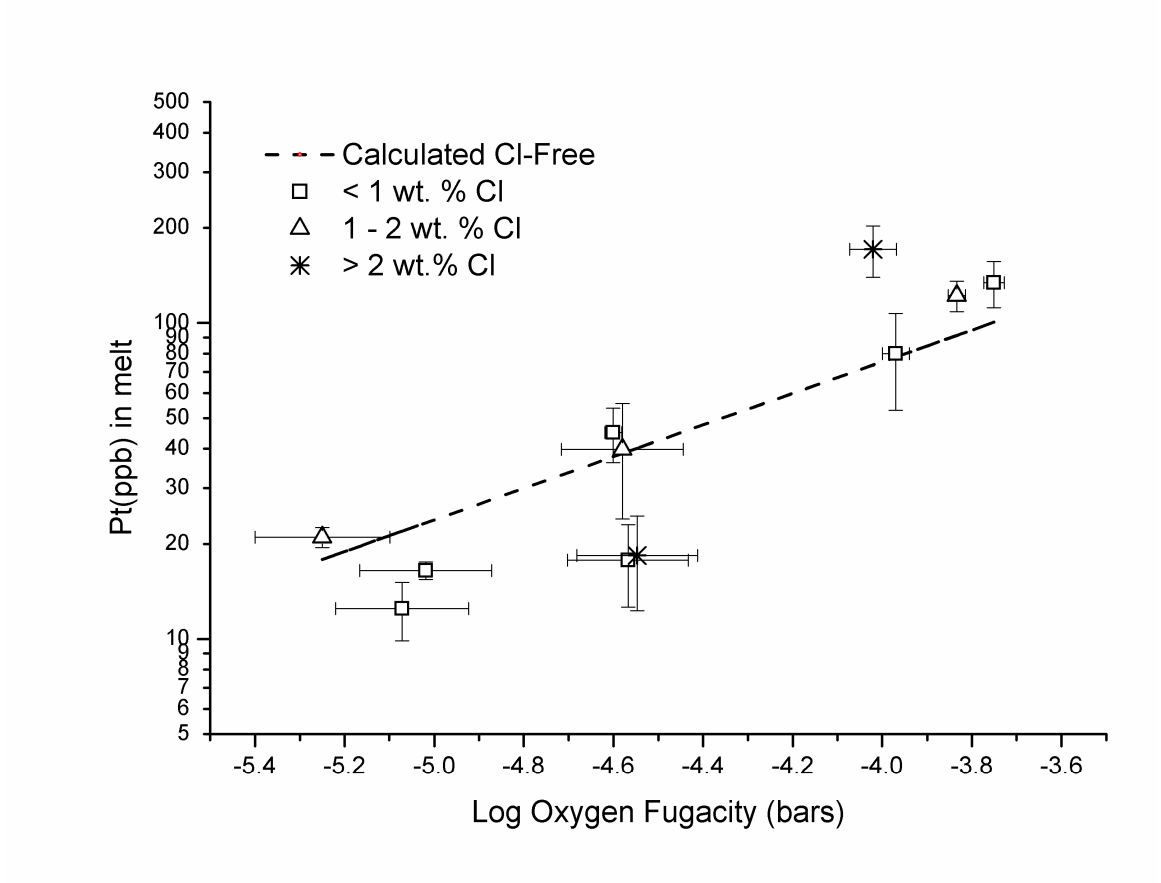

Figure 3.3 – Experimentally determined activity-corrected platinum solubility data of this study with varying Cl contents for experiments with run durations 96 hours or longer. Platinum contents determined by LA-ICPMS with micronuggets removed, plotted with hydrous, Cl-free calculated Pt solubilities (taken from Blaine et al. 2005 and consistent with anhydrous studies by Borisov and Palme, 1997; Ertel et al., 1999; and Fortenfant et al. 2003).

The solubility values obtained in this study are much lower than those obtained by Simon and Pettke (2009) for rhyolitic melts coexisting with an aqueous vapor phase and brine. The data of Simon and Pettke (2009) were obtained at 1073 °K (0.1 and 0.14 GPa) and indicate that Pt solubility in a melt containing ~ 0.15 wt% Cl is in the range 0.15 - 0.45 ppm, whereas the maximum solubility in our study is found to be ~ 0.1 ppm at higher oxygen fugacities where solubility would be expected to be greater. The experiments of Simon and Pettke (2009) were conducted in the presence of a Ni-NiO solid buffer and at the corresponding oxygen fugacity ($\log fO_2 = -6.95$; O'Neill and Pownceby, 1993) expected Pt solubility would be less than 2 ppb in a melt composition similar to that used in this study. This significant difference is difficult to explain considering our present knowledge on the solubility of PGEs in volatile-bearing silicate melts at high pressure, however the effect of melt composition on PGE solubility is not well constrained.

3.5.1 Explanation of high Pt anomalies in experimental data and formation of micronuggets

Although the Pt solubility data obtained using bulk solution ICP-MS from shorter run duration experiments were determined to be non-representative of equilibrium platinum solubilities in the melt, there exist some intriguing trends in the data that are worthy of discussion.

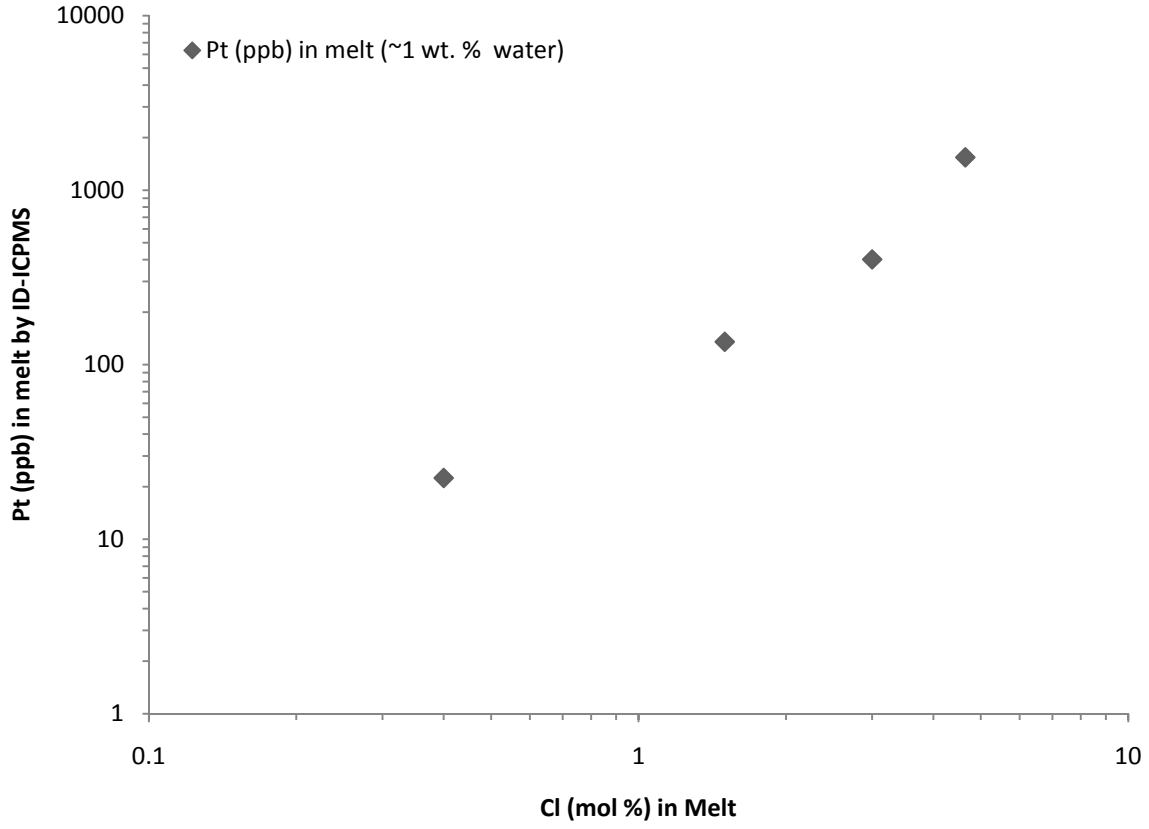

Figure 3.4 - Plot of apparent Pt solubility determined by isotope dilution ICP-MS versus Cl content in the run products containing approx. 1wt. % total water content (absolute log f_{O_2} between -5.4 and -5.6 bars).

Bulk solution isotope dilution ICP-MS analyses show a systematic increase in apparent Pt solubility with an increase in Cl content (Figure 3.4) for experiments with approximately 1 wt. % water, holding everything except Cl-content constant. This dataset could suggest an influence of Cl on Pt solubility in the melt, indicating the formation of complexes between Cl and PGE in the silicate melt. However, the platinum concentrations determined by LA-ICPMS do not vary with chlorine

concentration and using LA-ICPMS, it has been demonstrated that the high Pt concentrations in the products from short run duration are due to the contribution of Pt in micronuggets.

A model is herein proposed (represented in Figure 5), that can explain the increase in Pt content in the run products analyzed by the bulk solution ICP-MS method by taking into account the different steps by which Cl and H_2O are dissolved into the melt during the early stages of an experiment. The initial capsule charge consists of a powder of Fe-free basaltic glass, water and a chlorine source ($CaCl_2$ and $MgCl_2$) (Figure 3.5-I). Prior to heating and during the initial heating stages the Cl-source will dissolve into the water present within the capsule, resulting in two phases present in the capsule, a Cl-rich fluid phase and a solid glass phase (Figure 5-II). During heating the Cl-rich fluid will only dissolve very slightly into the glass (this process is controlled by the diffusivity of water and Cl) but it is possible that the fluid can dissolve significant Pt from the capsule (Figure 3.5-II). This Cl-rich fluid will continue to dissolve Pt but will not diffuse significantly into the glass until high temperatures (close to the water-saturated melting of a basaltic composition) are reached (Figure 3.5-III). As the fluid dissolves into the glass (or melt), the Pt incorporated into the fluid cannot be accommodated within the melt structure and is left behind initially along the relict boundaries between glass particles (Figure 3.5-IV). As the melting of the glass and the dissolution of the volatiles reaches completion, the micronuggets would be left as discreet phases suspended in the melt. It is assumed that migration of the Pt contained within the micronuggets out of the melt would occur slowly, either by settling (hindered by the very small size of the micronuggets), or by Ostwald ripening.

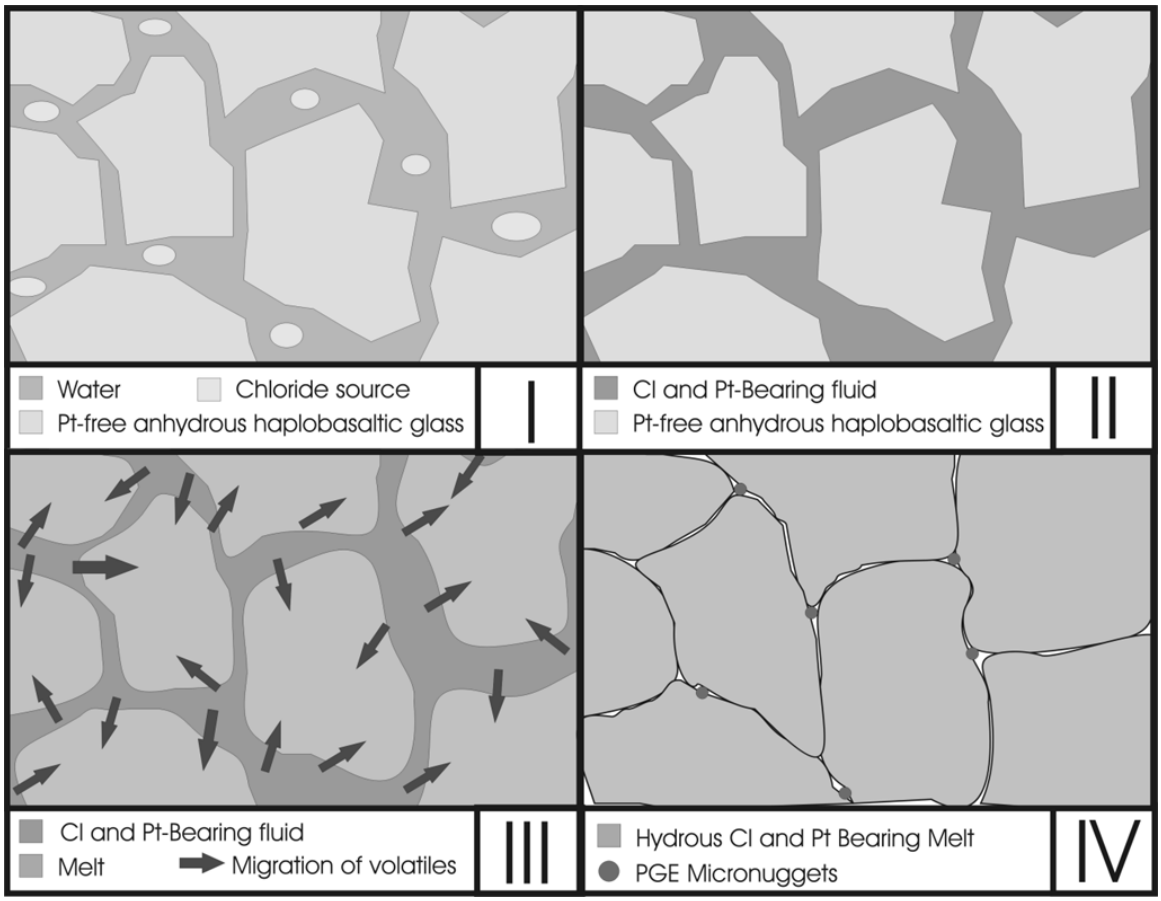

Figure 3.5 – Schematic description of the proposed processes involved in the early stages of experimental runs and explaining the formation of elevated Pt contents and "micronuggets" in experimental products. Details explained in text.

Taking the model proposed above into account, Figure 2 can be re-interpreted. The LA-ICPMS spectra of three separate samples with similar chlorine (~2 wt.%) and water (~2 wt.%) contents but with varying run durations are shown in Figure 2. In the shortest of the three experiments, PtIr-11 at 68 hours, the count-rate is high, unstable, and shows a high apparent solubility in the glass without individual "micronuggets", though the baseline is difficult to determine. With longer durations the count-rates drop significantly and strong variations are localized to individual discreet peaks within the analytical run. In the analysis of experiment Cl-5 after 74 hours, it can be seen that the count-rates are much lower, although still variable and discreet high intensity peaks are visible, baseline solubility still produces relatively high concentrations of Pt when integrated. In experiment Cl-13 after 130 hours run duration, concentrations are lower and LA analysis shows a consistently low inherent (micronugget-free) solubility with discreet micronugget phases. This

behaviour suggests that initially the residual Pt, left behind as the fluid dissolves into the melting glass, is distributed relatively evenly along the particle boundaries and with increasing time, the excess Pt coalesces to form individual "micronuggets". These particles may eventually move along the relic particle boundaries, if any residual pathways remain and out of the glass or melt (towards the capsule wall).

There have been a number of theories on the formation of micronuggets in experimental systems (Borisov and Palme, 1997; Ertel et al., 1999; Blaine et al., 2005; Brenan et al., 2005, Cottrell and Walker, 2006, among others) and although this model is applicable to the experiments detailed here, it will not be applicable to the formation of all micronuggets in experimental systems. Using the model described here it is not believed that micronuggets will form in, or from, the fluid during the heating stages unless physically transported as Pt particles from the capsule; lack of micronuggets in H_2O-only bearing experiments (Blaine et al., 2005) indicate this is unlikely. It is also demonstrated by the decrease in micronugget abundance and concentration with experimental duration, that at least the bulk of the micronuggets formed are not formed on quench as has been proposed by Cottrell and Walker, 2006 (discussed in detail in Chapter 7). The formation of micronuggets proposed here would be isolated to multiple-phase systems where Pt (or other PGEs) is partitioned strongly into one phase which is then dissolved into the other. Analogous systems and mechanisms are present in natural systems specifically ore-forming PGE systems and this proposed mechanism could also contribute to the formation of micronuggets in natural systems and is discussed below.

3.5.2 Estimating Pt solubility in a Cl-bearing volatile phase

Based on the model outlined above is assumed, that because the starting glasses have very low Pt contents (<60ppb) and chlorine has no discernable influence on Pt solubility in the melts, the source for the excess Pt present within the experimental glasses is related to the existence of a free fluid phase in the first steps of the experiments. If this model is correct, the anomalously high Pt determined by ID-ICPMS in the run products of experiments with shorter run durations can provide information on the amounts of Pt that can be dissolved in the fluid phase and the Pt concentration in the fluid can be estimated through mass balance. By subtracting the Pt solubility (determined by LA-ICPMS) from the bulk concentration (using bulk isotope dilution ICP-MS), the amount of excess Pt contributed by the fluid phase prior to fluid dissolution into the glass can be determined (Equation 4) and an estimate on solubility can be obtained. These calculations indicate that the Cl-bearing fluids present in the capsules prior to dissolution into the glass (up to ~1448K) can contain very significant amounts of Pt, up to hundreds of ppm (Table 3.3).

These estimates are admittedly rough as there is a lack of constraint on the system conditions and evidence that not all Pt contained in the fluid is still present in the glass, however the evidence suggests that these estimates are still significant and may in fact represent a lower-end estimate of Pt solubility in the fluid phase under the conditions of this study. The decrease in Pt determined by bulk solution with experiment duration indicates that some Pt present as micronuggets is lost from the melt over time and suggests higher levels of Pt in the fluid-melt system (attributed to the fluid as Pt solubility in the melt is low) prior to quench and would result in an underestimation of Pt in the fluid phase, using the calculations described.

As the fluid will not dissolve significantly into the melt until near the melting temperature and the micronuggets are assumed to form on dissolution, the estimated solubilities are assumed to be relevant at, and correspond to the temperature of dissolution at ~1473K, however for this to be true certain overriding assumptions are made. During the heating stages when a free fluid is present during the experiment, equilibration of the fluid with the Pt capsule will be very rapid and it is assumed that Pt solubility will show prograde solubility behaviour as proposed by Wood (1987) and Hanley (2005), and the maximum Pt solubility observed/calculated should be representative of the fluid at the temperature it dissolves into the melt. If platinum solubility does not show prograde behaviour throughout the heating and there is a maximum Pt solubility at a lower temperature it is possible that micronuggets could form above this temperature and calculated Pt solubility would be representative of this temperature, however this is believed not to be the case. Another potential complication is that during the heating stage the composition of the system will be constantly changing, as the temperature rises and the fluid and melt interact. As a result during the heating stages a solubility maximum, and micronugget formation, could also occur at a lower temperature. Because of these assumptions and potential complications the solubilities of Pt in the fluid are apparent solubilities only and should only be used qualitatively.

It can be noted that the estimations given in Table 3.3 are at least two orders of magnitude higher that the data published recently by Simon and Pettke (2009). This difference may be due to the temperature difference between the two datasets (1073K vs. approximately 1473K). In any case, even if we use the data of Simon and Pettke (2009) obtained for fluids at 1073K (~ 0.1 to 1.1 ppm Pt in aqueous vapor), it can be noted that the partitioning of Pt between Cl-bearing aqueous fluids and basaltic silicate melts would be higher than calculated in the study of Simon and Pettke (2009) because of the lower Pt solubility observed in this study for the basaltic melt.

$$Pt_{fluid} = [Pt_{ID-ICPMS} - Pt_{calculated}] \times \frac{m_{glass}}{m_{fluid}}$$ **Equation 3.4**

Table 3.3 – Tabulated results of Pt concentration in the fluid phase

Sample	Pt_{melt} (ppb) ID-ICPMS	Pt_{melt} (ppb) Calculated (Cl-free)	H_2O_{melt} content (wt. %)	Cl_{melt} content (wt. %)	Calculated Pt content of Fluid (ppb)
PtIr-8	13422	55	3.59	1.79	235000
PtIr-9	7311	75	2.96	1.85	143000
PtIr-10	1613	40	2.03	2.75	32000
PtIr-11	7304	46	2.25	2.25	154000
Cl-5	1375	30	2.14	2.00	31000
Cl-6	1543	10	1.01	2.53	42000

3.5.3 Application to natural systems

In the case of the vapour refinement model proposed for the formation of Pt deposits (Boudreau, 1999; Boudreau and Meurer 1999) the estimation of the Pt concentrations in the fluids from our experiments could be especially important. The values listed in Table 2 suggest that it is possible to significantly enrich and transport Pt and PGEs in a Cl-bearing fluid phase. At the end of the crystallization of magma chamber (late stage processes), PGEs should be partitioned into the fluid phase if a Cl-rich fluid exsolves from the melt. If the interstitial exsolved fluid travels upwards through a crystallizing magma (density contrast), and if the fluid interacts with an overlying volatile-undersaturated magma, the fluid will dissolve into the melt possibly leading to the formation of PGE-bearing micronuggets, as has occurred in our experiments. If the magma (melt) is saturated with respect to a sulfide melt, these PGE-bearing micronuggets could be readily scavenged by the sulfide resulting in a PGE-rich sulfide melt.

3.6 Conclusions

The presence of chlorine has no discernable effect on the solubility of Pt in a hydrous Fe-free melt at the investigated conditions (200 MPa, 1523K). The results also stress the necessity of using microanalytical techniques such as LA-ICPMS when performing solubility studies of PGEs. The results of the LA-ICPMS data combined with bulk analyses by isotope dilution ICP-MS indicate that extremely high (>100ppm) Pt contents may be incorporated in high-temperature Cl-bearing fluids at moderate oxygen fugacities.

The evidence for such high Pt contents in the Cl-bearing aqueous phase provides further evidence that fluids could play a significant role in the formation of PGE deposits in layered intrusions and the magmatic hydrothermal model of the formation of these deposits is a realistic model. The strong difference between our data (~1523K) in a hydrous, Fe-free haplobasalt and the recent dataset of Simon and Pettke (2009) obtained for rhyolite melts at 1073K also stress the need for further studies to quantify the high temperature fluid-melt partitioning of PGEs. Furthermore, if the estimates of Simon and Pettke are correct, this indicates that partitioning and solubility data and behavior of the PGEs cannot be applied outside of strict compositional brackets and much care must be taken when comparing experimental data with natural ore-forming systems.

Chapter 4 - The effect of oxygen fugacity and Cl content on Ir solubility in a haplobasaltic melt: Evidence of Cl complexing in basaltic melts and aqueous brines

4.1 Introduction

There have been a number of historical studies (Bezman et al., 1994; Peach et al., 1994; O'Neill et al., 1995; Borisov and Palme, 1995; Righter et al., 2004; and Brenan et al., 2005) that attempted to elucidate the behaviour of Ir with varying oxygen fugacity with varying levels of success. Two early comprehensive studies; O'Neill et al. (1995) and Borisov and Palme (1995); studied Ir solubility in an iron-free haplobasalt at atmospheric pressure and 1573/1753K and 1673K, respectively. Although nearly identical experimental conditions were used, contrasting results were obtained indicating that Ir is dissolved either in the 1+ (Borisov et al., 1995) or 2+ (O'Neill et al., 1995) valence state. However in both of these studies it was impossible to determine low level variations in Ir solubility at low oxygen fugacities making it appear that Ir solubility was independent of oxygen fugacity indicating that Ir was dissolved in the melt in a 0-valence state.

Recent technological advances in analytical methodology, most importantly the development of microanalytical techniques such as laser-ablation inductively coupled mass spectroscopy (LA-ICPMS) and ion microprobe, have made it possible to analyze microscale variations in concentration. The use of these techniques has identified the presence of PGE micronuggets in experimental run products, especially at low oxygen fugacities and correspondingly low PGE solubilities (Blaine et al. 2005; Ertel et al. 2006 and 2008). These micronuggets add to the observed concentration when analyzed by bulk analytical techniques and can mask true solubility trends. These microscale analytical techniques are very important for experiments on the PGEs, including Ir, and allow for baseline determination of PGE solubilities in experimental products in the presence of micronuggets. Using these analytical techniques, Brenan et al. (2005) determined that Ir was dissolved in the 2+ valence state indirectly through olivine-melt partitioning experiments; however, the melt composition differed from that used in previous studies as it was a Fe-bearing basaltic melt.

Direct Ir solubility experiments are needed to confirm the findings of Brenan et al. (2005) and confirm that Ir is dissolved in the 2+ valence state which is inconclusive based on previous direct experiments (Borisov et al., 1995 and O'Neill et al., 1995). It was demonstrated in Blaine et al. (2005) that the sealed-capsule technique paired with laser ablation analysis could be used to determine the solubility of Pt in hydrous basaltic melts at conditions relevant to the conditions of PGE deposit formation. Blaine et al. (submitted; Chapter 3) demonstrated that this method could be applied to a Cl- bearing system to observe the effect of Cl on Pt solubility. In the current study, these techniques are applied to determine the effect of water and chlorine on iridium and are summarized in this chapter.

4.2 Experimental methods

Iridium solubility experiments in chlorine-bearing or chlorine-free hydrous haplobasaltic melts were conducted through hydration and chlorination of a synthetic melt, and saturation of that melt with Ir at the temperature and pressure of interest. Iridium saturation was the result of equilibration of the melt with the sealed noble metal capsule used to contain the melt throughout the experiment.

Experimental charges were prepared by sealing approximately 300 mg of diopside-anorthite dry eutectic minima composition glass ($An_{42}Di_{58}$) with a grain size of <200μm, and varying amounts of distilled water (from approximately 3mg to 12mg, corresponding to 1 - 4 wt. % water) into a $Pt_{80}Ir_{20}$ alloy capsule (25mm length x 4mm outer diameter/3.6mm inner diameter), along with a source of chlorine. The $An_{42}Di_{58}$ composition was used to allow direct comparison of the data of this study with those of Borisov et al. (1995) and O'Neill et al. (1995); the two studies that had previously investigated Ir solubility. In this study, chlorine was added as solid $MgCl_2$ and $CaCl_2$ and mixed in stoichiometric proportions in order to maintain the Mg:Ca ratio of the starting glass. The salts were mixed with the haplobasaltic glasses prior to loading into the capsules in approximately 1 g batches, to obtain Cl contents between 1 and ~3 wt. %, mixed thoroughly, and were stored in a drying oven at 373K prior to loading.

Pure iridium metal is brittle, hard and has a very high melting temperature making experiments using pure iridium capsules impractical. As a solution to this problem, a $Pt_{80}Ir_{20}$ alloy was used for the capsule material which allows determination of the solubilities of both Pt and Ir during the same experiment. However, the use of alloys causes a reduction in the absolute concentrations due to reduced metal activities as compared to pure metals which increases the lower

quantification of Ir solubility. In order to determine metal solubilities, an activity correction was applied to account for the reduced activity of Pt and Ir. Iridium activities determined from Tripathi and Chandrasekhariah (1983), for a $Pt_{80}Ir_{20}$ alloy at 1383K, 1468K and 1573K is 0.27, differing from the ideal 0.20 due a perceived miscibility gap. However, more recent studies (Yamabe-Mitarai et al., 2009) indicate that there is no miscibility gap in the Pt-Ir system at the temperatures used within this study which would result in an Ir activity of 0.2. Consequently, ideal mixing in the alloy is assumed and an Ir activity of 0.20 is used. Even if this assumption is incorrect, the error on absolute Ir solubility will be constant and the relative solubility variations between experiments will be unaffected. To determine absolute solubilities (activity = 1), concentrations in the resultant experimental glasses were divided by the corresponding activities. The effect of pressure on metal activities was assumed to be negligible.

Experiments were conducted at 1523 K ± 10 K and 200 MPa + 0.4/ -0.02 MPa. Temperature was controlled using two S-type thermocouples and was monitored with the use of two additional S-type thermocouples. In the water-bearing system of Blaine et al. (2005), equilibrium solubility in the glass was determined through time-series experiments where constant Pt concentrations, within analytical error, were reached between 48 and 65.5 hours. Subsequently, all of the experiments in this study were run for at least 68 hours. However, the addition of Cl to the haplobasalt-H_2O system causes an increase in the amount of micronuggets that are formed and longer run times are required to develop nugget-free regions in the glasses that are large enough to be analyzed by LA-ICP-MS. The micronugget problem is addressed in detail below. Electron microprobe analysis (EMPA) of polished sections of the glasses showed homogeneous distribution of chlorine after these run durations using solid Cl-salts as the source for Cl. The oxygen fugacity of the experiments is imposed by the intrinsic hydrogen fugacity of the autoclave. The intrinsic fH_2 is well characterized through multiple experiments at different temperatures and the corresponding fO_2 falls on the MnO-Mn_3O_4 buffer curve at water-saturated conditions (Berndt et al., 2002). At the conditions of the experiments (i.e. 1523 K, 200 MPa and water-saturated conditions), the fO_2 is calculated from O'Neill and Pownceby (1993) to be $10^{-3.6}$ bar.

All experiments were conducted at the Institut für Mineralogie at the University of Hannover, Germany in a vertically mounted, internally heated pressure vessel equipped with a rapid quench device. This apparatus allows the melt to be quenched to a crystal- and bubble-free glass at a cooling rate of >200 K/min (Berndt et al., 2002). After quenching, the samples were removed from the sample holder and weighed to ensure there had been no loss of water during the experiment. The experimental glasses were removed from the capsule and broken into 3–4 large pieces for various

analyses. No visible Pt-Ir contamination was noted on the exterior of the glass samples, but steps were taken (see below) to ensure there was no surface contamination when using bulk solution methods for Pt-Ir analysis. All end-product glasses were clear with no noticeable coloration or crystallization. Results for individual runs are summarized in Table 4.1.

4.3 Analytical techniques

Analytical techniques used for this study were similar to those used in Blaine et al. 2005, and Blaine et al. (submitted; Chapter 3). Where necessary these techniques were modified for the determination of iridium in the silicate melt.

4.3.1 Microprobe

Glasses were analyzed for major elements using either a Cameca SX-100 electron microprobe at the University of Hannover or a Cameca SX-50 at the University of Toronto, with a 15 keV accelerating voltage, a 4-6 nA beam current, and a 10 μm defocused beam. Transects were performed to check for glass homogeneity and consisted of a minimum of ten analyses. In all glasses there was no indication of glass heterogeneity and composition varied only slightly between experiments due to the addition of the Cl salts. Average run product glass compositions in wt. %, normalized to the Cl and H_2O free composition are CaO = 23.24 (0.54), MgO = 10.13 (0.27), Al_2O_3 = 16.93 (0.93), and SiO_2 = 49.70 (0.31), with 1σ standard deviations given in brackets. Results for individual glasses for Cl-bearing experiments are included in table 3.2.

4.3.2 Karl Fischer Titration (KFT)

End-product glasses were analyzed for total water content using KFT (cf. Behrens et al., 1996 for details on the method). Glasses with greater than 3 wt. % water degassed violently, even with slow heating. This degassing may have led to incomplete collection of the water and consequently underestimation of water content, however this is estimated to be slight. Water contents determined by KFT were higher than calculated from water added to the capsule (by 42% to 90% relative), due to the hydroscopic nature of the salts which took on significant water during capsule preparation despite efforts to minimize this effect, this effect was not observed for Cl-free experiments which showed general disagreement by < 5wt. % however experiment PtIr-4 showed a 43% higher water content by KFT than calculated. However, the KFT values are representative of water contents that are dissolved in the glass under experimental conditions and were used to calculate the redox conditions of the experiments as outlined below. The error in the analysis is given in Table 1 and was used for calculating corresponding errors in oxygen fugacity.

Table 4.1 – Summary of run conditions and analyses of experimental glasses

Sample Name	Capsule material	Experiment Duration (h)	$Cl_{(melt)}$ (Wt.%)$_{(a)}$	$H_2O_{(melt)}$ KFT (Wt.%)$_{(c)}$	Log Oxygen Fugacity (bars)	$Ir_{(melt)}$ (LA) (ppb)$_{a,b}$ Activity corrected solubility	$Ir_{(melt)}$ (ID) (ppb) Activity corrected solubility
Short run duration experiments not used in interpretation as discussed in text							
PtIr-10*	$Pt_{80}Ir_{20}$	68	2.75 (.09)	2.03(.06)	-4.82	309(68)	974
PtIr-11	$Pt_{80}Ir_{20}$	68	2.25 (.06)	2.25(.06)	-4.65	33131(3596)	4245
PtIr-7	$Pt_{80}Ir_{20}$	92.8	2.12 (.07)	1.60(.05)	-5.10	926(124)	204
PtIr-8	$Pt_{80}Ir_{20}$	92.8	1.79 (.05)	3.59(.08)	-4.04	3718(690)	7767
PtIr-9	$Pt_{80}Ir_{20}$	92.8	1.85 (.06)	2.96(.09)	-4.27	14005(4016)	4058
Longer run duration experiments used for interpretation as discussed in text							
PtIr-13	$Pt_{80}Ir_{20}$	96	0.89 (.02)	3.63(.10)	-3.97	168(126)	240
PtIr-14	$Pt_{80}Ir_{20}$	96	0.69 (.05)	4.4(.10)	-3.75	192(91)	282
PtIr-15	$Pt_{80}Ir_{20}$	96.1	0.68 (.06)	2.12(.09)	-4.60	73(49)	241
PtIr-16	$Pt_{80}Ir_{20}$	96.1	2.52 (.08)	3.83(.08)	-4.02	199(85)	na
PtIr-17*	$Pt_{80}Ir_{20}$	96.1	1.90 (.07)	4.38(.08)	-3.83	36(27)$_{(d)}$	na
Cl-Free experiments							
PtIr-2	$Pt_{80}Ir_{20}$	75	Cl-Free	2.08(.04)	-4.57	67(13)	34
PtIr-3	$Pt_{80}Ir_{20}$	75	Cl-Free	3.98(.06)	-3.80	28(12)$_{(d)}$	201
PtIr-4	$Pt_{80}Ir_{20}$	109	Cl-Free	4.07(.06)	-3.78	20(15)$_{(d)}$	51

LA – Concentration as determined by laser-ablation ICP-MS
ID – Concentration as determined by bulk solution isotope dilution ICP-MS
a – 1 σ errors given in brackets
b – Calculated from 193-Ir signal using 195-Pt sensitivity factor as a proxy
c – Errors given in brackets
f – Values below quantification limits
* - Saturated in a volatile phase as evidenced by hissing on opening of capsule

4.3.3 Fourier Transform Infrared Spectroscopy (FTIR)

Selected pieces of run-product glasses were prepared as 500μm thick, doubly polished sections for FTIR analysis. Near-infrared spectra with a resolution of 4 cm^{-1} were collected using a Bruker IFS 88 spectrometer with an IR-Scope II microscope, a tungsten light source, a CaF_2 beam splitter, and a mercury cadmium telluride (MCT) narrow range detector. A slit aperture of 150 μm x 150 μm was used, and multiple measurements were made on the same polished section. The peak heights near 4500 cm^{-1} and 5200 cm^{-1} were compared and it was determined that the distribution of water was homogeneous throughout the sample.

In all experiments the water was distributed uniformly, even after the shortest run duration. Peak heights of a given sample were identical within error of the measurement. Measurement error is introduced by instabilities in the baseline, which varied by up to 0.003 absorbance units. This instability results in an estimated maximum variation in absolute water content of 0.2 wt. % for a given experiment.

4.3.4 Isotope Dilution ICP-MS

Iridium was analyzed in experimental glasses by isotope dilution inductively coupled mass spectrometry (ID-ICP-MS), using either the Micromass Isoprobe multicollector ICPMS at the University of Muenster, or a NU Instruments multicollector ICPMS at the Max Planck Institute (MPI) for Geochemistry in Mainz. All wet chemistry was also performed at the MPI in Mainz.

Contamination of the samples with Ir-bearing capsule material was a major concern using a bulk solution analytical method and care was taken to minimize this problem. Because of the small absolute amounts of iridium dissolved in the glasses, any contamination by capsule material would be readily apparent due to very high apparent solubilities.

For analysis, glasses were removed from the capsule and thoroughly cleaned in multiple stages. A large piece(s) of the glass (~100 mg) was placed in a Teflon Savillex bomb. To clean the sample, 1 mL of dilute (1:20) HF was added and the sample was placed in an ultrasonic bath for 1 minute. This process served to loosen any Pt-Ir alloy that may have been attached to the surface without leaching Ir from the sample. The samples and containers were then rinsed thoroughly with high-purity water. Water was then added to the container, and it was again placed in an ultrasonic bath for 5 minutes. The water was then discarded, and the sample was allowed to dry overnight. After the cleaning stages, the samples were crushed to a fine powder using an agate mortar and pestle, which was thoroughly cleaned between samples using distilled nitric acid. The samples were then weighed, placed in a clean Savillex bomb, and spiked with a ^{198}Pt- and ^{191}Ir- enriched platinum

solution. The samples and spike were then digested using a solution of 0.5 mL concentrated HF, 0.5 mL concentrated HCl and 0.5 mL concentrated HNO_3. All acids used were suitable for trace analysis; HCl and HNO_3 were distilled, and HF was doubly distilled. The containers were sealed and placed on a hot plate at 393 K for 24 hours. After 1 hour, the samples were removed from the hotplate and placed in an ultrasonic bath for 5 minutes before being returned to the hotplate. After 24 hours of digestion the containers were uncovered, returned to the hot plate, and the acids were allowed to evaporate. After the samples were thoroughly dried, 0.5 mL of concentrated HNO_3 was added to the sample and was allowed to evaporate on the hot plate. A further 0.2 mL concentrated HNO_3 was added and the sample allowed to evaporate. The final stage of the digestion process was the addition of 2 mL of 0.8N HNO_3 saturated with Br_2. The Savillex bombs were then sealed tightly and placed on the hotplate overnight. This final step ensured that the both platinum and iridium present were in their highest valence state which was required for subsequent column separation.

Bio-Rad AG 1X8 resin (200–400 mesh) was prepared the day before column separation by adding of 0.8N HNO_3 saturated with Br_2. Resin was added to the column and two 1-mL aliquots of 0.8N HNO_3 saturated with Br_2 were added and allowed to pass through the column. The samples were then loaded onto the column, and again two 1 mL aliquots of 0.8N HNO_3 saturated with Br_2 were added. The resin was then cleaned by adding 5 mL of 10N HNO_3 to the column. After the resin was cleaned, 10 mL of 14N HNO_3 was added to the column, eluting the Pt and Ir and the solution was collected. Samples were evaporated and then stored until analysis by MC-ICP-MS.

4.3.5 Laser ablation ICP-MS

Laser ablation ICP-MS analysis was used to determine both the possible presence of micronuggets and Pt and Ir concentrations in glasses at the Great Lakes Institute for Environmental Research, University of Windsor, Canada (see Blaine et al., submitted; Chapter 3). Laser ablation analysis was performed on polished chips of sample glass devoid of visible surface contamination using a 266nm Nd-YAG laser with 1.25 kA power and a 20Hz repetition rate. Use of a 2 mm diameter pinhole and 10X-objective resulted in a laser spot size of 140 μm and samples were analyzed by boring into the sample at a rate determined by the laser. Samples were analyzed using a Thermo Electron X Series II quadrupole ICP-MS using an argon carrier gas. Background acquisition was obtained for 60 seconds with the laser off, followed by sample acquisition for a maximum of 180 seconds. Data was collected for the following isotopes: ^{43}Ca and ^{25}Mg (high resolution, 20 ms dwell times) ^{191}Ir, ^{193}Ir, ^{195}Pt, ^{196}Pt (low resolution, 100 ms dwell times). Calcium was used as an internal standard using values obtained by electron microprobe analysis to correct for variances in ablation yield. Analyses were calibrated using a pair analyses of NIST 610 run at the beginning and end of

each acquisition set and if acquisition sets contained more than 20 analyses, a second pair of NIST analyses were performed mid way through the acquisition set. Due to poorly constrained and non-standardized values for Ir in NIST standards it was necessary to estimate Ir concentrations using Pt as an analog and adopting the sensitivity factor determined for Pt (Jenner et al., 1990). This was possible due to Pt and Ir having very similar masses and charges, although it should be noted this approximation may introduce errors in absolute values, relative values should not be affected. Using the sensitivity factors obtained for ^{195}Pt, acquired LA data were reduced and interpreted using a combination of Thermo Electron's Plasmalab software and in-house developed tools based on Longerich et al. (1996).

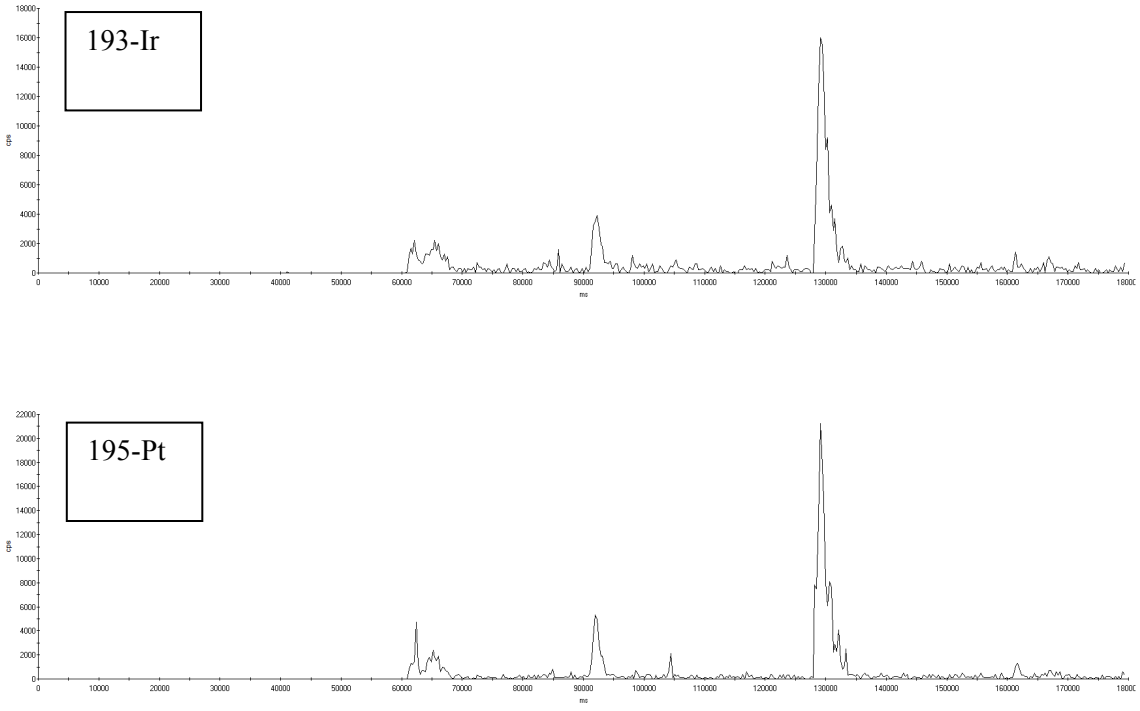

Figure 4.1 – Typical LA-ICPMS results for an LA-ICPMS analysis of run-product glasses for 195-Pt and 193-Ir showing two discreet "micronuggets" evident by the short-duration high intensity peaks in counts per second (cps) at 93000 and 130000 milliseconds (ms). The peaks are surrounded by regions of stable count rates which are used for the integration of the data to determine baseline "micronugget-free" solubilities. Laser switched on at 61000 ms and corresponding peak between 61000 and 68000 ms corresponds to an initially high ablation rate with commencement of ablation.

A typical analysis with two discreet micronuggets is shown in Figure 4.1, with the micronuggets appearing as the short-duration high-intensity peaks occurring at 93000 and 130000

milliseconds (ms). The high-intensity peak at 61000 ms corresponds to initially high ablation rates at the commencement of ablation and is not a result of micronugget ablation. Where peaks associated with micronuggets occur, they are excluded from the integrated regions in order to get a baseline concentration representing the concentration in the micronugget-free melt. As shown in Figure 4.1, the Pt and Ir peaks are coincident and the micronuggets have both Pt and Ir. Although Pt and Ir are both typically present in micronuggets, in some cases, the ablated micronuggets contain only Pt or Ir. A lower background, higher abundance made 193-Ir the most appropriate isotope for Pt concentration calculations and was used for calculating Ir concentrations.

4.4 Attainment of equilibrium

It was demonstrated by Blaine et al. (2005) that platinum concentrations reached equilibrium solubility within 48-66 hours in non-chlorine bearing experiments using the same methods used in this study. However, due to increased micronugget formation in Cl-bearing experiments, longer run durations (e.g. 96 hours and greater) were required (Blaine et al., submitted, Chapter 3) to allow reliable determinations of equilibrium solubilities using LA-ICPMS analysis. The same experiment duration cutoffs are used to determine Ir solubilities in this paper. As with Pt (Blaine et al. submitted; Chapter 3), increased Ir concentrations in the short run duration experiments, when analyzed by both ID-ICPMS and LA-ICPMS, are due to an increased abundance of micronuggets in the glasses. In the shortest run duration experiments, Ir distribution in the glasses is very inhomogeneous with a large number of micronuggets and it is not possible to measure baseline, micronugget-free concentrations. In longer run duration experiments, the micronugget distribution is more regular and reliable concentrations can be obtained using LA-ICPMS.

4.5 Results and discussion

The summary of run conditions and analytical results is given in Table 4.1. For the determination of the effect of Cl on Ir solubility in the melt, only the data obtained by LA-ICPMS can be considered due to the presence of micronuggets in the end-product glasses. ID-ICPMS analysis includes these micronuggets and the Ir concentrations in these glasses are much higher than the solubility. It was also determined that a minimum experiment length of 96 hours was required to produce glasses that had areas devoid of micronuggets so that LA-ICPMS was effective (Blaine et al. submitted; Chapter 3). Although in these shorter run duration experiments the glasses were more than likely saturated in Ir, the ubiquitous presence of micronuggets made interpretation of the LA-ICPMS analysis difficult. It is therefore considered that experiments longer than 96 hours when

analyzed by LA-ICPMS produced the most reliable results and are used for interpretation of the affects of Cl on Ir solubility.

4.5.1 Controls on solubility

4.5.1.1 Oxygen fugacity

Using the sealed-capsule technique in internally heated pressure vessels the oxygen fugacity is imposed by the intrinsic oxygen fugacity and corresponding hydrogen fugacity of the IHPV (MnO-Mn_3O_4 (Berndt et al., 2002). The capsule containing the experimental charge is permeable to hydrogen and therefore the hydrogen fugacity in the experimental charge is controlled by the intrinsic hydrogen fugacity of the autoclave which is constant. The prevailing oxygen fugacity in the capsules is a variable that is controlled by the water content of the melt through the dissociation reaction of water:

$$H_2O \leftrightarrow H_2 + \tfrac{1}{2}O_2 \qquad \textbf{Equation 4.1}$$

Increasing the water content in the melt increases the activity of water in the melt and therefore increases the oxygen fugacity of the experiment. Water activities in the experimental charges were calculated from the water content of the melt using Equation 4.2 from Burnham (1994), assuming that Cl content has little to no effect on water activity within the melt at volatile undersaturated conditions (as discussed in Blaine et al., submitted, chapter 3):

$$aH_2O = k \times (XH_2O)^2 \; at \; XH_2O < 0.5 \qquad \textbf{Equation 4.2}$$

From the water activities, the oxygen fugacity of the experiments can be calculated using Equation 4.3 (modified from Whitney, 1972):

$$\log fO_{2\,(experiment)} = \log fO_{2\,(water\ saturated)} + 2 \log aH_2O_{(experiment)} \qquad \textbf{Equation 4.3}$$

Iridium dissolves in a silicate melt through the oxidation of Ir in the metallic zero-valence state into a charged valence bonded with oxygen within the silicate melt structure. This reaction can be approximated by Equation 4.4:

$$Ir^0\,(s) + xO_{2(melt)} \leftrightarrow IrO_{2x(melt)} \qquad \textbf{Equation 4.4}$$

This reaction is dependent on oxygen fugacity and the valency of Ir can be estimated from the relation between Ir solubility and oxygen fugacity (Equation 4.5), where the valence of Ir is equal to 4x:

$\log [Ir] = x \log fO_2 + constant$ **Equation 4.5**

Figure 4.2 provides a compilation of previous studies (Borisov and Palme 1995; O'Neill et al. 1995; and Brenan et al, 2005) and the data of this study and shows the variation in Ir solubility with varying oxygen fugacity. Due to the low activities of Ir in these experiments and a detection limit of 2ppb, corrected solubilities less than approximately 50ppb are beneath the quantification levels ($[5 \times detection\ limit] \div aIr$), of the LA analysis indicated on Figure 4.2, and are not used for further calculations. The results of this study can be compared directly with those of Borisov and Palme (1995) and O'Neill et al. (1995) which use the same Fe-free haplobasaltic melt composition. It should be noted that this study was conducted at slightly lower experimental temperatures. Brenan et al. (2005) uses a Fe-bearing basaltic melt and, although shown on Figure 4.2 for demonstration purposes, should not be directly compared to this study.

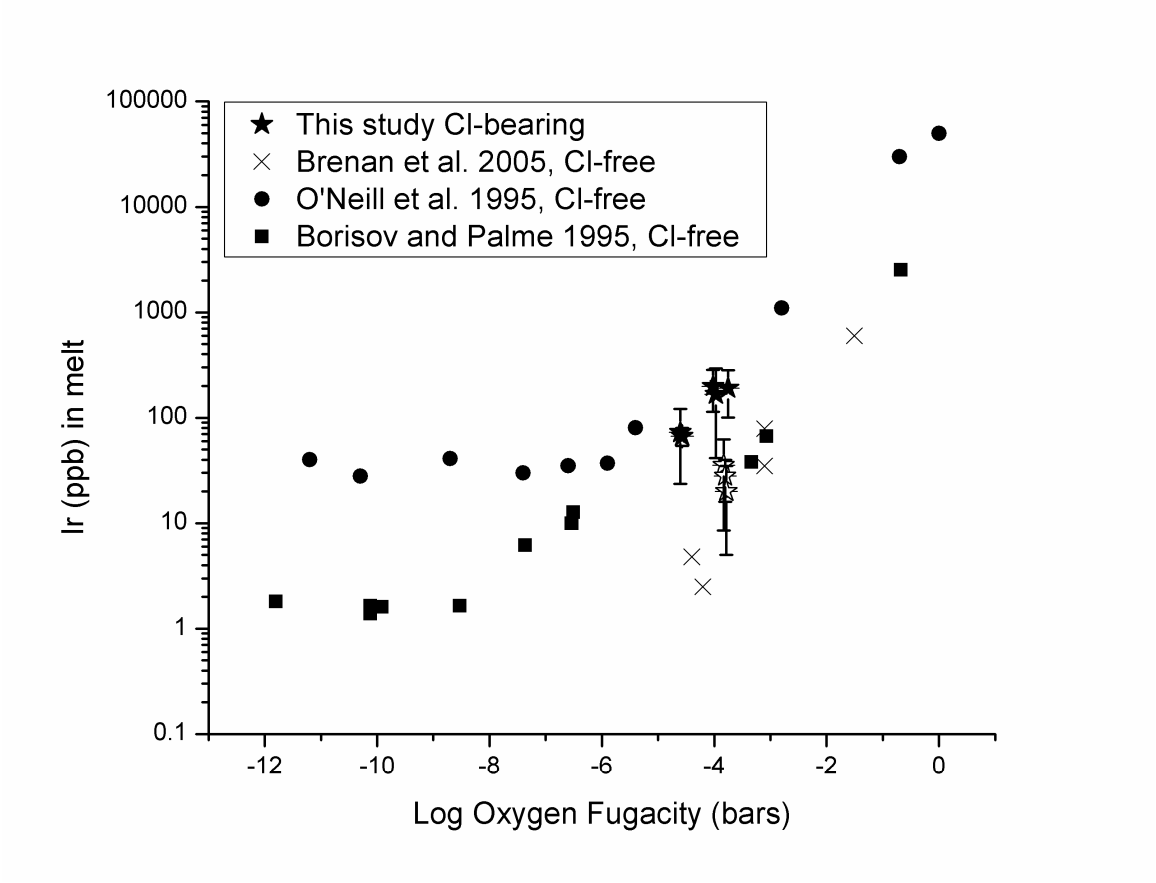

Figure 4.2 - Summary of historical data and the data from this study. Values below quantification levels of the technique for this study are shown as open symbols. Quantifiable data of this study fall on a linear trend between low oxygen fugacity data of Borisov and Palme (1995) and high oxygen fugacity data of O'Neill et al. (1995). Data of Brenan et al. (2005) are for a Fe-bearing melt and fall below those of the other studies using Fe-free melt compositions, although solubility trends are consistent.

The data of Borisov and Palme (1995) and O'Neill et al. (1995) show a deflection from a trend of decreasing Ir solubility with decreasing fO_2, causing a minimum apparent solubility below which there is no deviation in Ir solubility with oxygen fugacity. This trend is attributed to the formation/inclusion of micronuggets at lower oxygen fugacities and is not believed to be the result of Ir dissolved in a zero-valent state within the melt. As shown in Figures 4.3 and 4.4, the data of this study plot well between the low fO_2 data ($<10^{-6}$ bars) of Borisov and Palme (1995) and the high fO_2 data ($>10^{-3}$ bars) of O'Neill et al. (1995) and produce a consistent linear trend of log[Pt] for oxygen fugacities ranging from 10^{-9} to 10^{1} bars. This indicates that any effect of Cl on Ir solubility observed in this study is slight and the overriding control on Ir solubility is oxygen fugacity. Fitting a slope of ½, corresponding to a 2+ valence for Ir (Equation 4.5), through the data provides a very good

correlation and generates a relation between Ir solubility and oxygen fugacity given in Equation 4.6, and shown in Figure 4.4.

$\log [Ir] = 0.5 \log fO_2 + 4.234$ adj. R-squared = .873 Equation 4.6

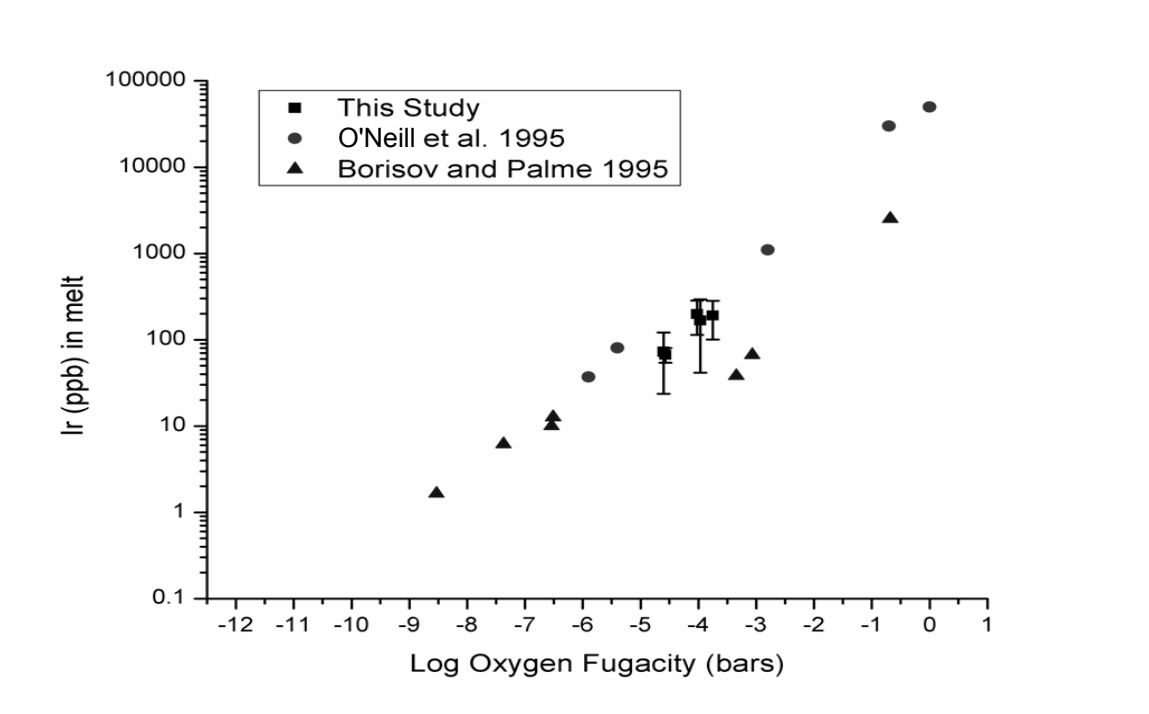

Figure 4.3 – Selected data from Borisov and Palme (1995) and O'Neill et al. (1995) (explained in text) and the data of this study showing a strong linear correlation on a log-log plot of Ir solubility and oxygen fugacity.

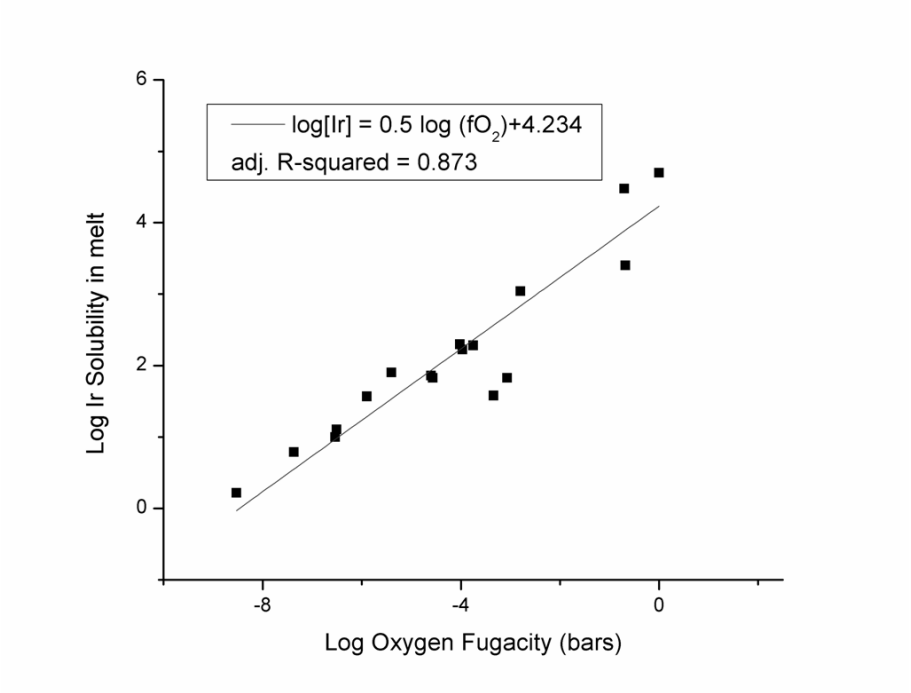

Figure 4.4 – Plot of a fixed slope of ½, corresponding to a 2+ valence state for Ir, through the data of this study and selected data of Borisov and Palme (1995) and O'Neill et al. (1995).

All of the data of this study fall along this line, within the error of analysis. However, the slight negative bias could be due to the underestimation of the sensitivity factor for laser ablation interpretation and/or the slightly lower experimental temperatures of the current experiments; Borisov and Palme (1995) determined a slight positive temperature dependence of Ir solubility with temperature. In Blaine et al. (2005), it was possible to perform a non-linear regression for Pt solubility against oxygen fugacity to estimate the influence of Pt^{4+} in the melt. Non-linear regression of the form of Equation 4.7, using the Ir solubility data of Borisov and Palme (1995) and O'Neill et al. (1995) could not produce a better fit than the linear regression with a fixed slope of ½ and did not show any perceivable influence of Ir^{4+} in the solubility data.

$$[Ir]_{(total)} = a\,(fO_2) + b\,(fO_2)^{1/2} \equiv [Ir^{4+}] + [Ir^{2+}] \qquad \textbf{Equation 4.7}$$

4.5.1.2 Evaluation of the effect of water and Cl on the solubility of Ir

Initially, the study was designed to provide series of data with varying Cl contents at specific oxygen fugacities to provide a means of interpreting the effect of Cl and water content on Ir solubility. However, due to analytical difficulties of lower run duration experiments and values near detection limits, the dataset has become significantly reduced. In order to evaluate the effect of H_2O and Cl on the solubility of Ir, a less direct approach must be utilized. If it can be assumed that Ir dissolves in the 2+ valence state, which all experimental data indicate, then it is possible to calculate the relative deviation (RD) from that trend (Equation 4.7) and compare that to the water and Cl content to identify any effects of either Cl or water. An effect of either volatile will be seen as a systematic deviation, with varying mole fraction of the volatile, from the calculated solubility. By contrast if there is no effect, no trends should be evident and any variation should be random.

$$\frac{\left([Ir_{ppb}]_{observed} - [Ir_{ppb}]_{calculated}\right)}{[Ir_{ppb}]_{calculated}} \qquad \textbf{Equation 4.8}$$

Figure 4.5 shows the relative deviation from the calculated trend in Ir solubility with varying water contents. No systematic variation is noted which would indicate that water does not have a direct effect on Ir solubility outside of varying the oxygen fugacity; all data are negatively biased (as discussed above) but produce a random distribution.

In order to clearly demonstrate any effect of Cl evident in these experiments, the relative deviation calculated in Equation 8 above is calculated using an equation of Ir solubility as a function of oxygen fugacity that is forced to include the Cl-free solubility (PtIr-2; 67ppb, $\log(fO_2) = -4.75$) as determined in this study (shown in Equation 4.9)

$$\log [Ir] = 0.5 \log fO_2 + 4.11 \qquad \textbf{Equation 4.9}$$

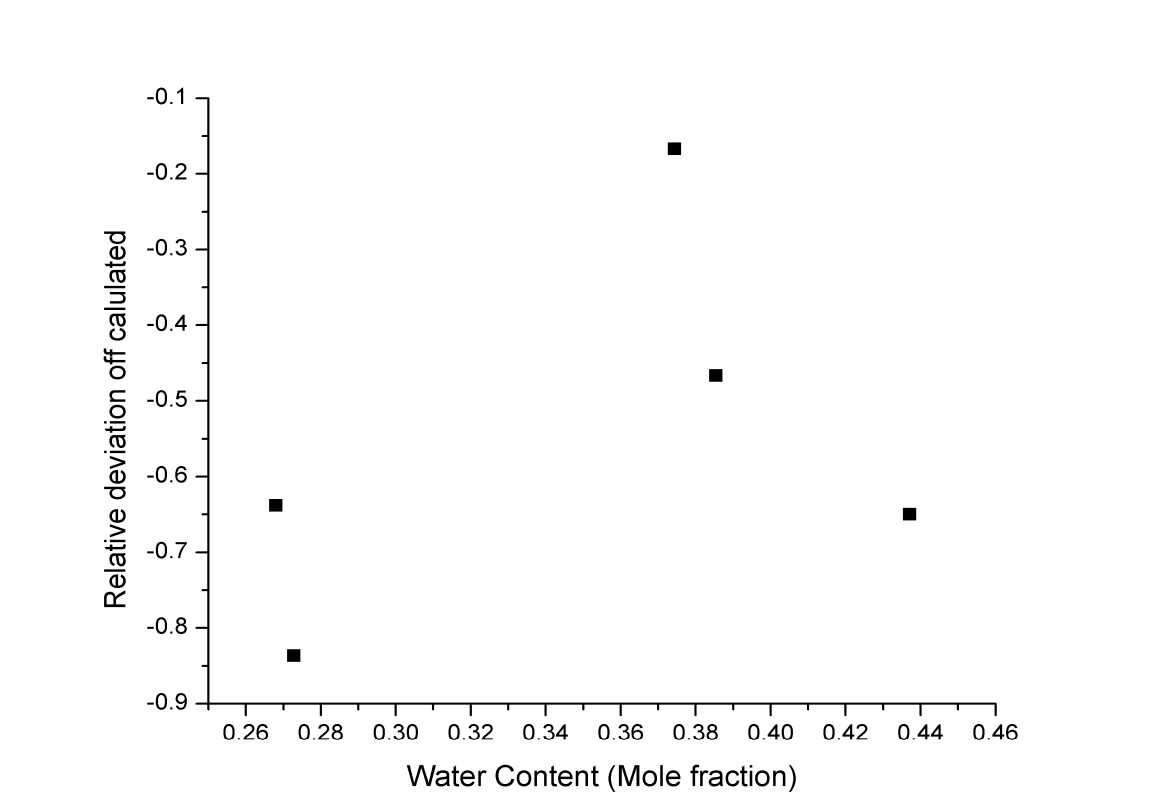

Figure 4.5 – Variation in relative solubility with varying water content. Data indicate negative bias but show no systematic variation that would indicate that water content has an intrinsic effect on Ir solubility (explained in text)

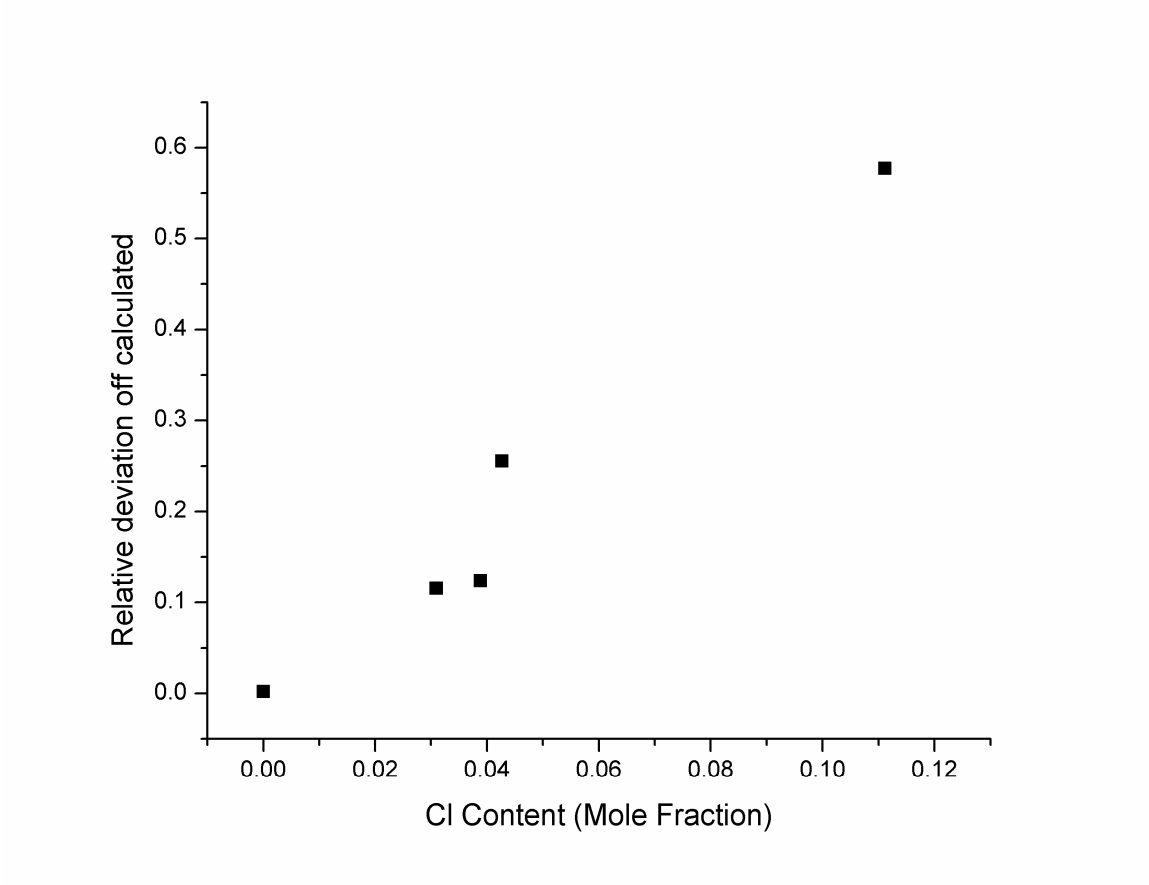

Figure 4.6 – Variation in relative solubility with varying chlorine content. Data show a systematic variation, indicating that Ir solubility is influenced by chlorine content in the melt, suggesting chlorine complexing (explained in text).

Figure 4.6 shows a well developed trend of increasing deviation from calculated Ir solubility with increased Cl content. This result indicates an increase in Ir solubility relative to the calculated Ir^{2+} solubility trend with increasing Cl content. Increased solubility of Ir with increasing Cl content is strong indication for Cl-complexing of Ir in the silicate melt. The increase in solubility appears to be minor with a 60% relative increase in solubility with an increase in mole fraction Cl in the melt (X_{Cl}) from 0 to 0.15 (i.e. from 0 to 2.75 wt. % Cl); however, a lack of data at a specific oxygen fugacity precludes a calculation of the stoichiometry of the Pt-Cl complex.

4.5.2 Estimating Ir solubility in a Cl-bearing volatile phase

Because the starting glasses have low Ir concentrations and chlorine has only a moderate effect on Ir solubility in the melts, the source for the excess Ir present within the experimental glasses of short run duration experiments must be the fluid. In experiments with shorter run durations and

anomalously high Ir concentrations as analyzed by ID-ICPMS, the "extra" Ir can be attributed to the fluid phase(s). It is therefore possible to estimate the Ir concentration in the fluid through mass balance using the same method as used in Blaine et al., (submitted; Chapter 3) for Pt and represented by Equation 9. All assumption outlined for Pt in Chapter 3 are also applicable for Ir. Results of these calculations are summarized in Table 4. 2. From these calculations, it is evident that the Cl-bearing fluids present in these capsules prior to dissolution into the glass (up to ~1448K) can contain very significant amounts of Ir, up to hundreds of ppm. However, lack of constraint on the system conditions and evidence that not all Ir contained in the fluid is still present in the glass make it a rough albeit significant estimate.

$$Ir_{fluid} = [Ir_{ID-ICPMS} - Ir_{calculated}] \times \frac{m_{glass}}{m_{fluid}} \qquad \textbf{Equation 4.10}$$

Table 4.2 – Tabulated results of Ir concentration in the fluid phase

Sample	Ir_{melt} (ppb) ID-ICPMS	Ir_{melt} (ppb) Calculated (Cl-free)	H_2O_{melt} content (wt. %)	Cl_{melt} content (wt. %)	Calculated Ir content of Fluid (ppb)
PtIr-8	7767	164	3.59	1.79	134000
PtIr-9	4058	126	2.96	1.85	78000
PtIr-10	973	67	2.03	2.75	18000
PtIr-11	4245	81	2.25	2.25	88000

4.6 Importance of Cl-complexation and implications

Recently, Botcharnikov et al. (2010) demonstrated Cl-complexing of Au in silicate melts and Farges et al. (2006) also showed that Mo-S complexing is possible in silicate melts. Evidence that Cl-complexing occurs for Ir holds important implications for the modelling of PGE deposits in layered intrusions even more so if the potential for Cl-complexing in silicate melts exists for all PGEs (inconclusive for Pt; Chapter 3, submitted).

Using isotopic evidence, it has been shown that the Cl found in the Bushveld deposit was introduced with the parental magma, and was not from an outside source (Willmore et al., 2002). The presence of Cl can have a multistage effect on PGEs in the magma. Firstly the presence of Cl in the magma can allow for enhanced solubility of PGEs in the magma as shown in this study for Ir.

This could at least partially account for the apparently elevated, above saturation levels of PGE (Blaine et al., 2005; Borisov et al, 1994; and Ertel et al. 1999) in the parental magmas for the Bushveld and Stillwater deposits (Naldrett et al., 2009). Secondly, because Cl is an incompatible element, during crystallization Cl contents would continue to increase in the residual melt, further increasing the residual magma's capacity for the PGEs. This would allow the PGEs to concentrate in the residual magma without becoming saturated and forming PGE alloys, or forcing them out of solution. Water and Cl concentrations would continue to rise with crystallization and upward migration of the residual magma, due to compaction and density differences and would cause the PGEs to be transferred along with the residual magma to higher elevations in the magma chamber.

Furthermore, following the processes involved in the melt, in the case of the vapour refinement model (Boudreau, 1999; Boudreau and Meurer, 1999) the behaviour observed in these experiments could be especially important. Upon saturation, Cl would partition strongly into the aqueous fluid and/or brine mixture (Webster et al., 1999). The reduced Cl levels in the magma would cause an abrupt decrease in solubility of the PGEs, forcing them out of the silicate melt.

Upon saturation of an interstitial Cl-rich fluid, Ir contained within the melt will be partitioned into that fluid phase, owing to the high fluid-melt partition coefficients. If the interstitial exsolved fluid travels upwards through a crystallizing magma due to settling and compression, and fluid interacts with an overlying volatile undersaturated melt, the fluid will dissolve into the melt leaving residual Ir micronuggets behind, analogous to the processes involved in these experiments. This process could be repeated with the undersaturated melt crystallizing and eventually exsolving a fluid which in turn could dissolve and transport the Ir further up the column. Upon saturation of the melt in sulfide, a sulfide melt would form and the Ir micronuggets could be readily scavenged by the sulfide resulting in an Ir-rich sulfide melt.

The experiments summarized herein demonstrate that it is possible to enrich and transport Ir in a Cl-bearing fluid phase and in Chapter 3 it was demonstrated a similar behaviour is possible for Pt. Furthermore, it follows that other PGEs may behave similarly, to varying extents. The moving front of PGE saturation caused by the above scenario could possibly help to explain the reef structures of PGE occurrences in layered intrusions.

4.7 Conclusion

As with platinum in Blaine et al. (2005) and Chapter 3 the sealed capsule technique paired with LA-ICPMS analysis has allowed for the determination of Ir solubility as a function of both water

content (oxygen fugacity) and chlorine content. Water has no intrinsic effect on Ir solubility under the range of conditions of this study. Iridium has been determined to be dissolved in the melt in a 2+ valence state with no evidence of Ir 1+ or 4+ over the range of fO2 conditions covered by these experiments. In contrast to platinum, which did not show any compelling evidence of Cl-complexing in the melt, Ir shows an apparent increase in solubility with increasing Cl content with a relative increase of approximately 60%. More work needs to be done to constrain the behaviour of Ir with respect to Cl content at varying oxygen fugacities to determine the speciation of Ir within the melt. Mass balance calculations have allowed the calculation of Ir solubilities in a Cl–bearing fluid which range from 18 to 134 ppm, allowing for the possibility for Ir to be transported and enriched in magmatic Cl-bearing fluids.

Chapter 5 – The effect of CO_2 on the solubility of Pt in a haplobasaltic melt at 1523K and 0.2 GPa and evidence for Pt-carbonyl complexing in magmatic fluids

5.1 Introduction

Carbon dioxide plays an important role in many mafic-ultramafic magmatic systems. Although CO_2 is not as prevalent, or as influential on melt properties as water, mafic melts generally become saturated first in CO_2. The fluids that are generated at CO_2 saturation are generally mixed H_2O-CO_2 fluids with water present in the silicate melt being partitioned from the silicate melt and into the fluid (Botcharnikov et al., 2005; and references therein). These mixed fluids have the potential to be powerful enrichment and transportation media for metals. Analysis of fluid inclusions from the PGE-bearing Merensky Reef of the Bushveld igneous complex in South Africa indicates that mixed H_2O-CO_2 fluids were present during the formation of the Merensky Reef (Ballhaus and Stumpfl, 1986) and may have played a role in the transport and enrichment of the PGE hosted within. To date the behaviour of PGE in CO_2-bearing fluid-melt systems has not been studied to address the fact of whether mixed H_2O-CO_2 fluids have the capacity to transport PGE and what the effect of CO_2 is on the solubility of PGE in a silicate melt.

Although carbon dioxide is used to control oxygen fugacity in nearly every experimental study looking at metal solubility in 1-atm mixed-gas furnaces, to the author's knowledge the effect of CO_2 on metal solubility in silicate melts has never been assessed in literature. Carbon dioxide solubility is very low in silicate melts at 1 atm; however, it has been noted in previous studies that there is a change in the behaviour of Pt solubility at low oxygen fugacity conditions, generally corresponding to the conditions where a carbon dioxide/carbon monoxide mixture is introduced to control oxygen fugacity (Borisov and Palme, 1994; Ertel et al., 1999). Under these reduced conditions, PGE solubility studies show micronugget formation/contamination, causing an increased apparent solubility in the melt when using a bulk solution analytical method (Borisov and Palme 1994; Ertel et al., 1999; Amosse et al., 2000). It was postulated (Ertel et al., 1999) that the formation of micronuggets could be a result of the formation of PGE-carbonyl complexes in the presence of CO/CO_2, however no follow up studies were conducted.

At increased pressures, relevant to the conditions of magmatic ore-forming systems, CO_2 solubility is increased and any subtle effects of CO_2 on metal solubility present at low pressure could be substantially increased. In this chapter, the effect of CO_2 on Pt solubility is assessed for a haplobasaltic melt at relevant magmatic P-T-oxygen fugacity conditions through experiments using the methods outlined in Chapter 1 and adding varying amounts of CO_2 to the hydrous haplobasaltic system. Solubility is investigated for a range of CO_2 contents up to saturation including experiments at saturation where the silicate melt coexists with a free fluid phase.

5.2 Experimental methods

Platinum solubility was determined for a hydrous, CO_2-bearing, Fe-free basalt melt at increased pressure and temperature using a sealed-capsule technique, modified from that used in Chapters 2 (Blaine et al., 2005) and 3. The method described in Chapters 2 and 3 was modified with the addition of a CO_2 source while maintaining approximately 1 wt. % water, due to temperature limitations of the internally heated pressure vessel (IHPV). While providing rapid quench and redox control, which are essential for studies of this nature (Blaine et al. 2006, Chapter 2), the temperature is limited to 1523K and is not sufficient to melt the diopside-anorthite eutectic composition under H_2O-absent conditions. By maintaining approximately 1% water in the experiments the liquidus temperature was reduced sufficiently to allow complete melting under experimental conditions at 1523k and 0.2 GPa. The solubility of CO_2 in the silicate melt at experimental conditions is low (~2500ppm, discussed later) and as CO_2 is added in greater concentrations, the experiments will become saturated in CO_2 and concentrations of CO_2 in the glass will vary based on the CO_2:H_2O ratio in the fluid phase.

Experimental charges were prepared by sealing approximately 300mg of glass with a composition corresponding to that of the eutectic point of the dry diopside-anorthite system ($An_{42}Di_{58}$, the same composition as in Chapters 2 through 4 and described therein) in a Pt capsule (25mm length x 4mm outer diameter/3.6mm inner diameter), along with distilled water (approx. 1 wt. %) and a source of carbon dioxide. Prior to loading, the glass was powdered to a grain size <200μm to increase homogeneity. One of two separate sources of CO_2 was used for each experiment; either silver oxalate (AgC_2O_4, with 96% liberation of CO_2 upon thermal decomposition, ranging from 2.55-14.13 mg added) or calcium carbonate ($CaCO_3$, ranging from 0.54 - 2.02 mg added). Early experiments in this study used silver oxalate as the CO_2 source which was subsequently replaced by the carbonate mixture after early experiments using silver oxalate showed a ubiquitous presence of micronuggets in the resultant experimental glasses. The potential for Ag-Pt complexes to form,

causing the formation of micronuggets, lead to the modification of the technique to use $CaCO_3$ as a metal-free CO_2 source. The presence of micronuggets in the resultant experimental glasses is discussed in detail later in this chapter.

In these experiments, the capsules containing the experiment were composed of pure platinum and were used as the source of Pt for the saturation of the melt. For solubility calculations, the activity of platinum is assumed to have been unity at the P-T-X conditions of the experiments and the effect of pressure on metal activities is assumed to be negligible. In silver oxalate bearing experiments the activity of Pt was assumed to be one although the formation of a Ag-Pt alloy could reduce the activity of Pt, though the reduction would be slight (Ag:Pt ratio >300).

All experiments were conducted at the Institut für Mineralogie at the Leibniz University of Hannover, Germany, in a vertically mounted, internally heated pressure vessel equipped with a rapid quench device. This apparatus allows the melt to be quenched to a crystal- and bubble-free glass at a cooling rate of >200 K/min (Berndt et al., 2002). The oxygen fugacity of the experiments is imposed by the intrinsic hydrogen fugacity of the autoclave. The intrinsic fH_2 is well characterized through multiple experiments at different temperatures and the corresponding fO_2 falls on the $MnO\text{-}Mn_3O_4$ buffer curve at water-saturated conditions (Berndt et al., 2002). Experiments were conducted at 1523 K ± 10 K and 200 MPa + 0.4/ -0.02 MPa. The fO_2 at water-saturated conditions is calculated from O'Neill and Pownceby (1993) to be $10^{-3.6}$ bar.

Temperature was controlled using two S-type thermocouples and was monitored with the use of two additional S-type thermocouples. In a previous study on the investigation of the effect of water on Pt solubility in a synthetic basalt at the same P-T conditions (Blaine et al., 2005, Chapter 2), time series experiments were used to demonstrate that equilibrium between the Pt capsule and melt is reached between 48 and 65.5 hours (using the same melt composition and amount of added glass as in this study). All of the experiments in this study were run for at least 48 hours, except for two instances for which it was necessary to quench at 46 hours.

After quenching, the samples were removed from the sample holder and weighed to ensure that there had been no loss of water during the experiment. The experimental glasses were removed from the capsule and broken into 3 or 4 large pieces for various analyses. No visible Pt contamination was noted on the exterior of the glass samples, but steps were taken (see Chapters 2 through 4) to ensure that there was no surface contamination prior to Pt analysis. All end-product glasses were clear with no noticeable coloration or crystallization. Individual run conditions and results are summarized in Table 5.1.

5.3 Analytical methods

5.3.1 Fourier Transform Infrared Spectroscopy (FTIR)

Selected pieces of run-product glasses were prepared as ~500μm thick, doubly polished sections for FTIR analysis for water and a second ~90μm thick section for CO_2 for analysis by FTIR using a Bruker IFS 88 spectrometer outfitted with an IR-Scope II microscope. Sample thicknesses were measured to within +/- 2μm using a digital micrometer. Individual analytical conditions for H_2O and CO_2 are outlined below. The Lambert-Beers equation (Equation 1) was used to calculate volatile contents in the glasses (Fine and Stopler 1986; Ohlhorst et al. 2001,) using a calculated density of 2700 g l^{-1} for a diopside-anorthite melt with 1 wt. % water (calculated using the Appen method; Appen, 1952). Measurement error is introduced by instabilities in the baseline, which varied by up to 0.003 absorbance units for water and .002 absorbance units for CO_2. The observed instabilities result in an estimated maximum variation in absolute water content of 0.07 wt. % and in CO_2 content of 50 ppm.

$$\boldsymbol{Weight\ Fraction}\ (\boldsymbol{x}) = \frac{\boldsymbol{m_x \times a}}{\boldsymbol{\rho \times d}} \times \frac{\boldsymbol{1}}{\boldsymbol{\epsilon}} \qquad \textbf{Equation 5.1}$$

Where:

x is the compound of interest

a is the absorbance of the band of interest

m is the molecular weight of x in $g \cdot mol^{-1}$

d is the thickness of the sample in cm

ρ is the density of the sample in $g \cdot l^{-1}$

ε is the absorption coefficient in $l \cdot mol^{-1} \cdot cm^{-1}$

5.3.1.1 Water

Near-infrared (NIR) (6000-4000 cm^{-1}) spectra with a resolution of 4 cm^{-1} were collected to determine of water content using a tungsten light-source, a CaF_2 beam-splitter, and a mercury cadmium telluride (MCT) narrow range detector. Using a slit aperture of 150 μm x 150 μm, multiple measurements were made on the same polished section to determine average water concentrations and homogeneity within a given sample. Absorbances were determined for the 5200 cm^{-1} H_2O and

4500 cm^{-1} OH bands using straight-line baseline correction (Ohlhorst et al. 2001) for each peak. A linear absorption coefficient (ε) of 0.56 l mol^{-1} cm^{-1} for the H_2O and OH bands was used, as per Ohlhorst et al. (2001).

5.3.1.2 Carbon Dioxide

Mid-infrared (MIR) spectra (1200 – 4000 cm^{-1}) with a resolution of 2 cm^{-1} were collected for the determination of CO_2 contents using a globar light source, a KBr beam-splitter and a narrow range MCT detector. Using a slit aperture of 100 μm x 100 μm, multiple measurements were made on the same section to determine the concentration and distribution of CO_2 within the sample. Absorbance was measured using the 1522 cm^{-1} carbonate band of the two-band, 1300-1600 cm^{-1} system using a straight-line baseline correction. For concentration calculations a linear absorption coefficient (ε) of 398 l mol^{-1} cm^{-1} for the carbonate bands, as per Jendrzejewski et al., 2001.

5.3.2 Pt Analysis

All resultant glasses from this study were analyzed for platinum using the techniques and methods outlined in Chapters 2 and 3. All glasses were analyzed by bulk-solution isotope-dilution ICP-MS (ID-ICPMS) with follow-up laser ablation ICP-MS (LA-ICPMS). Initial analysis by laser ablation (CO_2-1 through CO_2-11) was only performed to assess the presence of micronuggets and was not used for quantification. It was observed that the addition of CO_2 to the haplobasalt-H_2O system caused an increase in the amount of micronuggets that are formed, as compared to the CO_2-free system observed in Chapter 2. This behaviour is believed to be analogous to the processes of micronugget formation discussed in Chapters 3 and 4 for Cl, and is discussed in detail later within this chapter. However, from an analytical standpoint the abundance of micronuggets was not as severe for CO_2–bearing glasses as compared to Cl-bearing glasses in Chapters 2 and 3, and as a result longer run times were not required to develop nugget-free regions in the glasses that were large enough to be analyzed and quantified by LA-ICP-MS (Figure 5.1).

Table 5.1 – Summary of experimental conditions and analytical results

Sample Name	CO_2 Source	Duration (h)	CO_2 Added (ppm)	$CO_{2(melt)}$ Measured $(FTIR)_{(b)}$	H_2O Added (Wt.%)	$H_2O_{(melt)}$ - Measured $(Wt.\%)_{(c)}$	Log Oxygen Fugacity (bars)	$Pt_{(melt)}$ (LA) $(ppb)_{(d)}$	$Pt_{(melt)}$ (ID) (ppb) +/- 5%	Calculated $Pt_{(melt)}$ (ppb) CO_2-free
CO_2-1	$Ag_2C_2O_4$	65	12900	1620	.94	n.a.	-5.5	n.a.	39	13
CO_2-2	$Ag_2C_2O_4$	48	12900	2430	.91	.72	-6.1	n.a.	46	7
CO_2-3	$Ag_2C_2O_4$	21	12600	2320	.91	.73	-6.1	n.a.	59	7
CO_2-4	$Ag_2C_2O_4$	48	6600	2000	.96	.95	-5.7	n.a.	59	11
CO_2-5	$Ag_2C_2O_4$	48	8700	2510	.93	.92	-5.7	n.a.	58	11
CO_2-6	$Ag_2C_2O_4$	48	2400	1630	.98	.94	-5.7	n.a.	16	11
CO_2-7	$Ag_2C_2O_4$	48	10500	2350	.94	.88	-5.8	n.a.	$3222_{(e)}$	10
CO_2-8	$Ag_2C_2O_4$	48	12000	2410	1.01	.93	-5.7	n.a.	638	11
CO_2-9	$Ag_2C_2O_4$	48	6100	1980	.94	.90	-5.7	28(6)	674	10
CO_2-10	$Ag_2C_2O_4$	48	3300	1850	1.02	1.25	-5.3	80(37)	505	18
CO_2-11	$Ag_2C_2O_4$	48	5500	2100	1.01	1.24	-5.3	19(5)	367	18
CO_2-12	$Ag_2C_2O_4$	48	3400	1580	.98	.90	-5.7	120(42)	499	10
CO_2-13	$CaCO_3$	46	1000	$n.a._{(a)}$	.95	$n.a._{(a)}$	-5.7	7(2)	101	11
CO_2-14	$CaCO_3$	46	800	$n.a._{(a)}$	.96	$n.a._{(a)}$	-5.6	7(2)	28	11
CO_2-15	$CaCO_3$	85	2600	$n.a._{(a)}$	.75	$n.a._{(a)}$	-6.0	11(2)	271	7
CO_2-16	$CaCO_3$	85	1200	$n.a._{(a)}$	.99	$n.a._{(a)}$	-5.6	19(4)	128	12
CO_2-17	$CaCO_3$	123	3000	$n.a._{(a)}$	.96	$n.a._{(a)}$	-5.6	9(2)	349	11

a – Concentrations not determined by FTIR, for calculations and display the amount added is used (explained in text)
b – error on analysis +/- 50 ppm
c – error on analysis +/- 0.07 wt. %
d – 1-sigma error on analysis given in brackets
e – Probable surface contamination, excluded from calulations

Cl-5 – 74 hours, 976 ppb Pt (LA-ICPMS)

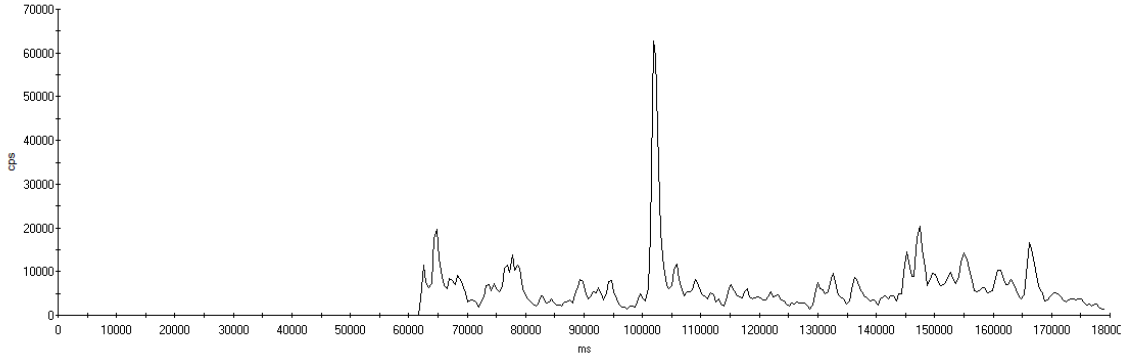

CO_2-13 – 46 hours, 7 ppb Pt (LA-ICPMS)

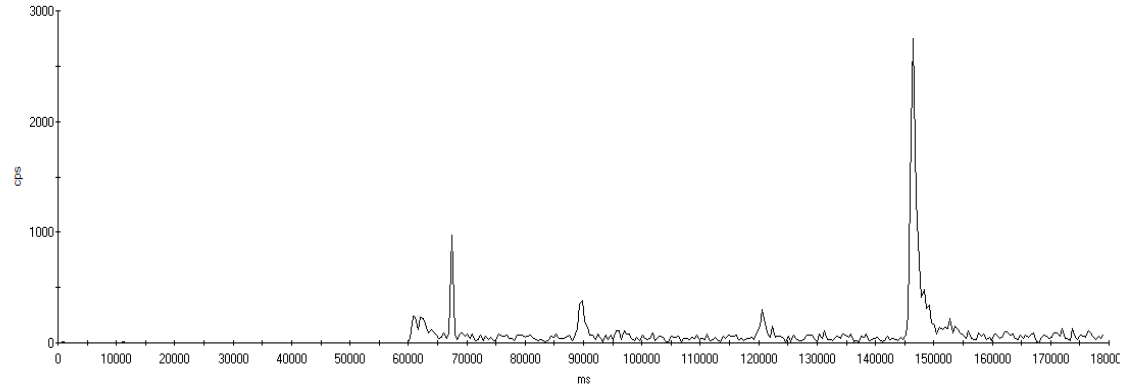

Figure 5.1 – LA-ICPMS spectra of a 74 hour chlorine-bearing experiment (Cl-5) and a 46 hour CO_2-bearing experiment (CO_2-13) showing the difference in micronugget distribution. Note that although CO_2-13 has a shorter run duration the distribution of micronuggets is more distinct and exclusion of micronugget signals is possible after a shorter run duration in CO_2 bearing experiments.

5.4 Results and discussion

5.4.1 Evolution of experiments

Silver oxalate was used in initial experiments as the source of CO_2. Initial analysis of these experiments by bulk solution isotope dilution ICP-MS indicated elevated levels of Pt in the glasses compared to the CO_2-free experiments of Blaine et al. (2005). Subsequent laser ablation analysis indicated the presence of Pt-bearing micronuggets in the experimental glasses, increasing in frequency with increasing CO_2 added to the capsule. In these early studies, LA-ICPMS was used

solely to check for inhomogeneities in PGE distribution (as per Blaine et al., 2005) as the analytical protocol was not yet optimized for determination of Pt concentrations at the low levels present in the run-product glasses.

The presence of the micronuggets was initially attributed to two possibilities; alloying of Pt with silver retained in the glass during the breakdown of the silver oxalate or the potential formation of Pt-carbonyl complexes, present as a colloidal suspension within the melt. Pt-carbonyl complexing was noted as a potential complicating factor causing micronugget formation in experiments performed in gas mixing furnaces at reduced oxygen fugacity, when CO/CO_2 mixtures are used (Ertel et al., 1999). Using the analytical techniques available it was not possible to distinguish the nature or source of the Pt micronuggets. As well, correlations could not be determined between Pt and Ag due to the use of silver paint in previous preparation of the samples for EMPA analysis. As a result of these two factors, the initial technique and initial experiments were abandoned.

Subsequently a modified experimental technique was implemented using $CaCO_3$ as the source for CO_2, somewhat analogous to the use of the Mg:Cl mixture used in Blaine et al. 2010, Chapter 2 and Chapter 3. Due to the small amounts of total carbonates added it was possible to add only $CaCO_3$ (fraction of a weight percent CO_2 versus weight percent Cl) without substantially changing the melt composition and a $CaCO_3$ and $MgCO_3$ mixture was not required. Using a silver-free CO_2 source it was possible to assess whether micronugget formation was potentially due to the formation of Ag-Pt alloys or whether micronugget formation was also as abundant in Ag-free melts and thus related to other mechanisms.

5.4.2 Solubility behaviour of CO_2 and H_2O

In all experiments measured by FTIR (CO_2-1 through CO_2-12), the water and CO_2 were distributed uniformly throughout the resultant glass. The concentration of CO_2 in the glass varies in the experiments from 1575 ppm to 2508 ppm and varies linearly, increasing with increasing amount of CO_2 added to the capsule, Figure 5.2. The concentrations of CO_2 obtained in this study are significantly higher than those determined for basalt at similar conditions by Botcharnikov et al. (2005) who determined CO_2 solubility at 1473K and 0.2GPa to be approximately 1000 ppm at 1 wt. % water in a synthetic ferrobasalt. The cause of this discrepancy is at this point unknown and may be due to the compositional differences (basalt vs. ferrobasalt) between the two studies. However, it was indicated in Botcharnikov et. al 2005, that at 0.5 GPa there is a strong effect of water on CO_2 solubility, increasing CO_2 solubility to from a modeled 2500 ppm (Newman and Lowenstern, 2002) to approximately 7000 ppm in a synthetic ferrobasalt. It is possible that this effect is evident at lower

pressures for the composition observed in this study. The majority of water contents measured in the resultant glasses were found to be lower (~5-20 wt. % relative) than estimated from the amount of water added to the capsule. In general, this discrepancy increases with increasing amounts of excess CO_2 (CO_2 added minus CO_2 measured), indicating that some water is drawn from the melt and into the fluid phase by the CO_2-rich fluid, which would be expected due to fluid melt partitioning of H_2O and CO_2 (Botcharnikov et al., 2005). There is no evidence that the addition of CO_2 affects the total solubility of water in the melt (Botcharnikov et al., 2005) and will only affect the concentration of water in the melt for a total given water content. Water activity can still be estimated from the concentration of water in the melt and therefore calculation of oxygen fugacity based on the water content in the glass (explained in detail in Chapters 1-3) is assumed to be valid.

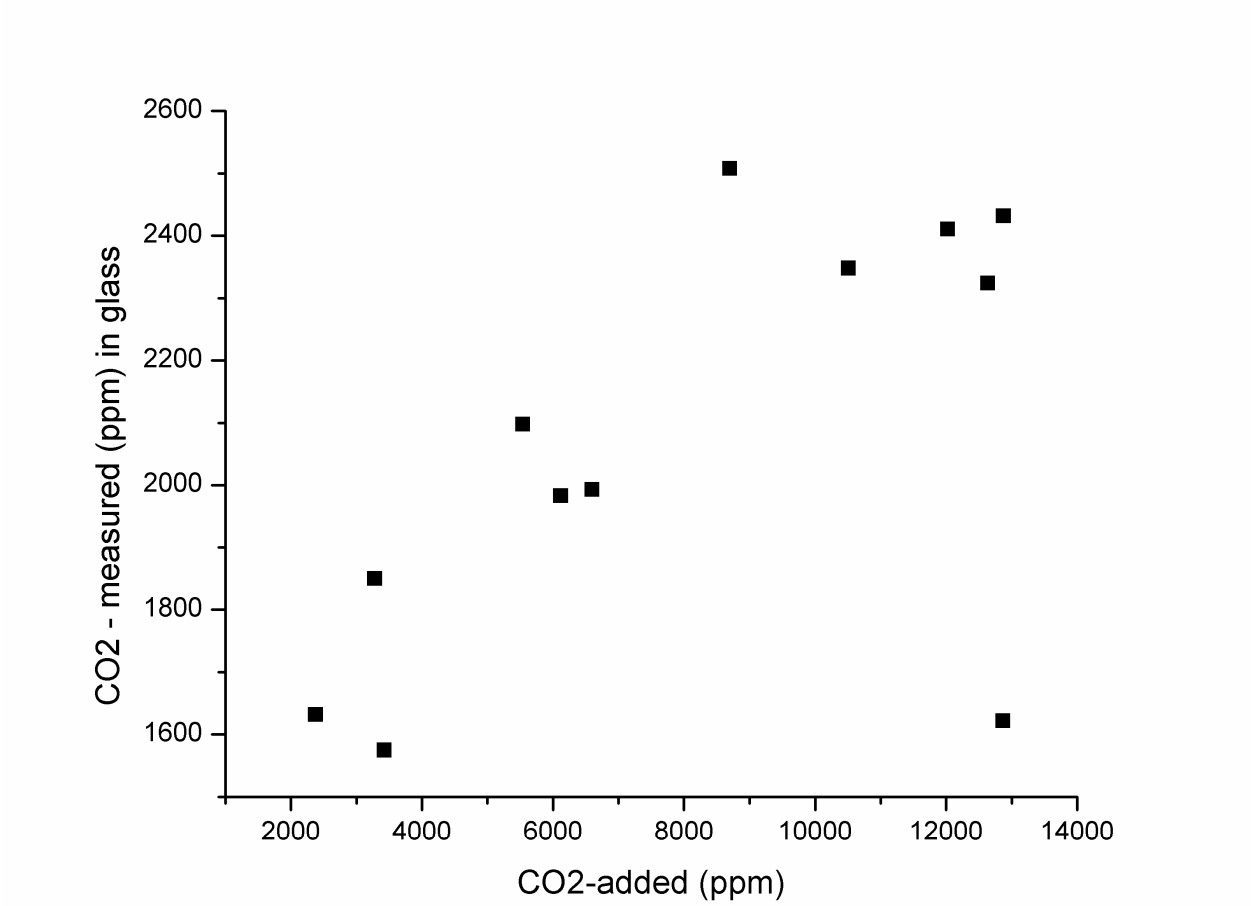

Figure 5.2- Variation in measured CO_2 content in glasses as a function of the CO_2 added to the experimental charge showing increasing CO_2 content in glasses with increased CO_2 added.

5.4.3 Estimation of oxygen fugacity

Oxygen fugacity is imposed by the IHPV and is controlled through the dissociation of water in the experiment; it is therefore highly dependent on the water content of the melt. The intrinsic oxygen fugacity of the autoclave falls along the MnO-Mn_3O_4 buffer curve and represents the oxygen fugacity imposed under water-saturated conditions. At lower water contents the oxygen fugacity is reduced and can be calculated from the water content in melt, full details of these calculations can be found in Chapters 2-4. Water contents in the experiments of this study varied within a narrow range (0.75-1.25 wt %; Table 1) between experiments and the resulting absolute oxygen fugacity (bars) variations were less than one order of magnitude between all experiments. Where FTIR determined water contents were not available, the water content was estimated to be equivalent to the amount of water added to the capsule. These assumptions should be valid because the experiments (where this is assumption is required) were conducted at low CO_2 contents minimizing the amount of H_2O lost to the fluid.

5.4.4 Solubility of Pt

5.4.4.1 $CaCO_3$ experiments

LA-ICPMS analysis of $CaCO_3$ experiments shows that at approximately 1% water and varying amounts of CO_2, the solubility of platinum is nearly constant, Figure 5.3 and 5.4. Any effect of CO_2 on platinum solubility would result in a systematic variation in Pt solubility with varying CO_2 content. The lack of variation in Pt solubility with varying CO_2 strongly indicates carbon dioxide does not have any discernable effect on Pt solubility in haplobasaltic melt. By contrast, Pt values determined by bulk solution ID-ICPMS show a strong positive correlation with added CO_2 (Figure 5.3), which taken on its own would indicate an effect of CO_2 on Pt solubility and suggest complexing. However, because LA-ICPMS analyses demonstrate that Pt solubility is constant within the melt, the increase in platinum concentration determined by ID-ICPMS with increasing CO_2 is contributed by platinum not dissolved within the melt but present as micronuggets. Increasing concentrations with increasing CO_2 indicate that the amount of Pt contributed by micronuggets increases with increasing CO_2 contents. Analogous to the Cl-bearing experiments in Chapters 3 and 4, this behaviour suggests increased Pt solubility in the fluid phase prior to dissolution in the melt and allows for an estimation of Pt content in the fluid (discussed in detail below). It is postulated that similar processes occur for CO_2 as occur for Cl, where during the initial heating stages the $CaCO_3$ either dissolves into the fluid present in the capsule or thermally decomposes to form $CaO + CO_{2(fluid)}$ resulting in a mixed CO_2-H_2O fluid which at the temperatures (<1073K) and pressures (2 kbar) during the heating of the experiment

should be a supercritical single phase fluid, although this system is not well characterized under these conditions.

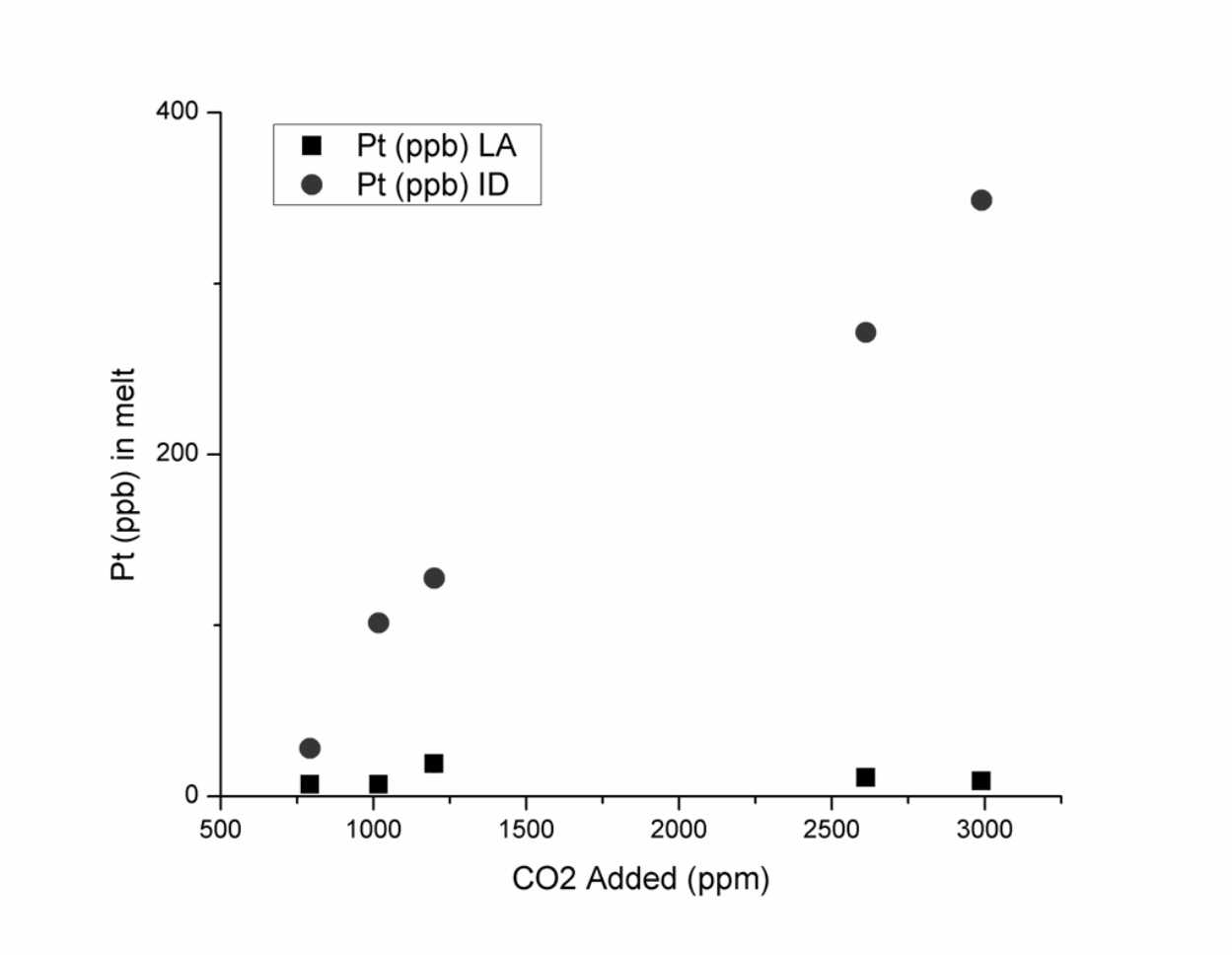

Figure 5.3 – Comparison between ID-ICPMS and LA-ICPMS for calcium carbonate bearing experiments. LA-ICPMS analysis shows consistent low-level Pt solubilities independent of CO_2 content. ID-ICPMS analyses vary linearly with increasing CO_2 showing an increase in micronugget contamination.

5.4.4.2 Silver oxalate experiments

Throughout the course this study it was found that experiments using silver oxalate show a proliferation of micronuggets evident in LA-ICPMS analysis, and as a result, bulk solution ID-ICPMS shows high apparent solubilities for Pt. After the discovery of the micronugget problem and due to the potential for the silver to alloy with the Pt in the experiments masking the effect of CO_2, the use of silver oxalate was discontinued. The silver oxalate experiments that were performed prior to the switch to $CaCO_3$ can be divided into two groups based on the apparent solubilities, as

determined by ID-ICPMS analysis. One group (CO_2-8 to CO_2-12) is distinguished by apparent solubilities in the 100s of ppm and shows a greater proliferation of micronuggets when analyzed by LA-ICPMS. The second group (CO_2-2 to CO_2-6) exhibits lower apparent solubilities closer to that of the calculated CO_2-free solubilities, Table 1. These two groups do not differ in experimental or analytical method; however, the concentrations are considerably different due to the abundance of micronuggets in the first group. No explanation is available at this time to explain this phenomenon occurring under nearly identical conditions. The experiments that were analyzed quantitatively by LA-ICPMS show lower measured solubilities than by ID-ICPMS; however, they still show increased concentrations as compared to the CO_2-free solubilities at equivalent oxygen fugacities, as determined by Blaine et al. (2005), Figure 5.4.

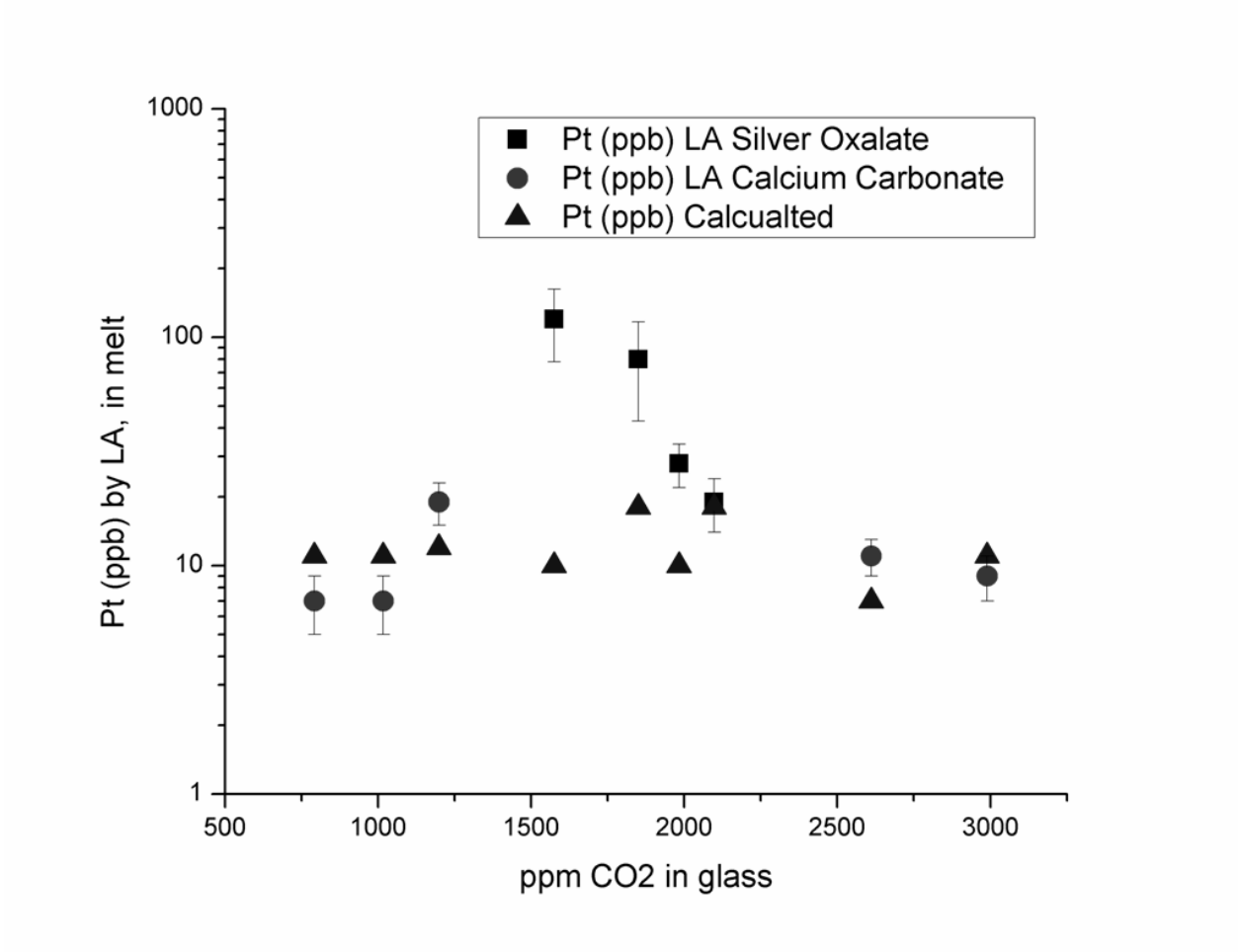

Figure 5.4 – Comparison between LA-ICPMS analysis for calcium carbonate and silver oxalate experiments. Included on the figure is the calculated CO_2-free Pt solubilities calculated after Blaine et al. 2005, Chapter 1. Note silver oxalate values tend to be higher than CO_2-free calculated values, based on Blaine et al. (2005).

5.4.5 Formation of micronuggets

It is believed that the micronuggets in these experiments form analogously to the mechanisms presented in Chapters 2 and 3 for Cl. Using an equivalent model, upon the heating of the experimental charge to the experimental temperature, the carbonate source decomposes releasing the CO_2 which mixes with the water present in the capsule. This H_2O-CO_2 mixture reacts with the platinum capsule dissolving Pt into solution. As the temperature increases and the glass begins to melt, the H_2O and CO_2 are dissolved into the melt. The platinum dissolved in the fluid cannot be incorporated into the melt and is left behind as a residual phase along the particle boundaries as the fluid dissolves. Increased run duration may indicate that the residual Pt phase will migrate out of the melt to the capsule walls. However, this effect was not observed due to the narrow range of relatively short run durations that were used for the CO_2-bearing experiments.

5.4.6 Estimation of Pt content in a mixed H_2O-CO_2 fluid

If we consider that this experimental system is analogous to the one presented for chlorine (Chapters 2 and 3), in that micronuggets are a result of dissolution of a PGE bearing fluid into the melt and depositing a PGE phase along the grain boundaries, then it is also possible to calculate a apparent solubility of Pt in a mixed H_2O-CO_2 phase. Assumptions made in chapter's 3 and 4, for Cl, are also applicable here for CO_2. As explained in Chapters 3 and 4, the excess Pt (ID-ICPMS concentration minus the CO_2-free concentration) can be attributed to the fluid phase and mass balance calculations can be used to calculate the potential solubility in the fluid phase using Equation 2. Tabulated results of this calculation are presented in Table 5.2.

$$Pt_{fluid} = \left[Pt_{ID-ICPMS} - Pt_{calculated}\right] \times \frac{m_{glass}}{m_{fluid}} \qquad \textbf{Equation 5.2}$$

Table 5.2 – Tabulated data for calculation of fluid-melt partitioning for Pt. Experiments were selected with increased concentrations measured by ID-ICPMS with no evidence of contamination.

Sample	Pt_{melt} (ppb) ID-ICPMS	Pt_{melt} (ppb) Calculated (CO_2-free)	H_2O_{melt} Added (wt. %)	CO_2 Added (ppm)	Pt_{fluid} (ppb) Calculated	Mol CO_2:H_2O Fluid	$D_{fluid-melt}$ Pt
CO_2-8	638	11	1.01	12000	27736	0.49	2500
CO_2-9	674	10	0.94	6100	42150	0.27	4200
CO_2-10	505	18	1.02	3300	35631	0.13	2000
CO_2-11	367	18	1.01	5500	21984	0.22	1200
CO_2-12	499	10	0.98	3400	36474	0.14	3600
CO_2-13	101	11	0.95	1000	8505	0.04	770
CO_2-14	28	11	0.96	800	1628	0.03	150
CO_2-15	271	7	0.75	2600	25885	0.14	3700
CO_2-16	128	12	0.99	1200	10291	0.05	860
CO_2-17	349	11	0.96	3000	26485	0.13	2400

The calculated apparent concentration of Pt in the fluid ranges from 1.6 to 42 ppm and results in a corresponding apparent Nernst partition coefficient ($D_{fluid-melt}$) of $1.5x10^3$ to $42x10^3$, indicating a substantial enrichment in the fluid phase. There is a clear increase in the calculated apparent concentration in the fluid with increasing CO_2 in the fluid; however, the increase is not consistent throughout the range of CO_2 contents, and the apparent concentrations levels out at mol CO_2:H_2O ratio higher approximately 0.2. The same holds true for the calculated $D_{fluid-melt}$ values (Figure 5.5) which are internally corrected for oxygen fugacity variations between experiments, and holds true for both the $CaCO_3$ and silver oxalate experiments. There is a clear increase until approximately mol CO_2:H_2O ratio equal to 0.15 above which the $D_{fluid-melt}$ values maintain a nearly constant value of 3600-4000. It should be noted that two $CaCO_3$ experiments have nearly identical mol CO_2:H_2O ratios as two corresponding silver oxalate experiments and result in nearly identical $D_{fluid-melt}$ values.

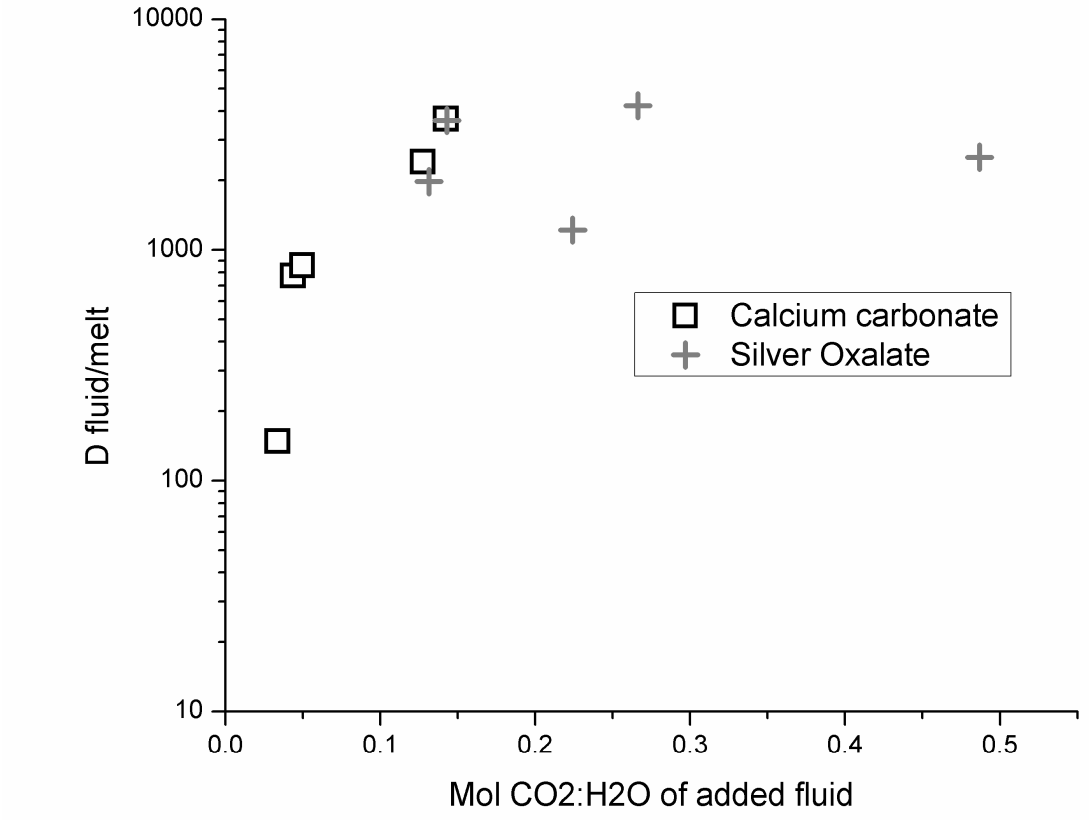

Figure 5.5 – Calculated apparent $D_{fluid\text{-}melt}$ values for Pt versus mol CO_2:H_2O ratio in the fluid phase. Note apparent maximum $D_{fluid\text{-}melt}$ is reached at approximately 0.15 above which $D_{fluid\text{-}melt}$ appears constant.

5.4.7 Implications to ore-forming systems

The results of this study could be an important step in the understanding of PGE ore-forming systems in the magmatic-hydrothermal environment, including PGE deposition in layer intrusions. It is demonstrated above that mixed CO_2-H_2O fluids have the capacity to enrich and transport Pt with high apparent $D_{fluid\text{-}melt}$ values ranging from 1.5×10^3 to 42×10^3. It is also likely that these results will translate to other PGEs, as well providing an efficient enrichment and transport mechanism for the PGEs in evolving mafic/ultramafic systems where mixed CO_2-H2O fluids will predominate.

Enrichment of PGE in CO_2-bearing fluids will be especially important in the early stages of deposit formation as the initial fluid generated will likely be a mixed CO_2-H2O fluid which will be

enriched in PGE relative to the melt. These fluids would form due to enrichment of the melt in CO_2 and H_2O during crystallization, as neither is incorporated significantly into early formed minerals, and as the temperature decreases decreasing solubility. These fluids when formed would migrate upward through the crystal mush at the base of the magma chamber due to compaction and density contrasts. When these fluids encounter a fluid-undersaturated magma higher in the magma chamber they can be reincorporated leaving behind micronuggets of PGE analogous to the formation of micronuggets in these experiments and discussed in Chapters 2-4. Repeated saturation and redissolution events would continue to enrich the successively generated fluids in PGE through redissolution of the previously generated micronuggets. This process is complimentary to the vapour-refinement model (Boudreau, 1999; Boudreau and Meurer, 1999) and as long as these fluids do not escape the system, essentially depleting the PGE, the process can continue to enrich the PGEs in the fluid until eventual deposition.

5.5 Conclusion

Data from this study indicate that CO_2 does not have a discernable effect on Pt solubility in a haplobasaltic melt over the conditions studied. The ubiquitous presence of micronuggets in experiments using both $CaCO_3$ and AgC_2O_4 again highlights the need for microscale analytical techniques such as LA-ICPMS to determine true solubilities of the PGE. The presence of micronuggets and their increase in abundance with increasing CO_2 content is attributed to Pt being dissolved in the mixed H_2O-CO_2 fluid prior to the fluid dissolving into the melt. Upon fluid dissolution into the melt the Pt which is not incorporated into the melt structure is left as a Pt-phase along the relict grain boundaries. Mass balance calculations indicate a $D_{fluid\text{-}melt}$ for Pt between $1.5x10^3$ and $42x10^3$, increasing with increasing mol CO_2:H_2O up to approximately 0.3, after which increasing CO_2 content does not further increase partitioning. These high apparent $D_{fluid\text{-}melt}$ values for Pt suggest a substantial enrichment in the fluid phase and suggest mixed H_2O-CO_2 fluids as potential enrichment and transport media for Pt and perhaps other PGEs in ore-forming systems.

Chapter 6 - A novel method for determining fluid-mineral-melt partitioning at elevated temperature and pressure – Application to platinum partitioning in a basaltic system

6.1 Introduction

Due to the potential role of fluids in the enrichment and transport of metals in evolving magmatic systems and their role in the formation of ore deposits, reliable partitioning data must be acquired to accurately model ore deposit formation. It has long been observed that fluids have played a key role in the formation of many ore deposits related to igneous rocks (Economic Geology 100th Anniversary Edition, J.F.H. Thompson, R.J. Goldfarb and J.P. Richards; editors), i.e.; volcanogenic massive sulfide (VMS), porphyry copper, intrusion-related gold, as well as a much debated role in the formation of Reef-type platinum group element (PGE) deposits in layered intrusions (Boudreau, 1988, 1999; Boudreau and Meurer, 1999; Boudreau et al., 1986, 1997; Willmore et al., 2000, 2002). The key to understanding the potential for fluid enrichment and transfer of metals is learning the fluid-melt partitioning or the capacity of the fluid to transport the metal at the conditions of deposit formation (Ballhaus and Stumpfl, 1986; Ballhaus et al., 1994). In historical studies it has been shown that PGEs can be transported as volatiles at magmatic temperatures (Fleet et al, 1993; 1995) and in sulphur-dominated vapour (Peregoedova et al. 2006); however transport by aqueous fluids at magmatic conditions is poorly constrained.

Platinum group element ore deposits are largely associated with ultramafic/mafic intrusions and validation of ore deposit models is reliant on relevant, experimentally determined partition coefficients ideally for comparable systems and conditions. Although there is an abundance of partitioning studies for sulphide melt-silicate melt (Ballhaus and Ulmer, 1995; Bezmen et al., 1994; Cottrell and Walker, 2006; Fleet et al.,1999; Makovicky and Karup-Moller, 2000; Peach et al., 1994 Van Orman et al., 2006), mineral-silicate melt (Brenan et al., 2003; 2005; Righter et al., 2004) and metal-silicate melt (Righter, 2003; Righter et al. 1997; 2007), there is a paucity of fluid-melt partitioning data for the PGEs for hydrous mafic systems at crustal conditions, due in part to the experimental difficulties in these systems (Hanley et al, 2005; Ertel et al., 2008). In general, fluid-

melt partitioning experiments are inherently quite difficult, require elaborate experimental set-ups in order to achieve reliable results and many of the current experimental techniques are problematic in key areas. Mafic systems are especially problematic where the low viscosity of the melt precludes the direct trapping of inclusions in a quenched glass which is a method available for use in felsic systems (Schaefer et al, 1999). It is also not possible in these systems to perform experiments where the capsule is simply quenched and the free fluid removed because of the formation of quench products due to the reduced solubility of components within the fluid phase at room temperature. Due to the use of platinum or noble metal capsules to contain the experiment, leaching of the capsule to dissolve quench products would also result in leaching of the capsule material giving non-representative results. The diamond-trap method (Kessel et al., 2004) allows sampling of fluid and quench products but is not a viable method for the conditions relevant to this study because diamond would not be stable. The conditions used for the study of basaltic magmatism in this study are 1523K, 0.2 GPa and NNO+3 and under these conditions diamonds will oxidize. A modified trap method was attempted using an alumina insert instead of diamond but it was found that the alumina was too reactive with the melt and also an abundance of quench products precluded the use of this modified method.

One method suitable for use in mafic systems to determine partitioning calculated from the amount of an element lost from a melt to a known amount of fluid. However, the most suitable capsule material for these experiments is generally a PGE or PGE alloy due to their hig-melting temperature and workability. Determination of a PGE's solubility using these materials would be overly complicated by potential contamination from the capsule and alloy formation which would reduce the activity of the PGEs in the system. Another possibility would be to use Re capsules but is too brittle for practical use in IHPV experiments (Paparoni et al., 2010, in press). This mass loss method, although unsuitable for PGEs, was used as part of this study to determine partitioning of other elements and is discussed later in this paper.

A second method to determine the solubility of metals at high temperature is to extrapolate low-temperature thermodynamic data; this method was used extensively in the nineties by authors such as Gammons and Bloom (1993), Gammons et al. (1992), Sassani and Shock (1990, 1998), Wood et al. 1994 and Gammons (1995, 1996) among others. Most of the data was determined from experiments that were performed at temperatures of less than 573K and were then extrapolated to magmatic temperatures. These extrapolations were very useful in demonstrating that, even at moderate hydrothermal temperatures, fluids have the potential to dissolve large amounts (ppm levels) of PGEs. It was determined that significant Pt solubilities can occur in the presence of complexing ligands such as HS and Cl. In the case of Cl it was found that significant solubilities only occur at

low pH and highly oxidizing conditions at low to moderate temperatures. It was suggested in these studies and by other researchers (Wood, 2002; Hanley 2005) that Pt becomes a "harder" Lewis acid with increasing temperature and that Cl could become a major complexing agent at magmatic temperatures. The major shortcoming of these experiments was that they do not provide direct experimental evidence of PGE solubility at the temperatures of mafic magma and extrapolation to these temperatures can introduce large amounts of uncertainty. Xiong and Wood (2000) also show that there are significant problems with PGE solubility data extrapolated to high temperature.

A third technique is the fractured-quartz method, which should be superior because it is possible to trap a fluid that coexists with a silicate melt, although due to experimental shortcomings it is difficult to achieve consistent data (Hanley et al. 2005, 2007; Simon and Pettke 2009). In the fractured-quartz method, pre-fractured quartz crystals are used in the experiment and healing of the fractures during the experiment traps fluid inclusions which are analyzed at the conclusion of the experiment using a microanalytical technique such as laser ablation ICP-MS (e.g., Hanley et al. 2005, 2007; Pettke et al. 2002, Simon and Pettke 2009). As well, any constituents which were dissolved at experimental conditions and precipitated during quench are also contained within the inclusion and analyzed when the inclusion is ablated; therefore the analysis is representative of the fluid that was trapped at the temperature and pressure of the experiment. However, the major limitation of this method is there is no control on the time at which the fractures heal and trap inclusions allowing inclusions to be trapped at any time during the experiment, even during the initial heating stages, thus trapping fluids that are not in equilibrium. Trapping of non-equilibrium fluids over a range of conditions results in spurious data non-representative of the fluids at the conditions of interest (Hanley et al. 2005, 2007; Pettke et al. 2002, Simon and Pettke 2008). Secondly, this method is only possible using SiO_2-rich melt compositions and cannot be used to examine mafic systems where PGE occurrences are found.

In order to obtain reliable and applicable data, a new method for determining fluid-melt partitioning is required. The method presented herein addresses the shortcomings of the two methods outlined above and allows the controlled trapping of fluid inclusions representative of a fluid in equilibrium with a coexisting mafic melt. As well, this method allows 3-phase, fluid-mineral-melt partitioning data to be obtained for mafic systems. Although in this study this method is applied to Pt in a basaltic system, this method can also be adopted for nearly any element and can also be modified to observe different systems as well.

6.2 Part I: Method development

6.2.1 Theory and requirements

The best known way for determining the properties of a fluid, apart from direct sampling, in either a natural or synthetic system is by analyzing fluid inclusions trapped in minerals or glasses (Schaefer et al., 1999; Heinrich et al., 1999). Fluid inclusion analysis is widely applied to natural systems and recent advances in laser ablation inductively coupled plasma mass spectrometry (LA-ICPMS) have resulted in a surge in the understanding of fluid behavior and evolution in magmatic systems (Audetat et al. 1998; Heinrich et al., 1999). Laser ablation ICP-MS fluid inclusion analysis ensures that the fluid, as well as any dissolved constituents that crystallize post trapping, are included in the analysis, thus the analysis is representative of the fluid at the trapping conditions. This is extremely important when analyzing fluid inclusions as solubilities can be much lower at ambient conditions and significant crystallization can occur within the inclusion. Due to the suitability of fluid inclusion analysis, it would be desirable to create a method to synthesize fluid inclusions in an experiment while controlling the timing and conditions of inclusion trapping, the major shortcoming of the fractured quartz method.

An effective way to control the timing of the trapping of the inclusions is to entrap fluid inclusions within a crystallizing (not healing) mineral (Student and Bodner, 1999) and the crystallization of many minerals can be controlled by temperature. Temperature can be varied during an experiment and periods of no crystal growth and crystal growth can be produced, fully controlling the timing of inclusion trapping. By controlling temperature, equilibrium can be obtained within the system prior to generating crystallization conditions and trapping of inclusions. In the method proposed here, only a small drop in temperature is necessary to promote crystallization which should have a negligible effect on equilibrium between the fluid and melt to be maintained.

The current method proposes using a single seed crystal placed within the experimental capsule to allow the trapping of fluid inclusions during the growth of this seed crystal. If only a single crystal is present and the degree of super-saturation is small, this crystal will grow and nucleation of abundant smaller crystals in the melt can be prevented. It is a requirement of the proposed method that a seed crystal will grow from the fluid phase trapping inclusions of a fluid that is in equilibrium with the melt. When crystals grow from a melt in the presence of a fluid the inclusions are likely to be small. This is because after bubbles nucleate in the melt they must coalesce and stick to a growing crystal face without buoyant rise through the melt. This can happen in nature but experiments are run at a much smaller scale and large bubbles cannot be trapped in a low

viscosity melt such as basalt. However, if it is possible to grow a crystal is from a fluid it may be possible to trap larger fluid inclusions because the fluid wets the complete crystal.

To summarize, the goals of the development of this technique are to:

- Effectively trap a fluid saturated in an element of interest in a fluid inclusion formed within a crystallizing mineral in equilibrium with a silicate melt.
- Control the timing of inclusion entrapment and allow for equilibrium to be reached before trapping.
- Entrap inclusions large enough for laser ablation analysis
- Analyze and quantify element solubility in the silicate melt phase, mineral and fluid inclusion, allowing determination of partitioning between melt, mineral and fluid

6.2.2 Development of the crystallization entrapment method to determine the fluid-melt partitioning of platinum

In order to achieve the above-mentioned conditions, a modified sealed-capsule technique was developed. In Blaine et al. (2005), a sealed-capsule technique was demonstrated to be an effective means of determining Pt solubility in a hydrous silicate melt by equilibrating a starting glass that is nearly Pt-free with the platinum capsule containing the experimental charge. To modify this technique for use in this study, a diopside seed crystal was also added to the capsule along with enough water to insure a free fluid phase would be present throughout the duration of the experiment.

Most previous studies on PGE solubility and partitioning have primarily utilized a diopside-anorthite dry eutectic composition ($An_{42}Di_{58}$) for the silicate melt component (Amosse et al. 1994; Bezmen et al. 1994; Borisov and Palme 1995, 1997; O'Neill et al 1995; Ertel et al, 1999; Blaine et al. 2005; among others), as a simple analog to a iron-free mafic melt. Iron present in the silicate melt can severely complicate solubility studies of the highly siderophile PGEs (e.g., the melt will be saturated in an FePt alloy so the activity coefficients in the alloy must be known and the Fe^{3+}/Fe^{2+} ratio in the melt also needs to be determined for experiments at moderately oxidized conditions such as the present study), so an iron-free analog is generally used. The phase equilibrium of the system diopside-anorthite is also well understood and by choosing a composition on the diopside side of the eutectic it is possible to create conditions favorable to diopside crystallization. It should be noted that the addition of water to the diopside-anorthite system could cause a deviation from a true binary system and allow the stabilization of another phase(s). Although deviation from the binary Di-An

system with the addition of water was not noted by Yoder (1968), evidence for a pseudobinary system is presented in this study, discussed later in this chapter.

A graphical representation of the experimental setup and a stepwise depiction of an experimental run are shown in Figure 6.1. Figure 6.1-I depicts the system prior to running the experiment with anhydrous haplobasaltic glass, a diopside seed crystal and water added to a platinum capsule as shown in inset. The diopside seed crystal is kept separate from the haplobasaltic glass by crimping the capsule as indicated in the inset diagram. The composition of the entire system is shifted with the addition of the diopside crystal from the diopside-anorthite eutectic glass composition toward diopside (determined by the relative weights of melt and diopside and the lever rule; point "A" on Figure 6.1-I). The capsule is then pressurized and heated (Figure 6.1-II), melting the glass powder and allowing a portion of the fluid to dissolve into the melt. As well at this temperature, some of the seed diopside will dissolve into the melt however the temperature is such that the system will be in the diopside + melt + vapor field (point "B" on Figure 6.1-II) and a portion of the diopside crystal will persist. At this point the temperature is held constant and the system is allowed to approach and ultimately reach equilibrium. During this period, due to the constant temperature, the crystal does not grow and inclusions are not trapped. After a given length of time, the temperature is then dropped (point "C" on Figure 6.1-III) to promote the crystallization of diopside (the amount of growth will be controlled by the liquidus and the lever rule). Again temperature is held constant, in this case to allow for crystallization to occur. To conclude the experiment the capsule is quenched rapidly to ambient temperature (Figure 6.1-IV) quenching the melt to a glass which can be analyzed for PGEs and halting crystal growth.

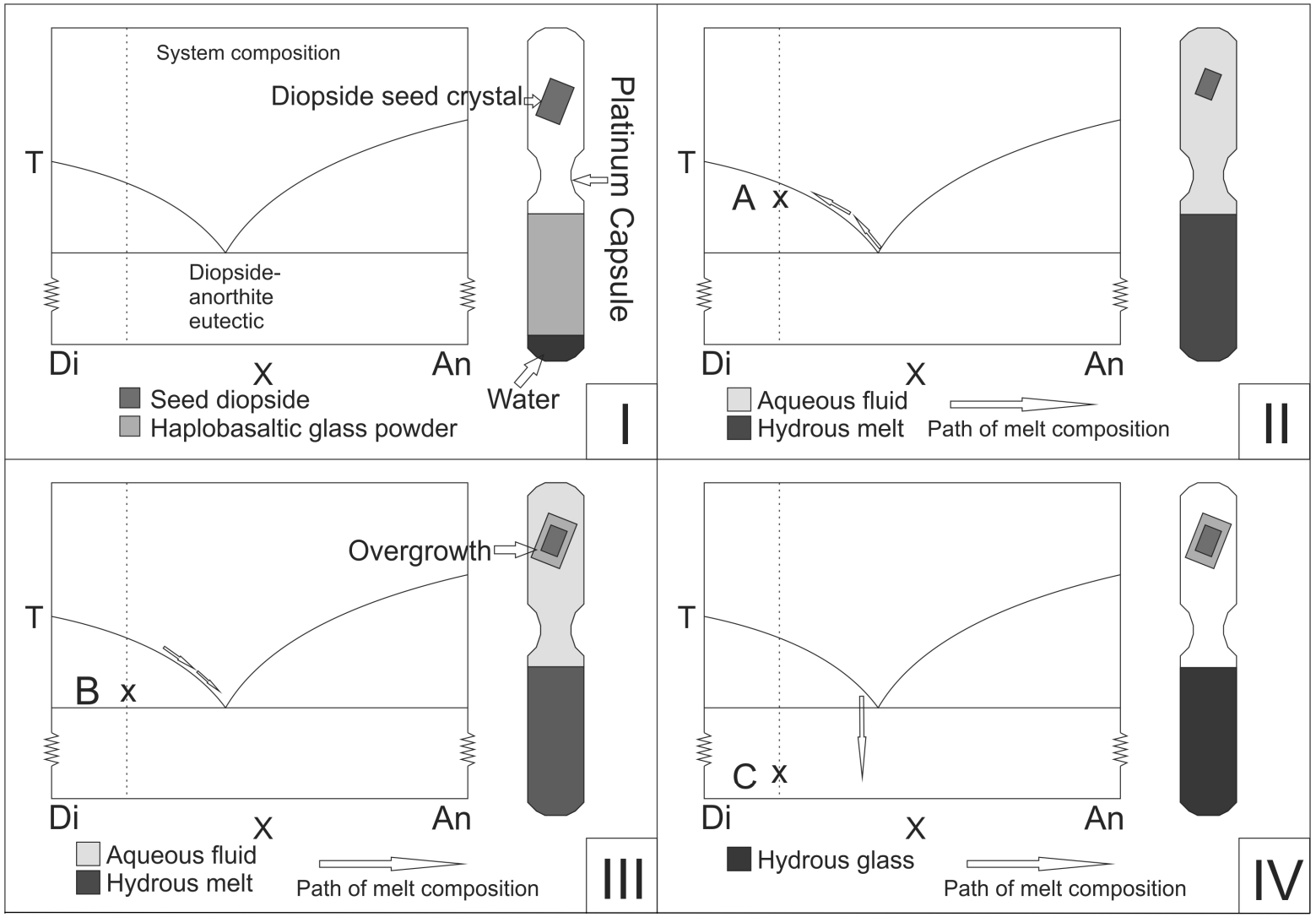

Figure 6.1 – Schematic of capsule design and step by step details of an experimental run.

6.2.3 Experimental conditions

Capsules were prepared using $An_{42}Di_{58}$ glasses synthesized from component oxides and carbonates in alumina crucibles in order to minimize Pt contamination in the starting glasses (cf. Blaine et al., 2005). Approximately 500 ppm of Ba, Sr, Cs and 300 ppb Rb were added as carbonates ($BaCO_3$, $SrCO_3$, Cs_2CO_3 and Rb_2CO_3) to the starting glass to serve as internal spikes require for quantification of platinum concentrations in the fluid inclusions and are discussed later. The composition of the starting glass was determined using a Cameca SX-100 electron microprobe with a 15 keV accelerating voltage, a 4 nA beam current and a 3 μm beam width. The microprobe analysis in weight percent normalized to 100% is, 49.0 (0.68) wt. % SiO_2, 17.3 (1.0) wt. % Al_2O_3, 23.3 (0.24) wt. % CaO and 10.1 (0.26) wt. % MgO, with 1σ errors given in brackets.

Experimental charges were loaded in either a platinum or platinum-iridium ($Pt_{80}Ir_{20}$) capsule, which also served as the source for the saturation of the experimental system in the metal of interest. Experimental charges were prepared by adding Millipore water followed by approximately 300mg of Di-An haplobasaltic glass powder to a 4cm long x 4mm o.d. (3.6mm i.d.) noble metal capsule which had been sealed at one end. The amount of water added was calculated by calculating the free volume with the capsule and determining the amount of water that would occupy that volume at the experimental conditions using the equations of state of Pitzer and Sterner (1994) for H_2O. The maximum water possible without causing over pressurization within the capsule was added to ensure that a free volume was maintained within the capsule throughout the experiment, insuring that the capsule did not collapse and prevent transfer of fluid throughout the capsule. After addition of the water and glass powder the capsule was tapped, compacting the glass powder and water mixture, and the capsule was crimped above the mixture creating a two chambered capsule. Care was taken to not entirely close off the conduit between the two chambers when crimping. A single diopside crystal was then added to the upper chamber and the capsule was crimped and sealed by arc welding. The capsule was dipped in liquid nitrogen prior to welding to prevent volatilization and loss of volatiles during sealing. Capsules were weighed after each stage of capsule preparation and again at the conclusion of the experiment to ensure that there was no loss of water.

Diopside crystals used in this study were from the Belvedere Mountain Quarries in Eden Mills, Vermont and were near end-member skarn-hosted Ca-Mg diopside. The composition of the diopside is 55.2 wt. % SiO_2, 26.3 wt. % CaO, 15.1 wt. % MgO with a small amount (3.4 wt. % FeO) of iron, determined by electron microprobe (Table 2) using the same operating conditions as those used for determining the compositions of the starting and resulting glasses. Prior to addition to the

experimental charges the diopside crystals were heated at ambient pressure to >973K and left for 2 hours to ensure that any inclusions present would be decrepitated and would not contain any fluid.

All experiments were conducted at the Institut fur Mineralogie at the University of Hannover, in a vertically mounted, internally heated pressure vessel (IHPV) equipped with a rapid quench device. The melt can be quenched using this apparatus to a crystal- and bubble-free glass at a cooling rate of >200 K/min (Berndt et al., 2001). Temperature was controlled to within +/-5K using two S-type thermocouples connected to a Eurotherm temperature controller which controlled two corresponding heating coils within the autoclave. Temperature was also monitored using two additional S-type thermocouples within the hotspot of the furnace ensuring a constant temperature during the experiment and no temperature gradients across the length of the capsule. Experiments were conducted at 0.2 GPa and oxygen fugacity was imposed by the intrinsic oxygen fugacity of the autoclave which falls along the MnO-Mn_3O_4 buffer curve. All experiments were conducted at water saturated conditions ($a_{H_2O} = 1$) resulting in an imposed oxygen fugacity equal to the intrinsic oxygen fugacity of the autoclave (full details in Blaine et al., 2005; Chapter 2), equal to NNO+3 or $10^{-3.7}$ bars (O'Neill et al. 1999) under the experimental conditions

In order to attempt to maximize the efficiency of inclusion entrapment and crystallization of the seed crystal a number of experimental time/temperature protocols were used, varying the rest and crystallization temperatures and times the experiment remained at each experimental stage. The effectiveness of the method appeared independent of the time protocols used and success of fluid entrapment was independent of experimental temperature. The run summaries are listed in Table 6.1.

Table 6.1 – Summary of run conditions

Experiment	Capsule Material	Fluid type	Temperature (K) "A"	Time (h) at "A"	Temperature (K) "B"	Time (h) at "B"	Comments
Cryst-1	Pt	H_2O	1493	6	1433	24	
Cryst-2	Pt	H_2O	1493	6	1433	41	
Cryst-3	Pt	H_2O	1493	6	1433	61	
Cryst-4	Pt	H_2O + 5% Cl	1483	6	1433	39	
Cryst-5	Pt	H_2O + 10% Cl	1483	6	1433	61	
Cryst-6	Pt	H_2O+ CO_2	1483	6	1433	60	
Cryst-7	Pt	H_2O	1483	48	1433	15.3	Spiked starting glass
Cryst-8	Pt	H_2O	1488	48	1433	24	Spiked starting glass
Cryst-9	Pt	H_2O	1488	48	1433	39.8	Spiked starting glass
Cryst-10	Pt	H_2O	1488	48	1433	18	Spiked starting glass
Cryst-11	$Pt_{80}Ir_{20}$	H_2O	1488	48	1433	36.3	Spiked starting glass

6.2.4 Method results

Using the method outlined above it was possible to create an overgrowth on the diopside seed crystal and inclusions were trapped within the overgrowth. Figure 6.2 shows a crystal before (Figure 6.2a) and after (Figure 6.2b) an experimental run. The remainder of the seed crystal after partial dissolution is readily evident in Figure 6.2b as a smaller, irregular shaped, darker center, as well as the overgrowth causing the final crystal to be slightly larger and a different shape than the seed crystal.

While removing the experimental products from the capsule certain observations were made:

1) Although evidence that the capsule expanded due to internal pressurization from fluid expansion, the crystal remained separated from the melt throughout the experiment, remaining "stuck" to the capsule wall.
2) Crystallization occurred solely from the fluid phase and not within the silicate melt, resulting in a crystal- and bubble-free experimental glass and single crystal at the termination of the experiment.
3) In the majority of experiments crystallization on seed crystals grew dominantly parallel to the capsule wall, forming a thin tabular crystal. The overgrowth in these experiments contained inclusions dominantly grouped along what were determined to be mineral contacts (discussed later), as shown in Figure 6.4.
4) In some experiments the resultant crystal was more tabular and appeared to be similar to the original seed crystal. These crystals contained numerous equidimensional inclusions, and fewer grouped inclusions as shown in Figure 6.5. These inclusions are believed to have formed through refilling and healing of decrepitated inclusions already present within the seed crystal and not within an overgrowth. These inclusions are analogous to those formed in the fractured quartz method and were not used for solubility determination.
5) No experimental differences were noted resulting in the two crystallization patterns

It is hypothesized that in these experiments, rapid transfer of ions through the fluid in conjunction with the presence of the large nucleation surface provided by the seed crystal caused the absence of crystallization in the melt. This behavior is quite interesting in itself as changes in the melt can cause crystallization of a mineral, from a fluid or vapor phase, physically removed from the melt, which suggests equilibrium between the fluid and melt phase.

Run-product crystals were mounted in epoxy disks and were polished for subsequent analyses. BSE imagery (Figure 6.3) shows that two mineral phases make up the bulk of the overgrowth. The two minerals were intimately intergrown and fluid inclusions formed generally at the contact of the two mineral phases. A third intermediary phase was also observed at the contact between the seed crystal and the overgrowth.

The three mineral phases were analyzed using a Cameca SX-100 electron microprobe at the University of Hannover, Germany. Analyses were made using a 15keV accelerating voltage, a 4 nA beam current and a 3 μm beam. Multiple analyses were made to determine homogeneity of the mineral phases; compositions and 1σ standard deviations of all microprobe analyses are tabulated in Table 6.2.

The three phases were determined by their stoichiometry to be diopside (with a small amount of Al), what would appear to be an unidentified very calcium-rich amphibole (does not correspond to a natural occurring composition), as well an intermediary composition between amphibole and pyroxene which is left as an unidentified "pyrobole". Further spectroscopic work would be required to determine the mineralogy of the two undetermined phases, however, as it is not fundamental to this study, the mineralogy of the two were not determined beyond their composition. The presence of the intermediary phase is believed to be the result of very rapid crystallization upon initial reduction in temperature and is not believed to be a stable phase and may be pseudocrystalline in nature. The subsequent crystallization of two intergrown mineral phases also suggests rapid although somewhat slower crystallization after the initial drop in temperature. The somewhat slower crystallization conditions are ideal for the trapping of inclusions from the fluid and is interpreted to occur during the desired times and conditions. As briefly noted above, due to the presence of abundant excess water it was foreseeable that another phase could become stable in addition to diopside. However using the phase rule at fixed T and P the system will still be invariant with 4 components (silicate melt, diopside, "amphibole" and aqueous fluid) and 4 phases (melt, 2 minerals and a single supercritical fluid).

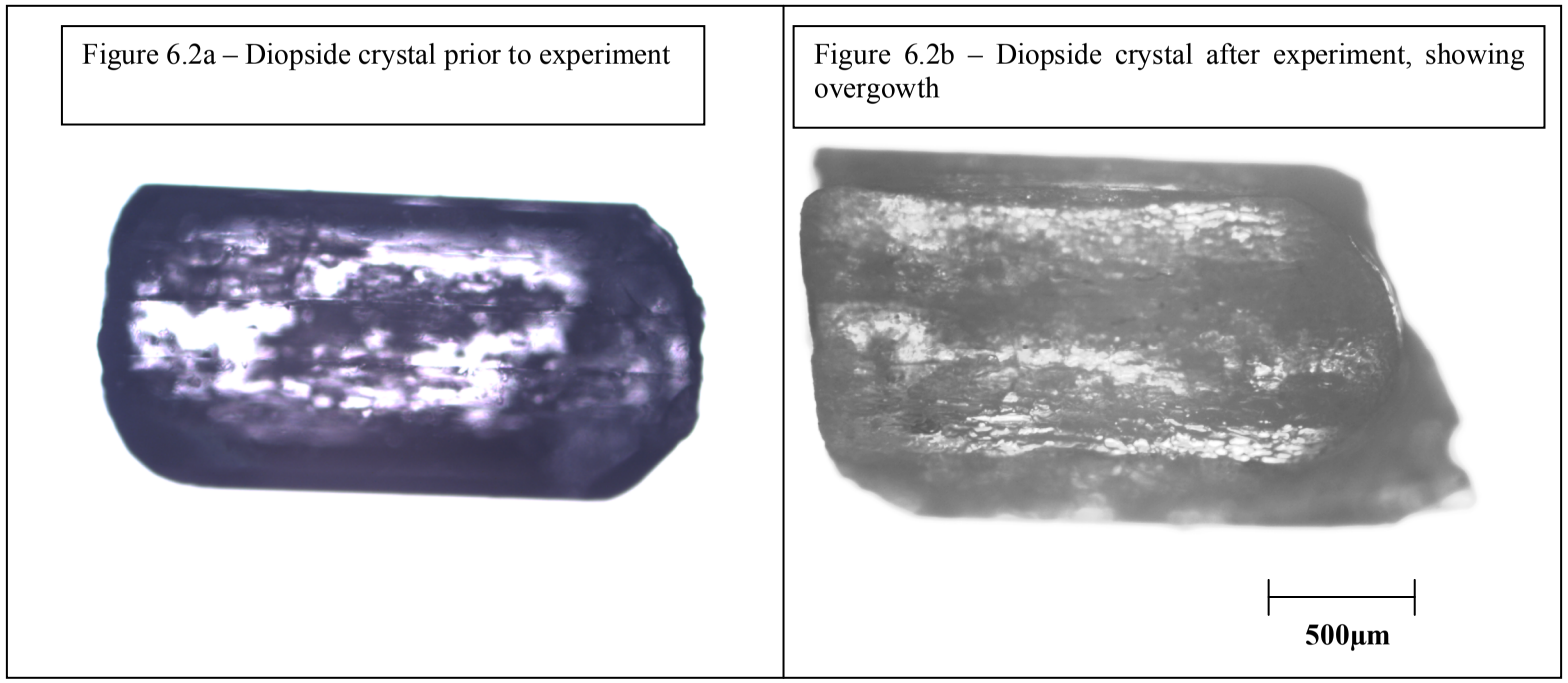

Figure 6.2 – Diopside crystal before (a) and after (b) experiment. Remainder of seed crystal is evident in Figure 6.1b as an irregular shaped core indicating some dissolution of the seed crystal prior to overgrowth, not the change in shape of the crystal with crystal growth occurring parallel to the capsule wall.

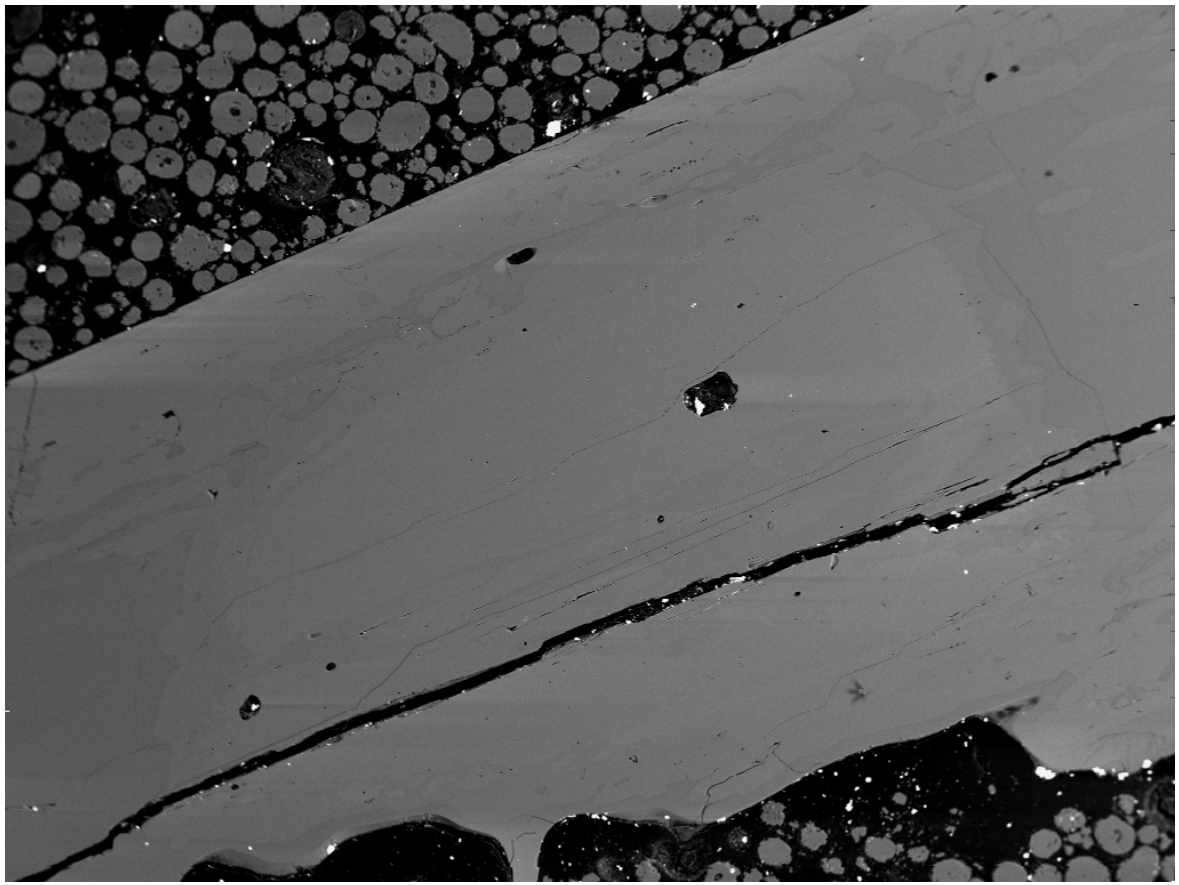

Figure 6.3 – BSE image of a run product diopside crystal. Shown in the image are the central remainder of the seed diopside crystal (lightest gray), a small rim of intermediate composition is found at the contact between the central seed crystal and outer overgrowths (not visible on this scale), the diopside overgrowth which appears as an intermediate gray and the amphibole which appears as the darkest gray. FOV = 2.5 mm.

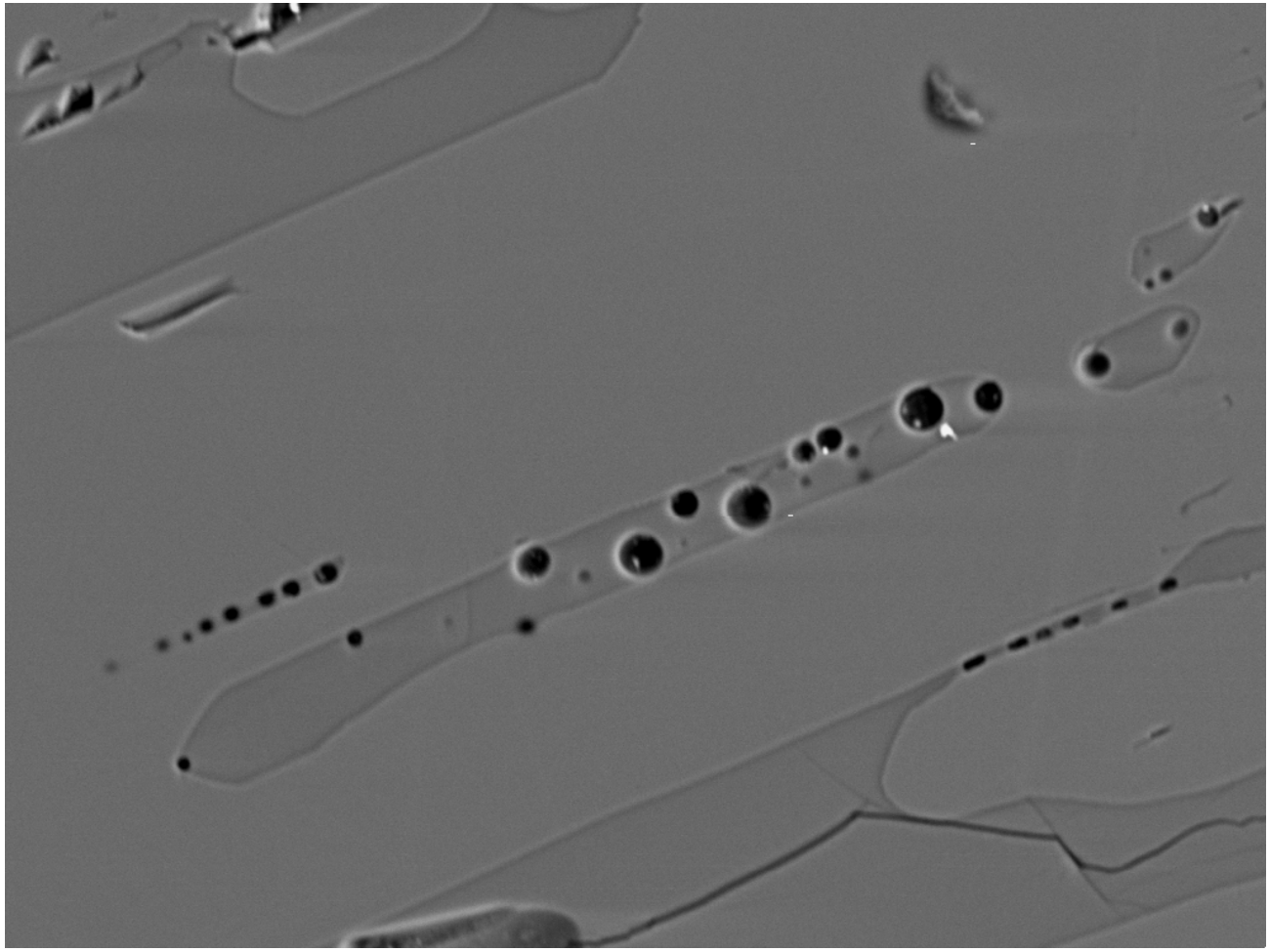

Figure 6.4 – Close up BSE image of inclusions polished to the surface, circular remainders of fluid inclusions can be seen at the contact between amphibole (dark gray) and diopside (light gray). FOV = 172 µm.

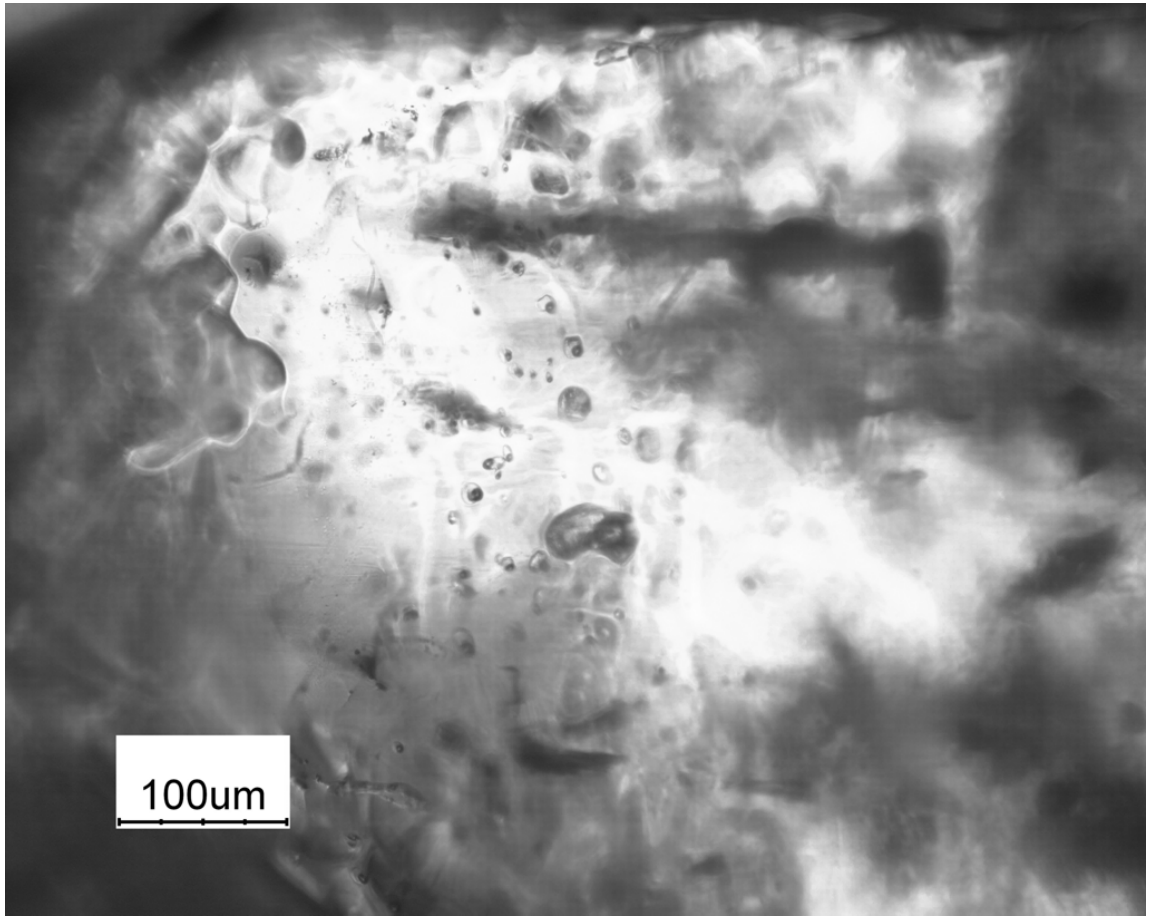

Figure 6.5 – Photomicrograph of equidimensional inclusions interpreted to be emptied inclusions present in the seed crystal, that were refilled during an experimental run.

Table 6.2 - Composition of phases pictured in Figure 2 as determined by EMPA. 1σ errors on analyses are shown in brackets.

Phase	# of Analyses	SiO_2 wt. %	Al_2O_3 wt. %	CaO wt. %	FeO wt. %	MgO wt. %	Total	Stoichiometry Si:Al:Ca:Fe:Mg:O:OH
Diopside (A)	12	54.4 (0.5)	2.7 (0.6)	26.0 (0.3)	0.2 0.2)	16.9 (0.3)	100.2	2:0:1:0:1:6:0
Amphibole (B)	17	48.18 (0.6)	16.2 (0.2)	23.3 (0.3)	0.1 (0.1)	7.6 (.4)	95.4	6.5:2.5:3.5:1.5:22:2_a
Pyrobole (C)	1	49.6	12.1	24.4	0.0	10.7	96.5	
Seed Diopside	7	55.2 (0.4)	0.09 (0.1)	26.4 (.4)	3.4 (.3)	15.1 (.2)	100.1	2:0:1:0:1:6:0

a - For calculation of "amphibole" composition the number of oxygen was set to 22 and (100-total) was apportioned to OH.

6.2.5 Fluid inclusion petrography

Fluid inclusions along mineral contacts were rounded to sub-rounded, two-phase L-V inclusions, and were abundant in the overgrowth. In Figure 6.4, a close up of an "inclusion" that has been polished to surface is shown; this "inclusion" consists of a group of fluid inclusions (circular) surrounding the central amphibole at the contact between amphibole and the surrounding diopside. There was no clear relation evident between experimental protocol (i.e., time at temperature "A" or "B", Figure 1 II and III) and the successful entrapment of inclusions or the nature of inclusions.

Microthermometric analysis was performed using a THMSG600 Linkham heating and cooling stage and was performed on a total of seven inclusions from crystallization run #2. The microthermometric analysis was done to double check the composition of the included fluid phase. Melting temperatures were consistent with a composition of pure water with a final melting temperature of 0° ± 0.2 Celsius. Homogenization temperatures were attempted however inclusions decrepitated and the sample became cloudy before homogenization was reached. Due to the lack of inclusion samples and the need to prevent the destruction of the inclusions prior to LA analysis, further attempts to obtain homogenization temperatures were not made.

6.3 Part II: Determination of the fluid-melt partitioning of Pt

Fluid-melt partitioning values were determined for this study using concentrations for the melt and the fluid obtained using LA-ICPMS. Utilizing LA-ICPMS it is possible to determine micronugget-free PGE solubilities in the resultant glasses from an experimental run as has been shown in previous chapters, also because of the microanalytical nature of the LA-ICPMS analysis it is possible to analyze concentrations in individual fluid inclusions. Determination of Pt concentration in an analyzed fluid inclusion requires specific ablation behaviour of the inclusion, knowledge of the composition of the fluid inclusion and the use of specialized algorithms, which are discussed in the following section. Initial LA-ICPMS analysis of fluid inclusions from preliminary experiments (Cryst-1 through Cryst-6) indicated enrichment in Pt when compared to the background crystal and demonstrated success in the method. Quantification of the Pt content within the inclusion was not possible however due a lack of internal standards in these experiments.

6.3.1 Development of internal standards

When using LA-ICPMS to analyze fluid inclusions it is impossible to ablate only the inclusion and a portion of the signal will be a result of ablation of the host crystal. In order to correct for this and calculate the concentration of an element in a fluid inclusion, the concentration of another element (an internal standard) must be known in the fluid. This allows correction for the volume of the inclusion ablated, the amount of host material included within the ablated material and the different ablation characteristics of the inclusion and host. Ideally the internal standard would have a much larger concentration in the fluid compared to the host material to provide a good contrast between the inclusion and the host. Very few previous experimental studies have examined the partitioning of elements between fluids and melt in basaltic systems, so it was necessary to design a set of experiments to determine the partitioning behaviour of an element to be used as an internal standard. For the purposes of this study three elements; Sr, Cs, Ba were chosen for their potential compatibility with the fluid and incompatibility with the host diopside.

To determine the fluid-melt partitioning of these elements simple mass-loss experiments were performed using the haplobasaltic starting glass composition as used above, containing approximately 500 ppm Sr, Ba and Cs and 300 ppm Rb. For these mass-loss experiments, approximately 100mg of powdered glass were added to a 1.5 cm long Pt capsules with varying amounts of Milli-Q water and sealed. Water was added in quantities enough to saturate the melt in water (~4.5 wt. %), leaving an excess fluid phase in the capsule at experimental conditions. During the experiment, elements are partitioned between the melt and the fluid in order to maintain equilibrium between the melt and the

fluid, which reduces the concentration of elements in the melt. At the end of the experiment the experimental charge is quenched resulting in a crystal- and bubble-free glass. By analyzing the resultant concentration in the glass by LA-ICPMS (method outlined below) it is possible to use mass balance to calculate the concentration in the fluid and the resulting distribution coefficient using Equation 6.1 and 6.2. In Equations 6.1 and 6.2 the initial concentration in the melt is compared to the final concentration after the experiment and the difference in these two values are attributed to loss of the element to the fluid, knowing the volume of fluid it is then possible to calculate the concentration of the element in the fluid and the corresponding partition coefficient. The results of these experiments are summarized in Table 6.3.

$$D_{fluid/melt}^{element} = \frac{C_{fluid}}{C_{glass}} \qquad \textbf{Equation 6.1}$$

Where;

$$C_{fluid} = \frac{(C_{initial} \times m_{glass}) - (C_{glass} \times m_{glass})}{m_{fluid}} \qquad \textbf{Equation 6.2}$$

The data for all partitioning experiments and calculated partition coefficients are summarized in Table 6.3. Experiment PART-A was conducted at fluid-undersaturated conditions and was used to calculate the bulk concentrations of Sr, Ba, Cs and Rb. The concentration in Part-A shows a depletion in the concentrations of Sr, Ba and Cs and Rb as compared to the starting glass due to dilution by the water dissolved into the melt. Starting glass concentrations are calculated from Part-A using Equation 6.3.

$$C_{calculated} = \frac{c_{initial} \times m_{glass}}{m_{glass} + m_{fluid}} \qquad \textbf{Equation 6.3}$$

Experiment PART-B shows inconsistent results and shows higher concentrations in all elements than was added to the system (i.e., relative to PART-A), this experiment is therefore considered to be contaminated and has been excluded. Cesium and strontium do not show a consistent depletion in concentration in the glass with increased water added to the capsule in PART-C and D. Cesium concentrations vary only slightly indicating a very low $D_{fluid/melt}^{Cs}$ value an indication that Cs is not partitioned strongly into the fluid. Strontium shows slightly different results with the two isotopes analyzed ^{86}Sr (9.86% abundance) and ^{88}Sr (82.58% abundance): the concentration of ^{86}Sr does not vary significantly but the concentration of ^{88}Sr in the glass increased slightly after the water saturated experiments. The behaviour of Sr indicates that Sr is not partitioned

significantly into the fluid phase. Rb shows a similar behaviour to Sr and Cs; the Rb concentration is not shown to be depleted in the glass with increased fluid content indicating that Rb as well does not partition significantly into the fluid phase. Barium shows a consistent depletion with increasing water content and produces a calculated partition coefficient $\left(D^{Ba}_{fluid/melt}\right)$ of 0.42-0.51. Therefore in subsequent experiments a fluid-melt partition coefficient of 0.46 for Ba will be used for all calculations of Pt concentrations in the fluid inclusions. The behaviour observed for Ba is broadly consistent with those obtained for bracketing compositions (trondhjemite and basanite) at 1173-1373K and 2.0GPa (Adam et al. 1997). In Adam et al. (1997), Ba showed moderately compatible behaviour in pure water with a fluid-melt partition value of 0.89 for trondhjemite and 0.05 for basanite. In Adam et al. (1997), Sr and Rb were also shown to be moderately compatible, however this behaviour was not demonstrated in this study. If the values calculated here for the partitioning of Ba are incorrect they will have a direct influence on the determined partition coefficients for platinum, underestimating the fluid-melt partitioning of Ba would result in an underestimation of the concentration of Ba in the fluid inclusions and result in an equal relative underestimation of Pt concentration, i.e. a 20% underestimation in Ba concentration would equal a 20% underestimation in Pt concentration.

Table 6.3 – Results of experiments for development of an internal standard. Errors are given in brackets. a – recalculated anhydrous composition from PART-A using Equation 6.5

Experiment	^{86}Sr	^{88}Sr	^{87}Rb	^{133}Cs	^{138}Ba	$D^{Ba}_{fluid/melt}$
PART-A	440 (2)	492 (5)	280	442 (38)	531 (12)	
Initial Concentration$_a$	458	513	292	460	553	
PART-B	443 (2)	504 (2)	296	483 (2)	559 (16)	-
PART-C	441 (2)	507 (1)	281	461 (32)	499 (15)	0.42
PART-D	443 (4)	514 (5)	283	462 (18)	495 (1)	0.51

6.3.2 Laser ablation analysis of glasses and fluid inclusions

Laser ablation ICP-MS analysis was used to determine both the possible presence of micronuggets and Pt and Ir concentrations in glasses and concentration of Pt in the synthetic fluid inclusions at the Great Lakes Institute for Environmental Research, University of Windsor, Canada. Ablation was achieved using a 266nm Nd-YAG laser and samples were analyzed using a Thermo Electron X series II quadrupole ICP-MS using an argon carrier gas. Background acquisition was obtained for 60 seconds with the laser off, followed by sample acquisition for a maximum of 180

seconds. Use of the Nd-YAG laser ablation was chosen over a femto-second laser which was also available at GLIER due to the availability of better optics using the Nd-YAG laser which was required due to the small inclusion size. The femto-second laser would provide more controlled ablation of the inclusions allowing "cold" ablation preventing rupturing and bleeding of the inclusions, however, the optics available that are suitable for the wavelength of the femto-second laser were of poor quality at that time.

For analysis of glasses, laser ablation analysis was performed on polished chips of sample glass devoid of visible surface contamination using 1.25 kiloampere power and a 20Hz repetition rate. Use of a 2 mm diameter pinhole and 10X-objective resulted in a laser spot size of 140 μm and samples were analyzed by boring into the sample at a rate determined by the laser. Data were collected for the following isotopes: ^{43}Ca, ^{44}Ca, ^{27}Al and ^{25}Mg (high resolution, 20-ms dwell times) ^{138}Ba, ^{195}Pt, ^{196}Pt (low resolution, 100-ms dwell times). Calcium was used as an internal standard for the glass analyses using values obtained by electron microprobe analysis to correct for variances in ablation yield. Analyses were calibrated using two analyses of the NIST 610 standard run at the beginning and end of each acquisition set and if acquisition sets contained more than 20 analyses, two additional NIST 610 analyses were performed mid way through the acquisition set. Using the sensitivity factors obtained for ^{195}Pt, acquired LA data were reduced and interpreted using a combination of Thermo Electron's Plasmalab software and in-house developed tools based on Longerich et al. (1996). The LA-ICPMS analysis technique used for the glasses is identical to that used in previous chapters for the determination of Pt except that Ba, Cs, and Sr are added in this study. Micronuggets were also handled in an identical manner by selecting areas of stable baseline micronugget-free analysis for calculation of Pt concentrations.

Inclusions were also analyzed using a power of 1.13 kiloampere and a 20 Hz repetition rate. The use of a 0.5 mm pinhole and a 20x objective resulted in a 22 μm beam size. Three experiments were chosen for analysis Cryst-8, Cryst-9 and Cryst-12 due to successful overgrowth and entrapment of numerous near surface inclusions. To analyze the synthetic fluid inclusions in the diopside crystals the crystals were analyzed as-is and were not prepared/polished. The thinness and fragile nature of the crystals, along with the potential of polishing out fluid inclusions prevented any preparation. The lack of polish on the surface added an extra challenge to the analysis as inclusions were difficult to see using the optics available on the LA microscope. As a result, only near-surface inclusions were able to be located and analyzed. Multiple methods were attempted when analyzing the fluid inclusions, including boring directly into the inclusion and traversing into the inclusion. Due to the near-surface nature of the inclusions, ablation of the inclusion occurred immediately after switching

the laser on when boring directly into the inclusions making interpretation impossible. Success was achieved by starting the ablation at a location adjacent to the inclusion, allowing a short acquisition of background crystal ablation, and slowly traversing into the inclusion. This was not always successful as the depth of the inclusion and depth of the ablation pit had to be estimated, as well it was possible to traverse and miss the inclusion because during ablation the inclusions were obscured. Visual confirmation of inclusion ablation was not possible and confirmation relied on the change in Ba signal which showed a marked increase upon inclusion ablation.

Table 6.4 – Summary of inclusion analysis and calculated $D_{fluid-melt}$ values for Pt.

Analytical ID	Internal Standard (^{138}Ba) ppm	Start ms	End ms	^{25}Mg ppm	^{27}Al ppm	^{44}Ca ppm	Ca:Mg	^{195}Pt ppm fluid	^{195}Pt ppm Melt	$D^{Pt}_{fluid-melt}$	Comment
Ma22A08-6	232	69932	85275	45624	52288	112414	2.5	0.888	0.078	11	
Ma22A08-15	232	64937	75998	401208	64235	391079	1.0	3.675	0.078	47	
Ma22B08-9	232	68327	76890	38277	39554	93501	2.4	0.957	0.078	12	
Ma22B08-10	232	68148	77604	24843	50686	84721	3.4	0.624	0.078	8	
Ma22B08-13	232	70111	79209	1201488	146958	1533197	1.3	2.238	0.078	29	Very weak Pt signal
Ma22B08-19	232	66186	76712	170693	58721	219885	1.3	0.180	0.078	2	

6.4 Results and discussion

After analysis was complete the spectra were assessed for coherent inclusion signals which were selected for processing. Pt concentrations were calculated using the calculated concentrations of Ba as an internal standard and an algorithm developed in-house at GLIER for analysis of fluid inclusions.

The analysis of the inclusions did not produce a straightforward set of analyses for interpretation. Four different scenarios occurred in the analyses and are listed below with their respective interpretations:

1) Coincident Ba and Pt peaks in laser-ablation spectra, this is ideal and provides convincing evidence of ablation of a Pt-bearing fluid inclusion. Coincident Ba and Pt signals primarily occurred along with larger Ba peaks >100000 counts/sec.
2) Barium-only peaks in the laser ablation spectra. This generally occurred with small Ba peaks <100000 cps for the more abundant ^{138}Ba isotope. This behaviour when paired with a low Ba value is attributed to smaller inclusions and the lack of a Pt peak is believed to be due to the small absolute amounts of Pt contained within the small inclusions which was too low to be detected. When this behaviour occurs with large Ba contents two scenarios are possible, either incomplete ablation of the inclusion (i.e. Ba-bearing fluid is bled off leaving residual solid Pt phase behind) or the ablation/liberation of the Pt is slow and creates a broader low amplitude signal which is too low for the detector to measure.
3) Platinum-only peaks in the laser ablation spectra. Because the samples are not prepared prior to analysis it is possible that some surficial Pt contamination is present on the surface of the inclusions either through contamination from the capsule or from quench products forming at the conclusion of the experiments.

Scenario 1, listed above is the optimum instance for determination of the concentrations of Pt within an inclusion. Of the three experimental crystals analyzed only Cryst-8 provided reliable results on the inclusions analyzed, however it should be noted that the bulk of the analyses were performed on Cryst-8 as it provided the most promising results during analysis. The numerical results are summarized in Table 6.4 and individual spectra are shown in Figure 6.5A-F.

As a whole, the concentrations of Pt found in the inclusions range from 180ppb to 3700 ppb, however the data can be split into two groups based on the overall chemistry of the inclusions. The first group

shows a Ca/Mg ratio of 3-4 and shows a depleted Ca, Mg, and Al signal. This group produces consistent results ranging from 620 to 960ppb. The second group shows a relatively elevated Ca, Mg and Al signal and has a Ca/Mg ratio of 1-1.5. This group of analyses shows on average higher Pt concentrations up to 3700 ppb, however one analysis has a lower Pt concentration of 180ppb. The differing Ca:Mg ratio may be indicative of the host mineral that the inclusion is contained within as the Ca:Mg ratio is higher in the "amphibole" phase than in diopside with Ca:Mg ratios of 3.6 versus 1.8, respectively. Visually, the inclusions are generally at the contact with the two mineral phases, contained within the "amphibole" phase and one would suspect that there would be a continuum of Ca:Mg ratios between the two end members, however this appears not to be the case. Increased numbers of analyses may indicate a complete continuum; however with the current dataset the data are limited. It is not believed that the data represent multiple trapping conditions as crystallization temperature is controlled and results are believed to be representative of a single fluid however some analytical relics may be present that are not clear at the present stage, increased analyses of inclusions in multiple experiments will hopefully clarify this effect if present.

6.4.1 Assessment of $D_{Fluid\text{-}melt}$ values for Pt

The calculated $D^{Pt}_{fluid-melt}$ range on the order of 10^1 showing a moderate enrichment in the fluid phase over the melt phase indicating that Pt would be compatible with an exsolved magmatic hydrous fluid. These results are consistent with the results determined in Chapters 2 and 4 with enrichment in a Cl- or CO_2-bearing phase showing higher $D^{Pt}_{fluid-melt}$ values (10^3-10^4) in the presence of a complexing agent in the fluid phase. Fluid compatibility with pure water although moderate is compelling evidence that the results obtained in previous chapters are correct and that magmatic fluids can be effective concentrating and transport agents for the PGEs.

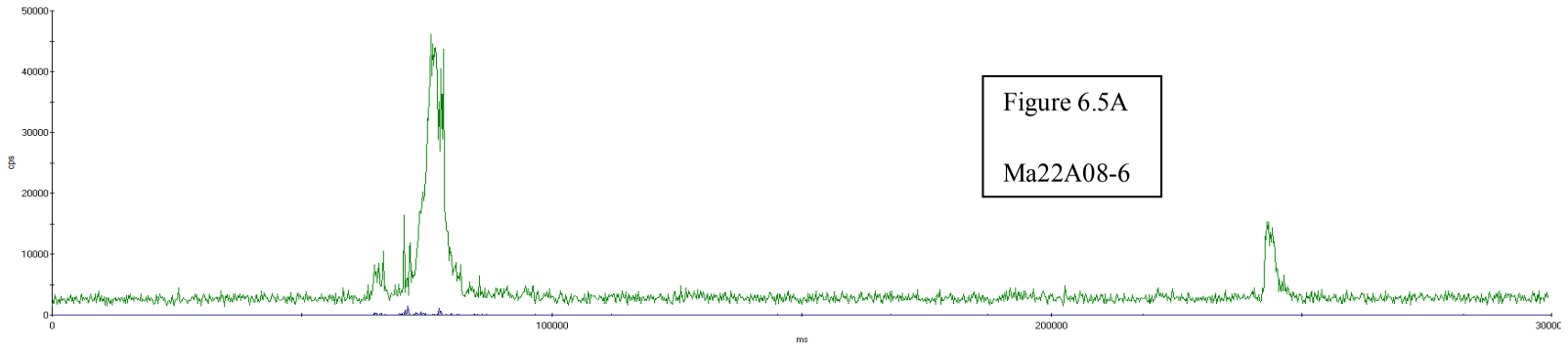

Figure 6.5A

Ma22A08-6

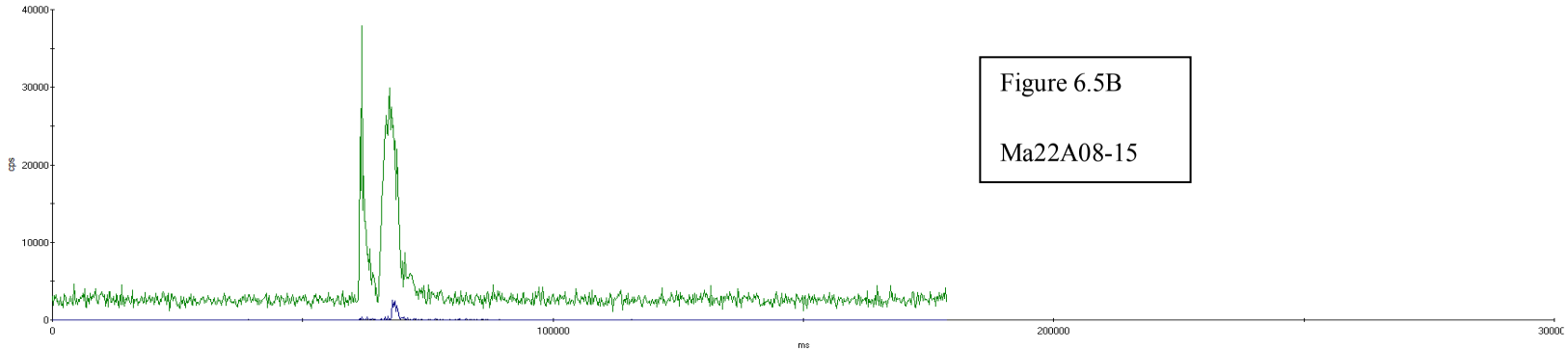

Figure 6.5B

Ma22A08-15

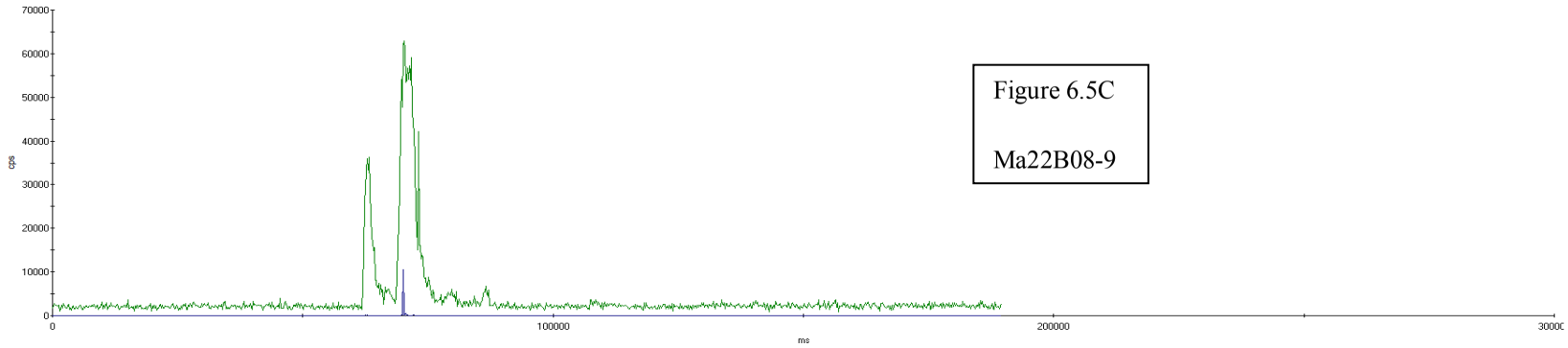

Figure 6.5C

Ma22B08-9

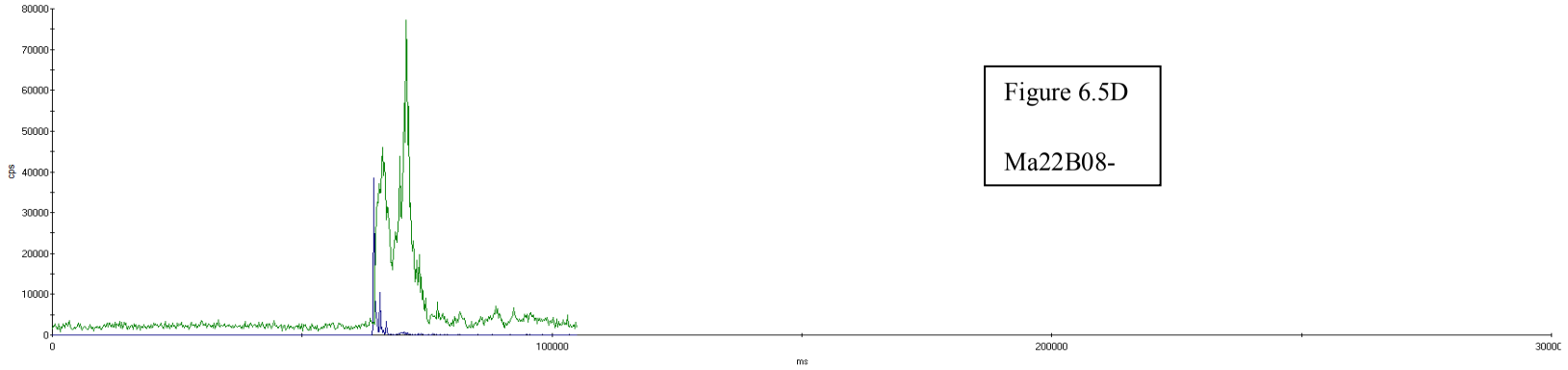

Figure 6.5D

Ma22B08-

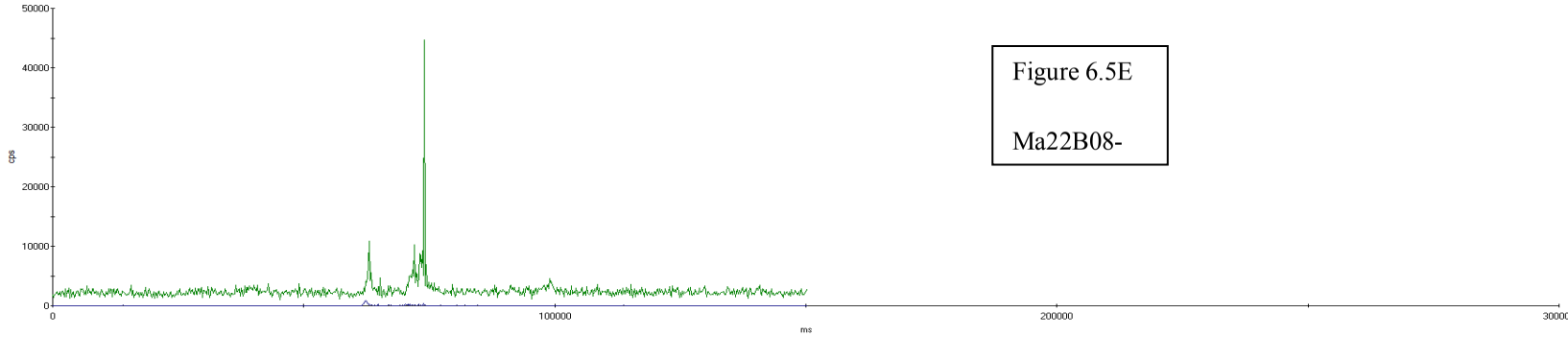

Figure 6.5E

Ma22B08-

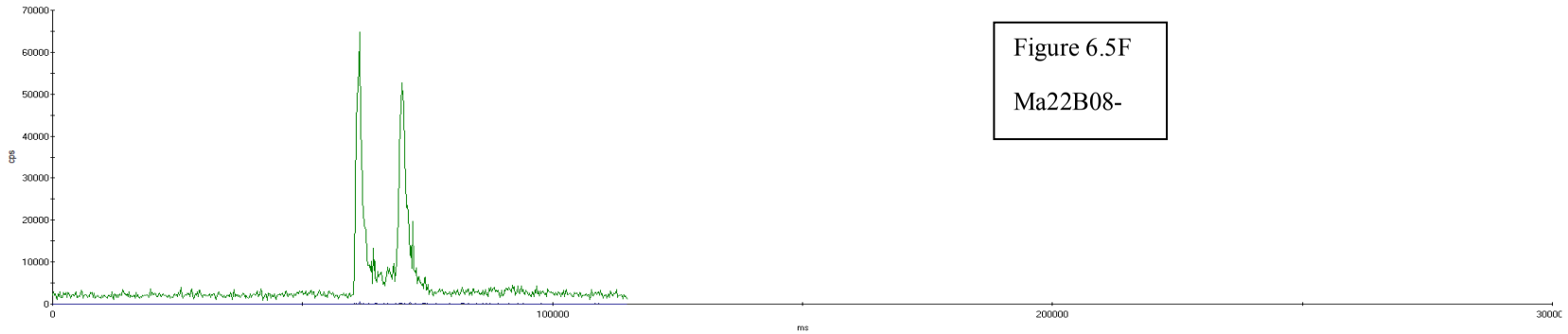

Figure 6.5F

Ma22B08-

Figure 6.5 A-F – Laser ablation spectra for the analysis of inclusion of Cryst-8. In all cases the ^{136}Ba signal is shown in green with the ^{195}Pt signal shown in blue. The ^{136}Ba signal was chosen as opposed to the ^{138}Ba signal used for calculations due to its lower abundance allowing both Pt and Ba to be shown on the same scale.

6.5 Conclusions

It has been demonstrated here that the crystallization entrapment method is successful at entrapping fluid inclusions that can be analyzed using LA-ICPMS to determine fluid-melt partition coefficient. Application of this method has provided an estimate of $D^{Pt}_{fluid-melt}$ on the order of 10^1-10^2 between an Fe-free diopside-anorthite haplobasaltic melt and pure water at magmatic conditions (1495K and 0.2 GPa) and moderately oxidizing conditions (NNO+3). This enrichment in the fluid phase indicates that magmatic hydrous fluids can act as an enrichment and transportation media for Pt in ore-forming systems. The determined $D^{Pt}_{fluid-melt}$ are consistent with the apparent partition coefficients determined for Cl- and CO_2-bearing fluids in Chapters 2 and 4 as it is likely that the addition of complexing agents in the fluid can substantially increase the partitioning into the fluid phase.

Currently the inclusions entrapped using this method are small, and in order to fully realize the potential for this method increased sensitivity and better optics will be required for the analytical equipment. Femto-second laser ablation analysis would allow more controlled ablation of the inclusions producing a cleaner signal however the optics available at the time of this study were of limited quality. With further refinement of the method it may be possible to produce larger inclusions or larger crystals which would allow sample polishing and preparation, allowing easier analysis.

Chapter 7 – Summary and Discussion

7.1 Effect of volatiles on platinum and iridium solubility

The primary and initial focus of this study was the fluid-melt partitioning of Pt and Ir, however it was soon realized that there were insufficient data available to assess the role of volatiles on the solubilities of Pt and Ir in the silicate melt that would be the focus of the study. Furthermore, at the commencement of this study nearly all experiments investigating PGE solubility were conducted in dry, volatile-free systems at atmospheric pressure. Experiments must be conducted at increased pressure and controlled redox conditions in order to assess any effect of volatiles on solubility and methods currently in use for PGE solubility were not suitable. The sealed capsule technique was deemed suitable for this purpose and was applied to three volatiles of interest, H_2O, CO_2 and Cl.

7.1.1 Water

Through the experiments of this study it was determined that water content did not have an intrinsic effect on the solubility of Pt or Ir, providing no evidence of OH-complexing, contrary to the results of Bezmen et al. 2008 ($Di_{55}An_{35}Ab_{10}$, 1473K, 0.2GPa and similar oxygen fugacities) , and discussed in Chapter 2. Although water had no intrinsic effect on solubility of Pt and Ir, due to the design of the experiments and the experimental apparatus used, water content exerts a strong control on Pt and Ir solubility by affecting/controlling the oxygen fugacity of the melt system. Metal dissolution is an oxidation reaction; oxidizing the zero-valent metal to dissolve as a charged species in the melt and as such the solubility of metals is highly dependent on the prevailing oxygen fugacity. By observing the solubility behaviour of Pt and Ir with varying oxygen fugacity it was possible to determine the valance state of these elements in the silicate melt, an area of some contention. Previous studies were able to determine that Pt dissolves in the 2+ valence state over a limited range of oxygen fugacities, below which micronugget contamination became a problem. In this study it was possible to confirm with a high degree of confidence that Pt dissolves in the melt in the 2+ valence to lower oxygen fugacities than previous work demonstrated; there was no evidence of Pt dissolved in the zero-valence state as had been previously suggested, and no evidence of micronugget contamination. At high oxygen fugacities, non-linear regression indicated the possible presence of Pt dissolved in the 4+ valence state, though at geologically relevant conditions, NNO+3 and below, Pt is dissolved primarily in the 2+ valence state. This is consistent with equivalent anhydrous studies by

Borisov and Palme (1997), Ertel et al. (1999) and Fortenfant et al., 2003. Platinum solubility can be modeled using equation 7.1, as described in Chapter 2. Under the same range of oxygen fugacities and experimental conditions, Ir was also found to dissolve primarily in the 2+ valence state. Non-linear regression of the Ir data did not provide any evidence of Ir in another valence state (0 or 1+) as suggested by Amosse et al. (1990; 2000), and is consistent with the study by Brenan (2005) under anhydrous conditions. Iridium solubility can be modeled using Equation 7.2, as described in Chapter 4.

$$[\boldsymbol{Pt}](\boldsymbol{ppb}) = \mathbf{1389}(\boldsymbol{fO_2}) + \mathbf{7531}(\boldsymbol{fO_2})^{\mathbf{1/2}} \qquad \textbf{Equation 7.1}$$

$$[\boldsymbol{Ir}](\boldsymbol{ppb}) = \mathbf{17140}(\boldsymbol{fO_2})^{\mathbf{1/2}} \qquad \textbf{Equation 7.2}$$

Lack of data at low oxygen fugacities in previous experimental studies was a result of the formation of micronuggets, high-concentration nanoscale inhomogeneities which presented a problem for analysis especially when performed using bulk-solution techniques (cf. Ertel et al., 2008). The sealed-capsule technique utilized in this study made it possible to determine the solubility of Pt at more reduced conditions than previously possible without the formation of micronuggets, as well the hydrous conditions and elevated pressure are more representative of natural conditions related to ore deposition. This was predominantly attributed to the use of a relatively Pt-free starting glass and conducting experiments at a single oxygen fugacity versus prior studies that had intermittent sampling of a single experiment while reducing oxygen fugacity over the length of the experiment. In this scenario the concentrations in the melt begin very high at highly oxidized conditions (in air) and as the oxygen fugacity is lowered the PGEs must vacate the melt, it is believed that at this point the micronuggets form and due to their small size and relative stability are maintained within the melt throughout the duration of the experiment (Ertel et al., 2008).

A lack of variation in PGE solubility versus anhydrous conditions suggests Pt is not complexed by OH^- groups within a hydrous diopside anorthite melt and, based on the data obtained in the study an enrichment of Pt is not expected with the addition of water to natural depolymerized mafic or ultramafic melts. Compositional differences with the addition of iron may produce differing results and this is an area for follow-up studies as the activity of iron may be affected by water content. Due to the propensity for Pt to alloy with iron it is foreseeable that varying the iron activity and/or speciation within the melt may vary the Pt solubility. However the addition of Fe to the melt would be expected to result in a reduction in Pt solubility, due to the potential formation of Fe-Pt

alloys reducing the Pt activity (Borisov and Palme, 1995), and it is not foreseeable that H_2O could increase the solubility above that determined in the equivalent Fe-free systems.

7.1.2 Chlorine

It was determined in Chapter 3 that Cl did not have an effect on the solubility of Pt in the silicate melt within the error of the analytical method up to and including saturation in Cl, over various water contents and oxygen fugacities. This suggests that there is no complexing of Pt with Cl in a hydrous diopside-anorthite melt. Iridium behaviour was found to be similar and as no increase in Ir solubility in the melt with increasing Cl content could be demonstrated *within the error* of the analytical technique, however a systematic relative increase in Ir solubility versus the calculated Cl-free Ir solubility was found with increasing Cl content resulting in a 60% increase in iridium solubility over calculated Cl-free solubilities at a Cl content of 2.52 wt. %. Limited data due to the necessary exclusion of short-duration experiments (as discussed in Chapter 3 and 4) as well as relatively large errors in analysis due to low concentrations and the presence of ubiquitous micronuggets (discussed below) prevents a conclusive statement indicating that Cl-complexing occurs for Ir in a hydrous diopside-anorthite melt. However, the systematic increase in Ir solubility observed certainly suggests that Cl complexing of Ir remains a possibility. If this is true the behaviour would not be isolated to Ir as a similar behaviour was noted for Au in a recent study, Botcharnikov (2009). The potential effect of Cl on the solubility of Ir is not profound (maximum observed increase of 60% only at levels nearing Cl saturation) and cannot reproduce the 1-2 order of magnitude increase in solubility (versus solubilities determined for dry volatile-free diopside anorthite) needed to explain the formation Merensky Reef proposed by Naldrett et al. (2009). However the increase is significant and could be especially important in crystallizing systems where increased Cl in residual magmas would allow Ir to be maintained within the melt to higher degrees of crystallization before becoming saturated, as discussed below.

7.1.3 Carbon dioxide

In solubility experiments investigating the effect of CO_2 on the solubility of Pt in a silicate melt, platinum solubilities with varying CO_2 contents were indistinguishable from those determined for CO_2-free systems at equivalent oxygen fugacities. The lack of variation in Pt solubility with increasing CO_2 content is strong evidence for the lack of CO_2 (CO, CO_3) complexation of Pt. The data of this study suggest the presence of CO_2 will not affect the solubility of Pt in a natural, depolymerized mafic or ultramafic melt, where the dominant dissolved carbon species in the silicate melt is CO_3 (Fine and Stolper, 1986; Behrens et al. 2004; Botcharnikov et al., 2005).

7.2 Micronuggets in solubility experiments

Micronuggets have long been an issue in experiments investigating PGE solubility and in this study was no exception. The formation of micronuggets in Pt solubility experiments investigating the effect of H_2O was avoided (Blaine et al., 2005, Chapter 2); however micronuggets were ubiquitous in all experiments that examine the effects of both Cl (Pt and Ir, Chapters 3 and 4) and CO_2 (Chapter 5). The effects of volatiles on solubilities were determined using LA-ICPMS and allowed the exclusion of the micronuggets from the analysis to determine Pt and Ir solubilities, resulting in the conclusions discussed above.

In the Cl-bearing experiments the abundance and intensities of the micronugget signals decreased with increasing experiment duration. The behavior may also be expected to occur in CO_2-bearing experiments, but run durations did not vary substantially between CO_2-bearing experiments and this effect is yet to be demonstrated. This observation suggests that the micronuggets are formed near the beginning of the experiment, are not in equilibrium with the melt and are depleted as the experiment progresses and the system attempts to approach equilibrium. This behaviour is in stark contrast to the proposed interpretation of micronugget formation by Cottrell and Walker (2006) who suggest that the PGE contained within micronuggets is dissolved within a melt at experimental conditions and the micronuggets form upon quenching of the experiments. If it was the case that micronuggets formed on quench, micronugget intensity and frequency should not display any time dependence. It should be noted that there is an ongoing debate on the formation of micronuggets (see Cottrell and Walker, 2006 and Ertel et al., 2008 for details) at reduced conditions in experimental systems, between those formed on quench (Cottrell and Walker, 2006); and stable, equilibrium "contaminant" phases, present throughout the experiment, which are dependent on the path of experimental conditions (Ertel et al., 1999; 2006; 2008). As stated by Ertel et al. (2008), using presently available experimental data it is not possible to rule out the formation of micronuggets on quench using the more slowly-quenched (piston cylinder) experiments of Cottrell and Walker, (2006). However, in the study presented here, using the sealed-capsule technique in a rapid-quench IHPV, at moderately reducing conditions there is significant evidence that the micronuggets do not form on quench, including the absence of micronuggets in water-only bearing experiments, (Chapter 2, Blaine et al. 2005) and time dependence of micronugget abundance/distribution.

The nature of the micronuggets, their propensity to form in ligand-bearing experimental systems of this study, and their behaviour with increasing run duration led to the conclusion that their formation was a result of enhanced solubility in the fluid phase. Because the experimental charge is

composed of a volatile-free diopside-anorthite glass and a separate source of volatiles, there is a period during heating, prior to the glass-transition temperature that the fluid can dissolve PGEs from the noble-metal capsule before dissolving into the melt. It was proposed (Chapters 3 -5) that the presence of Cl and CO_2 enhances the solubilities of PGEs to values much higher than the few parts-per- million solubility of Pt in pure water at these temperatures (Chapter 6). Because of this enhanced solubility, as these fluids dissolve into the melt where the contained PGEs are not accommodated (only up to ~100 ppb solubility, Chapters 2 and 3) the PGEs are left as residues forming the micronuggets. After formation, these micronuggets will potentially migrate back to the capsule walls with sufficient run durations. It is foreseeable that some of the PGE will remain suspended with the melt as Cl^- or carbonyl complexes regardless of run duration unless they are able to coalesce and become large enough to settle out.

The recognition of this as a possible mechanism for micronugget formation is important not only in assessing whether micronuggets form on quench (implying they must be included in concentration/ solubility calculations) which this study suggests they do not, but it also allows the calculation of an indication of the relative solubility of the PGEs in the fluid phase prior to dissolution through mass-balance calculations comparing micronugget-corrected analyses and bulk analyses including the micronuggets (discussed in Chapters 3-5 and below). As well, if this behaviour is confirmed it can provide new information on micronugget formation in natural systems as the experimental charge can be considered an analog to natural systems where previously exsolved or liberated fluids redissolve into a fluid undersaturated magma; this possibility is discussed below with application to current models of PGE ore deposition.

7.3 Fluid-melt partitioning of Pt and Ir

7.3.1 Water

In Chapter 6 the partitioning of Pt was investigated using a newly developed method designed to overcome many of the shortcomings of methods currently in use for study fluid-melt partitioning. The method was applied to determine partitioning between a diopside-anorthite melt and pure water at magmatic temperatures and pressures 1498K, and 0.2 GPa with a certain level of success. Inclusions were trapped and it was possible to analyze the inclusions and determine fluid melt partitioning indicating $D^{Pt}_{fluid-melt}$ values ranging from 2-47 with the most consistent results ranging between 8 and 12. This shows that there is Pt enrichment in the fluid phase over the melt

even if the added fluid is water without added ligands (such as Cl) and the solubility in the fluid phase is at or near ppm levels. Parts per million levels in the fluid represent a substantial enrichment but do not represent levels necessary for the formation of an ore deposit from exsolved fluids only, without significant volumes of fluid and an unreasonable amount of zone refinement. However, these elevated levels in pure water without any additional complexing agents is significant because enhanced solubility with the addition of complexing agents such as Cl^-, C and S species is expected to result in even higher solubilities. Evidence of this is provided in Chapters 3-5 and summarized below.

The method developed and presented in Chapter 6 is promising for the determination of fluid-melt partitioning and with further testing and with further refinement shows promise as a robust technique for the determination of multi-element partitioning. However there are some limitations and issues to address with the inclusions that are trapped and the nature of the system. The limitation of the method was not in its effectiveness of trapping fluids but rather in the size of the inclusions (<15 μm) that were trapped and limitations of the analysis; the small inclusions that were trapped were difficult to identify using the sub-optimal optics/lighting used on LA-ICPMS microscope due to poor translucence of the diopside crystal (both seed and overgrowth). As well, due to the small size and fragility of the crystals polishing was not an option. Because the inclusions were not able to be observed properly during ablation it was not possible to observe the point of ablation of the fluid inclusion, thus requiring the determination of ablation and ablation time from the interpretation of laser ablation spectra.

7.3.2 Chlorine

As a result of solubility experiments conducted and addressed in Chapters 3 and 4, it was possible to make some inferences about the fluid-melt partitioning of Pt and Ir between a diopside-anorthite melt and a Cl-bearing aqueous fluid. As discussed above and in Chapters 3-5 and above, the presence of micronuggets in Cl-bearing experiments is interpreted to be the result of initial dissolution of large amounts of Pt and/or iridium in the high temperature fluid, prior to dissolution of the fluid into the silicate melt. If it assumed that the Pt and/or Ir dissolved in the fluid is the source of excess platinum allowing the formation of the micronuggets, it is possible to use a mass-balance calculation to determine how much Pt or Ir was dissolved in the fluid. The concentration of metal dissolved in the glass determined by LA-ICPMS subtracted from the bulk metal content determined by bulk solution ID-ICPMS gives an estimation of the amount of PGE contributed by the micronuggets and hence the fluid, as described in Equation 7.3. Using the calculated metal content it

is possible to estimate the integrated concentration in the fluid and estimate the corresponding apparent fluid-melt partition coefficient. Though it cannot be demonstrated that the values obtained are representative of equilibrium conditions, if the hypothesis on the formation of micronuggets stated here is correct, they strongly suggest significant partitioning of Pt and Ir into a Cl-bearing fluid and at the least can be used to qualitatively assess the relative importance of different ligands.

Using these methods for Pt and Ir in Cl-bearing fluids, respective apparent partition coefficients ($D^{i}_{fluid-melt}$) of $1x10^3$ to $4x10^3$ and 300-1100 were determined (Chapters 3 and 4) and are on the same order as those suggested by Hanley et al. (2007), who also had problems demonstrating equilibrium. These estimates represent substantial enrichment in the fluid (100's of ppm Pt and 10's of ppm Ir), at levels that may be on the same order of importance as the partitioning between sulphide melt and silicate melt which are on the order of 10^4 (Fleet et al., 1999). Considering the number of variables, the apparent fluid-melt partition coefficients are very consistent; all estimates are on the same order of magnitude. If the hypothesis of micronugget formation is true these represent a viable first estimate for fluid-melt partitioning in the presence of Cl. Using these partition values, a fluid should be regarded as a potential enrichment and transport media and its role cannot be simply dismissed as it generally is when discussing the R-factor model. More discussion on the role of fluids in ore deposit formation and the comparison between the behaviours of Pt and Ir are discussed below in their respective sections.

Using this method the estimated solubilities in the fluid and hence the partition coefficients can potentially be considered minimum estimates as it has been demonstrated that the Pt and Ir micronuggets do leave the melt over time (Chapters 3 and 4) and some PGE will be lost to the capsule and not form micronuggets. However it must also be stressed that there are many processes involved in the heating stages and that prograde Pt solubility is assumed for the fluid. In order to test this hypothesis it would be possible to "zero-time" experiments where experiments are quenched immediately after reaching experimental temperature. These experiments would determine if the micronuggets were formed over the duration of the experiment and should provide the nearest to actual partition coefficients although some PGE will still have to be assumed to be lost to the capsule. These experiments are planned for the near future but time does not permit including the results here. Another test for this hypothesis would be to use a sealed capsule with a solid piece of diopside-anorthite glass surrounded by diopside-anorthite glass powder and run the experiments as described in Chapters 3 and 4. If the micronuggets are indeed a result of the Cl bearing fluid then micronuggets should form in the powdered portion of the glass and not within the solid glass portion. In order to test this hypothesis using this technique, the experimental glass of this experiment would have to be

carefully cut and polished to bisect the solid glass core allowing analysis of both types of glasses by LA-ICPMS. It may be possible to add a tracer (element with low diffusivity, e.g. P^{5+}, and at trace concentrations) during synthesis in the glass to be used for the solid piece of glass to mark the interface between the powdered glass and solid glass piece which would be detectable on analysis by LA-ICPMS.

7.3.2 Carbon dioxide

Using the methods discussed for Cl above it was possible to estimate the partitioning of Pt between an H_2O-CO_2 fluid and a silicate melt. Micronuggets were prevalent in these experiments and were believed to have formed in a manner analogous to that presented for Cl-bearing experiments. All of the assumptions and inferences made for Cl-bearing fluid partitioning discussed above are applicable to CO_2. Apparent fluid-melt partitioning of Pt ($D^{Pt}_{fluid-melt}$) between a CO_2-bearing aqueous fluid and a diopside-anorthite melt were determined to range between 150 and 4200. However in comparison to Cl there is a more consistent and extensive dataset with essentially constant H_2O contents (approximately 1 wt. % of the bulk composition) and varying CO_2 contents. It is noted that there is a strong positive correlation between the mol ratio of the fluid, CO_2:H2O, and the apparent $D^{Pt}_{fluid-melt}$ up to maximum of ~3700 at a mol CO_2:H2O = 0.14, above which the apparent $D^{Pt}_{fluid-melt}$ appears to be constant with some scatter. The observed maximum at CO_2:H2O = 0.14 is at this point not explained, but is supported by repeat experiments at this fluid composition.

These experiments indicate that CO_2 or CO_2-bearing aqueous fluids can be efficient transport and enrichment media for Pt. These fluids have a high capacity for transporting Pt with solubilities in the 10's of ppm at the conditions of these experiments and as these fluids are very prevalent in mafic and ultramafic magmatism they could be extremely important and their potential role in PGE deposit formation is discussed below.

7.4 Comparison of the behaviours of Pt and Ir

It has long been noted that the PGEs behave differently from one another and ratios of the PGEs are commonly used to interpret the influence of certain processes. One ratio that is used is Pt/Ir and is primarily looked at to determine the source of the PGEs. Iridium-bearing phases generally have higher melting points and are refractory (Barnes et al., 1985; Lorand et al. 2008; Mungall et al., 2008); higher Ir values are representative of more complete melting of source magmas as Ir can be maintained in the residual peridotite mantle residue whereas the Pt will be lost from the residue with

the melting of the sulphide. High Pt/Ir values can also be indicative of sea water influence. The study of both Pt and Ir in this study allows direct comparison between the behaviours of these two elements under the restricted conditions of these experiments.

Table 7.1 shows a summary of Pt and Ir solubility and partitioning data obtained in this study. Both Pt and Ir were found to dissolve in a haplobasaltic diopside-anorthite over geologically relevant oxygen fugacities with a primary valence of 2+. This statement can be extended to state that simple variations in oxygen fugacity will not cause fractionation of Pt and Ir, unless certain phases that exclude/incorporate one of the two elements are stabilized corresponding with the change in oxygen fugacity. It was observed that Ir solubility is higher than Pt by a factor of approximately 2 with a modeled Pt:Ir ratio of 0.44 using the equations developed (Chapters 2 and 4, Equations 7.1 and 7.2).

Data are available in this study to compare the integrated concentrations of Pt and Ir in a Cl-bearing aqueous fluid and combined with the melt solubility values, apparent $D^{i}_{fluid-melt}$ can also be compared. The integrated concentration of Pt in the Cl-bearing aqueous fluid is nearly double that of Ir and is very consistent between experiments (Table 7.1). Along with the lower solubility of Pt in the silicate melt this produces a significantly higher apparent partition coefficient $(D^{i}_{fluid-melt})$ for Pt as compared to that for Ir, with averages of 2700 and 700, respectively. The higher solubility of Pt in a Cl-bearing aqueous fluid, and higher apparent $D^{Pt}_{fluid-melt}$ introduce a possible mechanism for fractionation of Pt and Ir. Upon exsolution of a Cl-bearing fluid, Pt and Ir will partition into the fluid however this will deplete the silicate melt more strongly in Pt, increasing the Pt:Ir ratio in the fluid and decreasing it in the melt. The evidence here only shows that this could be true of mixed H_2O-Cl fluids and element behaviour may be different for other binary fluids such as H_2O-CO_2 and H_2O-S as well as multi-component fluids.

Table 7.1 – Tabulated results of calculated estimated integrated concentrations of Pt and Ir in the fluid phase and estimates of apparent $D_{fluid\text{-}melt}$

Experiment ID	$H_2O_{(melt)}$ Wt. %	$Cl_{(melt)}$ Wt. %	Mol Cl:H_2O added	$[Pt]_{fluid}$ ppb	$[Ir]_{fluid}$ ppb	$D^{Pt}_{fluid-melt}$	$D^{Ir}_{fluid-melt}$	$\frac{D^{Pt}}{D^{Ir}}$	Pt/Ir Fluid
PtIr-8	3.59	1.79	0.25	235000	134000	3300	820	4.0	1.8
PtIr-9	2.96	1.85	0.32	144000	78000	2600	620	4.2	1.8
PtIr-10	2.03	2.75	0.69	32000	18000	1100	270	3.9	1.7
PtIr-11	2.25	2.25	0.51	154000	88000	4300	1100	3.9	1.7
Cl-5	2.14	2	0.47	31000		900			
Cl-6	1.01	2.53	1.27	42000		4200			
average				106000	79000	2700	700		

7.5 Application of results to natural systems and ore-deposit modeling

This study assessed the effect of volatiles on Pt and Ir solubility, from their effect on PGE solubility in the melt, to partitioning of the PGE between a silicate melt and an exsolved fluid at magmatic conditions. The fluids used were simple binary fluids and an iron-free analog was used as the melt composition to isolate the affect of the individual volatiles. These studies were conducted to provide experimental data for researchers to assess their models, working toward understanding the complex systems and complex behaviours of the PGE that allow these elements to reach concentrations that are high enough to generate an ore deposit. The systems used here are simple analogs and caution must be used when applying the data and values to natural systems; however, the data of this study suggest that the volatiles studied can play an important role in PGE ore deposit formation, perhaps effecting solubility of the PGE in the parental/derivative silicate melts as in the case of Cl or as concentrating and transport media. As well, the proposed behaviours of Pt and Ir resulting in formation of micronuggets is an intriguing prospect and the potential for these micronugget-forming processes to occur in natural systems is something that must be considered as it could be an important step in the formation of ore deposits.

One of the major shortcomings of the R-factor model is the very low saturation levels for PGE in the parental magmas of deposits such as Bushveld, which is on the order of a few ppb at the proposed oxygen fugacity (FMQ) for Bushveld (Naldrett, 2009). These low saturation concentrations require that the PGEs that form the deposit are collected and concentrated from a very large volume of magma. Increasing the solubility/concentrations of PGE in the magma would require smaller volumes of magma to produce the same amount of ore. It was proposed at the beginning of this study that the incorporation of volatiles could result in enhanced solubility of the PGE in the silicate melt. Although some evidence of enhanced solubility with the addition of Cl was obtained for Ir (and perhaps Pt) the increases are less than 100% and would not produce the 100-fold increase in solubility over experimentally determined solubilities in dry, volatile-free, diopside-anorthite melts that have been suggested as necessary for the R-factor model (Naldrett, 2009). However the small increase in solubility may be important in another fundamental area, if the parental magmas are at or near saturation in PGE, and in the case of Bushveld it appears that this is so (Merkle et al., 1995), then only very small amounts of crystallization would be able to occur prior to the melt becoming saturated and depositing PGE. Chlorine, an incompatible element that will increase in concentration in the residual melt as early crystallization occurs, may increase the PGE solubility enough as it

increases in concentration to allow the PGEs to be maintained in the residual magma until saturation of the melt in a sulphide or volatile phase.

It was demonstrated in this study that significant concentrations of Pt can be dissolved in an aqueous fluid and solubility is enhanced in mixed H_2O-CO_2 and H_2O-Cl, with the highest solubilities occurring in the latter. Estimated solubilities of 10's to 100's of ppm in these fluids suggest that these fluids can indeed transport and concentrate PGEs adding experimental support to the magmatic-hydrothermal model. In the case of mixed H_2O-Cl fluids it appears that the fluids would be more efficient at scavenging Pt over Ir and field evidence comparing Pt:Ir ratios between parental and derivative magmas and ores may provide evidence whether fluids played a role. However more work is needed on the solubility of the individual PGEs in complex fluids, as a mixed H_2O-CO_2-Cl-(+/- S) fluids, which are more likely to be representative of complex natural fluids.

The results of this study indicate that timing of a volatile/sulphide saturation event is an important factor due to the high apparent $D^i_{fluid-melt}$ values. If the melt reaches saturation in sulphide and exsolves a sulphide melt which also liberates a Cl or CO_2-bearing aqueous phase (Ballhaus and Stumpfl, 1986) the PGE concentrations in these two phases may be broadly similar (factor of 10) reducing the effectiveness of the sulphide as a concentrating agent. This could be important because if these two phases separate and evolve separately it would essentially cause a dilution of the PGEs preventing significant enrichment. As well, if volatile saturation is reached before sulphide saturation and the volatile phase has been transported away, the melt will be left reduced in PGEs, reducing the PGE concentrations in later formed sulphides.

The processes proposed in this study for the formation of micronuggets (Chapters 3-6) offer some intriguing possibilities if analogous processes occur in natural systems. The process presented here is solely a hypothesis as to how the processes believed to occur in these experiments could apply to natural systems. It is foreseeable that as a melt evolves and eventually reaches saturation in a volatile phase and PGEs will be partitioned into that phase (magmatic-hydrothermal model). If generated in the crystal mush of a magma chamber the fluid will propagate upwards due to buoyancy and compaction of the crystal pile (also the magmatic-hydrothermal model), where eventually it can eventually come in contact with a fluid undersaturated magma. However, as the fluid dissolves into the magma which will be at or near PGE saturation, the PGEs dissolved within the fluid will not be able to be accommodated in the magma and will be left as a residue, analogous to the formation of micronuggets in these experiments. This process can continue with continual deposition of the PGE (potentially as micronuggets) at the interface of the fluid-undersaturated magma. As the interface of

the fluid-undersaturated magma propagates upwards as the crystal pile grows, this PGE-deposition front would migrate upwards with it as fluids that are generated beneath could re-dissolve the PGE micronuggets that were previously formed, transporting them upwards until again the fluid is dissolved in the magma re-depositing the PGE, this is similar to the vapour refinement model of Boudreau and Meurer (1999). However, Boudreau and Meurer (1999) did not take into account the formation of the micronuggets and instead interpreted that the PGEs would be concentrated into a sulphide phase directly and the model therefore relies on a sulphide phase being present. This model would be consistent with the observations and interpretations of Tredoux et al., (1995) and Ballhaus and Sylvester (2006) who estimate that the magmas were saturated in some PGEs and there were (non-sulphide) PGE-phases present at the time of the introduction of the Merensky magmas and the exsolution of the sulphide melt simply remobilized the PGEs. This model could also indeed work in conjunction with that proposed by Naldrett, 2009 for the formation of the Merensky Reef and would remove the reliance of the model on extreme concentrations of PGE in the silicate magma.

As proposed by Naldrett (2009) and authors cited therein, a later-stage magma was intruded into the Bushveld complex pooling out along the boundary between the crystal pile and the overlying magma, generating the Merensky Reef. Mixing of the magmas, as the later-stage magma propagated outwards resulted in saturation of the magmas in a sulphide melt. The generated sulphide melt is proposed to have mixed with the magmas due to turbulence and convection and during this mixing scavenged the PGEs from the magma. Using the current knowledge of PGE solubility in silicate melts it would require scavenging of PGE from 2500m of overlying magma (which is highly unlikely)(Naldrett, 2009), and it was therefore proposed that higher PGE solubilities would be required for the silicate melt.

If however, prior to the influx of the late stage magma, the processes of upward migration of PGE due to exsolution and redissolution of a volatile phase occurred, generating a PGE-rich horizon at the interface of the crystal pile and the overlying magma, a different scenario could occur. As the later-stage magma extruded outwards along the boundary between the crystal pile and overlying magma (currently the position of the Merensky Reef) causing sulphide saturation, the exsolved sulphide melt would mix with, and dissolve or assimilate the PGEs micronuggets that were deposited from the fluids at the interface enriching the sulphide in the PGE. This would thereby reduce the reliance of the model on the scavenging of the PGEs from an extremely large vertical column of magma, however it would be expected that some PGE would be scavenged from the overlying magmas as mixing occurred. After the PGEs were entrained and/or dissolved within the sulphide they would reside there and further redistribution would not occur.

The hybrid model explained here could explain the textural features noted in the sulphides of the Merensky Reef where the cores of the sulphides do not contain the highest levels of PGE (Ballhaus and Stumpfl, 1986), the association between the PGEs and elements with an aqueous affinity such as Cl in PGE-bearing layered intrusions (Boudreau and Meurer, 1998; Meurer et al., 1999; Willmore et al. 2000; Boudreau, 2008) and does not contradict the features supporting the R-factor model.

Chapter 8 - Conclusions

The purpose of this study was to study the effects of volatiles (i.e. H_2O, Cl and CO_2) on the solubility of Pt and Ir in a haplobasaltic melt, and furthermore determine the fluid-melt partitioning of Pt between a haplobasaltic melt and an aqueous fluid, at magmatic (P-T) conditions relevant to natural mafic magmas. Current experimental techniques were modified and new techniques were developed for the purposes of this study and were successfully applied to investigate these systems.

8.1 Solubility Experiments

This study used a sealed-capsule technique combined with rapid quench as an effective means for determining the effect of volatiles on Pt and Ir solubility in a haplobasaltic diopside-anorthite melt at 1523K and 0.2GPa; conditions analogous to natural systems. Using these techniques, three magmatic volatile conditions were investigated that are relevant to magmatic PGE ore forming systems: H_2O, Cl+H_2O andCO_2+H_2O.

In water-bearing experiments, it was determined that water content did not have an intrinsic effect on Pt or Ir solubility for water contents between 0.9 wt. % and 4.4 wt. % (saturation), showing identical solubility behaviours to those determined for dry 1-atm conditions. Water content controlled the oxygen fugacity of the experiment and the resulting variations in oxygen fugacity, and the corresponding solubilities of Pt and Ir, indicate that over geologically relevant conditions both Pt and Ir are dissolved primarily in the 2+ valence state. Pt data suggest minor influence of Pt^{4+} at higher oxygen fugacities; however, there is no evidence of higher valence states for Ir. The ability of the sealed capsule technique to produce micronugget-free run product glasses in water-only experiments, allowed the solubility of Pt to be determined in hydrous haplobasalt at lower oxygen fugacities (and concentrations) then was previously observed, without the influence of micronuggets. In these experiments, neither Pt nor Ir showed any evidence of dissolution in a neutral 0-valent state. Pt and Ir solubility can be represented as a function of oxygen fugacity (bars) by the following equations:

$$[\boldsymbol{Pt}](\boldsymbol{ppb}) = \mathbf{1389}(\boldsymbol{fO_2}) + \mathbf{7531}(\boldsymbol{fO_2})^{\mathbf{1/2}}$$

$$[\boldsymbol{Ir}](\boldsymbol{ppb}) = \mathbf{23714}(\boldsymbol{fO_2})^{\mathbf{1/2}}$$

In Cl-bearing experiments, experimental products from short run duration (<96hrs) experiments contained numerous micronuggets, preventing accurate determination of platinum and iridium solubility. Longer run duration experiments showed decreasing amounts of micronuggets, allowing

accurate determination of solubility; results indicate that under the conditions studied chlorine has no discernable effect on Pt solubility in the silicate melt from 0.6 to 2.75 wt. % Cl (saturation). Over the same conditions, a systematic increase in Ir solubility is found with increasing Cl content; however, the observed increase is within the analytical variation/error and is therefore not conclusive. If there is an effect of Cl on Ir solubility the effect is minor, resulting in increased Ir solubilities of 60% at chlorine saturation, relative to the determined values for a Cl-free melt. More work needs to be done to constrain the behaviour of Ir with respect to Cl content at varying oxygen fugacities to determine the speciation of Ir within the melt.

However, the abundance of micronuggets in short run duration experiments in Cl-bearing experiments, which decrease in abundance with time and increase with Cl-content, offers compelling evidence that Cl-bearing fluids have the capacity to transport significant amounts of Pt and Ir under magmatic conditions. It is suggested that platinum and iridium dissolved within the Cl-bearing fluid are left behind as the fluid dissolves into the melt during the heating stages of the experiment, leaving small amounts of Pt and Ir along the particle boundaries. With increasing run duration, the metal migrates back to the capsule walls decreasing the amount of micronuggets contained within the glass. Estimates based on this model, using mass balance calculations on the excess amount of Pt and Ir in the run product glasses (i.e. above equilibrium solubility) in short duration experiments, indicate non-equilibrium Pt and Ir concentrations in the Cl-bearing fluid ranging from 10s to a few hundred ppm, versus ppb levels in the melt. Respective apparent partition coefficients ($D^{i}_{fluid-melt}$) of 1x10^3 to 4x10^3 and 200-800 were determined for Pt and Ir in Cl-bearing fluids; suggesting that Cl-bearing fluids can be highly efficient at enriching and transporting PGE in mafic magmatic-hydrothermal ore-forming systems. The values obtained for Pt strongly contrast withrecent experimental results in felsic systems; the strong difference between our data (~1523K) in a hydrous, Fe-free haplobasalt and the recent dataset of Simon and Pettke (2009) obtained for rhyolite melts at 1073K also stress the need for further studies to quantify the high temperature fluid-melt partitioning of PGEs. Furthermore, if the estimates of Simon and Pettke are correct, this indicates that partitioning and solubility data and behavior of the PGEs cannot be applied outside of strict compositional brackets and much care must be taken when comparing experimental data with natural ore-forming systems.

Platinum solubility was also determined as a function of CO_2 content in a hydrous haplobasalt at controlled oxygen fugacity using the same sealed capsule techniques and melt composition as for H_2O and Cl.. Experiments were conducted with a water content of approximately 1 wt. %, fixing the log oxygen fugacity (bars) between -5.3 and -6.1 (log NNO = -6.95 @ 1523K and 0.2GPa) (O'Neill and Pownceby (1993). Carbon dioxide contents in the run product glasses ranged from 800-2500ppm;

and over these conditions, CO_2 was found to have negligible effect on Pt solubility in the silicate melt. Analogous to the Cl-bearing experiments, bulk concentrations of Pt in CO_2 bearing experiments increased with increasing CO_2 content due to micronugget formation. Using the models developed for Cl, apparent Pt concentrations in the H_2O:CO_2 fluid phase, prior to fluid dissolution, were estimated to be 1.6 to 42 ppm. These concentrations resulted in apparent partition coefficients $(D^{i}_{fluid-melt})$ between $1.5x10^2$ and $4.2x10^3$, increasing with increasing mol CO_2:H_2O up to approximately 0.15, above which increasing CO_2 content does not further increase partitioning. These high apparent $D_{fluid-melt}$ values for Pt suggest a substantial enrichment in the fluid phase and suggest mixed H_2O-CO_2 fluids as potential enrichment and transport media for Pt and perhaps other PGEs in ore-forming systems.

Apparent concentrations calculated for the fluid phase as well as the resulting partition coefficients are at this point estimations, due to two factors: 1) equilibrium cannot be established, as some Pt and/or Ir could be lost to the capsule, and during the heating of the experiment the system is in constant flux and 2) the hypothesis proposed for micronugget formation has yet to be irrefutably proven, although all available evidence indicates that it is the case. The estimates; however, are believed to be relevant estimates and indicate at the very least that these hydrothermal fluids can transport significant amounts of PGE.

8.2 Partitioning experiments

Experimental techniques were developed in this study to investigate the fluid-melt partitioning of Pt between a haplobasaltic melt and an aqueous fluid. It has been demonstrated here that the newly developed crystallization entrapment method is successful at entrapping fluid inclusions that can be analyzed using LA-ICPMS to determine fluid-melt partition coefficients. Application of this method has provided an estimate of $D^{Pt}_{fluid-melt}$ on the order of 10^1-10^2 between an Fe-free diopside-anorthite haplobasaltic melt and pure water at magmatic conditions (1495K and 0.2 GPa) and moderately oxidizing conditions (NNO+3.4) (O'Neill and Pownceby (1993). This enrichment in the fluid phase using this method also confirms that magmatic aqueous fluids can act as an enrichment and transportation media for Pt in ore forming systems. The determined $D^{Pt}_{fluid-melt}$ are consistent with those determined for Cl and CO_2 bearing fluids, as it is likely that the addition of complexing agents in the fluid can substantially increase the partitioning into the fluid phase.

Currently the inclusions entrapped using this method are small, and in order to fully realize the potential for this method increased sensitivity and better optics will be required for the analytical equipment. Femto-second laser ablation analysis would allow more controlled ablation of the

inclusions producing a cleaner signal however the optics available at the time of this study were of limited quality. With further refinement of the method it may be possible to produce larger inclusions or larger crystals which would allow sample polishing and preparation, allowing easier analysis.

This method shows very good promise and can be applied with further refinement to investigate the fluid melt-partitioning of a variety of different elements under various conditions and for various volatiles.

8.3 Application to natural ore forming systems

The results of this study indicate that the volatiles studied (i.e. H_2O, CO_2+H_2O, and Cl+H_2O) do not have a significant effect on Pt and Ir solubility in a haplobasaltic melt at magmatic conditions. These results suggest that complexing of Pt and Ir by OH, Cl, and carbonate species in a haplobasaltic melt is insignificant and the presence of these volatiles will not result in significantly increased PGE contents over their dry counterparts, as has been suggested in literature. Preliminary evidence of minor Cl-complexing of Ir is presented; however, resulting in only a slight increase (<100%) in Ir solubility at Cl-saturation. Significant partitioning of Pt and Ir into a fluid phase at magmatic conditions has been demonstrated; with estimates of fluid-haplobasaltic melt partition coefficients increasing from $1x10^1$ for pure water to up to $4x10^3$ with the addition of Cl or CO_2 to the system. This result indicates complexing of Pt and Ir with $OH < H_xCO_y \leq Cl$. Using these estimates, Cl- or CO_2-bearing magmatic fluids can be highly efficient at enriching and transporting platinum group elements (PGEs) in mafic magmatic-hydrothermal ore-forming systems supporting the magmatic-hydrothermal model.

Permissions

ELSEVIER LICENSE
TERMS AND CONDITIONS

Jun 11, 2010

This is a License Agreement between Fred A Blaine ("You") and Elsevier ("Elsevier") provided by Copyright Clearance Center ("CCC"). The license consists of your order details, the terms and conditions provided by Elsevier, and the payment terms and conditions.

All payments must be made in full to CCC. For payment instructions, please see information listed at the bottom of this form.

Supplier	Elsevier Limited The Boulevard,Langford Lane Kidlington,Oxford,OX5 1GB,UK
Registered Company Number	1982084
Customer name	Fred A Blaine
Customer address	3199 Capstan Crescent Coquitlam, BC V3c4H3
License Number	2446020152470
License date	Jun 11, 2010
Licensed content publisher	Elsevier
Licensed content publication	Geochimica et Cosmochimica Acta
Licensed content title	Platinum solubility in a haplobasaltic melt at 1250°C and 0.2 GPa: The effect of water content and oxygen fugacity
Licensed content author	Fred A. Blaine, Robert L. Linnen, Francois Holtz, Gerhard E. Brügmann
Licensed content date	1 March 2005
Volume number	69
Issue number	5
Pages	9
Type of Use	Thesis / Dissertation
Portion	Full article
Format	Both print and electronic
You are an author of the Elsevier article	Yes
Are you translating?	No
Order Reference Number	
Expected publication date	Jul 2010

Elsevier VAT number	GB 494 6272 12
Permissions price	0.00 USD
Value added tax 0.0%	0.00 USD
Total	0.00 USD

Terms and Conditions

INTRODUCTION

1. The publisher for this copyrighted material is Elsevier. By clicking "accept" in connection with completing this licensing transaction, you agree that the following terms and conditions apply to this transaction (along with the Billing and Payment terms and conditions established by Copyright Clearance Center, Inc. ("CCC"), at the time that you opened your Rightslink account and that are available at any time at http://myaccount.copyright.com).

GENERAL TERMS

2. Elsevier hereby grants you permission to reproduce the aforementioned material subject to the terms and conditions indicated.

3. Acknowledgement: If any part of the material to be used (for example, figures) has appeared in our publication with credit or acknowledgement to another source, permission must also be sought from that source. If such permission is not obtained then that material may not be included in your publication/copies. Suitable acknowledgement to the source must be made, either as a footnote or in a reference list at the end of your publication, as follows:

"Reprinted from Publication title, Vol /edition number, Author(s), Title of article / title of chapter, Pages No., Copyright (Year), with permission from Elsevier [OR APPLICABLE SOCIETY COPYRIGHT OWNER]." Also Lancet special credit - "Reprinted from The Lancet, Vol. number, Author(s), Title of article, Pages No., Copyright (Year), with permission from Elsevier."

4. Reproduction of this material is confined to the purpose and/or media for which permission is hereby given.

5. Altering/Modifying Material: Not Permitted. However figures and illustrations may be altered/adapted minimally to serve your work. Any other abbreviations, additions, deletions and/or any other alterations shall be made only with prior written authorization of Elsevier Ltd. (Please contact Elsevier at permissions@elsevier.com)

6. If the permission fee for the requested use of our material is waived in this instance, please be advised that your future requests for Elsevier materials may attract a fee.

7. Reservation of Rights: Publisher reserves all rights not specifically granted in the combination of (i) the license details provided by you and accepted in the course of this licensing transaction, (ii) these terms and conditions and (iii) CCC's Billing and Payment terms and conditions.

8. License Contingent Upon Payment: While you may exercise the rights licensed immediately upon issuance of the license at the end of the licensing process for the transaction, provided that you have disclosed complete and accurate details of your proposed use, no license is finally effective unless and until full payment is received from you (either by publisher or by CCC) as provided in CCC's Billing and Payment terms and conditions. If full payment is not received on a timely basis, then any license preliminarily granted shall be deemed automatically revoked and shall be void as if never granted. Further, in the event that you breach any of these terms and conditions or any of CCC's Billing and Payment terms and conditions, the license is automatically revoked and shall be void as if never granted. Use of materials as described in a revoked license, as well as any use of the materials beyond the scope of an unrevoked license, may constitute copyright infringement and publisher reserves the right to take any and all action to protect its copyright in the materials.

9. Warranties: Publisher makes no representations or warranties with respect to the licensed material.

10. Indemnity: You hereby indemnify and agree to hold harmless publisher and CCC, and their respective officers, directors, employees and agents, from and against any and all claims arising out of your use of the licensed material other than as specifically authorized pursuant to this license.

11. No Transfer of License: This license is personal to you and may not be sublicensed, assigned, or transferred by you to any other person without publisher's written permission.

12. No Amendment Except in Writing: This license may not be amended except in a writing signed by both parties (or, in the case of publisher, by CCC on publisher's behalf).

13. Objection to Contrary Terms: Publisher hereby objects to any terms contained in any purchase order, acknowledgment, check endorsement or other writing prepared by you, which terms are inconsistent with these terms and conditions or CCC's Billing and Payment terms and conditions. These terms and conditions, together with CCC's Billing and Payment terms and conditions (which are incorporated herein), comprise the entire agreement between you and publisher (and CCC) concerning this licensing transaction. In the event of any conflict between your obligations established by these terms and conditions and those established by CCC's Billing and Payment terms and conditions, these terms and conditions shall control.

14. Revocation: Elsevier or Copyright Clearance Center may deny the permissions described in this License at their sole discretion, for any reason or no reason, with a full refund payable to you. Notice of such denial will be made using the contact information provided by you. Failure to receive such notice will not alter or invalidate the denial. In no event will Elsevier or Copyright Clearance Center be responsible or liable for any costs, expenses or damage incurred by you as a result of a denial of your permission request, other than a refund of the amount(s) paid by you to Elsevier and/or Copyright Clearance Center for denied permissions.

LIMITED LICENSE

The following terms and conditions apply only to specific license types:

15. **Translation**: This permission is granted for non-exclusive world **English** rights only unless your license was granted for translation rights. If you licensed translation rights you may only translate this content into the languages you requested. A professional translator must perform all translations and reproduce the content word for word preserving the integrity of the article. If this license is to re-use 1 or 2 figures then permission is granted for non-exclusive world rights in all languages.

16. **Website**: The following terms and conditions apply to electronic reserve and author websites:
Electronic reserve: If licensed material is to be posted to website, the web site is to be password-protected and made available only to bona fide students registered on a relevant course if:
This license was made in connection with a course,
This permission is granted for 1 year only. You may obtain a license for future website posting,
All content posted to the web site must maintain the copyright information line on the bottom of each image,
A hyper-text must be included to the Homepage of the journal from which you are licensing at http://www.sciencedirect.com/science/journal/xxxxx or the Elsevier homepage for books at http://www.elsevier.com , and
Central Storage: This license does not include permission for a scanned version of the material to be stored in a central repository such as that provided by Heron/XanEdu.

17. **Author website** for journals with the following additional clauses:

All content posted to the web site must maintain the copyright information line on the bottom of each image, and
he permission granted is limited to the personal version of your paper. You are not allowed to download and post the published electronic version of your article (whether PDF or HTML, proof or final version), nor may you scan the printed edition to create an electronic version,
A hyper-text must be included to the Homepage of the journal from which you are licensing at http://www.sciencedirect.com/science/journal/xxxxx , As part of our normal production process, you will receive an e-mail notice when your article appears on Elsevier's online service ScienceDirect (www.sciencedirect.com). That e-mail will include the article's Digital Object Identifier (DOI). This number provides the electronic link to the published article and should be included in the posting of your personal version. We ask that you wait until you receive this e-mail and have the DOI to do any posting.
Central Storage: This license does not include permission for a scanned version of the material to be stored in a central repository such as that provided by Heron/XanEdu.

18. **Author website** for books with the following additional clauses:
Authors are permitted to place a brief summary of their work online only.
A hyper-text must be included to the Elsevier homepage at http://www.elsevier.com

All content posted to the web site must maintain the copyright information line on the bottom of each image
You are not allowed to download and post the published electronic version of your chapter, nor may you scan the printed edition to create an electronic version.
Central Storage: This license does not include permission for a scanned version of the

material to be stored in a central repository such as that provided by Heron/XanEdu.

19. **Website** (regular and for author): A hyper-text must be included to the Homepage of the journal from which you are licensing at http://www.sciencedirect.com/science/journal/xxxxx. or for books to the Elsevier homepage at http://www.elsevier.com

20. **Thesis/Dissertation**: If your license is for use in a thesis/dissertation your thesis may be submitted to your institution in either print or electronic form. Should your thesis be published commercially, please reapply for permission. These requirements include permission for the Library and Archives of Canada to supply single copies, on demand, of the complete thesis and include permission for UMI to supply single copies, on demand, of the complete thesis. Should your thesis be published commercially, please reapply for permission.

21. **Other Conditions**: None

v1.6

Gratis licenses (referencing $0 in the Total field) are free. Please retain this printable license for your reference. No payment is required.

If you would like to pay for this license now, please remit this license along with your payment made payable to "COPYRIGHT CLEARANCE CENTER" otherwise you will be invoiced within 48 hours of the license date. Payment should be in the form of a check or money order referencing your account number and this invoice number RLNK10798204.
Once you receive your invoice for this order, you may pay your invoice by credit card. Please follow instructions provided at that time.

Make Payment To:
Copyright Clearance Center
Dept 001
P.O. Box 843006
Boston, MA 02284-3006

If you find copyrighted material related to this license will not be used and wish to cancel, please contact us referencing this license number 2446020152470 and noting the reason for cancellation.

Questions? customercare@copyright.com or +1-877-622-5543 (toll free in the US) or +1-978-646-2777.

References

Aiuppa A. (2009) Degassing of halogens from basaltic volcanism; insights from volcanic gas observations. *Chem. Geol.* **263,** 99-109

Amosse J., Allibert M., Fischer W. and Piboule M. (1990) Experimental study of the solubility of platinum and iridium in basic silicate melts; implications for the differentiation of platinum-group elements during magmatic processes. *Chem. Geol.* **81,** 45-53.

Amosse J., Dable P., Alibert M. (2000) Thermochemical behaviour of Pt, Ir, Rh, Ru vs fO_2 and fS_2 in a basaltic melt. Implications for the differentiation and precipitation of these elements. *Mineralogy and Petrology* **68**, 29-62.

Andrews D. R. A. and Brenan J. M. (2002) The solubility of ruthenium in sulfide liquid; implications for platinum group mineral stability and sulfide melt-silicate melt partitioning. *Chem. Geol.* **192,** 163-181.

Aranovich L. Y. and Newton R. C. (1996) H (sub 2) O activity in concentrated NaCl solutions at high pressures and temperatures measured by the brucite-periclase equilibrium. *Contributions to Mineralogy and Petrology* **125,** 200-212.

Audetat A., Pettke T. and Heinrich C. (2007) The role of fluid immiscibility in the formation of magmatic-hydrothermal ore deposits. *Geochim. Cosmochim. Acta* **71,** A43-A43.

Audetat A., Guenther D. and Heinrich C. A. (1998) Formation of a magmatic-hydrothermal ore deposit; insights with LA-ICP-MS analysis of fluid inclusions. *Science* **279,** 2091-2094.

Bali E. and Audetat A. (2007) Synthetic fluid inclusions in rutile; a new technique to study mantle fluids; Abstracts of the 17th annual V. M. Goldschmidt conference. *Geochim. Cosmochim. Acta* **71,** A56.

Ballhaus C., Ryan C. G., Mernagh T. P. and Green D. H. (1994) The partitioning of Fe, Ni, Cu, Pt, and Au between sulfide, metal, and fluid phases; a pilot study. *Geochim. Cosmochim. Acta* **58,** 811-826.

Ballhaus C. G. and Stumpfl E. F. (1986) Sulfide and platinum mineralization in the Merensky Reef; evidence from hydrous silicates and fluid inclusions. *Contributions to Mineralogy and Petrology* **94,** 193-204.

Ballhaus C. G. and Ulmer P. (1995) Platinum-group elements in the Merensky Reef; II, Experimental solubilities of platinum and palladium in Fe (sub 1-x) S from 950 to 450 degrees C under controlled f (sub s2) and f (sub H2). *Geochim. Cosmochim. Acta* **59,** 4881-4888.

Ballhaus C. and Sylvester P. (2000) Noble metal enrichment processes in the Merensky Reef, Bushveld Complex. *J. Petrol.* **41,** 545-561.

Barnes S., Maier W. D. and Ashwal L. D. (2004) Platinum-group element distribution in the Main Zone and Upper Zone of the Bushveld Complex, South Africa; Highly siderophile element behavior in high temperature processes. *Chem. Geol.* **208,** 293-317.

Barnes S., Makovicky E., Makovicky M., Rose-Hansen J. and Karup-Moller S. (1997) Partition coefficients for Ni, Cu, Pd, Pt, Rh, and Ir between monosulfide solid solution and sulfide liquid

and the formation of compositionally zoned Ni-Cu sulfide bodies by fractional crystallization of sulfide liquid. *Canadian Journal of Earth Sciences = Journal Canadien des Sciences de la Terre* **34,** 366-374.

Barnes S., Naldrett A. J. and Gorton M. P. (1985) The origin of the fractionation of platinum-group elements in terrestrial magmas. *Chem. Geol.* **53,** 303-323.

Behrens H. and Jantos N. (2001) The effect of anhydrous composition on water solubility in granitic melts. *Am. Mineral.* **86,** 14-20.

Behrens H., Meyer M. , Holtz F., Benne D. and Nowak M. (2001) The effect of alkali ionic radius, temperature, and pressure on the solubility of water in MAlSi. *Chem. Geol.* **174,** 275-289.

Behrens H., Ohlhorst S., Holtz F. and Champenois M. (2004) CO (sub 2) solubility in dacitic melts equilibrated with H (sub 2) O-CO (sub 2) fluids; implications for modeling the solubility of CO (sub 2) in silicic melts. *Geochim. Cosmochim. Acta* **68,** 4687-4703.

Behrens H., Romano C., Nowak M., Holtz F. and Dingwell D. B. (1996) Near-infrared spectroscopic determination of water species in glasses of the system MAlSi (sub 3) O (sub 8) (M = Li, Na, K); an interlaboratory study; 5th Silicate melt workshop. *Chem. Geol.* **128,** 41-63.

Benne D. and Behrens H. (2003) Water solubility in haplobasaltic melts. *European Journal of Mineralogy* **15,** 803-814.

Berndt J., Liebske C., Holtz F., Freise M., Nowak M., Ziegenbein D., Hurkuck W., Koepke J., Aronson J. (. and Bish D. L. (. (2002) A combined rapid-quench and H (sub 2) -membrane setup for internally heated pressure vessels; description and application for water solubility in basaltic melts; Reynolds commemorative volume [modified]. *Am. Mineral.* **87,** 1717-1726.

Bezmen N. I., Asif M., Bruegmann G. E., Romanenko I. M. and Naldrett A. J. (1994) Distribution of Pd, Rh, Ru, Jr, Os, and Au between sulfide and silicate metals. *Geochim. Cosmochim. Acta* **58,** 1251-1260.

Bezmen N., Gorbachev P., Shalynin A., Asif M. and Naldrett A. (2008) Solubility of platinum and palladium in silicate melts under high water pressure as a function of redox conditions. *PETROLOGY* **16,** 161-176.

Bezmen N. I. (1997) Influence f (sub O2) on the solubility of Pd and Pt in hydrous silicate melt. *EOS Trans. Am. Geophys. Union* **78,** 781.

Blaine F. A., Linnen R. L., Holtz F. and Bruegmann G. E. (2005) Platinum solubility in a haplobasaltic melt at 1250 degrees C and 0.2 GPa; the effect of water content and oxygen fugacity. *Geochim. Cosmochim. Acta* **69,** 1265-1273.

Borisov A. (2001) Loop technique; dynamics of metal/melt equilibration. *Mineralogy and Petrology* **71,** 87-94.

Borisov A. and Palme H. (2000) Solubilities of noble metals in Fe-containing silicate melts as derived from experiments in Fe-free systems. *Am. Mineral.* **85,** 1665-1673.

Borisov A. and Palme H. (1997) Experimental determination of the solubility of platinum in silicate melts. *Geochim. Cosmochim. Acta* **61,** 4349-4357.

Borisov A. and Palme H. (1995) The solubility of iridium in silicate melts; new data from experiments with Ir (sub 10) Pt (sub 90) alloys. *Geochim. Cosmochim. Acta* **59,** 481-485.

Borisov A., Palme H. and Spettel B. (1994) Solubility of palladium in silicate melts; implications for core formation in the Earth. *Geochim. Cosmochim. Acta* **58,** 705-716.

Borisov A. and Walker R. J. (2000) Os solubility in silicate melts; new efforts and results. *Am. Mineral.* **85,** 912-917.

Botcharnikov R. E., Holtz F., and Linnen R. L. (2010) Solubility of Au in Cl- and S-bearing hydrous silicate melts. *Geochim. Cosmochim. Acta* **74,** 2396-2411.

Botcharnikov R., Freise M., Holtz F. and Behrens H. (2005) Solubility of C-O-H mixtures in natural melts; new experimental data and application range of recent models. *Annals of Geophysics* **48,** 633-646.

Boudreau A. E. (2005) Modeling C-O-H-S fluids and sulfides in igneous systems; Abstracts of the 15th annual V. M. Goldschmidt conference. *Geochim. Cosmochim. Acta* **69,** 853.

Boudreau A. E. (2005) On the hydrothermal origin of platinum-group element deposits in layered intrusions; Abstracts of 15th annual V. M. Goldschmidt conference. *Geochim. Cosmochim. Acta* **69,** 331.

Boudreau A. E. (1988) Investigations of the Stillwater Complex; 4, The role of volatiles in the petrogenesis of the J-M Reef, Minneapolis adit section. *The Canadian Mineralogist* **26,** 193-208.

Boudreau A. E., Love C. and Prendergast M. D. (1995) Halogen geochemistry of the Great Dyke, Zimbabwe. *Contributions to Mineralogy and Petrology* **122,** 289-300.

Boudreau A. E., Mathez E. A. and McCallum I. S. (1986) Halogen geochemistry of the Stillwater and Bushveld complexes; evidence for transport of the platinum-group elements by Cl-rich fluids. *J. Petrol.* **27,** 967-986.

Boudreau A. E. and McCallum I. S. (1992) Concentration of platinum-group elements by magmatic fluids in layered intrusions. *Econ. Geol. Bull. Soc. Econ. Geol.* **87,** 1830-1848.

Boudreau A. E. and McCallum I. S. (1989) Investigations of the Stillwater Complex; Part 5, Apatites as indicators of evolving fluid composition. *Contributions to Mineralogy and Petrology* **102,** 138-153.

Boudreau A. E. and Meurer W. P. (1999) Chromatographic separation of the platinum-group elements, gold, base metals and sulfur during degassing of a compacting and solidifying igneous crystal pile. *Contributions to Mineralogy and Petrology* **134,** 174-185.

Boudreau A. E., Stewart M. A. and Spivack A. J. (1997) Stable Cl isotopes and origin of high-Cl magmas of the Stillwater Complex, Montana. *Geology (Boulder)* **25,** 791-794.

Boudreau A. (1999) Fluid fluxing of cumulates; the J-M reef and associated rocks of the Stillwater Complex, Montana. *J. Petrol.* **40,** 755-772.

Boudreau A. (1995) Formation of chlor- and fluor-apatite in layered intrusions; a comment. *Mineralogical Magazine* **59,** 757-760.

Boudreau A. E. (2008) Modeling the Merensky Reef, Bushveld Complex, Republic of South Africa. *Contributions to Mineralogy and Petrology* **156,** 431-437.

Boudreau A. E. (2004) PALLADIUM, a program to model for the chromatographic separation of the platinum-group elements, base metals and sulfur in a solidifying pile of igneous crystals; Platinum-group elements; petrology, geochemistry, mineralogy. *The Canadian Mineralogist* **42,** 393-403.

Boudreau A. E. (2003) Vapor separation and migration in a solidifying and compacting crystal pile; AGU 2003 fall meeting. *EOS Trans. Am. Geophys. Union* **84,**

Boudreau A. E. and McCallum I. S. (1985) Evidence for mineral reactions and metasomatism by silica-undersaturated Cl-rich fluids in the main Pt-Pd zone, Stillwater Complex, Montana; Program and abstracts; Fourth international platinum symposium. *The Canadian Mineralogist* **23,** 296.

Bourgue E. and Richet P. (2001) The effects of dissolved CO (sub 2) on the density and viscosity of silicate melts; a preliminary study. *Earth Planet. Sci. Lett.* **193,** 57-68.

Brenan J. M., McDonough W. F. and Dalpe C. (2003) Experimental constraints on the partitioning of rhenium and some platinum-group elements between olivine and silicate melt. *Earth Planet. Sci. Lett.* **212,** 135-150.

Brenan J. M., McDonough W. F. and Ash R. (2005) An experimental study of the solubility and partitioning of iridium, osmium and gold between olivine and silicate melt. *Earth Planet. Sci. Lett.* **237,** 855-872.

Bruegmann G. E., Naldrett A. J., Asif M., Lightfoot P. C., Gorbachev N. S. and Fedorenko V. A. (1993) Siderophile and chalcophile metals as tracers of the evolution of the Siberian Trap in the Noril'sk region, Russia. *Geochim. Cosmochim. Acta* **57,** 2001-2018.

Burnham C. W. (1994) Development of the Burnham model for prediction of H (sub 2) O solubility in magmas; Volatiles in magmas. *Rev. Mineral.* **30,** 123-129.

Campbell I. H. and Naldrett A. J. (1979) The influence of silicate:sulfide ratios on the geochemistry of magmatic sulfides. *Econ. Geol. Bull. Soc. Econ. Geol.* **74,** 1503-1506.

Campbell I. H., Naldrett A. J. and Barnes S. J. (1983) A model for the origin of the platinum-rich sulfide horizons in the Bushveld and Stillwater complexes. *J. Petrol.* **24,** 133-165.

Carroll M. R. and Webster J. D. (1994) Solubilities of sulfur, noble gases, nitrogen, chlorine, and fluorine in magmas. *Rev. Mineral.* **30,** 231-279.

Chabiron A., Pironon J. and Massare D. (2004) Characterization of water in synthetic rhyolitic glasses and natural melt inclusions by Raman spectroscopy. *Contributions to Mineralogy and Petrology* **146,** 485-492.

Chakraborty S. (1995) Diffusion in silicate melts. *Rev. Mineral.* **32,** 411-503.

Chou C. L. (1978) Abundances of noble metals in the Earth's upper mantle; evidence for late heavy bombardment after core formation. *Meteoritics* **13,** 407-410.

Cottrell E. and Walker D. (2006) Constraints on core formation from Pt partitioning in mafic silicate liquids at high temperatures. *Geochim. Cosmochim. Acta* **70,** 1565-1580.

Dixon J. E. and Stolper E. M. (1995) An experimental study of water and carbon dioxide solubilities in mid-ocean ridge basaltic liquids; Part II, Applications to degassing. *J. Petrol.* **36,** 1633-1646.

Dixon J. E., Stolper E. M. and Holloway J. R. (1995) An experimental study of water and carbon dioxide solubilities in mid-ocean ridge basaltic liquids; Part I, Calibration and solubility models. *J. Petrol.* **36,** 1607-1631.

Ertel W., Dingwell D. B. and Sylvester P. J. (2008) Siderophile elements in silicate melts - A review of the mechanically assisted equilibration technique and the nanonugget issue. *Chem. Geol.* **248,** February.

Ertel W., O'Neill H. S. C., Sylvester P. J. and Dingwell D. B. (1999) Solubilities of Pt and Rh in a haplobasaltic silicate melt at 1300 degrees C. *Geochim. Cosmochim. Acta* **63,** 2439-2449.

Ertel W., Pichavant M. and Scaillet B. (1998) Experimentally determined solubilities of Pt in a haplobasaltic melt under well constraint conditions of f (sub O2) P, T, and H (sub 2) O activity; V. M. Goldschmidt conference; extended abstracts. *Mineralogical Magazine* **62A,** 425-426.

Ertel W., Walter M. J., Drake M. J. and Sylvester P. J. (2006) Experimental study of platinum solubility in silicate melt to 14 GPa and 2273 K; implications for accretion and core formation in Earth. *Geochim. Cosmochim. Acta* **70,** 2591-2602.

Farges F., Siewert R., Ponader C., Brown G., Pichavant M. and Behrens H. (2006) Structural environments around molybdenum in silicate glasses and melts. II. Effect of temperature, pressure, H2O, halogens and sulfur. *Canadian Mineralogist* **44,** 755-773.

Farges F., Neuville D. R. and Brown G. E.,Jr (1999) Structural investigation of platinum solubility in silicate glasses. *Am. Mineral.* **84,** 1562-1568.

Fine G. and Stolper E. (1986) Dissolved carbon dioxide in basaltic glasses; concentrations and speciation. *Earth Planet. Sci. Lett.* **76,** 263-278.

Finnigan C. S., Brenan J. M., Mungall J. E. and McDonough W. F. (2008) Experiments and models bearing on the role of chromite as a collector of platinum group minerals by local reduction. *J. Petrol.* **49,** 1647-1665.

Fleet M. E., Crocket J. H., Liu M. and Stone W. E. (1999) Laboratory partitioning of platinum-group elements (PGE) and gold with application to magmatic sulfide-PGE deposits. *Lithos* **47,** 127-142.

Fleet M. E. and Wu T. W. (1994) Experiments on the volatile transport of precious metals at 1000 degrees C. *Mineralogical Magazine* **58A,** 278-279.

Fleet M. E. and Wu T. (1995) Volatile transport of precious metals at 1000 degrees C; speciation, fractionation, and effect of base-metal sulfide. *Geochim. Cosmochim. Acta* **59,** 487-495.

Fortenfant S. S., Guenther D., Dingwell D. B. and Rubie D. C. (2003) Temperature dependence of Pt and Rh solubilities in a haplobasaltic melt. *Geochim. Cosmochim. Acta* **67,** 123-131.

Gammons C. H. (1995) Experimental investigations of the hydrothermal geochemistry of platinum and palladium; IV, The stoichiometry of Pt (IV) and Pd (II) chloride complexes at 100 to 300 degrees C. *Geochim. Cosmochim. Acta* **59,** 1655-1667.

Gammons C. H. and Bloom M. S. (1993) Experimental investigation of the hydrothermal geochemistry of platinum and palladium; II, The solubility of PtS and PdS in aqueous sulfide solutions to 300 degrees C. *Geochim. Cosmochim. Acta* **57,** 2451-2467.

Gammons C. H., Bloom M. S. and Yu Y. (1992) Experimental investigation of the hydrothermal geochemistry of platinum and palladium; I, Solubility of platinum and palladium sulfide minerals in NaCl/H (sub 2) SO (sub 4) solutions at 300 degrees C. *Geochim. Cosmochim. Acta* **56,** 3881-3894.

Gammons C. H. (1996) Experimental investigations of the hydrothermal geochemistry of platinum and palladium; V, Equilibria between platinum metal, Pt(II), and Pt(IV) chloride complexes at 25 to 300 degrees C. *Geochim. Cosmochim. Acta* **60,** 1683-1694.

Godel B., Barnes S. J. and Maier W. D. (2006) Stratigraphic variation of platinum-group element, rhenium, silver, gold, cobalt and zinc in sulphides of the Merensky Reef (Bushveld Complex, South Africa); GAC-MAC annual meeting; abstracts--AGC-AMC congres annual; resumes. *Abstract Volume (Geological Association of Canada)* **31,** 56.

Hanley J. J. (2005) The aqueous geochemistry of the platinum group elements (PGE) in surficial, low-T hydrothermal and high-T magmatic-hydrothermal environments. *Short Course Series - Mineralogical Association of Canada* **35,** 35-56.

Hanley J. J., Mungall J. E., Pettke T., Spooner E. T. C. and Bray C. J. (2005) Ore metal redistribution by hydrocarbon-brine and hydrocarbon-halide melt phases, North Range footwall of the Sudbury igneous complex, Ontario, Canada. *Miner. Deposita* **40,** 237-256.

Hanley J. J., Mungall J. E., Pettke T., Spooner E. T. C. and Bray C. J. (2008) Fluid and halide melt inclusions of magmatic origin in the ultramafic and lower banded series, Stillwater Complex, Montana, USA. *J. Petrol.* **49,** 1133-1160.

Hanley J. J., Pettke T., Mungall J. E. and Spooner E. T. C. (2005) The solubility of platinum and gold in NaCl brines at 1.5 kbar, 600 to 800 degrees C; a laser ablation ICP-MS pilot study of synthetic fluid inclusions. *Geochim. Cosmochim. Acta* **69,** 2593-2611.

Heinrich C. A., Ryan C. G., Mernagh T. P. and Eadington P. J. (. (1992) Segregation of ore metals between magmatic brine and vapor: a fluid inclusion study using PIXE microanalysis. *Economic Geology* **87,** 1566-1583.

Heinrich C. A., Guenther D., Audetat A., Ulrich T. and Frischknecht R. (1999) Metal fractionation between magmatic brine and vapor, determined by microanalysis of fluid inclusions. *Geology (Boulder)* **27,** 755-758.

Holtz F., Behrens H., Dingwell D. B. and Taylor R. P. (1992) Water solubility in aluminosilicate melts of haplogranite composition at 2 kbar. *Chem. Geol.* **96,** 289-302.

Holtz F., Roux J., Pichavant M. and Behrens H. (2000) Water solubility in silica and quartzofeldspathic melts. *Am. Mineral.* **85,** 682-686.

Jendrzejewski N., Trull T. W., Pineau F. and Javoy M. (1997) Carbon solubility in mid-ocean ridge basaltic melt at low pressures (250-1950 bar). *Chem. Geol.* **138,** 81-92.

Jenner G. A., Longerich H. P., Jackson S. E. and Fryer B. J. (1990) ICP-MS; a powerful tool for high-precision trace-element analysis in earth sciences; evidence from analysis of selected U.S.G.S. reference samples. *Chem. Geol.* **83,** 133-148.

Keppler H. and Bagdassarov N. (1999) The speciation of Ni and Co in silicate melts from optical absorption spectra to 1500 degrees C. *Chem. Geol.* **158,** 105-115.

Kerr A. and Leitch A. (2005) Self-destructive sulfide segregation systems and the formation of high-grade magmatic ore deposits.

Kessel R., Ulmer P., Pettke T., Schmidt M. W. and Thompson A. B. (2004) A novel approach to determine high-pressure high-temperature fluid and melt compositions using diamond-trap experiments. *Am. Mineral.* **89,** 1078-1086.

King P. L. and Holloway J. R. (2002) CO (sub 2) solubility and speciation in intermediate (andesitic) melts; the role of H (sub 2) O and composition. *Geochim. Cosmochim. Acta* **66,** 1627-1640.

King P. L., Vennemann T. W., Holloway J. R., Hervig R. L., Lowenstern J. B. and Forneris J. F. (2002) Analytical techniques for volatiles; a case study using intermediate (andesitic) glasses. *Am. Mineral.* **87,** 1077-1089.

Lange R. A. (1994) The effect of H (sub 2) O, CO (sub 2) and F on the density and viscosity of silicate melts. *Rev. Mineral.* **30,** 331-369.

Li C., Barnes S. J. and Fleet M. E. (1996) Partitioning of platinum-group elements and Au in the Fe-Ni-Cu-S system; experiments on the fractional crystallization of sulfide melt; discussion and reply. *Contributions to Mineralogy and Petrology* **123,** 435-440.

Li C., Barnes S. J., Makovicky E., Rose-Hansen J. and Makovicky M. (1996) Partitioning of nickel, copper, iridium, rhenium, platinum, and palladium between monosulfide solid solution and sulfide liquid; effects of composition and temperature. *Geochim. Cosmochim. Acta* **60,** 1231-1238.

Li C., Maier W. D. and De Waal S. A. (2001) The role of magma mixing in the genesis of PGE mineralization in the Bushveld complex: Thermodynamic calculations and new interpretations. *Economic Geology* **96,** 653-662.

London D., Hervig R. L. and Morgan G. B. (1988) Melt-vapor solubilities and elemental partitioning in peraluminous granite-pegmatite systems; experimental results with Macusani glass at 200 MPa. *Contributions to Mineralogy and Petrology* **99,** 360-373.

Longerich H. P., Jackson S. E., and Gunther D. (1996) Laser ablation inductively coupled plasma mass spectrometric transient signal data acquisition and analyte concentration calculation. *J. Anal. At. Spectrom.* **11,** 899-904.

Lorand J., Luguet A. and Alard O. (2008) Platinum-group elements; a new set of key tracers for the Earth's interior. *Elements* **4,** 247-252.

Lowenstern J. B. (2000) A review of the contrasting behavior of two magmatic volatiles; chlorine and carbon dioxide. *J. Geochem. Explor.* **69-70,** 287-290.

Maier W. D. (2005) Platinum-group element (PGE) deposits and occurrences; mineralization styles, genetic concepts, and exploration criteria. *J. Afr. Earth Sci.* **41,** 165-191.

Maier W. D. and Barnes S. J. (1999) Platinum-group elements in silicate rocks of the lower, critical and main zones at union section, western Bushveld Complex. *J. Petrol.* **40,** 1647-1671.

Makovicky E. and Karup-Moller S. (2000) Phase relations in the metal-rich portions of the phase system Pt-Ir-Fe-S at 1000 degrees C and 1100 degrees C. *Mineralogical Magazine* **64,** 1047-1056.

Manning C. E. and Boettcher S. L. (1994) Rapid-quench-hydrothermal experiments at mantle pressures and temperatures. *Am. Mineral.* **79,** 1153-1158.

Mathez E. A. (1995) Magmatic metasomatism and formation of the Merensky Reef, Bushveld Complex. *Contributions to Mineralogy and Petrology* **119,** 277-286.

Mathez E. A., Dietrich V. J., Holloway J. R. and Boudreau A. E. (1989) Carbon distribution in the Stillwater Complex and evolution of vapor during crystallization of Stillwater and Bushveld magmas. *J. Petrol.* **30,** 153-173.

Mathez E. A. and Peach C. L. (1989) The geochemistry of the platinum group elements in mafic and ultramafic rocks; Ore deposition associated with magmas. *Reviews in Economic Geology* **4,** 33-43.

Mathez E. A. and Webster J. D. (2005) Partitioning behavior of chlorine and fluorine in the system apatite-silicate melt-fluid. *Geochim. Cosmochim. Acta* **69,** 1275-1286.

Mavrogenes J. A. and O'Neill H. S. C. (. (1999) The relative effects of pressure, temperature and oxygen fugacity on the solubility of sulfide in mafic magmas. *Geochim. Cosmochim. Acta* **63,** 1173-1180.

McMillan P. F. (1994) Water solubility and speciation models. *Rev. Mineral.* **30,** 132-156.

Metrich N. and Rutherford M. J. (1992) Experimental study of chlorine behavior in hydrous silicic melts. *Geochim. Cosmochim. Acta* **56,** 607-616.

Meurer W. P., Willmore C. C. and Boudreau A. E. (1999) Metal redistribution during fluid exsolution and migration in the Middle Banded Series of the Stillwater Complex, Montana; Geodynamics of giant magmatic ore systems. *Lithos* **47,** 143-156.

Mitarai Y., Aoyagi T. and Abe T. (2009) An investigation of phase separation in the Ir-Pt binary system. *J. Alloys Compounds* **484,** 327-334.

Morgan G. B., V.I. and London D. (1996) Optimizing the electron microprobe analysis of hydrous alkali aluminosilicate glasses. *Am. Mineral.* **81,** 1176-1185.

Mountain B. W. and Wood S. A. (1988) Chemical controls on the solubility, transport and deposition of platinum and palladium in hydrothermal solutions; a thermodynamic approach. *Econ. Geol. Bull. Soc. Econ. Geol.* **83,** 492-510.

Mungall J. E. (2002) Empirical models relating viscosity and tracer diffusion in magmatic silicate melts. *Geochim. Cosmochim. Acta* **66,** 125-143.

Mungall J. E., Andrews D. R. A., Cabri L. J., Sylvester P. J. and Tubrett M. (2005) Partitioning of Cu, Ni, Au, and platinum-group elements between monosulfide solid solution and sulfide melt under controlled oxygen and sulfur fugacities. *Geochim. Cosmochim. Acta* **69,** 4349-4360.

Mungall J. E. and Naldrett A. J. (2008) Ore deposits of the platinum-group elements. *Elements* **4,** 253-258.

Mysen B. and Richet P (2005) *Silicate glasses and melts; properties and structure.* Elsevier, Amsterdam, Netherlands

Naldrett A. J. (1999) World-class Ni-Cu-PGE deposits; key factors in their genesis. *Miner. Deposita* **34,** 227-240.

Naldrett A. J. and Hawthorne F. C. (2005) A history of our understanding of magmatic Ni-Cu sulfide deposits; The Mineralogical Association of Canada 50th anniversary symposium volume. *The Canadian Mineralogist* **43,** 2069-2098.

Naldrett A. J., Wilson A., Kinnaird J. and Chunnett G. (2009) PGE tenor and metal ratios within and below the Merensky Reef, Bushveld Complex: Implications for its genesis. *J. Petrol.* **50,** 625-659.

Naldrett A. (2005) A history of our understanding of magmatic Ni-Cu sulfide deposits. *The Canadian Mineralogist* **43,** 2069-2098.

Newman S. and Lowenstern J. B. (2002) VOLATILECALC: A silicate melt-H2O-CO2 solution model written in Visual Basic for excel. *Computers and Geosciences* **28,** 597-604.

Nicholson D. M. and Mathez E. A. (1991) Petrogenesis of the Merensky Reef in the Rustenburg section of the Bushveld Complex. *Contributions to Mineralogy and Petrology* **107,** 293-309.

Ochs,Frederick A., I.,II and Lange R. A. (1999) The density of hydrous magmatic liquids. *Science* **283,** 1314.

Ohlhorst S., Behrens H. and Holtz F. (2001) Compositional dependence of molar absorptivities of near-infrared OH- and H (sub 2) O bands in rhyolitic to basaltic glasses. *Chem. Geol.* **174,** 5-20.

O'Neill H. S. C., Dingwell D. B., Borisov A., Spettel B. and Palme H. (1995) Experimental petrochemistry of some highly siderophile elements at high temperatures, and some implications for core formation and the mantle's early history; Chemical evolution of the mantle. *Chem. Geol.* **120,** 255-273.

O'Neill H. S. C. and Pownceby M. I. (1993) Thermodynamic data from redox reactions at high temperatures; II, The MnO-Mn (sub 3) O (sub 4) oxygen buffer, and implications for the thermodynamic properties of MnO and Mn (sub 3) O (sub 4). *Contributions to Mineralogy and Petrology* **114,** 315-320.

Pan P. and Wood S. A. (1994) Solubility of Pt and Pd sulfides and Au metal in aqueous bisulfide solutions; II, Results at 200 degrees C to 350 degrees C and saturated vapor pressure. *Miner. Deposita* **29,** 373-390.

Paparoni G., Webster J. D. and Walker D. (2010) Experimental techniques for determining tin solubility in silicate melts using silica capsules in 1 atm furnaces and rhenium capsules in the piston cylinder. *Am. Mineral.* **95,** 776-783.

Peach C. L. and Mathez E. A. (1996) Constraints on the formation of platinum-group element deposits in igneous rocks. *Econ. Geol. Bull. Soc. Econ. Geol.* **91,** 439-450.

Peach C. L., Mathez E. A., Keays R. R. and Reeves S. J. (1994) Experimentally determined sulfide melt-silicate melt partition coefficients for iridium and palladium; Trace-element partitioning with application to magmatic processes. *Chem. Geol.* **117,** 361-377.

Peregoedova A., Barnes S. and Baker D. R. (2006) An experimental study of mass transfer of platinum group elements, gold, nickel and copper in sulfur-dominated vapor at magmatic temperatures. *Chem. Geol.* **235,** 59-75.

Pettke T., Webster J. D., Halter W. E., Heinrich C. A., Aigner-Torres M. and De Vivo B. (2002) Advantages and limitations of quantifying melt inclusion chemistry by LA-ICPMS, EMP and SIMS; Abstracts of the 12th annual V. M. Goldschmidt conference. *Geochim. Cosmochim. Acta* **66,** 596.

Pettke T., Kessel R., Schmidt M. W. and Ulmer P. (2005) High-P-T fluids in diamond trap experiments analyzed frozen with LA-ICPMS; the technique; Abstracts of the 15th annual V. M. Goldschmidt conference. *Geochim. Cosmochim. Acta* **69,** 658.

Pitzer K.S. and Sterner M.S. (1994) Equations of state valid continuously from zero to extreme pressures for H_2O and CO_2. *The Journal of Chemical Physics* **101,** 3111.

Pruseth K. L. and Palme H. (2004) The solubility of Pt in liquid Fe-sulfides; Highly siderophile element behavior in high temperature processes. *Chem. Geol.* **208,** 233-245.

Righter K., Campbell A. J. and Humayun M. (2003) Experimental determination of spinel/melt, olivine/melt, and pyroxene/melt partition coefficients for Re, Ru, Pd, Au, and Pt. *Abstracts of Papers Submitted to the Lunar and Planetary Science Conference* **34,**

Righter K., Campbell A. J., Humayun M. and Hervig R. L. (2004) Partitioning of Ru, Rh, Pd, Re, Ir, and Au between Cr-bearing spinel, olivine, pyroxene and silicate melts. *Geochim. Cosmochim. Acta* **68,** 867-880.

Righter K., Drake M. J. and Yaxley G. (1997) Prediction of siderophile element metal-silicate partition coefficients to 20 GPa and 2800 degrees C; the effects of pressure, temperature, oxygen fugacity, and silicate and metallic melt compositions. *Phys. Earth Planet. Inter.* **100,** 115-134.

Righter K., Humayun M. and Danielson L. (2006) Highly siderophile elements in the terrestrial upper mantle require a late veneer? New results for palladium. 87-8.

Righter K. (2003) Metal-silicate partitioning of siderophile elements and core formation in the early Earth. *Annu. Rev. Earth Planet. Sci.* **31,** 135-174.

Righter K., Campbell A. J., Humayun M. and Hervig R. L. (2004) Partitioning of Ru, Rh, Pd, Re, Ir, and Au between Cr-bearing spinel, olivine, pyroxene and silicate melts. *Geochim. Cosmochim. Acta* **68,** 867-880.

Righter K. and Drake M. J. (1999) Effect of water on metal-silicate partitioning of siderophile elements; a high pressure and temperature terrestrial magma ocean and core formation. *Earth Planet. Sci. Lett.* **171,** 383-399.

Righter K. and Drake M. J. (1999) Effect of water on metal-silicate partitioning of siderophile elements; a high pressure and temperature terrestrial magma ocean and core formation. *Earth Planet. Sci. Lett.* **171,** 383-399.

Righter K., Humayun M. and Danielson L. (2007) Partitioning of Pd between Fe-S-C and mantle liquids at high pressure and temperature; implications for core formation. *Abstracts of Papers Submitted to the Lunar and Planetary Science Conference* **38,**

Rubie D. C., Melosh H. J., Reid J. E., Liebske C. and Righter K. (2003) Mechanisms of metal-silicate equilibration in the terrestrial magma ocean. *Earth Planet. Sci. Lett.* **205,** 239-255.

Sandland T. O., Du L., Stebbins J. F. and Webster J. D. (2004) Structure of Cl-containing silicate and aluminosilicate glasses; a (super 35) Cl MAS-NMR study. *Geochim. Cosmochim. Acta* **68,** 5059-5069.

Sassani D. C. and Shock E. L. (1998) Solubility and transport of platinum-group elements in supercritical fluids; summary and estimates of thermodynamic properties for ruthenium, rhodium, palladium, and platinum solids, aqueous ions, and complexes to 1000 degrees C and 5 kbar. *Geochim. Cosmochim. Acta* **62,** 2643-2671.

Sassani D. C. and Shock E. L. (1990) Speciation and solubility of palladium in aqueous magmatic-hydrothermal solutions. *Geology (Boulder)* **18,** 925-928.

Savard D., Barnes S. J., Bedard L. P. and Cox R. (2007) Sulfur/selenium ratios in Bushveld Complex, South Africa; Abstracts of the 17th annual V. M. Goldschmidt conference. *Geochim. Cosmochim. Acta* **71,** A878.

Schaefer B., Frischknecht R., Guenther D. and Dingwell D. B. (1999) Determination of trace element partitioning between fluid and melt using LA-ICP-MS analysis of synthetic fluid inclusions in glass. *European Journal of Mineralogy* **11,** 415-426.

Sekine K., Bignall G. and Tsuchiya N. (2004) Application of synthetic fluid inclusions to simultaneous temperature-pressure logging in high-temperature (sub- to supercritical) geothermal systems. *Geothermics* **33,** 775-793.

Shen A. (. and Keppler H. (. (1995) Infrared spectroscopy of hydrous silicate melts to 1000°C and 10 kbar: direct observation of H. *Am. Mineral.* **80,** 1335-1338.

Signorelli S. and Carroll M. R. (2000) Solubility and fluid-melt partitioning of Cl in hydrous phonolitic melts. *Geochim. Cosmochim. Acta* **64,** 2851-2862.

Sillitoe R. H. and Perello J. (2005) Andean copper province; tectonomagmatic settings, deposit types, metallogeny, exploration, and discovery. 845-890.

Simon A. C., Frank M. R., Pettke T., Candela P. A., Piccoli P. M. and Heinrich C. A. (2005) Gold partitioning in melt-vapor-brine systems. *Geochim. Cosmochim. Acta* **69,** 3321-3335.

Simon A. C., Frank M. R., Pettke T., Candela P. A., Piccoli P. M., Heinrich C. A. and Glascock M. (2007) An evaluation of synthetic fluid inclusions for the purpose of trapping equilibrated, coexisting, immiscible fluid phases at magmatic conditions. *Am. Mineral.* **92,** 124-138.

Simon A. C. and Pettke T. (2009) Platinum solubility and partitioning in a felsic melt-vapor-brine assemblage. *Geochim. Cosmochim. Acta* **73,** 438-454.

Stelling J., Botcharnikov R., Beermann O. and Nowak M. (2008) Solubility of H sub(2)O- and chlorine-bearing fluids in basaltic melt of Mount Etna at T=1050-1250 super(o)C and P=200 MPa. *Chem. Geol.* **256,** 101-109.

Student J. J. and Bodnar R. J. (1999) Synthetic fluid inclusions XIV; coexisting silicate melt and aqueous fluid inclusions in the haplogranite-H (sub 2) O-NaCl-KCl system. *J. Petrol.* **40,** 1509-1525.

Tredoux M., Lindsay N. M., Davies G. and McDonald I. (1995) The fractionation of platinum-group elements in magmatic systems, with the suggestion of a novel causal mechanism. *South African Journal of Geology* **98,** 157-167.

Tripathi S. N. and Chandrasekharaiah M. S. (1983) THERMODYNAMIC PROPERTIES OF BINARY ALLOYS OF II: Ir-Pt SYSTEM. *Journal of the less-common metals* **91,** 251-260.

Van Orman J. A., Keshav S. and Fei Y. (2006) High pressure solid-metal/liquid-metal partitioning of Os, Re and Pt in the Fe-S system. *Geochim. Cosmochim. Acta* **70,** A666.

Webster J. D. (2002) The exsolution of magmatic brine; Abstracts of the 12th annual V. M. Goldschmidt conference. *Geochim. Cosmochim. Acta* **66,** 826.

Webster J. D. (2004) The exsolution of magmatic hydrosaline chloride liquids. *Chem. Geol.* **210,** 33-48

Webster J. D., Kinzler R. J. and Mathez E. A. (1999) Chloride and water solubility in basalt and andesite melts and implications for magmatic degassing. *Geochim. Cosmochim. Acta* **63,** 729-738.

Webster J. D. and De Vivo B. (2002) Experimental and modeled solubilities of chlorine in aluminosilicate melts, consequences of magma evolution, and implications for exsolution of hydrous chlorine melt at Mt. Somma-Vesuvius. *Am. Mineral.* **87,** 1046-1061.

Webster J. D. and Mandeville C. W. (2007) Fluid immiscibility in volcanic environments. *Reviews in Mineralogy and Geochemistry* **65,** 313-362.

Whitney J. A. (1972) The effect of reduced H2O fugacity on the buffering of oxygen fugacity in hydrothermal experiments. *American Mineralogist* **57,** 1902-1908.

Willmore C. C., Boudreau A. E. and Kruger F. J. (2000) The halogen geochemistry of the Bushveld Complex, Republic of South Africa; implications for chalcophile element distribution in the lower and critical zones. *J. Petrol.* **41,** 1517-1539.

Willmore C. C., Boudreau A. E., Spivack A. and Kruger F. J. (2002) Halogens of Bushveld Complex, South Africa; delta (super 37) Cl and Cl/F evidence for hydration melting of the source region in a back-arc setting. *Chem. Geol.* **182,** 503-511.

Wood B. J., Corgne A. and Wade J. (2007) Fe-FeS-silicate partitioning of chalcophile and siderophile elements; implications for core formation. *Geochim. Cosmochim. Acta* **71,** A1126.

Wood S. A., Pan P., Zhang Y. and Mucci A. (1994) The solubility of Pt and Pd sulfides and Au in bisulfide solutions; I, Results at 25 degrees -90 degrees C and 1 bar pressure. *Miner. Deposita* **29,** 309-317.

Wood S. A. and Xiong Y. (2001) Experimental studies of the speciation and solubility of Os and Re in hydrothermal solutions. *LPI Contribution*3252.

Wood S. A. (1991) Experimental determination of the hydrolysis constants of Pt (super 2+) and Pd (super 2+) at 25 degrees C from the solubility of Pt and Pd in aqueous hydroxide solutions. *Geochim. Cosmochim. Acta* **55,** 1759-1767.

Wood S. A. (1987) Thermodynamic calculations of the volatility of the platinum group elements (PGE); the PGE content of fluids at magmatic temperatures. *Geochim. Cosmochim. Acta* **51,** 3041-3050.

Wyllie P. J. and Tuttle O. F. (1964) Experimental investigation of silicate systems containing two volatile components; Part 3, The effects of SO (sub 3) , P (sub 2) O (sub 5) , HCl, and Li (sub 2) O, in addition to H (sub 2) O, on the melting temperatures of albite and granite. *Am. J. Sci.* **262,** 930-939.

Yoder H. S., J. (1965) Diopside-anorthite-water at five and ten kilobars and its bearing on explosive volcanism. *Year Book - Carnegie Institution of Washington*82-89.

Zotov N. and Keppler H. (1998) The influence of water on the structure of hydrous sodium tetrasilicate glasses. *Am. Mineral.* **83,** 823-834.